UNIVERSITY OF CINCINNATI

Date: 05.06.09

I, Chittabrata Ghosh **,**

hereby submit this original work as part of the requirements for the degree of:

Doctor in Philosophy (Ph.D.)

in Computer Science and Engineering

It is entitled:

Innovative Approaches to Spectrum Selection, Sensing, and Sharing in Cognitive Radio Networks

Student Signature: Chittabrata Ghosh

This work and its defense approved by:

Committee Chair: Prof. Dharma P. Agrawal

Prof. Raj Bhatnagar

Prof. Chia-Yung Han

Prof. Yiming Hu

Prof. Marepalli B. Rao

Approval of the electronic document:

I have reviewed the Thesis/Dissertation in its final electronic format and certify that it is an accurate copy of the document reviewed and approved by the committee.

Committee Chair signature: Prof. Dharma P. Agrawal

Innovative Approaches to Spectrum Selection, Sensing, and Sharing in Cognitive Radio Networks

by

Chittabrata Ghosh

B.Tech. (Kalyani University, India) 2000
M.S. (Indian Institute of Technology (I.I.T) Kharagpur, India) 2004

A dissertation submitted in partial satisfaction of the
requirements for the degree of
Doctor of Philosophy

in

Computer Science and Engineering

in the

Department of Computer Science
of the
College of Engineering
of the
UNIVERSITY OF CINCINNATI, OHIO

Committee:
Professor Dharma P. Agrawal, Chair
Professor Raj Bhatnagar
Professor Chia-Yung Han
Professor Yiming Hu
Professor M. Bhaskara Rao

May 2009

Abstract

Innovative Approaches to Spectrum Selection, Sensing, and Sharing in Cognitive Radio Networks

In a cognitive radio network (CRN), bands of a spectrum are shared by licensed (primary) and unlicensed (secondary) users in that preferential order. It is generally recognized that the spectral occupancy by primary users exhibit dynamical spatial and temporal properties. In the open literature, there exist no accurate time-varying model representing the spectrum occupancy that the wireless researchers could employ for evaluating new algorithms and techniques designed for dynamic spectrum access (DSA). We use statistical characteristics from actual radio frequency measurements, obtain first- and second-order parameters, and define a statistical spectrum occupancy model based on a combination of several different probability density functions (PDFs).

One of the fundamental issues in analyzing spectrum occupancy is to characterize it in terms of probabilities and study probabilistic distributions over the spectrum. To reduce computational complexity of the exact distribution of total number of free bands, we resort to efficient approximation techniques. Furthermore, we characterize free bands into five different types based on the occupancy of its adjacent bands. The probability distribution of total number of each type of bands is therefore determined. Two corresponding algorithms are effectively developed to compute the distributions, and our extensive simulation results show the effectiveness of the proposed analytical model.

Design of an efficient spectrum sensing scheme is a challenging task, especially when false alarms and misdetections are present. The status of the band is to be monitored over a number of consecutive time periods, with each time period being of a specific time interval. The status of the sub-band at any time point is either free or busy. We proved that the status of the band over time evolves randomly, following a Markov chain. The cognitive radio assesses the band, whether or not it is free, and the assessment is prone to errors. The errors are modeled probabilistically and the entire edifice is brought under a hidden Markov chain model in predicting the true status of the band.

After spectrum sensing, our research direction is on spectrum sharing using cooperative communication. We discuss allocation strategies of unused bands among the cognitive users. We introduce a cooperative N-person Game among the N cognitive users in a CRN and then identify strategies that help achieve Nash equilibrium. When licensed users arrive in any of those sub-bands involved in unlicensed user communication, the affected cognitive users in those bands remove them out of the N-person game and assess their optional strategies with the licensed users using the 2-person game approach for coexistence with the licensed users. In the sequel of spectrum sharing, we present three novel priority-based spectrum allocation techniques for enabling dynamic spectrum access (DSA) networks employing non-contiguous orthogonal frequency division multiplexing (NC-OFDM) transmission.

The allocation of bandwidth to unlicensed users, without significantly increasing the interference on the existing licensed users, is a challenge for Ultra Wideband (UWB) networks. We propose a novel Rake Optimization and Power Aware Scheduling (ROPAS) architecture for UWB networks as multipath diversity in UWB communication encourages us to use a Rake receiver.

To

Dad and Mom for having confidence in me,

and

my sister and wife, Suprita for their continuous inspiration and support

Acknowledgments

I would like to express my sincere gratitude and specially "thank" my advisor, Dr. Dharma P. Agrawal for his unflinching support and continuous motivation for quality work. His momentum and spontaneity has always restored an aura of research excellence at the Center of Distributed and Mobile Computing (CDMC). Dr. Agrawal gave me the freedom to pursue inter-disciplinary research and encouraged me to publish and attend conferences to acquire knowledge that helped me in building a solid foundation in the area of Cognitive Radio Networks. For all his help, I am really indebted to him.

I would also like to extend my thanks to Dr. M. B. Rao for imparting valuable knowledge to me in the domain of Game Theory, Probability, and Statistics. This knowledge has become an integral part of my research work. I wold also like to thank Dr. Bhatnagar, not only for his help in the academics and administrative issues, but also for his kind support for our Computer Science Graduate Student Association. Dr. Berman and Dr. Han were really instrumental in providing subtle advices that accelerated my research work. I am indebted to all of them for acceeding to be members of my thesis committee.

Special thanks owes to Dr. A. M. Wyglinski for the enriched collaborative work on designing the innovative spectrum occupancy model. The real-time measurements performed by his students turned out to be an asset and invaluable for my research work.

I would also like to thank my colleagues at the CDMC laboratory as they have always been a source of inspiration and create a positive research atmosphere all the time. I would like to specially thank Bing, Junfang, Yun, Deepti, Asitha, Weihuang, Demin, Peter and Kuheli for their personal and professional assistance on myriad occasions. Special thanks to Dr. Bin Xie for teaching me the process of technical writing.

Last but not the least, I would take this opportunity to thank by dearest parents. Without their dream, I would not have sailed so far in life. My heartiest thanks to my sister, who is so very caring and loving all throughout my life. Special thanks to my wife, Suprita for always being so supportive and motivating me during my doctoral research.

Contents

List of Figures v

List of Tables ix

1 Introduction 2
- 1.1 Motivation . . . 6
- 1.2 Organization of the Thesis . . . 7
  - 1.2.1 Chapter 2: A Framework for Statistical Wireless Spectrum Occupancy Modeling . . . 8
  - 1.2.2 Chapter 3: Probabilistic Approach to Spectrum Occupancy . . . 8
  - 1.2.3 Chapter 4: Hidden Markov Model in Spectrum Sensing . . . 8
  - 1.2.4 Chapter 5: Game Theoretic Approach in Spectrum Sharing . . . 9
  - 1.2.5 Chapter 6: Priority-based Spectrum Allocation in Cognitive Radio Networks Employing NC-OFDM Transmission . . . 9
  - 1.2.6 Chapter 7: Cross-Layer Architecture for Joint Power and Link Optimization . . . 10
  - 1.2.7 Chapter 8: Conclusions and Future Work . . . 11

2 A Framework for Statistical Wireless Spectrum Occupancy Modeling 12
- 2.1 Introduction . . . 12
- 2.2 Real-time Data Measurements . . . 15
  - 2.2.1 USRP Measurements . . . 15
  - 2.2.2 Paging-band Measurements . . . 16
- 2.3 Proposed Spectrum Occupancy Model . . . 17
  - 2.3.1 Statistical Analysis of Spectrum Occupancy . . . 18
  - 2.3.2 Proposed Spectrum Occupancy Model Implementation . . . 20
- 2.4 M/M/1 Queuing Model Representation of Spectrum Occupancy . . . 22
  - 2.4.1 Case Study Using Real Time Measurements . . . 24
- 2.5 Performance Evaluation . . . 26
  - 2.5.1 Time Slice Validation . . . 27
  - 2.5.2 Frequency Slice Validation . . . 29

2.6 Conclusion . . . 32

3 Probabilistic Approach to Spectrum Occupancy 33
3.1 Introduction . . . 33
3.2 Related Work . . . 36
3.3 System Model and Problem Formulation . . . 38
3.3.1 Sub-band Free Probability Model . . . 38
3.3.2 Probability Distribution of N_{free} . . . 40
3.3.3 Approximation with Normal Distribution . . . 42
3.4 Probability Distribution of N_{free} . . . 45
3.4.1 Approximate Distribution of $N_{free_{small}}$ . . . 46
3.4.2 Approximate Distribution of $N_{free_{mod}}$ . . . 47
3.4.3 Approximate Distribution of $N_{free_{large}}$ . . . 47
3.4.4 Approximate Distribution of N_{free} . . . 48
3.5 Neighborhood Occupancy of Free Sub-bands . . . 50
3.5.1 Sub-band Types . . . 50
3.5.2 Probability Distribution of $X_I(N)$ . . . 52
3.5.3 Probability Distribution of $X_{II}(N)$ . . . 56
3.5.4 Probability Distribution of $X_{III}(N)$ . . . 57
3.5.5 Probability Distribution of $X_{IV}(N)$ . . . 58
3.5.6 Probability Distribution of $X_V(N)$ . . . 58
3.6 Implementation and Performance Evaluation . . . 59
3.6.1 Algorithm for Probability Distribution of N_{free} . . . 60
3.6.2 Algorithm for Probability Distribution of $X_I(N)$ . . . 62
3.6.3 Simulation Configuration . . . 63
3.6.4 Distribution of N_{free} . . . 64
3.6.5 Computational Efficiency . . . 65
3.6.6 Probability Distribution of $X_i(N)$ . . . 66
3.6.7 Statistical Analysis of $X_I(N)$ . . . 70
3.6.8 Special Case ($p_i = p_j$) . . . 71
3.7 Conclusion . . . 72

4 Hidden Markov Model in Spectrum Sensing 73
4.1 Introduction . . . 73
4.2 Related Work on Spectrum Sensing . . . 75
4.3 System Model and Problem Formulation . . . 76
4.4 Markov Chain Modeling of True States and its Validation . . . 78
4.4.1 Markov Chain Assumption Validation . . . 78
4.5 HMM Parameter Estimation . . . 80
4.6 Viterbi Algorithm and the Expectation Maximization Algorithm . . . 85
4.6.1 Viterbi-based Sensing Algorithm . . . 85
4.6.2 Expectation Maximization Algorithm . . . 87

4.7 Hidden Markov Model in Spectrum Sensing . . . 89
4.8 Validation and Simulation Results . . . 91
4.9 Conclusion . . . 98

5 Game Theoretic Approach in Spectrum Sharing 99
5.1 Introduction . . . 99
5.2 Related Work . . . 101
5.3 Spectrum Model and Basic Components of Spectrum Sharing . . . 103
5.4 Channel Capacity Optimization and Game Theoretic Formulation . . . 111
5.4.1 Channel Capacity Optimization . . . 112
5.4.2 Optimization, Game Theory, and Nash Equilibrium . . . 112
5.4.3 Case Study . . . 115
5.5 Game Theoretic Perspective using Spectrum Sensing Parameters . . . 119
5.5.1 Case Study . . . 120
5.6 Experimental Results . . . 124
5.7 2-Person Game Formulation for Coexistence of PUs and SUs . . . 128
5.8 Conclusion . . . 131

6 Priority-based Spectrum Allocation for Cognitive Radio Networks Employing NC-OFDM Transmission 133
6.1 Introduction . . . 133
6.2 System Model . . . 135
6.2.1 Wireless Multicarrier Transmission Format . . . 137
6.3 Proposed Priority-based Spectrum Allocation Techniques . . . 138
6.3.1 First Available First Allocate (FAFA) Spectrum Allocation Approach 139
6.3.2 Best Available Selective Allocate (BASA) Spectrum Allocation Approach . . . 140
6.3.3 Best Available Multiple Allocate (BAMA) Spectrum Allocation Approach . . . 143
6.4 Simulation Results . . . 144
6.4.1 Computation of Priority Metrics from Real-time Measurements . . . 145
6.4.2 Comparative Analysis of Proposed Algorithms . . . 146
6.5 Conclusion . . . 153

7 Cross-layer Architecture for Joint Power and Link Allocation 154
7.1 Introduction . . . 154
7.2 Related Work . . . 156
7.3 The ROPAS Architecture . . . 158
7.3.1 Rake Optimization Module . . . 162
7.3.2 Interference Measurement (IM) . . . 166
7.3.3 Channel Estimation Block (CEB) . . . 167
7.3.4 Channel Scanner . . . 168

7.3.5 Power Aware Scheduling 168
7.4 Priority Based Scheduling 171
7.5 Simulation Results 173
7.5.1 Multi-objective Rake Optimization 174
7.5.2 Power Aware Scheduling in ROPAS 176
7.5.3 Priority based Joint link and Power Scheduling 177
7.6 Conclusion 178

8 Conclusions and Future Work **180**
8.0.1 Future Work 182

Bibliography **188**

List of Figures

1.1 Advancement of technology and signal processing leading towards re-configurable SDRs. 3
1.2 Evolution of Software Defined Radio. 4
1.3 Technological evolution from SDR to AI-SR. 5
1.4 Various functionalities of a CR. 7

2.1 Snapshot of spectrum utilization (700-800 MHz) over an 18 hour period in Hoboken, New Jersey [4]. The shaded regions indicate primary user access while the *white spaces* imply no primary user activity. 12
2.2 Measured power spectrum obtained in the paging band (928-968 MHz). The measurement setup was located at Global Positioning System (GPS) latitude $42^{\circ}16'24.94''$ N and longitude $71^{\circ}48'35.29''$ W. During the measurement campaign, 500 scans or sweeps were conducted between 3:31 - 4:30 PM with frequency resolution of 20 KHz. 16
2.3 Measured power spectrum obtained in the paging band (928-968 MHz). The measurement setup was located at Global Positioning System (GPS) latitude $42^{\circ}16'24.94''$ N and longitude $71^{\circ}48'35.29''$ W. During the measurement campaign, 1500 scans or sweeps were conducted between 3:31 - 7:30 PM with frequency resolution of 5 KHz. 17
2.4 Queuing model representation of sub-band utilization by the BS. 22
2.5 Probability of time (wait and service) for the SUs with varying idle durations. The average service time for each SU is assumed to be 2 s and arrival rate of SUs into the queue is assumed to be 0.25. 25
2.6 Probability of waiting time in the queue for the SUs with varying idle durations. The average service time for each SU is assumed to be 2 s and arrival rate of SUs into the queue is assumed to be 0.25. 25
2.7 Comparison of CCDF plot against percentage ON time between model output and real-time measurements with threshold set to $(\mu + \sigma)$ and $(\mu + 3\sigma)$. CCDF plot against percentage ON time over 250 time sweeps. The training of our model is performed on the first 250 time sweeps. 27

2.8 Comparison of CCDF plot against percentage ON time between model output and real-time measurements with threshold set to $(\mu + \sigma)$ and $(\mu + 3\sigma)$. CCDF plot against percentage ON time over 500 time sweeps. The training of our model is performed on the first 1000 time sweeps. 28
2.9 Comparison of CCDF plot against percentage ON time between model output and USRP measurements with threshold set to $(\mu + \sigma)$ and $(\mu + 3\sigma)$. . . 29
2.10 Percentage of bandwidth occupied over 250 time sweeps. The variation in bandwidth occupancy is studied using threshold values $(\mu + \sigma)$. This comparison is performed using the real-time measurements. 30
2.11 Percentage of bandwidth occupied over 250 time sweeps. The variation in bandwidth occupancy is studied using threshold values $(\mu + 3\sigma)$. This comparison is performed using the real-time measurements. 30
2.12 Variation in total bandwidth occupied over the period of our experiment conducted for threshold values ranging from $\mu+\sigma$ to $\mu+10\sigma$ with n varying between 1 and 10 with step size of 0.5. 31

3.1 Spectrum utilization (446-740 MHz) by television broadcasting in Cincinnati, Ohio, USA 34
3.2 Spectrum occupancy of N sub-bands by primary users at time instant t . . . 40
3.3 Configuration of probabilities in a spectrum of (a) 16 sub-bands and (b) 30 sub-bands 41
3.4 Types of free sub-bands: (a) Type I, (b) Type II, (c) Type III, (d) Type IV, and (e) Type V 51
3.5 $(m + 1)$-spectrum derived from m-spectrum for Type I sub-bands 53
3.6 Exact distribution of N_{free} and its normal and Poisson-normal approximations for 16 sub-bands with 1 small and 6 large sub-band free probabilities . 64
3.7 Exact distribution of N_{free} and its normal and Poisson-normal approximations for 30 sub-bands with (a) 5 small and 5 large sub-band free probabilities and (b) 2 small and 16 large sub-band free probabilities 65
3.8 Comparison of probability distributions of N_{free} and $X_i(N)$, $i = I, II, III$ in a spectrum of 16 sub-bands 68
3.9 Comparison of probability distributions of N_{free} and $X_i(N)$, $i = I, II, III$ in a spectrum of 30 sub-bands with 5 small and 5 large sub-band free probabilities 69
3.10 Comparison of probability distributions of N_{free} and $X_i(N)$, $i = I, II, III$ in a spectrum of 30 sub-bands with 2 small and 16 large sub-band free probabilities 69

4.1 The system model implemented for enhanced spectrum sensing. 77
4.2 Power measurements obtained from paging bands over 500 time periods. . . 79
4.3 Estimation accuracy of our Markov chain model over paging bands for 99 observation periods performed over 1000 iterations. 81
4.4 Hidden Markov model representation in spectrum sensing 82

4.5 Expectation-maximization algorithm for estimating parameter values 91
4.6 Frequency distribution of prediction accuracy percentage of the Viterbi algorithm with mis-detection probability (Pmd) $\delta = 0.05$ and false alarm probability (Pfa) ϵ specified in the inset of each histogram (Case I, Scenario 1) 93
4.7 Frequency distribution of prediction accuracy percentage of the Viterbi algorithm with $\epsilon = 0.05$ and δ specified in the inset of each histogram (Case I, Scenario 2) 94
4.8 Frequency distribution of prediction accuracy percentage of the Viterbi algorithm with $\epsilon = 0.05$ and δ specified in the inset of each histogram (Case II, Scenario 2) 94
4.9 Frequency distribution of prediction accuracy percentage of the Viterbi algorithm with $\epsilon = 0.05$ and δ specified in the inset of each histogram (Case III, Scenario 2) 95
4.10 Normal approximation of the Viterbi algorithm for Case I with $\delta = 0.05$ and ϵ specified in the inset 96
4.11 Normal approximation of the Viterbi algorithm for Case I with $\epsilon = 0.05$ and δ specified in the inset 96

5.1 Distribution of PUs and SUs in one particular cell 103
5.2 Type classifications of various configurations of free channels 110
5.3 Free channel configurations for (a) SU_1 and (b) SU_2 115
5.4 Transmission power variation over 10 frequency slots, i.e., 928.8 MHz to 929 MHz. 125
5.5 Transmission power variation over 10 frequency slots, i.e., 929 MHz to 929.20 MHz. 125
5.6 Idle durations over 10 consecutive idle intervals in both paging bands, i.e., 928.8 MHz to 929 MHz and 929 MHz to 929.20 MHz. 126
5.7 Quality of channels over sweeps 80 to 100 based on their neighboring channels considered for both paging bands, i.e., 928.8 MHz to 929 MHz and 929 MHz to 929.20 MHz. 127
5.8 SNR computations based on our reward function defined in Eq. 5.17 for both paging bands, i.e., 928.8 MHz to 929 MHz and 929 MHz to 929.20 MHz. 128
5.9 SNR computations for SU 1 and SU 2 based on their utility functions defined in Eq. 5.24 for paging bands 929 MHz to 929.20 MHz. 129

6.1 Schematic diagram of the system model used for proposed priority scheduling techniques among SUs. 136
6.2 Flow diagram of the proposed FAFA approach. 139
6.3 Flow diagram of the proposed BASA approach. 140
6.4 Flow diagram of the proposed BAMA approach. 142

6.5 Proportion of active sub-carriers for NC-OFDM for all sub-bands for ten time instants. 145
6.6 BER of all the sub-bands in the spectrum for all ten time instants of our simulation. 147
6.7 Comparison between FAFA, BASA and BAMA schemes for the number of un-allocated requests per time instant for increasing PU occupancy. 148
6.8 Comparison between FAFA, BASA and BAMA schemes for the number of un-allocated requests per time instant for increasing SU requests. 148
6.9 Aggregate bandwidth utilization in BASA, and BAMA schemes for varying number of SU requests. 150
6.10 Aggregate throughput achieved in BAMA scheme for varying number of SU requests. 151
6.11 labelInTOC 152

7.1 Cross-layer design of the ROPAS architecture 159
7.2 Pseudo code for the Rake multi-objective optimization 165
7.3 Channel assignment based on the “free” channels detected by the IM in the UWB (3.1-10.6 GHz) 167
7.4 Sub-band division into multiple frmaes in Power Aware Scheduling illustrated in UWB 169
7.5 (a) Values of Lagrange multiplier’s, $\lambda_i^{'}s$ for all 10 paths and (b) Strategic selection of propagation paths based on BER values by our optimization algorithm when path P1 is already selected 174
7.6 Strategic selection of paths for optimal BER 175
7.7 Reduction of BER with increase in iteration of path selection 176
7.8 Magnitude of power vectors allocated in each subframe with unit frame interval 177
7.9 Magnitude of power vectors allocated in each subframe with frame interval=2units 179
7.10 Power allocations for each application request in 6 time slots 179
7.11 Number of slots assigned per frame for varying values of BER 179

List of Tables

3.1 Notation . . . 39
3.2 Comparison between Normal approximation and exact distribution with $\epsilon(k)$ for 16 sub-bands . . . 41
3.3 Comparison between Normal approximation and exact distribution with $\epsilon(k)$ for 30 sub-bands . . . 42
3.4 Boundary conditions for Type I, II, and III sub-bands for $X_i(N)$ at N = 3 . . 52
3.5 Computational efficiency comparison among the exact distribution and its normal and Poisson-normal approximations . . . 66
3.6 Probability distribution of N_{free} and $X_i(N)$ depicted in Figure 3.9 . . . 68
3.7 Probability distribution of N_{free} and $X_i(N)$ depicted in Figure 3.10 . . . 68
3.8 $[Mean \pm r * SD]$ intervals and probability of intervals . . . 69
3.9 Probability distribution of N_{free} and $X_i(N)$ . . . 70
3.10 Binomial distribution of N_{free} and $X_i(N)$ . . . 71

4.1 Statistical parameters of Estimation . . . 80
4.2 Emission Probability for Spectrum Sensing . . . 90
4.3 Estimation accuracy for the EM algorithm . . . 98

5.1 Reward table to achieve Nash Equilibria . . . 118
5.2 Reward table to achieve Nash Equilibria with 10 strategies for $SU1$ and 6 for $SU2$ . . . 123
5.3 Reward table to achieve Nash Equilibria with 10 strategies for $SU1$ and remaining 3 for $SU2$ . . . 123
5.4 Pay-off table to achieve Nash Equilibria . . . 130

Abbreviations used

BER	Bit Error Rate
CCDF	Complementary Cumulative Distribution Function
CR	Cognitive Radio
CRN	Cognitive Radio Network
DSA	Dynamic Spectrum Access
HMM	Hidden Markov Model
IF	Intermediate Frequency
NC – OFDMA	Non – contiguous Orthogonal Frequency Division Multiple Access
PDF	Probability Density Function
PFA	Probability of False Alarm
PMD	Probability of Mis – detection
PU	Primary User
RF	Radio Frequency
ROPAS	Rake Optimization and Power Aware Scheduling
SDR	Software Defined Radio
SR	Software Radio
SU	Secondary User
USRP	Universal Software Radio Peripheral
UWB	Ultra Wideband

Chapter 1

Introduction

The generation of mobile communication started with the advent of Analog Mobile Phone System back in the 1980's. These first generation phones were based on the cellular communication (using macro cells) and analog cellular technology. It took another decade (around 1991) for the transition into the second generation which supports digital voice, messaging and data services using macro, micro and pico cellular concepts. By 2001, the third generation mobile devices hit the market with enhanced data communication services and for the first time started supporting both narrowband and wideband multimedia services.

With a rapid growth of wireless and mobile communication as well as wide acceptance of the third generation mobile communication and beyond, integration and intercommunication of existing and future networks is not a far-sighted envision. In recent years, different types of networks, like self-organizing ah hoc networks, wireless mesh networks, etc. have rapidly evolved and exhibited much prospects in the wireless networking arena. The ubiquitous, seamless access between second and third generation mobile communication, broadband wireless access schemes, as well as inter-operation among the self organizing networks encouraged the market to have a common terminal for different network entities. To support universal access along with user satisfaction in terms of content, quality of service (QoS), and cost, reconfigurable **software radio** (SR) [1]- [2], or its practical form, **software defined radio** (SDR) terminals are indispensable. The need for additional bandwidth for different wireless technologies has further increased the search for new spectrum

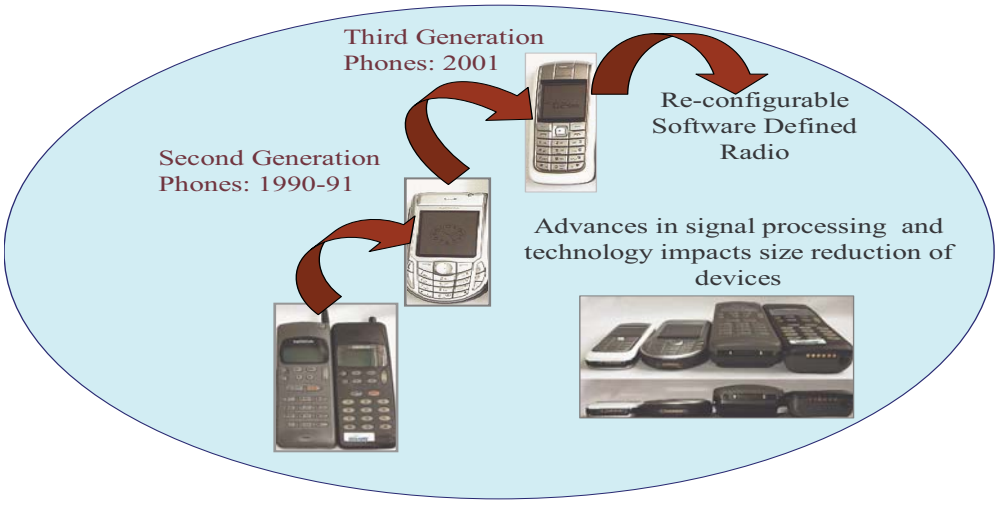

Figure 1.1: Advancement of technology and signal processing leading towards re-configurable SDRs.

and SDR is expected to provide a reasonable solution without any need to search for additional spectrum. The gradual transition from the first generation cellular communication to the advent of re-configurable terminals and base stations is depicted in Figure 1.1.

The central idea of implementing reconfigurable network and terminal equipments is to make international roaming services easy between different radio access networking standards, diversification of applications and provide flexibility in switching between appropriate radio access schemes. This intercommunication between multitude of networking standards leads to the so called *heterogeneous networks*.

Before discussing depth of research topics, a brief introduction about the evolution of SR from SDR is presented. Digital signal processing in any or all of the flexible functional blocks as shown in Figure 1.2 defines the characteristics of a radio. Some of the versions of the radios are defined for better appreciation of the evolution of SR from SDR based on Figure 1.2.

SDR: It is defined as a radio where the digitization is performed at the baseband stage, downstream from the receive antenna. This digitization is performed after the wideband filtering at the radio frequency (RF) section, low noise amplification and passband filtering at the intermediate frequency (IF) stage and down conversion of the signal to baseband

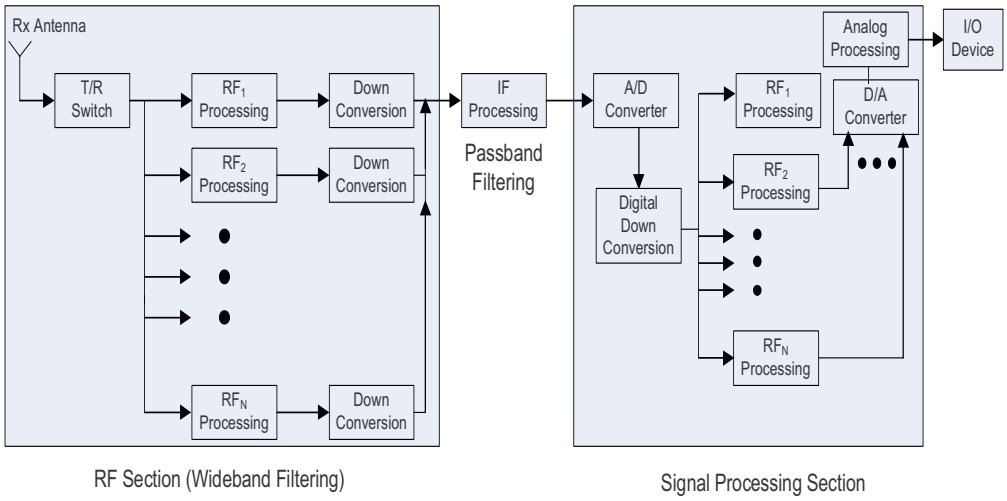

Figure 1.2: Evolution of Software Defined Radio.

frequency. The reverse operations are valid for the transmit digitization.

Digital radio: It is defined as a radio where digitization of signal is performed at any functional block between the antenna and the input/output (I/O) device as shown in Figure 1.2. A digital radio is not necessarily an SDR, if the signal processing after the A/D converter block is performed by a special purpose, application-specific integrated circuit (ASIC).

SR: It is defined as a modified version of SDR where the digitization of signal moves from the baseband processing section to the IF and RF sections. This transition is possible in future with the development of faster signal processors, memory chips as well as advancement in signal processing technology.

Adaptive Intelligent Software Radio (AI-SR) [1]- [2]: It is defined as a radio which is capable of all functionalities in a SR as well as can adapt to its operational environment for enhanced spectral efficiency and improved spectrum management.

The technological evolution of AI-SR from SDR is illustrated in Figure 1.3. As is evident, the transition from SDR to SR is possible with the advent of efficient signal processing techniques in conjunction with adept faster memory chips and signal processors technologies. This enables digitization of a radio to move from the baseband signal section all the way to IF and RF sections, making SR as a reality. Intelligent network algorithms

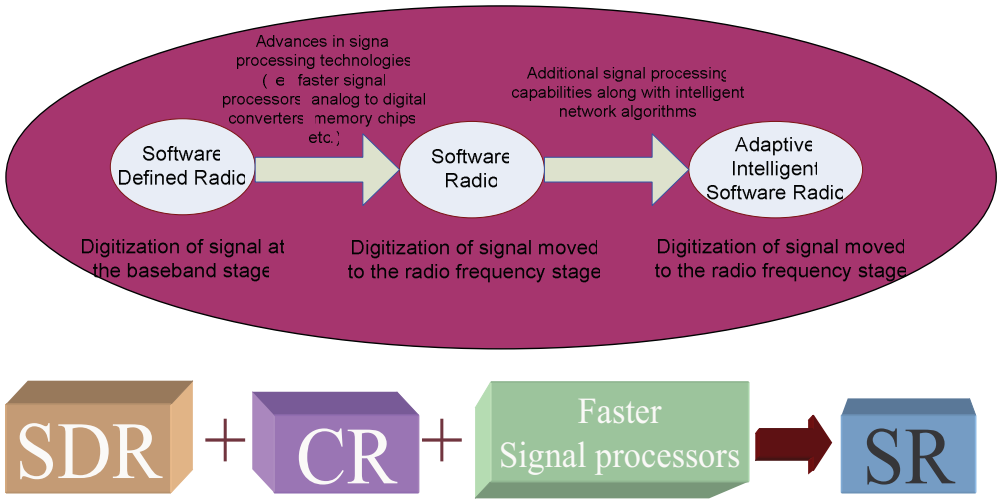

Figure 1.3: Technological evolution from SDR to AI-SR.

need to be plugged in for such possible transition from SR to AI-SR, which in turn will result in a higher spectral efficiency in a heterogeneous network environment.

The following are the two aspects of software functionality that may be incorporated into a radio:

- Software processing of the transmitted or received signal; and
- Software control which implies intelligent adaptation of radio parameters with respect to its environment.

Software signal processing is performed by a SDR since their operating frequencies and waveforms are controlled by using various software. Switching between modulations and protocols simply requires running different code by a special architecture called **Cognitive Radio** (CR) [3], [4]. Hence, a CR adds intelligence into an SDR. The term "intelligence" (also called intellect) is described in Wikipedia as "an umbrella term used to describe a property of the mind that encompasses many related abilities, such as the capacities to reason, to plan, to solve problems, to think abstractly, to comprehend ideas, to use language, and to learn. In some cases, intelligence may include traits such as creativity, personality, character, knowledge, or wisdom". In our context, we do not include the traits while referring to intelligent software control in a CR.

1.1 Motivation

Traditional research work in the domain of cognitive radio focuses on designing efficient and accurate spectrum sensing techniques as well as defining algorithms for better spectrum sharing of licensed spectrum among the SUs. Currently, there does not exist an accurate time-varying spectrum occupancy model for dynamic spectrum access (DSA) that could be used by wireless researchers in evaluating new algorithms and techniques designed. Chapter 2 primarily covers the representation of a spectrum occupancy model by probabilistic distribution functions. To validate this model, a qualitative analysis is made with respect to the real-time measurements obtained from the paging and television bands. These measurements are recently taken while conducting experiments at the Worcester Polytechnic Institute, MA. The innovative spectrum occupancy model accomplishes *spectrum occupancy analysis*, one of the important functions of CR as indicated in Figure 1.4.

A plethora of measurement data on spectrum occupancy is readily available while very little has been undertaken to exploit the information retrieved from these measurements in designing efficient spectrum sensing techniques. The probabilistic analysis carried out in Chapter 3 provides valuable qualitative and quantitative information about the spectrum occupancy. This information is useful in selecting an appropriate section of the spectrum before proceeding with spectrum sensing techniques. This procedure is proposed a term called *spectrum selection* in this dissertation. This is the second vital function of CR shown in Figure 1.4.

The *adaptive spectrum sensing* as one of the CR function shown in Figure 1.4 implies that the spectrum sensing is performed selectively using a-priori data information obtained from a reliable source. Existing spectrum sensing techniques primarily focus on reducing the persisting probability of mis-detection (PMD) and probability of false alarm (PFA). PMD is defined as the probability of failure in detecting an occupied sub-band and PFA is defined as the probability of detecting a section of a spectrum as occupied while is actually free. From the network layer perspective, a spectrum sensing technique should also be capable of retrieving the appropriate spectrum within minimum time duration. The word “appropriate” accommodates those sections of a spectrum which satisfies the number of requesting applications and their associated QoS. This leads to a time and spectral effi-

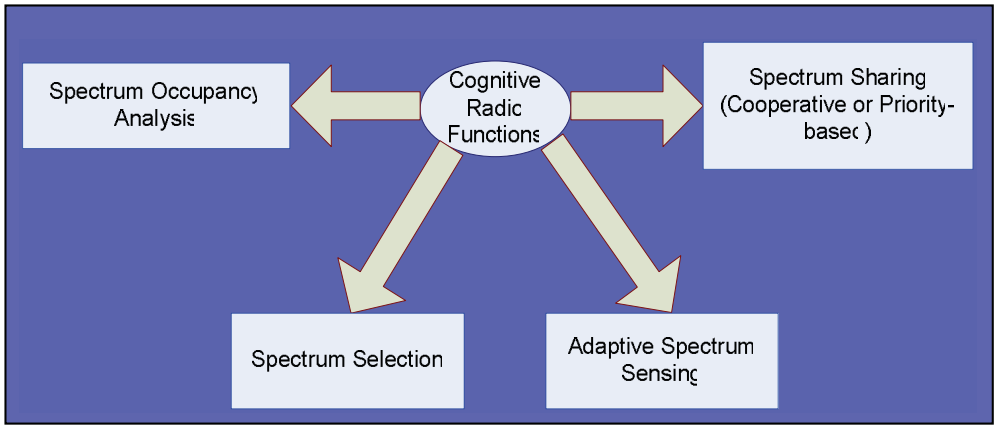

Figure 1.4: Various functionalities of a CR.

cient spectrum sensing. Existing research work assumes the prevalence of Markov chain in spectrum occupancy by licensed primary users. The work presented in this dissertation is essentially the first initiative in proving such an existence in Chapter 4. Real-time measurements in the paging band have been used in the process of validation. Later in the chapter, a time and spectral efficient sensing technique has been developed by using concepts from the Hidden Markov models.

Once the spectrum is sensed and idle sub-bands detected, the final function of a CR shown in Figure 1.4, is to allocate these sub-bands among the requesting unlicensed secondary users. This approach refers to *spectrum sharing*. The problem of spectrum allocation is dealt with in this dissertation in three different scenarios: (*i*) Cooperative communication is studied in CR networks while achieving maximum channel capacity using game theoretic and Nash equilibrium strategies in Chapter 5, (*ii*) Scheduling of sub-bands using a multiple access scheme namely, non-contiguous orthogonal frequency division multiple access (NC-OFDMA) in Chapter 6, and (*iii*) Cross-layer architectural design with multi-objective optimization of sub-band and power allocation in Chapter 7.

1.2 Organization of the Thesis

The rest of the thesis is organized into six chapters as follows:

1.2.1 Chapter 2: A Framework for Statistical Wireless Spectrum Occupancy Modeling

In this chapter, a novel spectrum occupancy model is designed in order to accurately generate both the temporal and frequency behavior of various wireless transmissions. Using statistical characteristics from actual radio frequency measurements, first- and second-order parameters are obtained and employed in a statistical spectrum occupancy model based on a combination of several different probability density functions (PDFs). In order to assess the accuracy of the model, output characteristics of proposed spectrum occupancy model are compared with actual radio frequency measurements.

1.2.2 Chapter 3: Probabilistic Approach to Spectrum Occupancy

In a cognitive radio network, sub-bands of a spectrum are shared by licensed (primary) and unlicensed (secondary) users in that preferential order. It is generally recognized that the spectral occupancy by primary users exhibit dynamic spatial and temporal properties and hence it is a fundamental issue to characterize the spectrum occupancy in terms of probability. With the sub-band free probabilities being available, an analytical model is proposed for spectrum occupancy in a cognitive network. To reduce the computational complexity of the actual distribution of total number of free sub-bands, we resort to efficient approximation techniques. Furthermore, we characterize free sub-bands into five different types, based on the occupancy of its adjacent sub-bands. The probability distribution of total number of each type of sub-bands is then determined. Two corresponding algorithms are effectively developed to compute different distributions and extensive simulation results show usefulness of the proposed probabilistic approach.

1.2.3 Chapter 4: Hidden Markov Model in Spectrum Sensing

Design of an efficient spectrum sensing scheme is a challenging task, especially when false alarms and mis-detections are present. The status of the sub-band is to be monitored over a sequence of consecutive time periods to determine if at any time point it is either free or busy. The status of the sub-band over time is proved to evolve randomly, following

a Markov chain. The cognitive radio assesses the sub-band, whether or not it is free, and the assessment is prone to errors. The errors are modeled probabilistically and the entire edifice is brought under a hidden Markov chain model in predicting the actual sub-band occupancy. Efficiency of our prediction method in identifying the true states of the sub-band is substantiated using simulations where Viterbi and Expectation Maximization algorithms are carried our for reducing the computational complexity.

1.2.4 Chapter 5: Game Theoretic Approach in Spectrum Sharing

In this chapter, we make a unique endeavor in computing channel capacity enhancement of licensed spectrum when the cognitive unlicensed users coexist with the licensed users using cooperative communication. We illustrate the probabilistic variations of idle durations, also called *white spaces*, and their dependence on the location of primary users. Then, we focus on the central idea of increasing the channel capacity by utilizing the white spaces for unlicensed users by allowing them to coexist within strict spectral power limits. We discuss strategies for allocating white spaces among the cognitive secondary users and seek to optimize the spectrum capacity. We introduce two cooperative N-person games among the N cognitive users in a Cognitive Radio Network (CRN) and then identify strategies that help achieve Nash equilibria. When licensed users arrive in any of those sub-bands currently being used by unlincensed users, they need to remove them out of the N-person game and assess their optional strategies with the licensed users using the 2-person game approach for coexistence.

1.2.5 Chapter 6: Priority-based Spectrum Allocation in Cognitive Radio Networks Employing NC-OFDM Transmission

In this chapter, we present three novel priority-based spectrum allocation techniques for enabling dynamic spectrum access (DSA) networks employing non-contiguous orthogonal frequency division multiplexing (NC-OFDM) transmission. The proposed techniques employs the novel results obtained from the spectrum occupancy statistics, illustrated in Chapter 2, in deciding the priorities for the spectrum allocations. Each sub-band in the tar-

get operating spectrum is prioritized based on its bit error rate (BER) support and number of unoccupied blocks. Our proposed techniques assign multiple blocks of these unoccupied wireless spectrum to secondary users by prioritizing based on their BER and delay requirements. Specifically, the proposed techniques assign blocks of spectrum possessing adequate aggregate bandwidth sufficient for supporting intended wireless data service over the communication link. Moreover, since several portions of the wireless spectrum may be heavily attenuated due to frequency-selective fading resulting from multipath propagation, communication links requiring high error robustness are assigned frequency bands located further away from these attenuated regions of spectrum. Consequently, the proposed spectrum allocation techniques aim at accommodating communication links supporting several different wireless services with dissimilar performance requirements.

1.2.6 Chapter 7: Cross-Layer Architecture for Joint Power and Link Optimization

The allocation of bandwidth to unlicensed users, without significantly increasing the interference on the existing licensed users, is a challenge for Ultra Wideband (UWB) networks. This chapter presents a novel Rake Optimization and Power Aware Scheduling (ROPAS) architecture for UWB networks. Since UWB communication is rich in multipath effects, a Rake receiver is used for path diversity. We develope an optimized Rake receiver by reducing the computation complexity in terms of the number of multiplications and additions needed for the weight assigned to each finger of the Rake receiver. Our work employs CR for dynamic channel allocation to requesting users while limiting the average transmit power in each sub-band. A dynamic channel allocation is achieved by a CR-based cross-layer design between the PHY and Medium Access Control (MAC) layers. Additionally, the maximum number of parallel transmissions within a frame interval is formulated as an optimization problem, based on distance between a transmitter-receiver pair, BER, and the frequency of request by a particular application. Moreover, the optimization problem improvises a differentiation technique by incorporating priority levels among requesting users. This provides fairness and higher throughput among services with varying power constraint and data rates required for a UWB network.

1.2.7 Chapter 8: Conclusions and Future Work

This chapter summarizes the salient features and achievements of the proposed schemes and algorithms and points out directions for future research.

Chapter 2

A Framework for Statistical Wireless Spectrum Occupancy Modeling

2.1 Introduction

With the advent of high bandwidth multimedia applications and the growing demand for ubiquitous information network access for mobile wireless devices, enhancing the efficiency of wireless spectrum utilization is essential for addressing the scarcity of available transmission bandwidth.

Results from spectrum occupancy measurement studies show that wireless spectrum is generally under-utilized in both the frequency and temporal domains [5]- [9]. Temporal and spatial variations of the usage by primary users (PUs) and opportunistic spectrum sharing

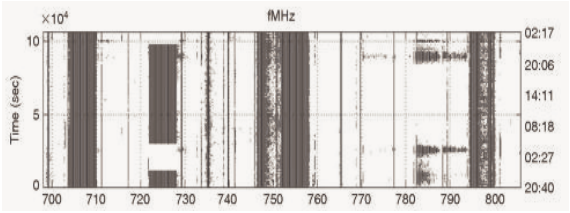

Figure 2.1: Snapshot of spectrum utilization (700-800 MHz) over an 18 hour period in Hoboken, New Jersey [4]. The shaded regions indicate primary user access while the *white spaces* imply no primary user activity.

is illustrated in Figure 2.1 which shows spectral usage of the 700-800 MHz bandwidth in Hoboken, New Jersey over a period of 18 hours (10:00 pm till 4:00 pm of the next day). As we can see from the figure, bands 705-709 MHz, 722-728 MHz, 746-758 MHz and 795-800 MHz are used spontaneously over the duration of the experiment. Sparse use of the bands 735 MHz, around 770 MHz and 782-790 MHz can be noticed during certain duration of the experiment. A more interesting fact about the white spaces detected in bands 710-720 MHz, 742-746 MHz, 760-770 MHz and 778-782 MHz is that they are never utilized for the entire duration of the experiment. The vital role of CR comes into play in the detection of such white spaces and in the opportunistic allocation among requesting users in varying time and space depicted by the colored rectangular time slots in Figure 2.1. This in turn, increases the spectral efficiency and the channel capacity.

To alleviate the spectrum scarcity problem, Mitola [3] first presented the concept of a CR, which could employ SDR technology to perform a wide variety of advanced communications and networking functions, including the sensing of unoccupied frequency subbands (*i.e.*, channels) for usage via secondary wireless access. This operation, known as DSA, is designed to enhance the utilization of existing spectral resources.

The fundamental concept behind DSA [3], [4] is that the licensed and *secondary users* (SUs) are allowed to coexist in the same frequency spectrum. The PUs maintain exclusive rights to their licensed spectrum. The SUs are required to sense spectrum usage and opportunistically utilize unoccupied bands while simultaneously respecting the rights of the incumbent primary transmissions. To obtain an estimate about the spectrum utilization by the PUs, spectrum occupancy measurement campaigns have been conducted [5]- [9]. However, the infrastructure and equipment needed to collect this data can be prohibitively expensive and not accessible by the majority of the wireless research community.

Nevertheless, there is a need for an accurate time-varying spectrum occupancy model to assess new DSA approaches and algorithms. As variations in the spectrum occupancy is unique to specific frequency band, geographical location, and time periods, a method is required that combines these characteristics into a comprehensive model. In [10], a unique probabilistic analysis of the spectrum occupancy has been performed using both Poisson and Poisson-normal approximations. The Markov chain and semi-Markov chain representation of spectrum occupancy by Gibson *et al.* [11] and Geirhofer *et al.* [12] possess serious

limitations for those bands with incessant occupancy by the PUs, *e.g.*, the frequency hopping sequences employed in the cellular frequency bands. Conversely, Poisson process emulation of the spectrum utilization [13–15] can be regarded as a positive step for the design of an accurate spectrum occupancy model. This idea can be further enhanced by incorporating the following unique characteristics: *(i)* center frequency selection by each primary user in its licensed band, and *(ii)* bandwidth occupied by primary users during each of their transmission durations.

In this chapter, we propose a novel time-varying statistical model for spectrum occupancy that uses actual wireless frequency measurements. The fundamental difference between our proposed model with respect to existing work is the realistic emulation of PU's occupancy in different sub-bands. To the best of our knowledge, there exists no other technique that combines all these parameters into a single model. The attributes of our proposed spectrum occupancy model are as follows:

- Utilization and idle periods are governed by two independent Poisson processes, an approach similar to [13];
- Transmission power during an utilization period is emulated by a Gaussian distribution with mean and standard deviation computed from real time measurements; and
- An inference from the real-time measurements is that the PU selects a different center frequency in each of its utilization period. A uniform distribution, governed by the mean and standard deviation of the corresponding Gaussian distribution, is employed to select the operating frequency during each utilization period.

The rest of this chapter is organized as follows: Section 2.2 presents collection of actual data in the paging band. Section 2.3 discusses our proposed spectrum occupancy model. Section 2.4 presents the idea of M/M/1 queuing model representation of the spectrum occupancy. Section 2.5 develops our proposed occupancy model and validates it using the measurements obtained in Section 2.2. Finally, concluding remarks are made in Section 2.6.

2.2 Real-time Data Measurements

To validate our proposed spectrum occupancy model, we have collected real-time data from both the paging band in Worcester, MA, USA as well as actual transmissions generated by several Universal Software Radio Peripheral (USRP) transceivers within a controlled laboratory environment in the industrial, scientific, and medical band (2.4 - 2.5 GHz). The details of both the conducted experiments are provided in the following two subsections.

2.2.1 USRP Measurements

In the ISM band (2.4 - 2.5 GHz), the transmit power values are collected from two USRPs operating at a close proximity. The measurements have been performed at Wireless Innovation Laboratory, Worcester Polytechnic Institute (WPI). The experimental setup consisted of an Advanced Technical Materials 07-18-440-NF horn antenna with a frequency range of $0.7 - 18$ GHz, an Agilent CSA series $N1996A$ spectrum analyzer (100 kHz - 3 GHz) with a low-noise amplifier, and a laptop installed with the SQUIRREL (Spectrum Query Utility Interface for Real-time Radio Electromagnetics) software tool for facilitating the collection of real-time data.

SQUIRREL is a software package developed at WPI by the Wireless Innovation Laboratory that provides an efficient way of communicating with the spectrum analyzer via a simple graphical user interface. The graphical user interface accepts details such as the center frequency, the span around the center frequency and the resolution bandwidth. SQUIRREL communicates with the spectrum analyzer using TCL (Tool Command Language) over TCP/IP. After the "sweep" action is performed by the spectrum analyzer, the data points are returned to the GUI in a comma spaced value format. In its current format, the GUI and the server are written in JAVA and can be deployed on a variety of operating systems and computers.

The experimental setup is used to collect the transmit power from the USRPs. We employed two USRPs which generate two sine waves in the ISM band, which are assumed to simulate the characteristics of the PU's signals which appear in the licensed bands. The

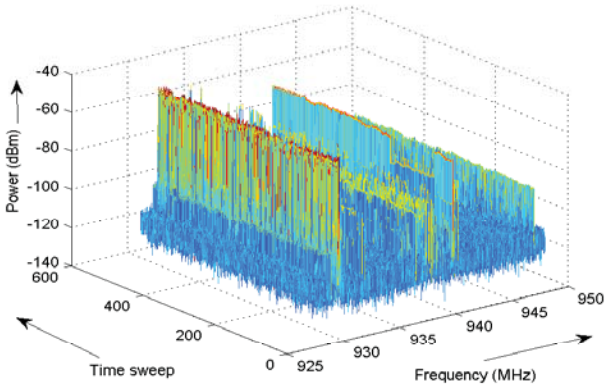

Figure 2.2: Measured power spectrum obtained in the paging band (928-968 MHz). The measurement setup was located at Global Positioning System (GPS) latitude $42°16'24.94''$ N and longitude $71°48'35.29''$ W. During the measurement campaign, 500 scans or sweeps were conducted between 3:31 - 4:30 PM with frequency resolution of 20 KHz.

center frequencies at which the sine waves are transmitted are 2.44 GHz and 2.46 GHz. The ON and OFF times of the licensed user signal transmission are set as uniform random variables.

2.2.2 Paging-band Measurements

In addition to using the data generated by the USRPs for validating our proposed model, we have also collected real-time data in the paging band (928-948 MHz). The measurement setup was located at the Global Positioning System latitude $42°16'24.94''$ N and longitude $71°48'35.29''$ W. During the measurement campaign, 500 scans or sweeps were conducted between 3:31 - 4:30 PM over the entire paging band. The frequency resolution was set to 20 KHz while the duration for each time sweep is 1.68 seconds. The power distribution over the entire paging band is shown in Figures 2.2 and 2.3. The received power spectrum obtained from our real time measurements in the paging band is shown in Figure 2.2. The x-axis represents the frequencies constituting the paging band, y-axis the time sweeps ranging from 1 to 500, and z-axis the received power (in dBm) measured at every instant of time. It is evident from Figure 2.2 that the noise floor is at around -110 dBm. Distinct primary user paging signal is identified near frequencies 929.5 MHz till 929.95 MHz, 937.4 MHz

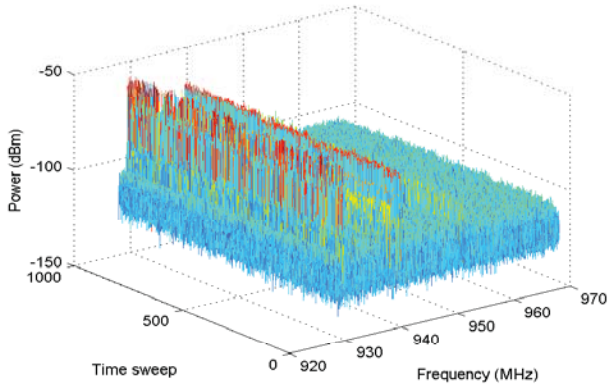

Figure 2.3: Measured power spectrum obtained in the paging band (928-968 MHz). The measurement setup was located at Global Positioning System (GPS) latitude $42°16'24.94''$ N and longitude $71°48'35.29''$ W. During the measurement campaign, 1500 scans or sweeps were conducted between 3:31 - 7:30 PM with frequency resolution of 5 KHz.

till 938.5 MHz, and 946.2 MHz. The maximum received signal power over the entire period of our experiment is recorded to be -45.6885 dBm. The minimum received signal power is -130.6880 dBm. Similar power spectrum values are also obtained from the USRP measurement set-up over 500 time sweeps. Further, for better statistical evaluation, a large sample space of power measurements were collected over the paging band 928-968 MHz for 1500 time sweeps and is shown in Figure 2.3.

2.3 Proposed Spectrum Occupancy Model

The spectrum occupancy by the PUs is known to possess dynamic temporal and spatial characteristics. In this chapter, we develop a novel spectrum occupancy model based on the real-time data from the measurement detailed in Section 2.2. In fact, the major contribution of our chapter lies in validating our proposed spectrum occupancy model in predicting the arrival rate of PUs in the operating spectrum. Our proposed model is significantly different from the previously mentioned Markov chain modeling of spectrum occupancy. In Markov chain modeling [11] - [12], the current state of spectrum occupancy is assumed to depend on its previous state. In our research, no such assumption is considered. Moreover, in our

paper, the assumption of Poisson distribution is on the arrival rates of PUs and the exponential distribution of idle durations. The advantage of our proposition is the flexibility of our approach over the Markov chain approach in such sections of the radio frequency spectrum where the property of Markov chain is not appropriate. The other advantage of our proposed model over the Markov chain assumption is with respect to memory constraints. Different sections of the spectrum may have varying transitional matrices and initial probabilities, unless steady-state probabilities have been defined. These parameters, defining the Markov chain, needs to be stored for efficient Markov chain estimation of spectrum occupancy. Such memory constraints are not essential for our spectrum occupancy model design.

2.3.1 Statistical Analysis of Spectrum Occupancy

Let the set of N sub-bands is represented by SB = $1, 2, \cdots, N$. At this point, we assume that each sub-band is licensed to one and only one PU. The utilization of the i^{th} licensed sub-band SB_i by the i^{th} PU is modeled as a Poisson process, with arrival rate λ_i, where $i = 1, 2, \cdots, N$. The entity λ_i, $i = 1, 2, \cdots, N$ is extracted from the real time measurements of Section 2.2. A single duration of utilization of the i^{th} sub-band by a PU is denoted by $t_{\text{ON}}(i)$. Similarly, an idle duration of the i^{th} sub-band is denoted by $t_{\text{OFF}}(i)$. If the number of utilization times for an SB_i is k with arrival rate λ_i, then the probability of having k utilization periods during the experiment conducted can be expressed as [16]:

$$f(k, \lambda_i) = \frac{\lambda_i^k e^{-\lambda_i}}{k!}, \; i = 1, 2, \cdots, N. \tag{2.1}$$

Hence, the duration between two utilization periods, *i.e.*, the inter-arrival rate of the i^{th} PU, $i = 1, 2, \cdots, N$, follows an exponential distribution. The probability density function of $t_{\text{OFF}}(i)$ for the i^{th} sub-band can be expressed as:

$$f(t_{\text{OFF}}(i); \lambda_i) = \begin{cases} \lambda_i e^{-\lambda_i t_{\text{OFF}}(i)}, & t_{\text{OFF}}(i) \geq 0 \\ 0, & t_{\text{OFF}}(i) < 0. \end{cases} \tag{2.2}$$

Similarly, the probability density function of $t_{\mathrm{ON}}(i)$ for the i^{th} sub-band can be expressed as:

$$f(t_{\mathrm{ON}}(i);\lambda_i) = \begin{cases} \lambda_i e^{-\lambda_i t_{\mathrm{ON}}(i)}, & t_{\mathrm{ON}}(i) \geq 0 \\ 0, & t_{\mathrm{ON}}(i) < 0. \end{cases} \tag{2.3}$$

The central idea of exploiting the Poisson and exponential distributions is to track the arrival rate of PUs for each sub-band, as well as their departure over the duration of the simulation. This can further assist SUs to perform spectrum sensing only on the detected ON times of the sub-bands and judiciously use the sub-bands during the OFF times. It is intuitive that higher values of OFF time enhances the chances of SUs using those sub-bands for longer duration of time. An additional feature has been incorporated in our simulation. Each time a PU arrives (*i.e.*, its ON time), it selects an operating frequency different from the frequency in its previous ON time.

Assuming that the power distribution of a PU in its sub-band follows a Gaussian distribution, the peak at which a transmission is detected gives us its operating frequency. Ideally, the operating frequency of a transmission in a sub-band is at the center of the band, *i.e.*, the mean operating frequency, with variance indicating the extent of the distribution.

The PDF of the operating frequency f_i is expressed as [16]:

$$f(f_i) = \frac{1}{\sqrt{2\pi\sigma_i^2}} e^{-\frac{(f-\mu_i)^2}{2\sigma_i^2}}. \tag{2.4}$$

In real time, it has been observed that the operating frequency f_i of an i^{th} PU transmission deviates from its ideal frequency for most of the times, though it ranges between its mean operating frequency μ_i and its variance σ_i^2 of its Gaussian distribution. Hence, in our model, the entity f_i for an i^{th} PU transmission is chosen from a uniform distribution governed by the values of μ_i and σ_i^2. Theoretically a PU can assume a frequency that is equally allowable within a band. Wireless spectrum measurements in the paging band indicate that PU frequency allocations are usually discretized on the number of frequencies allocated. Hence, the spectrum occupancy can be governed by an uniform distribution. The

probability density function for the i^{th} operating frequency f_i can be expressed as [16]:

$$f(f_i) = \begin{cases} \frac{1}{2\sqrt{\sigma_i^2}}, \text{ for } \mu_i - \sqrt{\sigma_i^2} \leq f_i \leq \mu_i + \sqrt{\sigma_i^2} \\ 0, \text{ otherwise.} \end{cases} \tag{2.5}$$

2.3.2 Proposed Spectrum Occupancy Model Implementation

The implementation of our spectrum occupancy model can be illustrated as follows. The basic input to our model are the statistical parameters extracted from our experiments conducted on the USRP measurement system. These parameters are namely, λ_i for the inter-arrival rate of each PU occupancy, $\lambda_i^{'}$ for the inter-arrival rate of the non-occupancy of PUs, the mean μ_i and the variance σ_i^2 of the i^{th} PU, $i = 1, 2, \cdots, N$. The output obtained from our model are the transmission times $t_{\text{ON}(i)}$ and $t_{\text{OFF}(i)}$, $i = 1, 2, \cdots, N$. Thus the inputs and outputs of the algorithm can be described in the following two steps.

1. Input: Set of $\lambda_1, \cdots, \lambda_N$, set of $\lambda_1^{'}, \cdots, \lambda_N^{'}$, $\mu_1, \cdots, \mu_N$, and $\sigma_1^2, \cdots, \sigma_N^2$.

2. Output: $t_{\text{ON}}(i)$, $t_{\text{OFF}}(i)$, $i = 1, 2, \cdots, N$.

Next, our model generates M (equal to 1000) PUs arriving into the spectrum, assuming that each PU is licensed to a distinct sub-band, different from other $(M - 1)$ PUs. This is to replicate the 1000 frequencies considered in our real-time measurements as well as the USRP measurements. We assume that each PU is licensed to a distinct sub-band, different from any other PU. The counters C_1 and C_2 keeps track of the overall simulation (validation) time and $t_{\text{ON}(i)}$, respectively. Also, the algorithm ensures that the model time does not exceed the validation time (herein taken to be 250 units, similar to the last 250 time sweeps under validation). Once the operating frequency f_i is selected using Eq. (2.5), the i^{th} PU starts with its transmission bursts for a time duration $t_{\text{ON}}(i)$, deduced from the exponential distribution with mean $\lambda_i^{'}$ as in Eq. (2.3), derived from the Poisson process of its OFF times. The vector $PU_{\text{transmit}}[\text{freq}_i, C_2]$ stores binary values with a "1" implying presence of a PU and a "0" its absence as in line 12 for the duration $t_{\text{ON}(i)}$. The vector $PU_{\text{transmit}}[\text{freq}_i, C_2]$ is assigned 1 to indicate occupancy of the i^{th} sub-band with the transmission burst time denoted by L. Finally, the counter C_1 is increased to $C_1 + C_2$ taking into account its transmission time. This is illustrated from Line 3 to Line 15. The "for" loop in Line 8 iterates

for the ON time duration.

3. Generate 1000 PUs at time t arriving in their respective sub-bands

4. for i = 1 to M do

5. Initialize counters C_1 and C_2 to 0

6. **while** $C_1 \leq 250$ **do**

7. Select the operating frequency freq_i using Eq. (2.5)

8. **for** $t_{\text{ON}}(i) = 1$ to L

9. **if** $C_1 + t_{\text{ON}}(i) < time$ **then**

10. $C_2 = C_1 + t_{\text{ON}}(i)$

11. i^{th} PU activates $t_{ON}(i)$, $i \in$ set of arrived PUs

12. $PU_{\text{transmit}}[\text{freq}_i, C_2] = 1$

13. **end if**

14. **end for**

15. $C_1 = C_1 + C_2$

Then, we define the idle times for each PU. This is critical as these slots of time are viewed as white spaces for opportunistic sharing by the SUs. The entity $t_{\text{OFF}}(i)$ is derived from Eq. (2.3) and Eq. (2.1) similar to that of $t_{\text{ON}}(i)$. The variable $t_{\text{OFF}}(i)$ is the time duration derived from the inter-arrival rate λ_i in Line 16. The variable $t_{\text{OFF}}(i)$ is the duration from the end of ON time C_1 till $(C_1 + t_{OFF})$. During the time duration C_1 to $t_{\text{OFF}}(i)$, the vector $PU_{\text{transmit}}[\text{freq}_i, C_2]$ is assigned 0 to imply the idle time in the i^{th} sub-band. During the time duration C_1 to $t_{\text{OFF}}(i)$, the vector $PU_{\text{transmit}}[\text{freq}_i, C_2]$ is assigned 0 to imply the idle time in the i^{th} sub-band. The counter C_1 is incremented by $t_{\text{OFF}(i)}$. This process is iterated until the end of the validation time. The model thus generates the $t_{\text{ON}}(i)$'s and $t_{\text{OFF}}(i)$'s during the entire validation time for i^{th} PU. At the end of this procedure, the spectrum occupancy model generates the $t_{\text{ON}}(i)$'s and $t_{\text{OFF}}(i)$'s for all users arrived during the validation time. This is summarized by Lines 16 to 22. The "for" loop in line 17 iterates only for the OFF time duration.

16. Generate $t_{\text{OFF}}(i)$ based on λ_i using Eq. (2.1) and exponential distribution using Eq. (2.3)

17. **for** $t_2 = C_1$ to $T_{\text{OFF}}(i)$ **do**

18. $PU_{\text{transmit}}[\text{freq}_i, t_2] = 0$

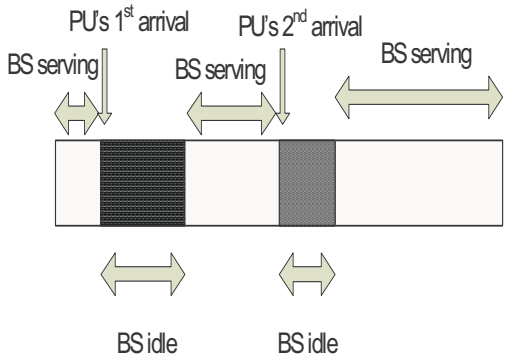

Figure 2.4: Queuing model representation of sub-band utilization by the BS.

19. $C_1 = C_1 + t_{\mathrm{OFF}}(i)$

20. end for

21. end while

22. end for

Hence, the model computes the $t_{\mathrm{ON}}(i)$ and $t_{\mathrm{OFF}}(i)$ for each i^{th} PU over the validation time of 250 units. The bandwidth utilization during a specific time unit over all 1000 frequencies or by a specific frequency over 250 time units are now computed using the output from our model. In the following section, we validate our model output with respect to the data collected from the paging band as well as the ISM band using the USRP transceivers.

2.4 M/M/1 Queuing Model Representation of Spectrum Occupancy

In an M/M/1 queuing model [17], the first *M* represents distribution of arrival processes, the second *M* represents the service time of each of the queued processes and 1 represents a single server. In this queuing model, arrival of processes are assumed to be Poisson distributed and service times to be exponentially distributed. The processes are arranged in a first-come-first-serve queue.

Utilization of a sub-band in the target spectrum by SUs can be modeled by an $M/M/1$ queue. The server in such a scenario is a centralized base station (BS), which maintains the

queue of arriving SUs and allocates idle durations in a sub-band to waiting SUs. The arrival of SUs into a queue is assumed to be Poisson distributed with arrival rate λ. The average service time T_s is the time required to serve an average SU. Hence, the BS utilization is $U_b = \lambda T_s$. Sub-band utilization by a PU and SUs in a sub-band is illustrated in Figure 2.4. As evident from the figure, the BS remains idle during the transmission durations by PUs in their corresponding sub-bands. Hence, $U_b = 0$ in the shaded sections of the sub-band in Figure 2.4. The queuing time T_q is expressed as:

$$T_q = T_i + \frac{T_s}{(1 - U_b)}, \tag{2.6}$$

where T_i is the average idle duration of the BS and is expressed as:

$$T_i = \frac{\sum_{j=0}^{N-1} e^{(\frac{1}{\lambda_{j_{OFF}}})}}{N}, \tag{2.7}$$

where N is the number of BS idle durations over a sub-band. One BS service duration is located in between two idle durations. The average service duration T_{avg} is expressed as:

$$T_{avg} = \frac{\sum_{j=0}^{M-1} e^{(\frac{1}{\lambda_{j_{ON}}})}}{M}, \tag{2.8}$$

where M is the number of BS busy durations. The number of SUs served during one busy duration is given by:

$$\begin{aligned} N_{SU} &= \frac{T_{avg}}{T_s}, \\ &= \frac{\sum_{j=0}^{M-1} e^{(\frac{1}{\lambda_{j_{ON}}})}}{MT_s}. \end{aligned} \tag{2.9}$$

The SUs wait in the queue behind the queued SUs. The waiting time depends on two reasons: (i) number of queued SUs waiting before the newly arrived SU and (ii) service time of the SU by the base station. The probability of the total time (waiting in the queue and being served by the BS) spent by an SU in the system is expressed as [17]:

$$\text{Prob(time in system} \leq t) = 1 - exp(-\frac{t}{T_q}) \tag{2.10}$$

On the other hand, it will be interesting to study the time spent by an SU waiting in the queue. The probability of the waiting time by an SU in a queue is expressed as [17]:

$$\text{Prob(wait time} \leq t) = 1 - U_b exp\left(-\frac{(1 - U_b)t}{T_q}\right) \tag{2.11}$$

2.4.1 Case Study Using Real Time Measurements

In this section, we show the usefulness of M/M/1 queuing model with respect to the real time measurements detailed in Section 2.2. We have arbitrarily chosen frequency 929.56 MHz for the illustration. In the context of PU transmission time or the BS idle time, we have used four distinct threshold values ($\mu + \sigma$, $\mu + 3\sigma$, $\mu + 6\sigma$, and $\mu + 10\sigma$) to obtain four average ON time duration as 4.55, 3.65, 2.13, and 1.16, respectively. The arrival of SUs into the queue is assumed to be a Poisson distribution with inter-arrival rate $\lambda = 0.25$. The average service time for each SU is assumed to be 2 seconds in accordance with the duration for each time sweep of 1.68 seconds.

We now compute the parameters described in the previous section for frequency 929.56 MHz with threshold set to $\mu + 3\sigma$. Using Eq. (2.6), the queuing time $T_q = 10.1320$ seconds. The arrival rate of the PUs λ_{ON} is 0.1440 while the arrival rate of idle durations λ_{OFF} is 0.1480. The average ON time duration T_i using Eq. (2.7) is 6.1320 seconds. Using Eq. (2.8), the average busy duration T_{avg} for a BS is 5.2214 seconds. During a T_{avg} of 5.2214 seconds, two SUs can be served.

The probability distribution of the total time in the system is evaluated using Eq. (2.10) and shown in Figure 2.5. The average ON time durations are varied using different threshold values for PU signal power detection. Higher the threshold value, lesser is the average ON time duration. As seen from Figure 2.5, with very high probability, an SU has to wait for substantial amount of time in the system before it can leave the system. Additionally, decreasing average ON time duration increases the chances of finding an SU, even with small waiting times.

The probability distribution of only waiting time in the system is studied using Eq. (2.11) and shown in Figure 2.6. In contrast to the distribution of total waiting time, SUs are found with very high probability even with low waiting times. Therefore, service time for each SU plays a vital role since its presence substantially decreases the probability as is shown in Figure 2.5.

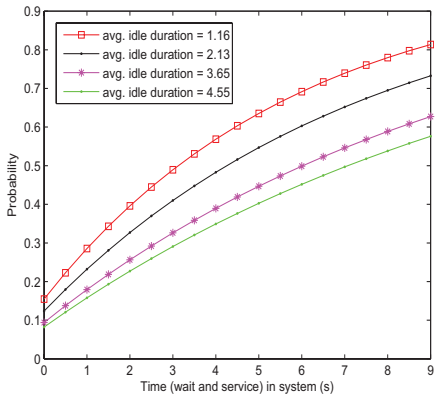

Figure 2.5: Probability of time (wait and service) for the SUs with varying idle durations. The average service time for each SU is assumed to be 2 s and arrival rate of SUs into the queue is assumed to be 0.25.

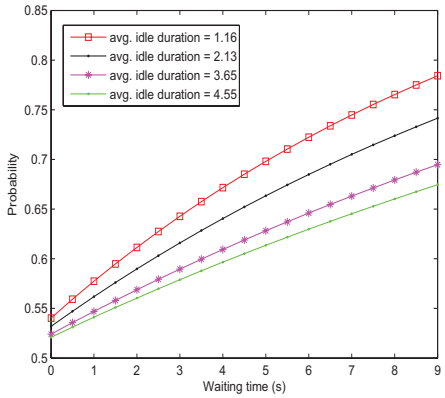

Figure 2.6: Probability of waiting time in the queue for the SUs with varying idle durations. The average service time for each SU is assumed to be 2 s and arrival rate of SUs into the queue is assumed to be 0.25.

2.5 Performance Evaluation

In this section, we validate our proposed spectrum occupancy model using the results obtained from the real-time measurements as well as the data from the USRP measurements.

A cross-validation approach is used to prove the efficacy of our proposed spectrum occupancy model. The validation is performed for two different threshold values required for signal detection namely, ($\mu + \sigma$) and ($\mu + 3\sigma$). In each time sweep, we observe that the received signal power over all the 1000 frequencies follows a Gaussian distribution with μ and σ, distinct from other time sweeps. This implies that the threshold is computed for every time sweep. During our spectrum measurements in the paging band, we have observed the band for 500 time sweeps. In such a scenario, we used the first 250 (half of the total time sweeps) to train our model and last 250 sweeps to validate our model based on the percentage of ON time (for time slice validation) and the percentage of bandwidth occupation (for frequency slice validation). The number "250" may not be substantial for statistical problems. Therefore, we have performed another extensive measurement campaign to collect signal power over 1500 time sweeps. Then, we use the first 1000 time sweeps to train our model and the previously collected 500 time sweeps to validate our model.

As explained in Section 2.3, the ON and OFF time durations for a single primary user are governed by two exponential random variables. In other words, the inter-arrival rate of ON times defines the mean value of the exponential random variable that defines an idle duration. Similarly, the inter-arrival rate of OFF times defines the mean value of the exponential random variable that defines an ON duration. The inter-arrival rates of ON and OFF times over the first 250 time sweeps are extracted from the real-time measurements. These values serve as the input to our model. We have addressed occupancy in time and frequency domains. In other words, the parameters of interest are temporal occupancy for fixed frequency (percentage ON time) and frequency occupancy for fixed time (percentage bandwidth occupied). Two cases of validation arise with respect to the last 250 time sweeps: (i) *time slice validation*: considering each frequency of bandwidth 20 KHz, compare the ON time, in percentage, between the real-time and model output and (ii)

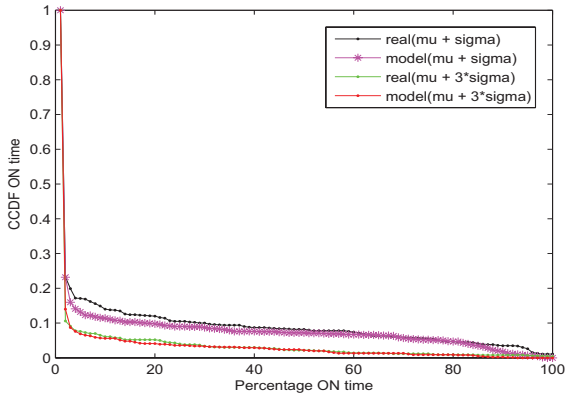

Figure 2.7: Comparison of CCDF plot against percentage ON time between model output and real-time measurements with threshold set to $(\mu + \sigma)$ and $(\mu + 3\sigma)$. CCDF plot against percentage ON time over 250 time sweeps. The training of our model is performed on the first 250 time sweeps.

frequency slice validation: considering each time sweep, compare the ON time, in percentage, between the real-time and model output. The following two sub-sections explain the validated results in details.

2.5.1 Time Slice Validation

As explained earlier, we consider an individual frequency of 20 KHz bandwidth and compute the percentage of ON time out of 250 time sweeps. Then we repeat the same process over all 1000 frequencies. We use the complementary cumulative distribution function (CCDF) metric to validate our model. In general, the CCDF metric indicates the number of times a random variable is above a given threshold. Figures 2.7, 2.8, and 2.9 compare the CCDF ON time given by our model with respect to that obtained from the real-time frequency measurements and USRP data, respectively. In Figure 2.7, the CCDF ON time decreases monotonically with increasing percentage of ON time. As shown in Figure 2.7, majority of the frequencies have ON time below 2% resulting in CCDF of 0.23 with threshold set to $(\mu + \sigma)$. With a threshold set to $(\mu + 3\sigma)$, the CCDF is 0.1 and 0.12 for real-time and model output, respectively. Another interesting point is that the CCDF ON times for a threshold set to $(\mu + 3\sigma)$ are lower than that for threshold set to $(\mu + \sigma)$. This implies that

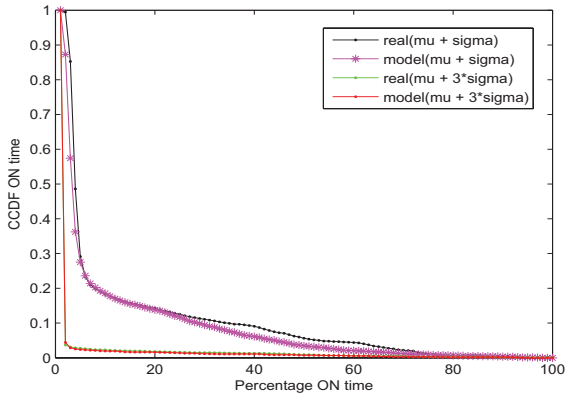

Figure 2.8: Comparison of CCDF plot against percentage ON time between model output and real-time measurements with threshold set to $(\mu + \sigma)$ and $(\mu + 3\sigma)$. CCDF plot against percentage ON time over 500 time sweeps. The training of our model is performed on the first 1000 time sweeps.

the threshold plays a critical role in signal detection where a low threshold may detect even some thermal noise as a PU signal. The model output is observed to closely follow the results obtained from the real-time measurements. This proves the efficacy of our spectrum occupancy model design. For better statistical evaluation, we have validated our model output over a sample space of 1500 time sweeps. Here, we have trained our model using the measurements from the first 1000 time sweeps. Then, we validated our model using the measurements from the last 500 time sweeps. The CCDF plots for both the thresholds are shown in Figure 2.8.

Similar CCDF plots are also obtained in Figure 2.9 using the data collected from our USRP measurement set-up using two different threshold values. For the threshold set to $(\mu + \sigma)$, a staircase plot is observed with step size of 20%. With the threshold set to $(\mu + 3\sigma)$, minimal signal power is detected above 2%. Comparing Figures 2.7, 2.8, and 2.9, it can be concluded that with threshold set to $(\mu + \sigma)$, there is a high probability of getting considerable received signal energy in the ISM band, even with increasing percentage ON time when compared to real-time measurements in the paging band. On the contrary, there is a sharp decrease in the probability of received signal energy in the ISM band when threshold value is increased to $(\mu + 3\sigma)$. Therefore, the choice of the threshold value plays

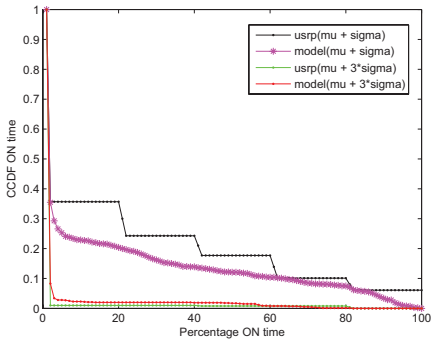

Figure 2.9: Comparison of CCDF plot against percentage ON time between model output and USRP measurements with threshold set to $(\mu + \sigma)$ and $(\mu + 3\sigma)$.

a critical role in the ISM band as compared to the paging band.

As shown in Figure 2.9, the results from the real-time measurements does not converge that much for threshold value set to $(\mu + \sigma)$, but matches quite well for $(\mu + 3\sigma)$. Our proposed model will not suit well for spread spectrum type signals where modulation schemes perform below noise floor. However, our model is useful for spectra used for television broadcasting, FM, and wireless Local Area Networks (LAN).

2.5.2 Frequency Slice Validation

In frequency slice validation, we consider an individual time sweep and compute the percentage of frequencies out of 1000 of them are ON at that sweep. This value provides us with the percentage bandwidth occupied for that time sweep. Similarly, the same process is carried over all the 250 time sweeps. The validation is performed for two different threshold values required for signal detection. Figures 2.10 and 2.10 give the scatter plot of percentage bandwidth occupied for both our model output and the real-time measurements. To better estimate the efficacy of our model design, we use "*line of best fit*" (LBF). We have used the curve fitting tool in MATLAB to generate the LBF in each case. The linear model polynomial is used for the LBF and is mathematically expressed as:

$$f(x) = p_1 x + p_2, \tag{2.12}$$

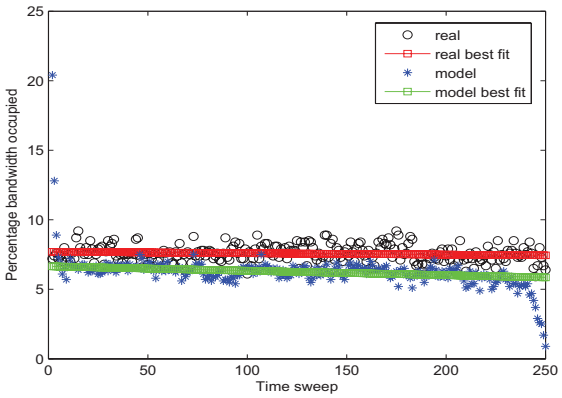

Figure 2.10: Percentage of bandwidth occupied over 250 time sweeps. The variation in bandwidth occupancy is studied using threshold values ($\mu + \sigma$). This comparison is performed using the real-time measurements.

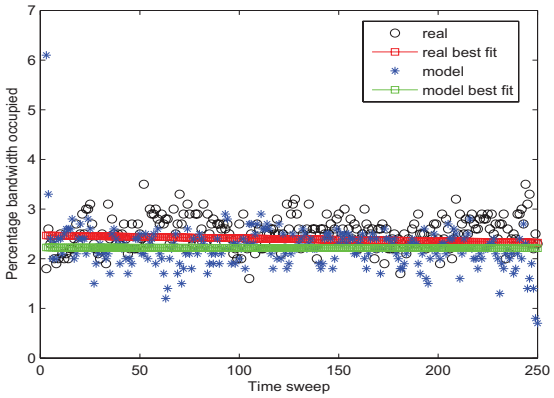

Figure 2.11: Percentage of bandwidth occupied over 250 time sweeps. The variation in bandwidth occupancy is studied using threshold values ($\mu + 3\sigma$). This comparison is performed using the real-time measurements.

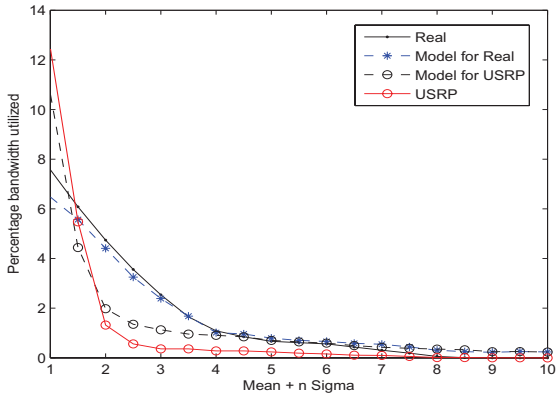

Figure 2.12: Variation in total bandwidth occupied over the period of our experiment conducted for threshold values ranging from $\mu + \sigma$ to $\mu + 10\sigma$ with n varying between 1 and 10 with step size of 0.5.

where p_1 and p_2 are the coefficients with 95% confidence bounds. In Figure 2.10, the coefficients for the real-time measurements are computed to be $p_1 = -0.00102$ and $p_2 = 7.699$. Similarly, the coefficients for our model are $p_1 = -0.003197$ and $p_2 = 6.654$. For Figure 2.11, coefficients for the real-time measurements are $p_1 = -0.0005798$ and $p_2 = 2.47$ while that for our model are $p_1 = -0.00006259$ and $p_2 = 2.227$. As noted from Figure 2.10, our model output deviates from the real-time measurements when the threshold for signal detection is set to $(\mu + \sigma)$. On the contrary, in Figure 2.11, the LBF for our model overlaps considerably to the LBF obtained from the real-time measurements when the threshold is set to $(\mu + 3\sigma)$. Figure 2.12 has a critical connotation in the context of signal detection. In this figure, we study the variation in the percentage of bandwidth occupancy while increasing the threshold for signal detection. Higher threshold values reduce the chance of detecting thermal noise as PU's signal. On the contrary, for higher threshold values, weak signals are not detected. This may have a serious concern resulting in inadmissible interference on the PU. Therefore, at threshold vale set to $(\mu + 10\sigma)$, only strong primary user signals are detected, thereby resulting in a very low percentage of bandwidth occupancy over the entire paging band of 20 MHz. The bandwidth utilization decreases sharply with an increase in the threshold from $(\mu + \sigma)$ to $(\mu + 2\sigma)$ in case of USRP measurements when compared to the real-time measurements. The output from our proposed model follows

both the results obtained from the real-time and the USRP measurements. Once again, the efficiency of our model is justified.

As shown in Figure 2.12, higher threshold values decreases the proportion of activity in the paging band. In other words, percentage ON time and percentage of bandwidth occupied decreases with increasing value of 'n'. Interference metric can be a deciding parameter for an appropriate selection of 'n'. For higher sensitivity of PUs to interference, a smaller value of 'n' is advisable. For robust communications by PUs, higher values of 'n' are permissible. The sensed environment and equipment are also deciding factors in the selection of an appropriate value of 'n'.

2.6 Conclusion

We have proposed a novel spectrum occupancy model to accurately generate both the temporal and frequency behavior of various wireless transmissions. Using statistical characteristics from actual radio frequency measurements, the first and second-order parameters are obtained and employed in a statistical spectrum occupancy model based on a combination of several different probability density functions (PDFs). The output characteristics of the proposed spectrum occupancy model are compared with spectrum measurements obtained from the real-time frequency measurements in the paging band (928-948 MHz) as well as data collected from the USRP measurement set-up.

Acknowledgments

This work was generously supported by the National Science Foundation (NSF) via grant CNS-0754315, as well as the University Research Council (URC) Graduate Student Research Fellowship Program at the University of Cincinnati. The authors would also like to thank Mr. Alexander Camilo for developing the SQUIRREL software package, and Ms. Robyn Colopy, Mr. Michael Leferman, and Ms. Di Pu for implementing the USRP random wireless signal generator.

Chapter 3

Probabilistic Approach to Spectrum Occupancy

3.1 Introduction

Spectral occupancy in the 446 MHz - 740 MHz bandwidth licensed to different television broadcasting stations in Cincinnati, OH, USA are depicted in Figure 3.1. The abbreviations in Figure 3.1 stand for different television broadcasting stations. For example, the frequency band 446 - 452 MHz is designated to The Cincinnati Post (WCPO-TV). The spectrum utilization of the primary users is not uniform and provides different levels of opportunity to the SUs. Certain portions of the spectrum are found to be highly utilized (e.g., $\geq 75\%$) by PUs, while some other sections of the spectrum are scarcely used ($\leq 5\%$) or unused for a long period of time. For example, the band 446 MHz - 452 MHz is used by the television stations for 24 hours a day, except for a certain duration of time. In contrast, the band 506 MHz - 512 MHz has a request pending from "We're Block Communications Queen City (WBQC)", which offers a high potential for the SUs.

The occupancy of sub-bands exhibits dynamic spatial and temporal property due to randomness of access by the PUs. For example, the occupancy in a single sub-band at any time instant can be determined by SUs in a cooperative manner [20] - [22] as opposed to being determined individually by each user [23] - [26]. However, the instantaneous statistics of sub-band occupancy in the entire spectrum over time is very difficult to determine due to

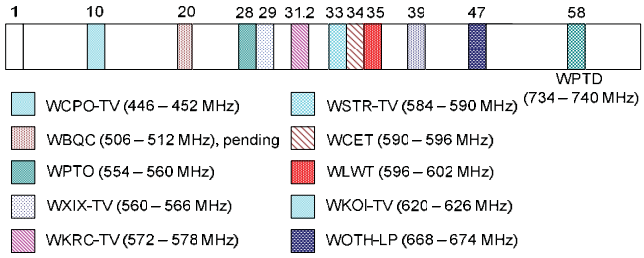

Figure 3.1: Spectrum utilization (446-740 MHz) by television broadcasting in Cincinnati, Ohio, USA

its time complexity. An instantaneous resource map is only available after the CRN has the knowledge of the utilization of every sub-band in the entire spectrum. For this purpose, the CRN has to instantly monitor and collect the spectrum occupancy data for all sub-bands all the time. Additionally, larger is the bandwidth monitored or scanned, higher will be the energy consumption for the SUs. McHenry *et al.* [5], [6] have monitored the spectrum occupancy for different sub-bands at Chicago as well as at Vienna, Virginia. The results show that the utilization of a sub-band can be small, moderate, or large, depending on the traffic load at a given time. However, the instantaneous resource maps in the entire spectrum are still not available due to complexity of monitoring all the sub-bands over time. Hence, instead of monitoring or sensing the entire spectrum, it is advisable to exploit the historical data [9] to select a set of preferable sub-bands for further sensing.

Instead of a direct map of occupancy, we analyze the sub-band occupancy in terms of the probability of capturing the dynamic spatial and temporal property. The probability of each sub-band being free, can be determined individually, without simultaneously monitoring all other sub-bands, thereby significantly reducing the complexity. In particular, the following two aspects are evaluated to reflect the sub-band availability for SUs:

- **Total number of free sub-bands** (N_{free}): At any given time instant, let N_{free} be the total number of sub-bands that are not used by the PUs. The entity N_{free} indicates how many SUs can simultaneously access the network. N_{free} also represents the probability that a SU can transmit packets, given the total number of SUs. Finally, the average and variance of N_{free} indicates spectrum utilization by PUs over a period of time.

- **Occupancy of a free sub-band's neighborhood**: Given a free sub-band, the information about adjacent sub-bands' occupancy is critical in mitigating interference to its adjacent PUs. If two neighboring sub-bands, i.e., $(i-1)^{st}$ and $(i+1)^{st}$ sub-bands of an i^{th} free sub-band, are occupied by PUs, the transmission power from the i-th sub-band interferes with both its adjacent neighbors. Hence, to reduce inadmissible interference, the transmission power in the i-th sub-band has to be restricted. If two networks have the same number of free sub-bands, the network with higher number of three contiguous free sub-bands can support a larger number of transmissions with high power if we ignore other factors that affect the transmission power.

By taking advantage of the probability of a sub-band being free, we provide a statistical estimation of N_{free} and of a free sub-band based on the occupancy of its immediate neighbors. The probability distribution of N_{free} allows selection of preferable sections of the spectrum for further sensing so that spectrum sensing is performed accordingly on those selective sub-bands with high probabilities of being free. The importance of our research is further emphasized by Wellens et al. [9], which stated that if the corresponding statistical analysis is available, the adaptive spectrum sensing could improve the probability of sensing by 70% over random spectrum sensing. In addition, given a free sub-band, knowledge of occupancy of the adjacent sub-bands can enable efficient power management [25] among requesting SUs. Thus, the allowable transmission power on a free sub-band can be adjusted based on the occupancy of its adjacent sub-bands. Furthermore, the prioritized allocation of sub-bands to SUs [27], [28] can be implemented in a way such that a high priority SU is allocated a sub-band with higher transmission power when compared to a low priority SU.

The traditional approach to estimate probability distribution of N_{free} is computationally complex. Therefore, we use approximation theory to compute the distribution of N_{free} by considering N_{free} as a sum of independent but not identically distributed Bernoulli random variables. The distribution of N_{free} is computed by using Poisson and normal approximations. In order to analyze the occupancy of the neighborhood of free sub-bands, we define five types of free sub-band (i.e., Type $I-V$ sub-band) in terms of the occupancy of its two adjacent sub-bands (having zero, one, or two free neighbors). To the best of our knowl-

edge, this is the first work on probabilistic analysis of spectrum occupancy [10]. The main contributions of this chapter are:

- Given the probability of a sub-band being free, we derive the probability distribution of N_{free} in any spectrum range.
- We derive the probability distribution of the total number of free bands of a specific type (i.e., Type $I-V$ sub-band). A probabilistic recurrence relationship is established to calculate probability distribution of the total number of these free bands types.
- The accuracy and efficiency of the proposed analytical models are verified by our simulation results.

The rest of this chapter is organized as follows. Section 3.2 discusses the related work. Section 3.3 illustrates the network model and formulates the problem. In Section 3.4, we present the analytical model for probability distribution of N_{free}. In Section 3.5, we characterize a free sub-band based on the occupancy of contiguous sub-bands. Section 3.6 discusses the implementation of algorithms and evaluates the accuracy and efficiency of our analytical models. Section 3.7 concludes the chapter.

3.2 Related Work

In a CRN, study of spectrum occupancy involves three critical aspects: spectrum measurement, spectrum sensing, and sub-band allocation. The first two aspects, in turn, facilitates the sub-band allocation for SUs.

The current research efforts mainly focus on spectrum sensing ([20] - [22], [27], and [29]) and sub-band allocation ([23] - [26] and [28]). For example, Ganesan *et al.* [21] proposed a cooperative spectrum sensing approach in a two-user cognitive network. This approach has been further improved for multi-user cognitive networks [22], enhancing the detection capability of cognitive radio users by exploiting the spatial diversity. Ganesan *et al.* [29] then discussed a spectrum sensing technique for a base station-controlled centralized cognitive network. It allows some cognitive users to act as relays for occupancy sensing of sub-bands while others transmit data in order to reduce average detection time.

For efficient spectrum sensing, Tu *et al.* [27] exploit physical layer attributes of PU transmissions like existence of cyclic prefix or fundamental symbol rate of signals.

Allocation of free sub-bands involves many issues such as routing, traffic, and power constraints. For example, based on spectrum stability, Deng *et al.* [24] present a method of selecting a set of sub-bands for a pre-determined path between a source and a destination. Demestichas *et al.* [25] describe a joint allocation of spectrum and radio access technologies using a learning and adaptation approach. The joint allocation models user requirements like traffic intensity, mobility characteristics, and quality of service guarantees. Wang *et al.* [26] discussed a graph theoretic approach for joint route and spectrum selection. A time schedule improves the channel usage to ensure quality of service guarantees among the real-time applications. Chu *et al.* [28] jointly optimize the power, time slots, and sub-carriers among the SUs in Orthogonal Frequency Division Multiple Access (OFDMA) cognitive radio systems.

Spectrum measurement is critical to assess spectrum occupancy in the network. McHenry *et al.* [5], [6] have experimentally monitored spectrum occupancy for different sub-bands at multiple locations. They deploy a high dynamic range spectrum measurement system for spectrum monitoring ranging from hours to days. Sanders *et al.* [7] use the Radio Spectrum Measurement System to collect observations periodically on sub-bands in the 108 MHz to 10 GHz spectrum providing a vast trove of occupancy data. Roberson *et al.* [8] use passive monitoring over the range of frequencies (30 MHz to 3 GHz) in order to categorize the degree of utilization of the sub-bands into four different classes: (i) sub-bands seldom used, (ii) sub-bands used during specific intervals of time, (iii) sub-bands infrequently used, and (iv) sub-bands heavily used.

In contrast to these spectrum measurement approaches, our target is to perform probabilistic analysis of sub-band occupancy. Luo *et al.* [23] assume an independent and identically distributed (i.i.d) model for the spectrum occupancy. This means that the occupancy of sub-bands are statistically independent with constant probability of occupancy over the entire spectrum. With this model, they developed some search strategies for the detection of a free sub-band based on an average search time. However, this model using a constant probability of occupancy does not reflect practical temporal and spatial variations in the spectrum. In our model, we keep independence assumption while occupancy probabilities

need not be constant for every sub-band. This model can be used to develop a searching strategy for free sub-bands in a practical way. In addition, the model and the attendant analysis can be utilized to define protocols for adaptive spectrum sensing [9], *i.e.*, selecting preferable sections of the spectrum for further sensing and allocation decisions.

3.3 System Model and Problem Formulation

In the following sub-sections, we describe the sub-band free probability model and discuss its computational complexity. We pursue a normal approximation and scrutinize the resultant approximation error.

3.3.1 Sub-band Free Probability Model

A cognitive radio divides an operational radio frequency spectrum into N non-overlapping sub-bands. The set of sub-bands is denoted by $Sub = \{1, 2, \ldots, N\}$ and we introduce a generic term *N-spectrum* for such a collection of sub-bands. In particular, the Federal Communications Commission (FCC) is currently considering 54 – 72 MHz, 76 – 88 MHz, 174 – 216 MHz, and 470 – 806 MHz spectra [30] for prospective spectrum sharing among the cognitive radio users. As a television transmission requires a bandwidth of 6 MHz, the above specified spectra effectively give a total of 68 sub-bands. Consequently, a typical value of N can be less than or equal to 68. The spectral occupancy of *N-spectrum* exhibits temporal and spatial characteristics. This means that if $A_t \subset Sub$ is the subset of sub-bands utilized at time instant t, the composition of A_t varies from one time instant to another. The term 'time instant' in the context of cognitive radio can also mean a specific duration of time. For example, Figure 3.2 shows the occupancy of N sub-bands at a given time t.

Let $\{x_1, x_2, \cdots, x_N\}$ be the set of N random variables, where $x_i = 0$ if i^{th} sub-band is occupied by a primary user and $x_i = 1$ if it is free, $i = 1, 2, \cdots, N$. For example, the fourth sub-band in Figure 3.2 is occupied and its status is expressed as $x_4 = 0$. Similarly, the status of the $(i + 5)^{th}$ sub-band in Figure 3.2 is depicted as $x_{(i+5)} = 1$. The occupancy of the i^{th} sub-band at any given time instant is characterized by the probability p_i of it being free, and hereafter referred to as the *sub-band free probability*. Note that for a period, $p_i =$

Table 3.1: Notation

N	Number of sub-bands in operating spectrum
Sub	Set of sub-bands
x_i	Binary random variable to indicate occupancy of i^{th} sub-band
p_i	i^{th} sub-band free probability
A_t	Subset of sub-bands occupied at time instant t
A	Subset of free sub-bands in Sub
N_{free}	Total number of free sub-bands
$Pr(N_{free} = k)$	Exact probability of having k free sub-bands
$\epsilon(k)$	Approximation error
ϵ	Overall approximation error
X	Any discrete random variable
$\mathcal{S}_X$	Essential support of X
θ	Decision threshold of $\mathcal{S}_X$
$Pr_{Normal}(N_{free} = k)$	Probability of $N_{free} = k$ using normal approximation
$\overline{N}_{free}$	Mean of the normal approximation
C_N	Variance of the normal approximation
P_{th1}	Threshold for segregating sub-bands with small p_i's
P_{th2}	Threshold for segregating sub-bands with large p_i's
Sub_{small}	Set of sub-bands with $0 < p_i \leq P_{th1}$
m	Size of Sub_{small}
$N_{free_{small}}$	Number of free sub-bands in Sub_{small}
Sub_{mod}	Set of sub-bands with $P_{th1} < p_i < P_{th2}$
n	Size of Sub_{mod}
$N_{free_{mod}}$	Number of free sub-bands in Sub_{mod}
Sub_{large}	Set of sub-bands with $p_i \geq P_{th2}$
$N_{free_{large}}$	Number of free sub-bands in Sub_{large}
λ_s	Mean value of Poisson approximation of $N_{free_{small}}$
Z	Random variable with Poisson distribution
X_i	i^{th} Bernoulli random variable with p_i
S	Sum of all X_i
λ_l	Mean value of Poisson approximation of $N_{free_{large}}$
$Pr_{Poi-Normal}(N_{free} = k)$	Poisson-normal approximated probability of $N_{free} = k$
$X_i(N)$	Random variable for total number of Type i sub-bands

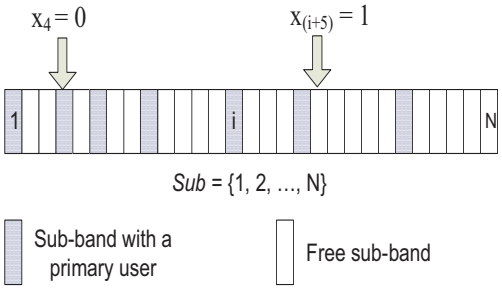

Figure 3.2: Spectrum occupancy of N sub-bands by primary users at time instant t

$Pr(x_i = 1)$, which can be determined empirically by observing each sub-band in a spectrum (for example as in [5] - [6] and [7] - [8]) at the same time instant. In the entire spectrum, the sub-band occupancy is statistically independent, i.e., the arrival of a primary user in one sub-band does not depend on the arrival of another primary user in any other sub-band at the same time instant. Therefore, x_i's are modeled as independent Bernoulli random variables. However, variables $x_1, x_2, \cdots, x_N$ are not necessarily identically distributed, i.e., $Pr(x_i = 1)$ and $Pr(x_j = 1)$ are not necessarily the same. We further define a random variable N_{free} to represent the total number of free sub-bands in the *N-spectrum*. In other words, N_{free} is the sum of all N random variables x_i's, i.e., $N_{free} = \sum_{i=1}^{N} x_i$. The possible values of N_{free} are $0, 1, \cdots, N$. Table 3.1 lists the most used notation whose meanings will be further explained when they appear for the first time.

3.3.2 Probability Distribution of N_{free}

We start with the simple case where all p_i's are equal to p. In this case, $x_1, x_2, \cdots, x_N$ are i.i.d. Bernoulli random variables with $Pr(x_i = 1) = p$. Then, $N_{free} = x_1 + x_2, \cdots + x_N \sim Binomial(N, p)$ with:

$$Pr(N_{free} = k) = \binom{N}{k} p^k (1-p)^{N-k}, \tag{3.1}$$

where $k = 0, 1, 2, \cdots, N$. Further, the mean is given by Np and the variance is $Np(1-p)$, where $(1-p) = Pr(x_i = 0)$.

The computation of the exact distribution of N_{free} becomes complex when p_i's are not equal. If we define the complexity as the total number of multiplications and additions in

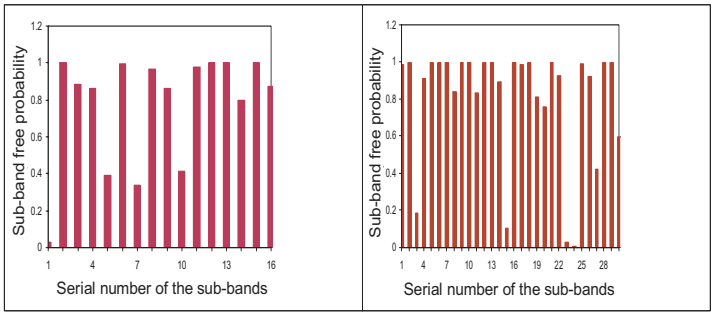

(a) (b)

Figure 3.3: Configuration of probabilities in a spectrum of (a) 16 sub-bands and (b) 30 sub-bands

Table 3.2: Comparison between Normal approximation and exact distribution with $\epsilon(k)$ for 16 sub-bands

	$N_{free} = k$							
	8	9	10	11	12	13	14	15
$Pr(N_{free} = k)$	0.0008	0.0079	0.0468	0.1617	0.311	0.3028	0.1417	0.0267
$Pr_{Normal}(N_{free} = k)$	0.0069	0.0483	0.1715	0.3109	0.2881	0.1365	0.0330	0.0040
$\epsilon(k)$	0.0061	0.0404	0.1247	0.1492	0.0229	0.1663	0.1087	0.0227

the computation, we have the following lemma.

Lemma 1 *When p_i's are not equal, the complexity involved in computing $Pr(N_{free} = k)$ in an N-spectrum is given by:*

$$\left[\binom{N}{k} \times N\right] - 1, \tag{3.2}$$

where $k = 0, 1, 2, \cdots, N$.

Proof: *Let A represent a generic symbol for any subset of* Sub *representing free sub-bands and $A^{'}$ its complement. Then,*

$$Pr(N_{free} = k) = \sum_{A} \left(\prod_{i \in A} p_i\right)\left(\prod_{j \in A'} (1 - p_j)\right). \tag{3.3}$$

The summation is taken over all subsets $A \subset$ Sub with cardinality of $A = k$. Each expression inside the summation symbol of Eq. (3.3) is a product of N terms and the summation

Table 3.3: Comparison between Normal approximation and exact distribution with $\epsilon(k)$ for 30 sub-bands

	$N_{free} = k$								
	19	20	21	22	23	24	25	26	27
$Pr(N_{free} = k)$	0.0004	0.0035	0.0199	0.0753	0.1876	0.2932	0.2664	0.1253	0.0262
$Pr_{Normal}(N_{free} = k)$	0.0023	0.0178	0.0784	0.1996	0.2928	0.2478	0.121	0.0341	0.0055
$\epsilon(k)$	0.0019	0.0143	0.0585	0.1243	0.1052	0.0454	0.1454	0.0912	0.0207

involves a total of $\binom{N}{k}$ *summands. Therefore, the computational complexity of Eq. (3.3) is given by* $\left(\binom{N}{k} \times N\right) - 1$. □

Lemma 1 illustrates that the computational complexity involved in the calculation of the probability of $N_{free} = k$ is extremely high. According to Lemma 1, the probability of getting exactly 15 free sub-bands $Pr(N_{free} = 15)$ in a 30-spectrum, for example, incurs $\binom{30}{15}$ $\simeq$ 155 *million* possible scenarios where 30 numbers need to be multiplied in each scenario. As indicated, a typical value of N can even surge up to 68. As a result, the humongous amount of computation becomes a memory constraint for the network. Furthermore, considering all probabilities of $N_{free} = k$, we have the following Corollary by using Lemma 1.

Corollary: The complexity involved in computing the distribution of N_{free} is given by:

$$\sum_{k=0}^{N} \left[\left(\binom{N}{k} \times N \right) - 1 \right] = 2^N \times N - (N + 1). \tag{3.4}$$

Eq. (3.4) represents the complexity in computing all probabilities of $N_{free} = k$, for $k = 0, 1, \ldots, N$. According to our tests, the time taken on a Pentium IV machine with Intel 3.2 GHz processor and 512 Megabyte RAM to compute the exact distribution of N_{free} with $N = 30$ is 2650.20 seconds.

3.3.3 Approximation with Normal Distribution

It is imperative to find an efficient way to significantly reduce the computational complexity in calculating the distribution of N_{free}. One such approach is to use the approxima-

tion theory as long as the accuracy could be maintained. We determine the error using the following definition.

Definition 3.1 (*Approximation error* $\epsilon(k)$): For any approximation, let $Pr_{app}(N_{free} = k)$ represent the approximate value of $Pr(N_{free} = k)$. For each $k = 0, 1, 2, \cdots, N$, let $\epsilon(k)$ be expressed as:

$$\epsilon(k) =\mid Pr(N_{free} = k) - Pr_{app}(N_{free} = k) \mid . \tag{3.5}$$

Let $\epsilon = max_{0\leq k\leq N}\, \epsilon(k)$ be the *over-all approximation error* under scrutiny. Eq. (3.5) indicates that a distribution of N_{free} with smaller ϵ provides a better approximation of the exact distribution.

For computational efficiency, we further define essential support of a probability distribution. We choose a number $0 < \theta < 1$, typically very small.

Definition 3.2 (*Essential support:* $\mathcal{S}_X$): Let X be a discrete random variable. The essential support, denoted by $\mathcal{S}_X$, is defined to be the set $\mathcal{S}_X = \{k; Pr(X = k) \geq \theta\}$.

The basic idea is to weed out events with a very small probability of occurrence and without significantly affecting the approximation. When comparing how close $Pr(N_{free} = k)$ and $Pr_{app}(N_{free} = k)$ are, there is no need to make a comparison when $Pr(N_{free} = k) < \theta$. $Pr(N_{free} = k) < \theta$ is very small if θ is small enough. With this provision, we redefine *over-all approximation error* to be

$$\epsilon = max_{k\in\mathcal{S}_{N_{free}}}\, \epsilon(k). \tag{3.6}$$

We evaluate the normal approximation over the N-spectrum. In the context of probability distributions, Central Limit Theorem [31] provides a way for approximating complicated distributions. Let $\overline{N}_{free} = \sum_{i=1}^{N} p_i$ be the mean and $C_N = Var(N_{free}) = \sum_{i=1}^{N} p_i(1-p_i)$ be the variance of N_{free}. If N and C_N are large, N_{free} can be approximated by $Normal(\overline{N}_{free}, C_N)$. Since N_{free} is a discrete random variable and the normal distribution is continuous, the approximation is

$$\begin{aligned} Pr(N_{free} = k) &\approx \int_{k-\frac{1}{2}}^{k+\frac{1}{2}} \frac{1}{\sqrt{2\pi C_N}}\, e^{-\left(\frac{\left(x-\overline{N}_{free}\right)^2}{2C_N}\right)} dx \\ &= Pr_{Normal}(N_{free} = k), \end{aligned} \tag{3.7}$$

where $k = 0, 1, \cdots, N$.

We test the normal approximation by observing its computational overhead and the approximation error. For this purpose, we have considered two typical spectra of 16-spectrum and 30-spectrum. For the spectrum with 16 sub-bands, the sub-band free probabilities p_i's are randomly generated from the $Beta(0.5, 0.2)$ distribution as shown in Figure 3.3(a). We illustrate *Beta* distributions in the simulation part (Section 3.4). The exact distribution of N_{free} is computed by using Eq. (3.3) and the normal approximation of N_{free} is computed using Eq. (3.7). We use $\theta = 0.0004$ and neglect $Pr(N_{free} = k) < 0.0004$. The exact probabilities, approximate probabilities, and approximation errors for each k in $\mathcal{S}_{N_{free}}$ are provided in Table 3.2. In summary, the essential support $\mathcal{S}_{N_{free}} = \{8, 9, \cdots, 15\}$ and the over-all approximation error ϵ is 0.1663 at $N_{free} = 13$. The computation time involved in the normal approximation is 1.11 seconds while using the same hardware configuration as in Section 3.3-B.

In the spectrum with 30 sub-bands, the probabilities p_i's are randomly generated from the $Beta(0.6, 0.1)$ distribution as shown in Figure 3.3(b). With $\theta = 0.0002$, the essential support $\mathcal{S}_{N_{free}} = \{19, 20, \cdots, 28\}$. The exact probabilities, approximate probabilities, and approximation errors for each k in $\mathcal{S}_{N_{free}}$ are provided in Table 3.3. The over-all approximation error ϵ is 0.1454 at $N_{free} = 25$. Computation time involved in the normal approximation is 1.14 seconds while using the same hardware configuration as in Section 3.3-B.

The experimental results show that the normal approximation is not acceptable in terms of its accuracy, although the computational time is far less. The approximation errors in both cases exhibit wide deviations between some exact probabilities and corresponding normal approximations. Accuracy of normal approximation depends on the following:

- Generally, the approximation provided by the Central Limit Theorem has a very high accuracy if all p_i's are equal or the variation among p_i's is very less.
- If p_i's vary widely, the approximation is good provided N and C_N are large.

But in our scenarios, variation among p_i's is large. Furthermore, N and C_N are not large enough to mitigate variations present in p_i's. To improve the accuracy, we propose a way of finding an approximate distribution of N_{free} by forging the Law of Rare Events, Very High Frequency Events, and Moderate Events. The proposed approximation method also achieves an enhanced efficiency in computing the distribution of N_{free}.

3.4 Probability Distribution of N_{free}

As has been pointed out in Section 3.3, computation of exact distribution of N_{free} is both complex and time-consuming. If the number of sub-bands is greater or equal to 45, it is impossible to calculate the exact distribution. An easy way out of this computational quagmire is to resort to normal approximation as discussed in Section 3.3 but the approximation is of dubious value and unacceptable margin of error. In this section, we present our approach to mitigate computational complexity by using the Poisson-normal approximation. As we discussed, p_i for a sub-band, can be small, moderate, or large. For this, we define a lower threshold P_{th1} and an upper threshold P_{th2}, which alternatively can be written as $0 < P_{th1} < P_{th2} < 1$. All p_i's within the range $0 < p_i \leq P_{th1}$ relate to sub-bands with small sub-band free probabilities. For p_i's $\geqslant P_{th2}$, sub-bands are classified into a group with large sub-band free probabilities. Otherwise, sub-bands within the range $P_{th1} < p_i < P_{th2}$ are categorized into a group with moderate sub-band free probabilities. With this, we have the following definitions.

Definition 3.3 (Sub_{small}): This is a set of all sub-bands having $0 < p_i \leq P_{th1}$. Let m be the size of Sub_{small} and $N_{free_{small}}$ be the number of free sub-bands in Sub_{small}.

Definition 3.4 (Sub_{mod}): This is a set of all sub-bands having $P_{th1} < p_i < P_{th2}$. Let n be the size of Sub_{mod} and $N_{free_{mod}}$ be the number of free sub-bands in Sub_{mod}.

Definition 3.5 (Sub_{large}): This is a set of all sub-bands having $p_i \geqslant P_{th2}$. The size of Sub_{large} is $(N - m - n)$. Let $N_{free_{large}}$ be the number of free sub-bands in Sub_{large}.

Note that P_{th1} is typically close to zero and P_{th2} is close to one. In order to find the distribution of N_{free}, we first compute the approximate distributions for each of $N_{free_{small}}$, $N_{free_{mod}}$, and $N_{free_{large}}$. Therefore, the distribution of N_{free} can be computed by using the relation:

$$N_{free} = N_{free_{small}} + N_{free_{mod}} + N_{free_{large}}. \tag{3.8}$$

3.4.1 Approximate Distribution of $N_{free_{small}}$

The distribution of $N_{free_{small}}$ can be approximated by a Poisson distribution and the probability that there are k free sub-bands is:

$$\begin{aligned} Pr(N_{free_{small}} = k) &\simeq \frac{{\lambda_s}^k e^{-\lambda_s}}{k!} \\ &= Pr_{Poi}(N_{free_{small}} = k), \end{aligned} \tag{3.9}$$

where $\lambda_s = \sum_{i \in Sub_{small}} p_i$. This approximation follows a so-called Law of Rare Events. We have the following lemma that gives an upper bound of the approximation error.

Lemma 2 *Let Z be a random variable that has a Poisson distribution with parameter λ_s. We have:*

$$\begin{aligned} \mid Pr(N_{free_{small}} = k) - Pr(Z = k) \mid &\leq \frac{1 - e^{-\lambda_s}}{\lambda_s} \times \sum_{i \in Sub_{small}} p_i^2 \\ k &= 0, 1, 2, \ldots . \end{aligned} \tag{3.10}$$

***Proof**: We apply the Law of Rare Events [32] in proving this. Suppose that $X_1, \ldots, X_s$ are independent Bernoulli random variables with success probabilities $p_1, \ldots, p_s$. If the p_i's are small and $\lambda = \sum_1^s p_i$ is moderate in size, then the Law of Rare Events asserts that the sum $S = \sum_1^s X_i$ is also approximately Poisson distributed. More precisely, if Z is a Poisson random variable with mean λ, then:*

$$\begin{aligned} \mid Pr(S = k) - Pr(Z = k) \mid &\leq \frac{1 - e^{-\lambda}}{\lambda} \times \sum_{i=1}^{s} p_i^2 \\ k &= 0, 1, 2, \ldots . \end{aligned} \tag{3.11}$$

In our context, $S = N_{free_{small}} = \sum_{i \in Sub_{small}} x_i$ and $\lambda = \lambda_s$. Therefore, Inequality (3.10) follows from Inequality (3.11). □

Lemma 2 shows that the upper bound of approximation error depends on the magnitude of $\sum_{i \in Sub_{small}} p_i$. Note that $\frac{1-e^{-\lambda}}{\lambda} \leq 1$. If p_i is very small, p_i^2 gets much smaller. For example, if $N = 10$, each $p_i \leq 0.03$, then $\sum_{i=1}^{10} p_i^2 \leq 0.009$. The exact probability $Pr(N_{free_{small}} = k)$ and Poisson probability $Pr(Z = k)$ should agree in the first two decimal places. We have observed that if sub-band free probabilities hover around 0.03, the approximation error is less than 0.001. Therefore, in our analysis, we have taken $P_{th1} = 0.03$ as the threshold value for small sub-band free probability.

3.4.2 Approximate Distribution of $N_{free_{mod}}$

The distribution of $N_{free_{mod}}$ in Sub_{mod} can be approximated by a normal distribution and the probability that there are k free sub-bands is:

$$\begin{aligned} Pr(N_{free_{mod}} = k) &\simeq \int_{k-\frac{1}{2}}^{k+\frac{1}{2}} \frac{1}{\sqrt{2\pi C_n}} e^{-\left(\frac{\left(x-\overline{N}_{mod}\right)^2}{2C_n}\right)} dx \\ &= Pr_{Normal}(N_{free_{mod}} = k), \end{aligned} \tag{3.12}$$

where n is the size of Sub_{mod}, $k = 0, 1, \cdots, n$, $\overline{N}_{mod} = E[N_{free_{mod}}] = \sum_{i \in Sub_{mod}} p_i$, and $C_n = \sum_{i \in Sub_{mod}} p_i(1 - p_i)$ represents the variance of $N_{free_{mod}}$.

The main difference between Eq. (3.12) and Eq. (3.7) is that the approximation of $N_{free_{mod}}$ in Sub_{mod} excludes those sub-bands having small or large probabilities of being free.

3.4.3 Approximate Distribution of $N_{free_{large}}$

The approximation of the distribution of $N_{free_{large}}$ follows essentially the path set by $N_{free_{small}}$. Note that $(1 - p_i)$ is small for $i \in Sub_{large}$. Using the Law of Rare Events, the distribution of $N_{free_{large}}$ can also be approximated by a Poisson distribution. The following lemma facilitates computation of $N_{free_{large}}$ probability distribution.

Lemma 3 *For $k = 0, 1, \cdots, (N - m - n)$, we have*

$$\begin{aligned} Pr(N_{free_{large}} = k) &\simeq \frac{e^{-\lambda_l} \lambda_l^{(N-m-n-k)}}{(N - m - n - k)!} \\ &= Pr_{Poi}(N_{free_{large}} = k), \end{aligned} \tag{3.13}$$

where $\lambda_l = \sum_{i \in Sub_{large}} (1 - p_i)$.

***Proof**: Let*

$$\begin{aligned} U &= \sum_{i \in Sub_{large}} (1 - x_i) \\ &= (N - m - n) - \sum_{i \in Sub_{large}} x_i \\ &= (N - m - n) - N_{free_{large}}. \end{aligned} \tag{3.14}$$

Note that $(1 - x_i)$ *is a Bernoulli random variable with* $Pr(1 - x_i = 1) = Pr(x_i = 0) = (1 - p_i)$*, which is small for* $i \in \text{Sub}_{large}$*. By the Law of Rare Events, U approximately follows a Poisson distribution with parameter* λ_l*. Consequently,*

$$\begin{aligned} Pr(N_{free_{large}} = k) &= Pr((N - m - n - U) = k) \\ &= Pr(U = (N - m - n - k) \\ &\simeq \frac{e^{-\lambda_l} \lambda_l^{(N-m-n-k)}}{(N - m - n - k)!}. \end{aligned}$$

□

In the following lemma, we give an upper bound for the approximation error involved in Lemma 3.

Lemma 4 *Let Z be a random variable that has a Poisson distribution with parameter* λ_l*. We have:*

$$| \, Pr(N_{free_{large}} = k) - Pr(Z = k) \, | \leq \frac{1 - e^{-\lambda_l}}{\lambda_l} \times \sum_{i \in Sub_{large}} (1 - p_i)^2, \tag{3.15}$$

where $k = 0, 1, 2, \ldots$.

Proof*: This Lemma is analogous to Lemma 2 once we replace* p_i *with* $(1 - p_i)$ *and* λ_s *by* λ_l*.* □

3.4.4 Approximate Distribution of N_{free}

In this section, we illustrate a procedure for computing the distribution of N_{free}, $N_{free_{mod}}$, and $N_{free_{large}}$. For better computational efficiency, only the essential supports, $\mathcal{S}_{N_{free_{small}}}$ and $\mathcal{S}_{N_{free_{large}}}$ of $N_{free_{small}}$ and $N_{free_{large}}$ respectively, are used in the computation. In other words, any probability less than θ will not be considered. From Eq. (3.8), we have $N_{free} = N_{free_{small}} + N_{free_{mod}} + N_{free_{large}}$. As an illustration, we first consider two cases: $N_{free} = 0$ and $N_{free} = 1$.

The entity $N_{free} = 0$ means that there are no free sub-bands in the entire spectrum. Equivalently, there are no free sub-bands in Sub_{small}, Sub_{mod}, or Sub_{large}. By Eqs. (3.8), (3.9), (3.12) and (3.13):

$Pr(N_{free} = 0)$

$$
\begin{aligned}
&= Pr(N_{free_{small}} = 0, N_{free_{large}} = 0, N_{free_{mod}} = 0) \\
&= Pr(N_{free_{small}} = 0)\, Pr(N_{free_{large}} = 0)\, Pr(N_{free_{mod}} = 0) \\
&\simeq e^{-\lambda_s} \frac{e^{-\lambda_l} \lambda_l^{(N-m-n)}}{(N-m-n)!} Pr(-\frac{1}{2} < N_{free_{mod}} < \frac{1}{2}) \\
&\simeq e^{-\lambda_s} e^{-\lambda_l} \frac{(\lambda_l)^{(N-m-n)}}{(N-m-n)!} \int_{-\frac{1}{2}}^{\frac{1}{2}} N(\overline{N}_{mod}, C_n) dx \\
&= Pr_{Poi-Normal}(N_{free} = 0).
\end{aligned}
$$

Similarly, $N_{free} = 1$ means that there is only one free sub-band in the spectrum of N sub-bands. This free sub-band can be in one of Sub_{small}, Sub_{mod}, and Sub_{large}. By Eqs. (3.8), (3.9), (3.12) and (3.13):

$Pr(N_{free} = 1)$

$$
\begin{aligned}
&= Pr(N_{free_{small}} = 1, N_{free_{large}} = 0, N_{free_{mod}} = 0) + \\
&\quad Pr(N_{free_{small}} = 0, N_{free_{large}} = 1, N_{free_{mod}} = 0) + \\
&\quad Pr(N_{free_{small}} = 0, N_{free_{large}} = 0, N_{free_{mod}} = 1) \\
&= Pr(N_{free_{small}} = 1)\, Pr(N_{free_{large}} = 0) \times \\
&\quad Pr(-\frac{1}{2} < N_{free_{mod}} < \frac{1}{2}) + \\
&\quad Pr(N_{free_{small}} = 0)\, Pr(N_{free_{large}} = 1) \times \\
&\quad Pr(-\frac{1}{2} < N_{free_{mod}} < \frac{1}{2}) + \\
&\quad Pr(N_{free_{small}} = 0)\, Pr(N_{free_{large}} = 0) \times \\
&\quad Pr(\frac{1}{2} < N_{free_{mod}} < \frac{3}{2}) \\
&\simeq \left(e^{-\lambda_s} \lambda_s\right) \left(\frac{e^{-\lambda_l} \lambda_l^{(N-m-n)}}{(N-m-n)!}\right) \int_{-\frac{1}{2}}^{\frac{1}{2}} N(\overline{N}_{mod}, C_n) dx + \\
&\quad (e^{-\lambda_s}) \left(\frac{e^{-\lambda_l} \lambda_l^{(N-m-n-1)}}{(N-m-n-1)!}\right) \int_{-\frac{1}{2}}^{\frac{1}{2}} N(\overline{N}_{mod}, C_n) dx + \\
&\quad (e^{-\lambda_s}) \left(\frac{e^{-\lambda_l} \lambda_l^{(N-m-n)}}{(N-m-n)!}\right) \int_{\frac{1}{2}}^{\frac{3}{2}} N(\overline{N}_{mod}, C_n) dx \\
&= Pr_{Poi-Normal}(N_{free} = 1).
\end{aligned}
$$

Following the *modus operandi* in the illustration presented above, we now obtain a general expression for the probability of k free sub-bands. Some k_1 of these free sub-bands could be in Sub_{small}, k_2 in Sub_{mod}, and k_3 in Sub_{large} with the provision that $k_1 + k_2 + k_3 = k$.

$$
\begin{aligned}
Pr(N_{free} = k) & \\
&= \sum Pr(N_{free_{small}} = k_1, N_{free_{mod}} = k_2, N_{free_{large}} = k_3) \\
&= \sum Pr(N_{free_{small}} = k_1)\, Pr(N_{free_{mod}} = k_2)\, Pr(N_{free_{large}} = k_3) \\
&\simeq Pr_{Poi}(N_{free_{small}} = k_1) Pr_{Normal}(N_{free_{mod}} = k_2) \times \\
&\quad Pr_{Poi}(N_{free_{large}} = k_3) \\
&= Pr_{Poi-Normal}(N_{free} = k), \qquad (3.16)
\end{aligned}
$$

where the summation is taken over all $k_1 \geq 0$, $k_2 \geq 0$, and $k_3 \geq 0$ with $k_1 + k_2 + k_3 = k$.

By focusing on $k_1 \in \mathcal{S}_{N_{free_{small}}}$ and $k_3 \in \mathcal{S}_{N_{free_{large}}}$ in Eq. (3.16), the number of calculations can be drastically reduced. In any practical situation, the sets $\mathcal{S}_{N_{free_{small}}}$ and $\mathcal{S}_{N_{free_{large}}}$ are determined first, and then Eq. (3.16) is used in obtaining an approximate distribution of N_{free}. The corresponding algorithm is presented in Section 3.6.

3.5 Neighborhood Occupancy of Free Sub-bands

In this section, we define certain types of free sub-bands based on the occupancy of their adjacent sub-bands. Then, we compute the probability distribution of the total number of each type sub-band.

3.5.1 Sub-band Types

Consider any interior free sub-band i, i.e., $i \neq 1$ and $i \neq N$. In this case, it has two adjacent neighbors. Each adjacent neighbor is either occupied by a PU or is free. This results in three different types of free sub-bands based on the number of free adjacent neighbors. The number of possible free adjacent sub-bands is either 0, 1, or 2. The three types are depicted in Figure 3.4 (b), (a), and (c), respectively. If the free sub-band is not

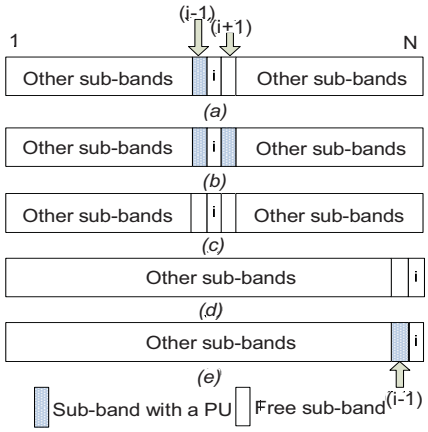

Figure 3.4: Types of free sub-bands: (a) Type I, (b) Type II, (c) Type III, (d) Type IV, and (e) Type V

interior, i.e., $i = 1$ or $i = N$, then two types are possible. Figures 3.4 (d) and (e) depict the case $i = N$. The five types of free sub-bands are defined formally as below.

- **Type I sub-band**: It is a free sub-band i having a PU as the $(i-1)^{st}$ neighbor and a free sub-band as the $(i+1)^{st}$ neighbor, or vice versa, making three contiguous sub-bands $(i-1)^{st}$, i^{th}, and $(i+1)^{st}$ as *Occupied, Free, Free* or *Free, Free, Occupied* as shown in Figure 3.4(a). Let $X_I(N)$ be the random variable that represents the total number of Type I sub-bands in the N-spectrum. Possible values of $X_I(N)$ are $0, 1, \ldots, N-2$.

- **Type II sub-band**: It is a free sub-band i with two PUs as $(i-1)^{st}$ and $(i+1)^{st}$ neighbors as shown in Figure 3.4(b). Let $X_{II}(N)$ be the random variable that represents the total number of Type II sub-bands in the N-spectrum. Possible values of $X_{II}(N)$ are $0, 1, \ldots, N-2$.

- **Type III sub-band**: It is a free sub-band i with two free sub-bands as $(i-1)^{st}$ and $(i+1)^{st}$ neighbors, resulting in three contiguous free sub-bands as shown in Figure 3.4(c). Let $X_{III}(N)$ be the random variable that represents the total number of Type III sub-bands in the N-spectrum. Possible values of $X_{III}(N)$ are $0, 1, \ldots, N-2$.

- **Type IV sub-band**: It is a free sub-band i at the left or right edge of the spectrum with a free sub-band as its neighbor, resulting in two contiguous free sub-band on the

Table 3.4: Boundary conditions for Type I, II, and III sub-bands for $X_i(N)$ at N = 3

$X_i(3)$	Probabilities of Types I, II, and III		
	$Probability(TypeI)$	$Probability(TypeII)$	$Probability(TypeIII)$
0	$1-(1-p_1)p_2p_3-p_1p_2(1-p_3)$	$1-(1-p_1)p_2(1-p_3)$	$1-p_1p_2p_3$
1	$(1-p_1)p_2p_3+p_1p_2(1-p_3)$	$(1-p_1)p_2(1-p_3)$	$p_1p_2p_3$

edge of the spectrum as shown in Figure 3.4(d). Let $X_{IV}(N)$ be the random variable that represents the total number of Type IV sub-bands in the N-spectrum. Possible values of $X_{IV}(N)$ are 0, 1, and 2.

- **Type V sub-band**: It is a free sub-band i at the left or right edge of the spectrum with a PU as its neighbor as shown in Figure 3.4(e). Let $X_V(N)$ be the random variable that represents the total number of Type V sub-bands in the N-spectrum. Possible values of $X_V(N)$ are 0, 1, and 2.

Following the above definitions, we determine the probability distribution of $X_i(N)$ for each type of sub-band. The recurrence relation enables us to develop an algorithm to compute the probability distribution of $X_i(N)$.

3.5.2 Probability Distribution of $X_I(N)$

The approach described in Section 3.4 is not applicable to $X_I(N)$ since the probability of a free sub-band also depends on its two neighbors. In view of this, we develop a recurrence relation to compute $X_I(N)$.

Lemma 5 *Let $X_I(m+1)$ be the total number of Type I sub-bands in the $(m+1)$-spectrum represented by $\{1,2,\cdots,(m+1)\}$ with sub-band free probabilities $p_1, p_2, \cdots, p_{(m+1)}$. Let $X_I(m)$ be the total number of Type I sub-bands in the m-spectrum represented by $\{1,2,\cdots,m\}$ with sub-band free probabilities $p_1, p_2, \cdots, p_m$. Then,*

$$X_I(m+1) = \begin{cases} [X_I(m)+1] \text{ with probability } p_I(m) \\ X_I(m) \text{ with probability } (1-p_I(m)), \end{cases} \tag{3.17}$$

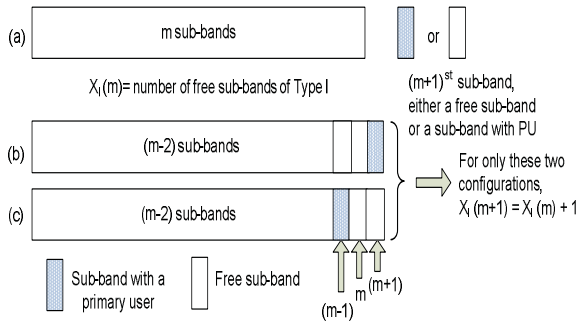

Figure 3.5: $(m+1)$-spectrum derived from m-spectrum for Type I sub-bands

where $p_I(m) = (1 - p_{(m-1)})p_m p_{(m+1)} + p_{(m-1)}p_m(1 - p_{(m+1)})$, $m = (N-1), (N-2), \cdots, 3$.

Proof: *We focus on the status of occupancy in the sub-bands* $(m-1), m$, *and* $(m+1)$. *Each of these sub-bands is either free or occupied, giving rise to* $2^3 = 8$ *possibilities indicated by the following three cases:*

- *Case I: Sub-bands* $(m-1)$ *and* m *are free, and sub-band* $(m+1)$ *is occupied as depicted in Figure 3.5(b). This occurs with probability* $p_{(m-1)}p_m(1 - p_{(m+1)})$. *Sub-band* m *is at the edge of the* m*-spectrum and therefore it cannot be a Type I sub-band in the spectrum. On the other hand, sub-band* m *is of Type I in the* $(m+1)$*-spectrum. Consequently,* $X_I(m+1) = X_I(m) + 1$*;*

- *Case II: Sub-band* $(m-1)$ *is occupied and sub-bands* m *and* $(m+1)$ *are free as shown in Figure 3.5(c). This occurs with probability* $(1 - p_{(m-1)})p_m p_{(m+1)}$. *Therefore,* $X_I(m+1) = X_I(m) + 1$*;*

- *Case III: It consists of the remaining six possibilities. In all such possibilities,* $X_I(m+1) = X_I(m)$.

Consequently, $X_I(m+1) = X_I(m) + 1$ *with probability* $p_I(m)$ *and* $X_I(m+1) = X_I(m)$ *with probability* $1 - p_I(m)$. □

Lemma 5 enables us to compute the distribution of $X_I(m+1)$ once we know the distribution of $X_I(m)$ as detailed below. The possible values of $X_I(m)$ are $0, 1, 2, \cdots, (m-2)$. From

Eq. (3.17), it is clear that the number of possible values of $X_I(m+1)$ are $0, 1, 2, \cdots, (m-1)$. A possible value of $X_I(m+1)$ is represented by r. For the computation of $Pr\,(X_I(m+1) = r)$, we identify three cases: $1 \leq r \leq (m-2)$; r=0; and r=$(m-1)$. If $1 \leq r \leq (m-2)$, the events $X_I(m+1)$=r can arise from $X_I(m)$=$(r-1)$ or $X_I(m)$=r. Consequently, by Eq. (3.17),

$$Pr\,(X_I(m+1) = r)$$

$$= p_I(m) \times Pr\,(X_I(m) = (r-1)) + (1 - p_I(m)) \times Pr\,(X_I(m) = r)\,. \tag{3.18}$$

The event $X_I(m+1)$=0 can occur if and only if $X_I(m)$=0. Therefore,

$$Pr\,(X_I(m+1) = 0) = (1 - p_I(m)) \times Pr(X_I(m) = 0). \tag{3.19}$$

Finally,

$$Pr(X_I(m+1) = (m-1)) = p_I(m) \times Pr(X_I(m) = (m-2)). \tag{3.20}$$

Thus, once we know the distribution of $X_I(m)$, the distribution of $X_I(m+1)$ can be determined using Eqs. (3.18), (3.19), and (3.20).

The ultimate goal is to find the distribution of $X_I(N)$. For this, we need the distribution of $X_I(3)$ which helps in finding the distribution of $X_I(4)$ using Eqs. (3.18), (3.19), and (3.20). We continue this process until we reach $X_I(N)$. The distribution of $X_I(3)$ is given in Table 3.4.

We further consider the special case that all p_i's are equal, i.e., $p_i = p$. The following theorem gives the exact distribution of the random variable $X_I(N)$.

Theorem 3.1: If all p_i's are equal, then $X_I(N)$ has Binomial $\Big((N-2), 2p^2(1-p)\Big)$.

Proof: The proof is by induction. If $p_i = p$, the distribution of $X_I(3)$ is given by:

$$\begin{aligned} Pr(X_I(3) = 0) &= 1 - 2p^2(1-p) \\ Pr(X_I(3) = 1) &= 2p^2(1-p). \end{aligned}$$

Therefore, $X_I(3)$ follows *Binomial* $\Big(1, 2p^2(1-p)\Big)$. By using Lemma 5, the recurrence relation of $X_I(4)$ in terms of $X_I(3)$ is given by:

$$\begin{aligned} X_I(4) &= X_I(3) + 1 \;\; with \;\; probability \; 2p^2(1-p) \\ &= X_I(3) \;\; with \;\; probability \;\; 1 - 2p^2(1-p). \end{aligned}$$

The distribution of $X_I(4)$ is given by:

$$\begin{aligned} Pr(X_I(4)=0) &= \left[1-2p^2(1-p)\right]^2 \\ Pr(X_I(4)=1) &= 2\left[1-2p^2(1-p)\right]2p^2(1-p) \\ Pr(X_I(4)=2) &= \left[2p^2(1-p)\right]^2. \end{aligned}$$

It is clear that $X_I(4)$ follows the $Binomial\left(2, 2p^2(1-p)\right)$.

Suppose $5 \leq n \leq N-1$ and the inductive hypothesis that $X_I(n) \sim Binomial\left((n-2), 2p^2(1-p)\right)$ is true. We prove that $X_I(n+1) \sim Binomial\left((n-1), 2p^2(1-p)\right)$. The Binomial distribution of $X_I(n)$ is given by:

$$\begin{aligned} Pr(X_I(n)=0) &= \left[1-2p^2(1-p)\right]^{(n-2)} \\ Pr(X_I(n)=1) &= \binom{(n-2)}{1}2p^2(1-p)\times \\ &\quad \left[1-2p^2(1-p)\right]^{(n-3)} \\ \cdots &= \cdots \\ Pr(X_I(n)=(n-2)) &= \left[2p^2(1-p)\right]^{(n-2)}. \end{aligned}$$

From Lemma 5, we have:

$$\begin{aligned} X_I(n+1) &= X_I(n)+1 \ \ with \ \ probability \ 2p^2(1-p) \\ &= X_I(n) \ \ with \ \ probability \ \ 1-2p^2(1-p). \end{aligned}$$

Possible values of $X_I(n+1)$ are $0, 1, \cdots, (n-2), (n-1)$. The probabilities for each of these values are computed separately as follows:

$Pr(X_I(n+1)=0)$

$$\begin{aligned} &= Pr(X_I(n)=0)\times\left[1-2p^2(1-p)\right] \\ &= \left[1-2p^2(1-p)\right]^{(n-2)}\times\left[1-2p^2(1-p)\right] \\ &= \left[1-2p^2(1-p)\right]^{(n-1)}. \end{aligned}$$

For $1 \leq r \leq (n-2)$, we have:

$$
\begin{aligned}
&Pr(X_I(n+1) = r) \\
&\quad = Pr(X_I(n) = r) \times \left[1 - 2p^2(1-p)\right] + \\
&\quad\quad Pr(X_I(n) = (r-1)) \times \left[2p^2(1-p)\right] \\
&\quad = \binom{(n-2)}{r} \left(2p^2(1-p)\right)^r \times \left(1 - 2p^2(1-p)\right)^{(n-2-r)} \times \\
&\quad\quad (1 - 2p^2(1-p)) + \binom{(n-2)}{(r-1)} \left(2p^2(1-p)\right)^{(r-1)} \times \\
&\quad\quad \left(1 - 2p^2(1-p)\right)^{(n-2-r+1)} \times \left(2p^2(1-p)\right) \\
&\quad = \left(2p^2(1-p)\right)^r \times \left(1 - 2p^2(1-p)\right)^{(n-1-r)} \times \\
&\quad\quad \left[\binom{(n-2)}{r} + \binom{(n-2)}{(r-1)}\right] \\
&\quad = \binom{(n-1)}{r} \times (2p^2(1-p))^r \times \left(1 - 2p^2(1-p)\right)^{(n-1-r)}.
\end{aligned}
\tag{3.21}
$$

Now, the probability of having $(n-1)$ Type I sub-bands is expressed as:

$$
\begin{aligned}
&Pr(X_I(n+1) = (n-1)) \\
&\quad = Pr(X_I(n) = (n-2)) \times \left[2p^2(1-p)\right] \\
&\quad = \left[2p^2(1-p)\right]^{(n-1)}.
\end{aligned}
\tag{3.22}
$$

From these probabilities, it is evident that $X_I(n+1) \sim Binomial\left((n-1), 2p^2(1-p)\right)$. □

3.5.3 Probability Distribution of $X_{II}(N)$

As evident from the analysis performed for Type I sub-bands, we develop a similar recurrence relation for computing total number of Type II sub-bands. The methodology is similar to that of Type I.

Lemma 6 *Let $X_{II}(m+1)$ be the total number of Type II sub-bands in the $(m+1)$-spectrum represented by $\{1, 2, \cdots, (m+1)\}$ with sub-band free probabilities $p_1, p_2, \cdots, p_{(m+1)}$. Let*

$X_{II}(m)$ be the total number of Type II sub-bands in the m-spectrum represented by $\{1, 2, \cdots, m\}$ *with sub-band free probabilities* $p_1, p_2, \cdots, p_m$. *Then,*

$$X_{II}(m+1) = \begin{cases} [X_{II}(m) + 1] \text{ with probability } p_{II}(m) \\ X_{II}(m) \text{ with probability } (1 - p_{II}(m)), \end{cases} \tag{3.23}$$

where $p_{II}(m) = (1 - p_{(m-1)})p_m(1 - p_{(m+1)})$, $m = (N-1), (N-2), \cdots, 3$.

A proof can be given similar to the one given in Lemma 5. The boundary condition which gives the distribution of $X_{II}(3)$ is provided in Table 3.4. This distribution can be used to obtain the distribution of $X_{II}(N)$.

Theorem 3.2: If all p_i*'s are equal, i.e.,* $p_i = p$, *then* $X_{II}(N)$ *has Binomial* $\Big((N-2), p(1-p)^2\Big)$.

□

3.5.4 Probability Distribution of $X_{III}(N)$

The recurrence relation for computing the total number of sub-bands of Type III is given by the following lemma.

Lemma 7 *Let* $X_{III}(m+1)$ *be the total number of Type III sub-bands in the* $(m+1)$*-spectrum represented by* $(1, 2, \cdots, (m+1))$ *with sub-band free probabilities* $p_1, p_2, \cdots, p_{(m+1)}$. *Let* $X_{III}(m)$ *be the total number of Type III sub-bands in the m-spectrum represented by* $\{1, 2, \cdots, m\}$ *with sub-band free probabilities* $p_1, p_2, \cdots, p_m$. *Then,*

$$X_{III}(m+1) = \begin{cases} [X_{III}(m) + 1] \text{ with probability } p_{III}(m) \\ X_{III}(m) \text{ with probability } (1 - p_{III}(m)), \end{cases} \tag{3.24}$$

where $p_{III}(m) = p_{(m-1}p_m p_{(m+1)}$, $m = (N-1), (N-2), \cdots, 3$.

The proof is omitted. The boundary condition which gives the distribution of $X_{III}(3)$ is provided in Table 3.4. This distribution is used to obtain the distribution of $X_{III}(N)$.

Theorem 3.3: If all p_i *are equal, i.e.,* $p_i = p$, $X_{III}(N)$ *has Binomial* $\Big((N-2), p^3\Big)$. □

3.5.5 Probability Distribution of $X_{IV}(N)$

As every spectrum has two edges, the number of Type IV sub-bands is $0, 1$, or 2. The probability distribution of the number of Type IV sub-bands is given by:

$$\begin{aligned} P(X_{IV}(N)=0) &= 1 - P(X_{IV}(N)=1) - P(X_{IV}(N)=2) \\ P(X_{IV}(N)=1) &= p_1 p_2 [p_{N-1}(1-p_N) + (1-p_{N-1})p_N + \\ &\quad (1-p_{N-1})(1-p_N)] + p_{N-1}p_N[(1-p_1)p_2 + \\ &\quad p_1(1-p_2) + (1-p_1)(1-p_2)]. \\ P(X_{IV}(N)=2) &= p_1 p_2 p_{N-1} p_N. \end{aligned} \tag{3.25}$$

The distribution of $X_{IV}(N)$ under the following special case is evident.

Theorem 3.4: If $p_1 = p_2 = p_{(N-1)} = p_N = p$, then the distribution of $X_{IV}(N)$ is given by:

$$\begin{aligned} Pr(X_{IV}(N=0)) &= 1 - 2p^2 + p^4 \\ Pr(X_{IV}(N=1)) &= 4p^3(1-p) + 2p^2(1-p)^2 \\ Pr(X_{IV}(N=2)) &= p^4, \end{aligned}$$

with $E[X_{IV}(N)] = 2p^2$. □

3.5.6 Probability Distribution of $X_V(N)$

The probability distribution of the number of Type V sub-bands is given by:

$$\begin{aligned} P(X_V(N)=0) &= 1 - P(X_V(N)=1) - P(X_V(N)=2) \\ P(X_V(N)=1) &= p_1(1-p_2)[p_{N-1}p_N + p_{N-1}(1-p_N) + \\ &\quad (1-p_{N-1})(1-p_N)] + (1-p_{N-1})p_N[p_1p_2 + \\ &\quad (1-p_1)p_2 + (1-p_1)(1-p_2)]. \\ P(X_V(N)=2) &= p_1(1-p_2)(1-p_{N-1})p_N. \end{aligned} \tag{3.26}$$

Theorem 3.5. If $p_1 = p_2 = p_{(N-1)} = p_N = p$, then the distribution of $X_V(N)$ is given by:

$$\begin{aligned} Pr(X_V(N=0)) &= 1 - p(1-p)(p^2 - p + 2) \\ Pr(X_V(N=1)) &= 2p(1-p)(p^2 - p + 1) \\ Pr(X_V(N=2)) &= p^2(1-p)^2, \end{aligned}$$

with $E[X_{IV}(N)] = 2p(1-p)$. □

Corollary: If all p_i's are equal, i.e., $p_i = p$, then the expected value of the total number of free sub-bands is the sum of the expected values of all types of sub-bands, i.e.,

$$E[N_{free}] = Np$$
$$= E[X_I(N)] + E[X_{II}(N)] + E[X_{III}(N)] + E[X_{IV}(N)] + E[X_V(N)]. \quad (3.27)$$

Proof: Any free sub-band has to be one and only one of Type I, Type II, Type III, Type IV, and Type V sub-bands. Therefore,

$$N_{free} = X_I(N) + X_{II}(N) + X_{III}(N) + X_{IV}(N) + X_V(N). \quad (3.28)$$

Hence the result follows. □

Comments: For the validity of Eq. (3.27), the assumption that all p_i's are equal is not essential. In the general case, $E[N_{free}] = \sum_{i=1}^{N} p_i$. However, $E[X_I(N)]$, $E[X_{II}(N)]$, and $E[X_{III}(N)]$ do not have any compact formulae.

3.6 Implementation and Performance Evaluation

In this section, we present algorithms to compute the distribution of N_{free} and that of the total number of Type I sub-bands. This is followed by a comparative study of the exact distribution, normal, and Poisson-normal approximations under three different scenarios. We further analyze probability distributions of the total number of each type of sub-bands. Finally, properties of the distributions are studied.

In the following two sub-sections, we develop algorithms to compute the distributions of N_{free} and $X_I(N)$. For clarification, we use $Pr(N_{free} = k)$ to represent the exact probability of $N_{free} = k$ obtained by using Eq. (3.3). The entity $Pr_{Normal}(N_{free} = k)$ is the probability of $N_{free} = k$ following a normal approximation and computed by using Eq. (3.7). Furthermore, $Pr_{Poi-Normal}(N_{free} = k)$ is the probability of $N_{free} = k$ using a Poisson-normal approximation as given by Eq. (3.16).

3.6.1 Algorithm for Probability Distribution of N_{free}

The rationale of Poisson-normal approximation of N_{free} distribution is explained in Section 3.4 and Algorithm 1 is its implementation. The basic input of this Algorithm is a given set of sub-band free probabilities $p_1, \cdots, p_N$ (Line 1) and the output is a set of probabilities $P[0], P[1], \cdots, P[N]$ (Line 2), where $P[k] = Pr_{Poi-Normal}(N_{free} = k)$. These discrete probabilities $P[0], P[1], \cdots, P[N]$ give the probability distribution of $N_{free} = k$.

The probabilities p_i's are classified into three groups Sub_{small}, Sub_{mod}, and Sub_{large} (Line 4), based on the lower and upper thresholds (i.e., P_{th1} and P_{th2}) as discussed in Section 3.4. The probabilities $Pr_{Poi}(N_{free_{small}} = i)$'s and $Pr_{Poi}(N_{free_{large}} = i)$'s are calculated separately using Eqs. (3.9) and (3.13), respectively. The essential supports $\mathcal{S}_{N_{free_{small}}}$ and $\mathcal{S}_{N_{free_{large}}}$ of these distributions are created (Line 4) according to *Definition 2* and $\theta = 0.001$.

In Algorithm 2, for reduced time complexity, only probabilities stemming from essential support $\mathcal{S}_{N_{free_{small}}}$ and $\mathcal{S}_{N_{free_{large}}}$ are considered. Two counters C_{small} and C_{large} are allocated to register values of essential supports (Lines 3 and 5). The variable k keeps track of all possible values of N_{free} (Line 6). Since values between $Pr_{Poi}(N_{free_{large}} = 0)$ to $Pr_{Poi}(N_{free_{large}} = C_{large} - 1)$ are less than θ, k from 0 to $(C_{large} - 1)$ are neglected by setting them as zero. For the same reason, the algorithm only considers values of k_1 from 1 to C_{small} (Line 8) and k_3 from C_{large} to N (Line 9).

Lines 6 – 17 facilitate Algorithm 2 to compute $Pr[C_{free}]$ for all possible combinations of free sub-bands in Sub_{small}, Sub_{mod}, and Sub_{large}. Each combination satisfies the constraint of $k_1 + k_2 + k_3 = C_{free}$. In particular, C_{free} tracks all possible combinations of k_1, k_2, and k_3 to yield a value of N_{free} as given in Eq. (3.16). $P[k]$ is initialized to zero for every iteration of k (Line 7). Then, the algorithm in Lines 8 – 16 accommodates all possible combinations of $N_{free_{small}} = k_1$, $N_{free_{mod}} = k_2$, and $N_{free_{large}} = k_3$ that sum up to $N_{free} = k$. Line 10 ensures non-negative values of $N_{free_{mod}} = k_2$. Line 12 computes $Pr_{Normal}(N_{free_{mod}} = k_2)$ using Eq. (3.12). Now the probability $Pr(C_{free})$ is obtained by multiplying the marginal probabilities of $N_{free_{small}} = k_1$, $N_{free_{mod}} = k_2$, and $N_{free_{large}} = k_3$ (Line 13). Each possible combination increments C_{free} by one (Line 14).

At the end of i^{th} iteration (Lines 18-20), for all possible combinations of m ranging from 1 to C_{free}, computed values $Pr(m)$ are added as in Eq. (3.16). This finally generates $P[k]$

1: **Input**: Set of sub-band free probabilities $p_1, \cdots, p_N$
2: **Output**: Probabilities $P[0]$, $P[1]$, $\cdots$,$P[N]$
3: Initialization: $C_{small} = 0$, $C_{large} = 0$, and $C_{free} = 0$
4: Classify and compute $Pr_{Poi}(N_{free_{small}} = i)$ and $Pr_{Poi}(N_{free_{large}} = i)$ using Eqs. (3.9) and (3.13)
5: Counters C_{small} and C_{large} updated with essential supports of $\mathcal{S}_{N_{free_{small}}}$ and $\mathcal{S}_{N_{free_{large}}}$
6: **for** $k = C_{large}$ to N **do**
7: $P[k] = 0.0$
8: **for** $k_1 = 1$ to C_{small} **do**
9: **for** $k_3 = C_{large}$ to N **do**
10: **if** $(k - k_1 - k_3) \geq 0$ **then**
11: k_2=$(k - k_1 - k_3)$
12: $Pr_{Normal}[k_2]$ is then computed using Eq. (3.12)
13: $Pr[C_{free}]$ is computed using the term inside the summation symbol of Eq. (3.16)
14: $C_{free} = C_{free} + 1$
15: **end if**
16: **end for**
17: **end for**
18: **for** $m = 1$ to C_{free} **do**
19: Add $Pr[m]$ as depicted in Eq. (3.16) for each value of m to obtain $P[k]$
20: **end for**
21: **end for**

Algorithm 1: Computation of distribution of N_{free} using Poisson-normal approximation

for $N_{free} = k$. The above process is repeated for possible values of k ranging from C_{large} to N so that for every $k \in [0, N]$ P[k] is computed sequentially.

1: **Input**: Set of sub-band free probabilities $p_1, \cdots, p_N$
2: **Output**: Probability of number of Type I free sub-bands $P[X_I(3:N)]$
3: Initialization: $P[X_I(3:(N-2))] = 0$
4: Compute $P[X_I(3) = 0]$ and $P[X_I(3) = 1]$ using expressions for Type I in Table IV
5: **for** $i = 4$ to N **do**
6: $P[X_I(i) = 0]$ is computed using Eq. (3.19)
7: $P[X_I(i) = (i-2)]$ is computed using Eq. (3.20)
8: **for** $j = 1$ to $(i-3)$ **do**
9: $P[X_I(i) = j]$ is computed using Eq. (3.18)
10: **end for**
11: **end for**

Algorithm 2: Computation of the probability distribution of $X_I(N)$ in a spectrum of N sub-bands

3.6.2 Algorithm for Probability Distribution of $X_I(N)$

Computation of distribution of total number of free sub-bands of Type I is explained in Algorithm 2. The input is still the set of sub-band free probabilities $p_1, \cdots, p_N$ (Line 1). The algorithm computes the probabilities $P[X_I(i) = j]$, $j = 0, 1, \cdots, (i-2)$ and $i = 3, 4, 5, \cdots, N$ (Line 2). The boundary condition is the distribution of $X_I(3)$, which is separately computed in Line 4 following the Table 3.4. Now, we use the recurrence relation given by Eq. (3.17) to compute the distributions of $X_I(4), \cdots, X_I(N)$ (Lines 5-11). The computations are carried out in two stages. First, for any value $4 \leq i \leq N$, compute $Pr[X_I(i) = 0]$ and $Pr[X_I(i) = (i-2)]$ using Eqs. (3.19) and (3.20), respectively (Lines 6-7). Second, compute $Pr[X_I(i) = j]$, $1 \leq j \leq (i-3)$, i.e., using Eq. (3.18) (Lines 8-10). Similar algorithms are developed to deal with distributions of $X_{II}(N)$ and $X_{III}(N)$. Due to space limitations, details are not presented here.

3.6.3 Simulation Configuration

For simulation purpose, a Beta distribution is used to generate p_i's, $i = 1, 2, \cdots, N$. The probability density function of a Beta distribution has two parameters $\alpha > 0$ and $\beta > 0$ and is given by:

$$f(x; \alpha, \beta) = \frac{1}{B(\alpha, \beta)} x^{\alpha-1}(1-x)^{\beta-1}, 0 < x < 1, \tag{3.29}$$

where $B(\alpha, \beta)$ is the Beta function defined as:

$$B(\alpha, \beta) = \int_0^1 t^{\alpha-1}(1-t)^{\beta-1} dt. \tag{3.30}$$

The entity $B(\alpha, \beta)$ is a normalization constant to ensure that the function in Eq. (3.29) integrates to unity. Any continuous probability distribution on $(0, 1)$ can reasonably be approximated by a Beta distribution [33]. This is the main reason we have chosen Beta distribution for randomly generating a set of sub-band free probabilities. By varying the values of the parameters α and β, we have generated three sets of probabilities.

As discussed earlier, a television transmission typically occupies a bandwidth of 6 MHz in the licensed bands. In view of this, the bandwidth of each sub-band is considered to be $6MHz$. In the simulation, p_i's are generated under the following three scenarios:

- *Scenario-1*: This scenario mimics the spectrum bandwidth $710 - 806MHz$ that can be divided into N=16 sub-bands. A set of p_i's as 16 sub-band free probabilities is generated from $Beta(0.5, 0.2)$ distribution. The output of the distribution has one small, six large, and nine moderate p_i's as shown in Figure 3.3(a).

- *Scenario-2*: This scenario mimics the spectrum bandwidth $628 - 806MHz$ that can be divided into N=30 sub-bands. A set of p_i's as 30 sub-band free probabilities is generated from $Beta(0.5, 0.5)$ distribution. The output of the distribution has five small, five large, and 20 moderate p_i's.

- *Scenario-3*: This scenario mimics the spectrum bandwidth $470 - 650MHz$ that can be divided into N=30 sub-bands. For simulation, a different Beta distribution is used to create an imbalance between small and large sub-band free probabilities,

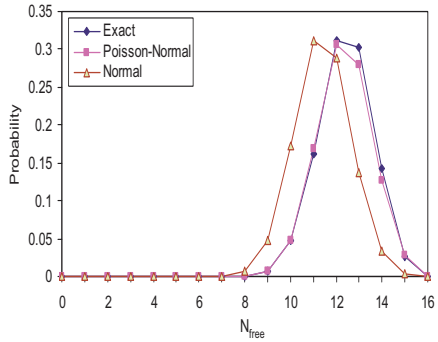

Figure 3.6: Exact distribution of N_{free} and its normal and Poisson-normal approximations for 16 sub-bands with 1 small and 6 large sub-band free probabilities

unlike *Scenario-2*. A set of p_i's as 30 sub-band free probabilities is generated from $Beta(0.6, 0.1)$ distribution. The output of the distribution has two small, 16 large, and 12 moderate p_i's as shown in Figure 3.3(b).

As discussed in Section 3.4, for computation of approximate distribution of N_{free}, we take $p_{th1} = 0.03$ and $p_{th2} = 0.97$ as the lower threshold and upper threshold values, respectively. Algorithm 1 is implemented on each scenario. In the following two sub-sections, we compare the exact distribution of N_{free} with its normal and Poisson-normal approximations in terms of approximation error and computation efficiency. We then discuss about the distributions of $X_i(N)$'s wherein Algorithm 2 is implemented on each scenario.

3.6.4 Distribution of N_{free}

The exact distribution of N_{free} and its normal and Poisson-normal approximations under *Scenario-1* are plotted in Figure 3.6. In a similar way, Figure 3.7 deals with *Scenarios-2* and *3*. As can be seen from the figures, the normal approximation deviates substantially from the exact distribution. The over-all approximation errors ϵ's are 0.1663, 0.0602, and 0.1454 for *Scenarios-1, 2*, and *3*, respectively. It seems that ϵ for *Scenario-2* is much lower than the other two. This is because the sub-band free probabilities are balanced, i.e., having the same number of small and large sub-band free probabilities. On the other hand, Poisson-normal approximation follows the exact distribution closely. The over-all approximation

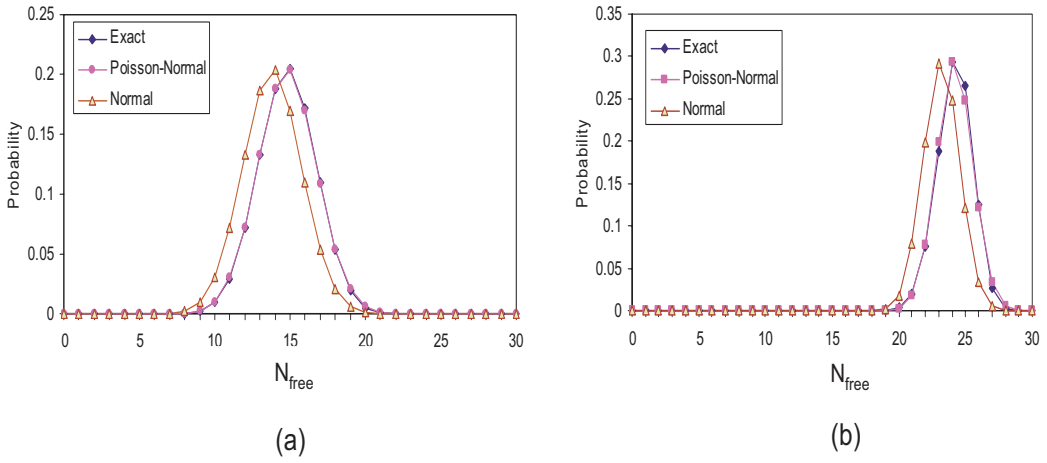

Figure 3.7: Exact distribution of N_{free} and its normal and Poisson-normal approximations for 30 sub-bands with (a) 5 small and 5 large sub-band free probabilities and (b) 2 small and 16 large sub-band free probabilities

errors ϵ's are 0.0236, 0.0019 and 0.0181 for *Scenarios-1, 2*, and *3*, respectively.

As seen from Figure 3.7(a), the normal approximation achieves a modal probability 0.2033 at $N = 14$. On the other hand, both the exact and Poisson-Normal approximation achieve respective modal probabilities of 0.2046 and 0.2034 at $N = 15$. In addition, the essential support $\mathcal{S}_{N_{free}}$ of the Poisson-Normal approximation is $\{8, \cdots, 22\}$ which closely follows the essential support $\{7, \cdots, 22\}$ of the exact distribution. In contrast, the essential support of the normal approximation is $\{6, \cdots, 21\}$.

From Figure 3.7(b), the modal probabilities for the exact distribution and its Poisson-normal approximation are 0.2932 and 0.2933, respectively achieved at $k = 24$. As seen from the figures, all distributions are more or less symmetric so far as their essential support is concerned. The location of the distributions on its essential support depends of its set of large sub-band free probabilities.

3.6.5 Computational Efficiency

Table 3.5 shows the computational efficiency in calculating the exact distribution of N_{free} and its normal and Poisson-normal approximations. It is evident that the normal

Table 3.5: Computational efficiency comparison among the exact distribution and its normal and Poisson-normal approximations

N	Computational time (seconds)		
	Exact	*Normal*	*Poisson − Normal*
16	1435.14	1.11	4.08
30	2650.20	1.14	4.17

approximation is highly efficient in computing the distribution of N_{free} when compared to the exact distribution. However, the normal approximation suffers from a higher over-all approximation error. The computation of $Pr_{Poi-Normal}(N_{free})$ achieves a high accuracy and is still considered as time efficient.

3.6.6 Probability Distribution of $X_i(N)$

Analytical model of the types of sub-bands based on its neighbors is described in Section 3.5. In this sub-section, we obtain simulation results for the distributions of $X_i(N)$, $i = I, II, III$. The distribution of $X_{IV}(N)$ and $X_V(N)$ are not included since each of them takes only three values, namely 0, 1, and 2 and their distributions have no significant contribution to our probabilistic analysis.

The distributions of $X_i(N)$ depend on the spatial and temporal variations of the sub-band occupancy by the PUs and as well as the magnitude of sub-band free probabilities. For example, the distribution of $X_I(N)$ for Type I sub-bands based on $p_1, p_2, \cdots, p_N$ is different from the distribution of $X_I(N)$ when $p_1, p_2, \cdots, p_N$ are permuted. On the other hand, the distribution of N_{free} is invariant under permutations.

Figure 3.8 illustrates the distributions of N_{free}, $X_I(N)$, $X_{II}(N)$, and $X_{III}(N)$ for *Scenario-1* with $N = 16$. This scenario has an imbalance in the cardinalities of Sub_{small} and Sub_{large}. Figure 3.9 compares the distribution of $X_i(N)$'s with that of N_{free} under *Scenario-2*, in which Sub_{small} and Sub_{small} have the same cardinalities. Finally, Figure 3.10 deals with *Scenario-3* with an imbalance in the cardinality of Sub_{small} and Sub_{small}. The distributions of N_{free}, $X_I(N)$, $X_{II}(N)$, and $X_{III}(N)$ reflect the temporal and spatial occupancy of sub-bands in each scenario.

From Figure 3.8, we observe specific features about distribution of N_{free} and $X_i(N)$'s.

A Type III sub-band is more likely than a Type I or Type II sub-band. The mode of N_{free} is 12 and that of $X_I(N)$, $X_{II}(N)$, $X_{III}(N)$ are 6, 4, and 1, respectively.

We compare some of the properties of the distributions under *Scenarios-2* and *3*, in view of the fact that they have the same number of sub-bands, i.e., $N = 30$. The mean, mode, variance, and essential support of their distributions are summarized in Table 3.6 and Table 3.7. The numbers of small p_i's and large p_i's have an impact on the modes of the distributions. In the balanced case of 5 small and 5 large p_is (i.e., *Scenario-2*), the mode is 15, which is located at the center of the range of the distribution of N_{free}. In the unbalanced case of 2 small and 16 large p_i's (i.e., *Scenario-3*), the mode of N_{free} distribution is 24. On the other hand, the distributions of $X_i(N)$'s depend on the order of the probabilities of Type i sub-band and its neighbors.

The analysis indicates the extent of proliferation of sub-bands of each type. If we compare the results of distribution in Figures 3.9 and 3.10, the spectrum associated with Figure 3.10 is preferable. This conclusion is based on the following observations:

- *Number of free sub-bands* (N_{free}): The mode of N_{free} distribution from Figure 3.10, namely 24, is much larger than the mode (i.e., 15) of N_{free} distribution from Figure 3.9. A SU is more likely to get a higher number of free sub-bands from the spectrum of Figure 3.10.

- *Number of Type III sub-bands*: A Type III sub-band is preferable to Type I or Type II sub-band. The spectrum of Figure 3.10 gives a mode of 14 for the distribution of $X_{III}(N)$ where as the mode is 2 for the underlying spectrum of Figure 3.9. Therefore, the spectrum of Figure 3.10 is preferable in terms of Type III sub-bands.

- *Number of Type II sub-bands*: A Type II sub-band is the least preferable since both the neighbors are occupied by PUs. The mode of distribution of $X_{II}(N)$ for the spectrum depicted in Figure 3.10 is *zero* where as the mode in Figure 3.9 is 2. In this respect, the spectrum of Figure 3.10 is again preferable.

Hence, this preferential selection of one N-spectrum over the other can help in adaptive spectrum sensing, i.e., selecting a set of preferred sub-bands for further sensing.

Table 3.6: Probability distribution of N_{free} and $X_i(N)$ depicted in Figure 3.9

Number of free sub-bands	Probability Distribution			
	Mode and modal prob.	Mean	Variance	Support
N_{free}	15 (P = 0.2034)	14.8189	3.8205	7 - 22
$X_I(N)$	9 (P = 0.2710)	7.0424	3.6821	3 - 16
$X_{II}(N)$	2 (P = 0.2739)	2.6001	1.9035	0 - 8
$X_{III}(N)$	2 (P = 0.3065)	2.1762	1.6750	0 - 8
$X_{IV}(N)$	2 (P = 0.6206)	1.3860	0.2501	0 - 2
$X_V(N)$	0 (P = 0.6831)	0.3200	0.2239	0 - 2

Table 3.7: Probability distribution of N_{free} and $X_i(N)$ depicted in Figure 3.10

Number of free sub-bands	Probability Distribution			
	Mode and modal prob.	Mean	Variance	Support
N_{free}	24 (P = 0.2933)	24.1801	2.1900	19 - 29
$X_I(N)$	8 (P = 0.2271)	8.1872	3.8169	2 - 15
$X_{II}(N)$	0 (P = 0.8711)	0.1348	6.1286	0 - 3
$X_{III}(N)$	14 (P = 0.2058)	13.6783	9.3174	7 - 21
$X_{IV}(N)$	2 (P = 0.5885)	1.5831	0.2539	0 - 2
$X_V(N)$	0 (P = 0.9997)	0.4169	0.2539	0 - 2

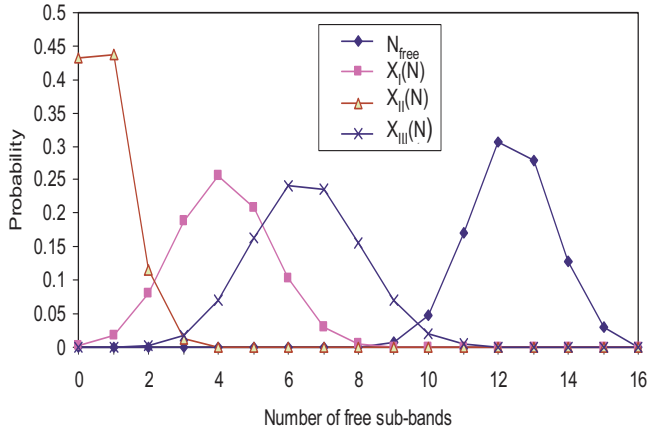

Figure 3.8: Comparison of probability distributions of N_{free} and $X_i(N)$, $i = I, II, III$ in a spectrum of 16 sub-bands

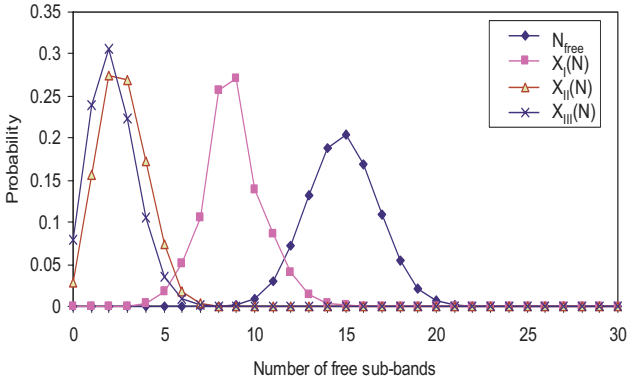

Figure 3.9: Comparison of probability distributions of N_{free} and $X_i(N)$, $i = I, II, III$ in a spectrum of 30 sub-bands with 5 small and 5 large sub-band free probabilities

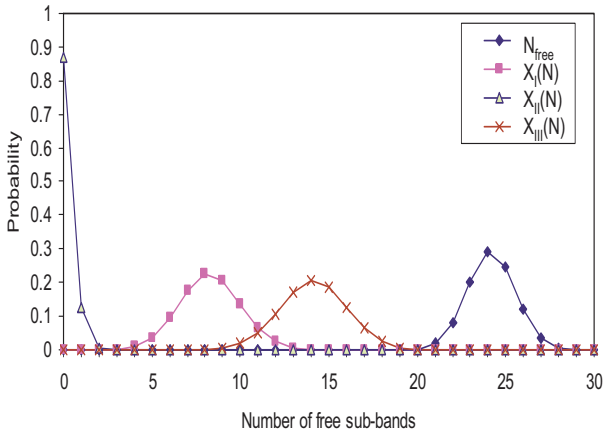

Figure 3.10: Comparison of probability distributions of N_{free} and $X_i(N)$, $i = I, II, III$ in a spectrum of 30 sub-bands with 2 small and 16 large sub-band free probabilities

Table 3.8: $[Mean \pm r * SD]$ intervals and probability of intervals

No. of free sub-bands	Mean and mean ± SD			
	Mean	$[Mean \pm \sigma]$, (p)	$[Mean \pm 2 * \sigma]$, (p)	$[Mean \pm 3 * \sigma]$, (p)
N_{free}	24.1801	[22, 25], (0.8185)	[21, 27], (0.9907)	[19 - 28], (0.9989)
$X_I(N)$	8.1872	[6, 10], (0.8433)	[4, 12], (0.9875)	[2, 14], (0.9987)
$X_{II}(N)$	0.1348	[0, 0], (0.8711)	[0, 1], (0.9943)	[0, 2], (0.9999)
$X_{III}(N)$	13.6783	[10, 16], (0.8691)	[7, 19], (0.9881)	[4, 22], (0.9991)

Table 3.9: Probability distribution of N_{free} and $X_i(N)$

Number of free sub-bands	Equal probability p = 0.857			
	Mode and modal prob.	Mean	Variance	Support
N_{free}	26 (P = 0.2034)	25.7100	3.6765	18 - 30
$X_I(N)$	6 (P = 0.1736)	5.8523	4.6434	0 - 15
$X_{II}(N)$	0 (P = 0.6095)	0.4899	0.4808	0 - 5
$X_{III}(N)$	18 (P = 0.2073)	17.6203	6.5298	6 - 21
$X_{IV}(N)$	2 (P = 0.5394)	1.4689	0.3901	0 - 2
$X_V(N)$	0 (P = 0.7699)	0.2451	0.2151	0 - 2

3.6.7 Statistical Analysis of $X_I(N)$

Since the spectrum associated with *Scenario-3* is preferable to the one under *Scenario-2*, we make an in-depth statistical analysis of the former spectrum. Note that this spectrum has 2 small and 16 large sub-band free probabilities. The distributions of N_{free} and $X_i(N)$, $i = I, II, III$ are shown in Figure 3.10. It seems that the distributions are nearly normal. To assess their normality, we calculate $[mean \pm i * SD]$, the probability mass of interval $[mean \pm i * SD]$, $i = 1, 2, 3$ for each of these distributions, where SD represents the standard deviation. These results are detailed in Table 3.8. If normality prevails, the probability masses carried by the intervals $[mean \pm i * SD]$, $i = 1, 2, 3$ are approximately 67%, 95%, and 99.9%, respectively.

Determination of the distribution of free sub-bands helps cognitive radio users to assess the range of numbers of free sub-bands with high probability which are available during spectrum sensing. The following are some of the highlights:

- N_{free}: The number of free sub-bands could be any number in the interval $[21, \cdots, 27]$ with more than 99% probability.
- $X_I(N)$: The number of free sub-bands could be any number in the interval $[6, \cdots, 10]$ with probability close to 85%.
- $X_{II}(N)$: A type II sub-band is very unlikely, i.e., around (87)%.

Table 3.10: Binomial distribution of N_{free} and $X_i(N)$

Number of free sub-bands	Equal probability p = 0.857		
	Mode	Mean	Variance
N_{free}	26	25.7100	3.6765
$X_I(N)$	6	5.8815	4.6461
$X_{II}(N)$	0	0.4907	0.4821
$X_{III}(N)$	18	17.6238	6.5310
$X_{IV}(N)$	2	1.4689	0.3901
$X_V(N)$	0	0.2451	0.2151

- $X_{III}(N)$: The number of free sub-bands is any number within the interval $[10, \cdots, 16]$ with (87)% probability.

- The distributions of free sub-bands of any type and any specific type are not normal. The actual distributions are narrower around the mean value than the normal distribution.

3.6.8 Special Case ($p_i = p_j$)

We use the algorithms developed for the special case of $p_1, p_2, \cdots, p_{30}$ equal to the mean of Beta (0.6, 0.1), as used in *Scenario-3*, i.e., p_i = 0.857. The mean, mode and variance of distributions of N_{free} and $X_i(N)$ stemming from our algorithms are depicted in Table 3.9. We have also shown in Section 3.5 that the distribution of each $X_i(N)$ is Binomial. Of course, the probability distribution of N_{free} is Binomial. For any Binomial distribution, formulae for its mode, mean and variance are available. These values are presented in Table 3.10. We see that the results of Table 3.9 match with those of Table 3.10, reflecting correctness of our algorithms.

3.7 Conclusion

In this chapter, we have done a probabilistic analysis of free and contiguous sub-bands in a cognitive radio network. The critical entity in our analysis is the distribution of total number of free sub-bands. As we have shown, the computation of the exact distribution of the total number of free sub-bands (i.e., N_{free}) is prohibitively time-consuming and an approach for efficient approximation is presented and analyzed. We label this approach as Poisson-normal approximation and the execution time is reasonable as indicated by the simulation. In addition, we focus on the analysis of contiguous sub-bands in characterizing five different types of free sub-bands. An algorithm is developed to compute the distribution of total number of sub-bands of each type. Once the probability distributions have been computed, we outline ways of selecting preferable section of the target spectrum.

Chapter 4

Hidden Markov Model in Spectrum Sensing

4.1 Introduction

Spectrum selection, proposed in the previous chapter, selects preferable sections of the spectrum for further sensing and detecting idle sub-bands. Sensing techniques exploit the information provided by the statistical analysis of historical data collected on such preferable sections of the spectrum.

The sub-band occupancy at any time instant can be considered as a state, which can be either free (unoccupied by a PU) or busy (occupied by a PU). The states of a sub-band are monitored over L consecutive time periods, where each time period is of a given time interval. Existing research [34]- [38] assume existence of a Markov chain, representing utilization of each sub-band by a PU over L time periods. However, to our best knowledge, this fundamental assumption has never been validated while ought to be done for each frequency band of interest. Further, the constituents of a Markov chain, namely, initial probability and transition matrix need to be estimated and then utilized in analytical modeling. In this chapter, we validate existence of a Markov chain by collecting real-time measurements [39] in the paging spectrum (928-948 MHz). While in this chapter, we focus on the paging spectrum, the same methodology can be applied to any other spectrum band.

Since the true states (occupancy by PUs in reality) of a sub-band are never known (i.e.,

hidden) to the CR, the authors of [34]- [37] have extended their idea of improvising the Hidden Markov model (HMM) for the spectrum sensing. One of the critical parameters of HMM is the set of emission probabilities [40], i.e., emission of an alphabet out of a set of alphabets by a hidden state. The authors have used well-known algorithms to predict the set of emission probabilities. In this chapter, we exploit a novel idea of defining the emission probabilities. Additionally, given the parameters of the HMM and error probabilities, obtaining the likelihood solution is faced with computational complexities. In this chapter, we use the Viterbi algorithm to reduce complexity. We assess the effectiveness of our method in predicting the true states of the sub-band by performing extensive simulations. The code for the Viterbi algorithm is developed and its usefulness is checked using simulations.

There are two possible cases. The first option is to deal with the situation when the parameters of the Hidden Markov model and error probabilities are known. Obtaining the likelihood solution is faced with computational difficulties which we overcome using the Viterbi algorithm. We assess the effectiveness of our method in predicting the true states of the sub-band by performing extensive simulations [41]. The second alternative is to deal with the situation when the parameters of Markov chain and the error probabilities are unknown. We employ Expectation-Maximization (EM) algorithm to estimate these parameters. A code for executing both the Viterbi algorithm and EM algorithm are provided and their usefulness is checked using simulations.

The rest of the chapter is organized as follows. Section 4.2 talks about the issues already dealt with in spectrum sensing and detection. Section 4.3 presents the system model using Markov Chain. Section 4.4 validates the assumption of Markov chain in spectrum occupancy by licensed users. Section 4.5 deals with the estimation of Hidden Markov Model parameters in probabilistic spectrum sensing. Section 4.6 deals with the underlying concepts of Viterbi algorithm and Expectation-Maximization algorithm required in predicting the path of the Hidden Markov Chain. Section 4.7 deals with the significance of Hidden Markov Models in probabilistic spectrum sensing. Section 4.8 evaluates our application of Hidden Markov Model approach for CR spectrum sensing in a Cognitive Radio Network (CRN) through simulation results. Finally, Section 4.9 draws the conclusion.

4.2 Related Work on Spectrum Sensing

In this section, we describe various avenues of work taken in the area of spectrum sensing, a primary role performed by a CR in the licensed bands. The work in [42] deals with an eigenvalue based sensing algorithm and employs a decision process approach based on the maximum and the minimum Eigen values for transformed covariance matrix obtained by sampling and filtering the received signal. The simulation results [42] indicate minimal signal-to-noise ratio (SNR), much below than the probability of false alarm and mis-detection. But, the algorithm accuracy in a real scenario, has never been dealt with. Fast Fourier Transform (FFT)-based pilot sensing algorithm discussed in [43] detects pilot signal in ATSC Vestigial Sideband (VSB) television signals. Varying length FFTs are utilized based on limiting the sensing period in a chosen sensing window. The squared FFT output is compared with a predetermined threshold value that relates to the desired probability of false alarm. The concept of a Frequency-Phase Locked Loop (FPLL) is introduced in [44] where the convergence of the results in two frequency tracking blocks are compared, even at lower SNR values of the ATSC VSB television signal. Numerous signal processing techniques have been used in [45]- [48]. Spectral correlation method [45] is used to compare the spectral components of the received signal with the pre-stored values of spectral information for NTSC or DTV signals. If the value of the received spectral component is higher than the predetermined value, this method declares the presence of a NTSC or a DTV signal. Similar technique is used in [45] to detect wireless microphones as the PUs. The cyclostationary feature of the ATSC television signals has been exploited in [46] since this feature distinctly identifies desired signal from noise as Gaussian noise does not possess this characteristic. The authors in [46] used spectrum sensing techniques in detecting peaks of the cyclic spectrum in the received signal to decide the presence of the ATSC signals. Finally, the authors in [47] and [48] use similar concepts of computing covariance matrix and maximum and minimum Eigenvalues to detect the ATSC television signals as well as wireless microphones.

In [45]- [48], instead of focusing on the percentage accuracy of detection by a CR, the authors focus on the efficiency of their spectrum sensing algorithms based on the parameters like sensing period and the sensitivity of incumbent detection at lowest possible SNR

values. Our research work focuses on the following aspects of spectrum sensing:

• Adapt the Viterbi algorithm to find the likelihood solution to the prediction of true states problem with the knowledge of the probability of false alarm and mis-detection and compute the percentage prediction accuracy in sub-band availability sensing and detection of PUs

• The authors in [38] assume Markovian model while considering the scenario of availability of PUs in a certain sub-band. Any Markov model requires a-priori knowledge of the initial probability distribution of states and all possible transitions. In the worst case, these parameter values may be unknown to the CR. We have addressed the estimation problem using the Expectation-Maximization algorithm and evaluate the efficiency of the EM algorithm by estimating the unknown parameters needed for the Markovian model.

4.3 System Model and Problem Formulation

The configuration of our proposed spectrum sensing model for a specific sub-band is shown in Figure 4.1. The same model can be applied for several sub-bands in an operating spectrum. Power measurements are collected for a sub-band over regular time intervals (in seconds) spanning an observation period (typically, hundreds of seconds). These measurements transformed into binary occupancy data Y serve as the historic data for offline reference by the CR as shown in Figure 4.1. Based on retrieved measurements, CR is trained to perform a validation check to ensure Markovian property of spectrum occupancy by PUs over time for the sub-band under consideration. If the sub-band occupancy follows a Markov chain, associated parameters are estimated. Simultaneously, the CR also senses the spectrum, using any of the existing spectrum sensing techniques [42] - [48], for PU occupancy and passes this information X to the HMM block. With this information under the purview of HMM, the Viterbi algorithm generates the predicted results. This predicted output $X^{'}$, as well as the output X generated by the CR, can now be compared with the actual PU occupancy Y to scutinize the efficiency of our proposed prediction mechanism. The details of each block is illustrated in the following sections.

We define an observation period $\tau = \{1, 2, \cdots, \mathcal{T}\}$, where each i in τ represents the i^{th}

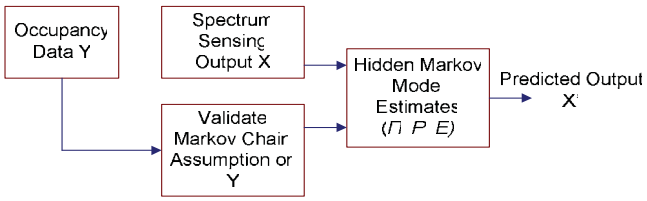

Figure 4.1: The system model implemented for enhanced spectrum sensing.

sensing duration. We also define a sequence $Y = \{y_1, \cdots, y_{\mathcal{T}}\}$, which represents the true states of the sub-band in the corresponding time periods. The entity y_i=1 if the sub-band is free at the i^{th} time instant and y_i=0 otherwise. The CR output generated by a sensing mechanism is represented by a sequence $X = \{x_1, \cdots, x_{\mathcal{T}}\}$ of sensed states in the corresponding time periods. The entity $x_i = 1$ if the state of the sub-band is sensed to be free at the i^{th} sensing slot and $x_i = 0$ otherwise. The sequence X represents the prediction of the true state sequence $Y = \{y_1, \cdots, y_{\mathcal{T}}\}$.

In practice, the true state sequence Y is unobservable. Collecting real-time measurements is laborious, time-consuming and expensive. Hence, various sensing mechanisms [42] - [48] have been proposed to monitor the utilization of a sub-band. The results of these sensing mechanisms gives rise to the sensed sequence X as described earlier. The readings provided by the sensing mechanisms are prone to errors of order of about 10%, namely the mis-detections and false-alarms [38]. More formally, the error probabilities are expressed as $Pr(x_i = 1|y_i = 0)$ for the probability of mis-detection and $Pr(x_i = 0|y_i = 1)$ for the probability of false-alarm. Our research work is an endeavor of enhancing the sensing accuracy of any sensed state sequence X obtained from a sensing mechanism under the assumption that the true state vector Y and predictor X are governed by a Hidden Markov model.

4.4 Markov Chain Modeling of True States and its Validation

The sub-band occupancy by a PU in any time slot is not predictable and thus taken to be random. As an example, Wyglinski *et al.* [10] monitored the paging band with center frequencies at 929.04 MHz and 929.56 MHz over 500 consecutive time slots using two patch antennas and the power patterns shown in Figure 4.2(a) and (b) are observed on a spectrum analyzer. If the power ≥ -70 dBm, it signifies that the sub-band is used by its PU and power below -70 dBm implies that the sub-bad is free.

The sequence Y is modeled as a Markov chain, which is characterized by an initial distribution $\pi = (p_0, p_1)$ and one-step transition matrix $P = (p_{ij})_{(2\times 2)}$, $i, j \in S$. More formally, $Y = y_1, y_2, \cdots, y_{\mathcal{T}}$ is a Markov chain with state space $S = \{0, 1\}$, the distribution of y_1 is π and

$$\begin{aligned} Pr(y_n = j | y_1 = i_1, \cdots, y_{n-2} = i_{n-2}, y_{n-1} = i \\ &= Pr(y_n = j | y_{n-1} = i), \\ &= p_{ij}. \end{aligned} \tag{4.1}$$

for every $i_1, i_2, \cdots, i_{n-2}, i, j \in S$ and $2 \geq n \leq \mathcal{T}$.

These stipulations gives the joint distribution of $y_1, y_2, \cdots, y_{\mathcal{T}}$ and is expressed as:

$$Pr(y_1 = i_1, y_2 = i_2, \cdots, y_{\mathcal{T}} = i_{\mathcal{T}}) = p_{i_1} p_{i_1 i_2} p_{i_2 i_3} \cdots p_{i_{\mathcal{T}-1} i_{\mathcal{T}}} \tag{4.2}$$

for all $i_1, i_2, \cdots, i_{\mathcal{T}} \in S$.

4.4.1 Markov Chain Assumption Validation

Previous research works have considered that the spectrum occupancy by the PUs follows a Markov chain model. This assumption is substantiated with results obtained from the real-time measurements while experiments have been conducted on the paging band (928 MHz to 948 MHz) as shown in Figure 4.2. The details of the measurement set-up is in Section 2.2.

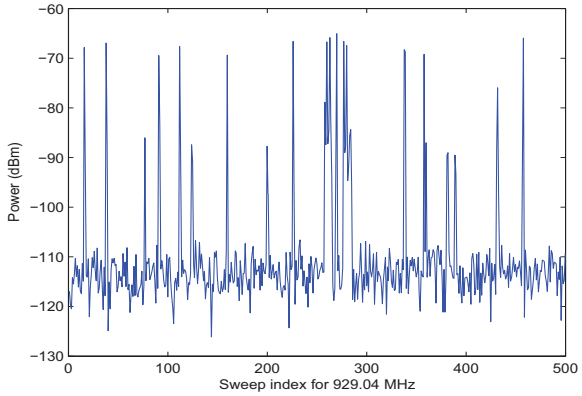

(a) Power pattern observed on a paging band with center frequency 929.04 MHz.

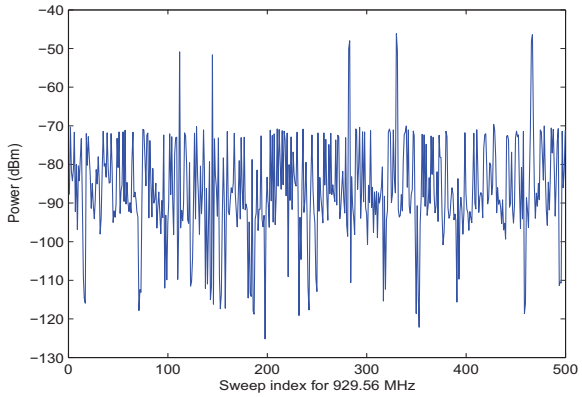

(b) Power pattern observed on a paging band with center frequency 929.56 MHz.

Figure 4.2: Power measurements obtained from paging bands over 500 time periods.

Table 4.1: Statistical parameters of Estimation

Freq. (MHz)	Estimation Statistics (%)				
	Min	Max	I Quartile	III Quartile	Mean
929.04	89	100	95	97	95.7230
929.06	83	98	90	93	91.2740
929.08	84	98	90	93	91.2090
929.10	83	97	90	93	91.2660
929.56	91	99	95	97	95.8170

To show that the Markov chain model fits well with the PU occupancy, we followed a cross-validation technique. First, we defined a hard threshold of -70 dBm for the power values obtained from the experiment. Now for each observation period, ranging from 1 to 500, we decided whether the power value is higher (state is 0) or lower (state is 1) than the defined threshold. Once we have the states over the observation period of 500 durations, we extract the probabilities required to obtain the transition matrix of the Markov chain using the first 400 readings. Now, we would estimate the remaining 100 states using the transition matrix parameter. Since we conducted the experiment for one day, the initial distribution of the paging bands are not available. Hence, we assumed that out of the 100 readings, the first reading, i.e., the 401^{th} power measurement is known to us. With this information, and the extracted transition matrix from the previous 400 readings, we estimated the remaining 99 states for each paging band. The statistical parameters of our estimation are provided in Table 4.1. The histogram plots of estimation for two frequency bands are shown in Figure 4.3 over 1000 iterations.

4.5 HMM Parameter Estimation

The key idea in this chapter is to introduce a HMM in representing the evolution of occupancy/non-occupancy of a sub-band by its PU over time and measurements of the CR. In this section, we outline the basic operational system of an HMM and then bring the model under the purview of CR.

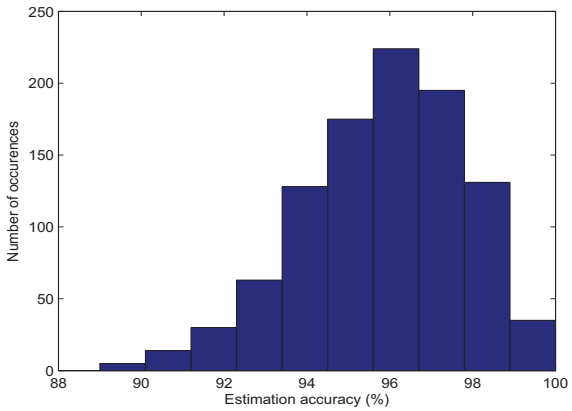

(a) Depiction of estimation accuracy of states in paging band (929.04 MHz).

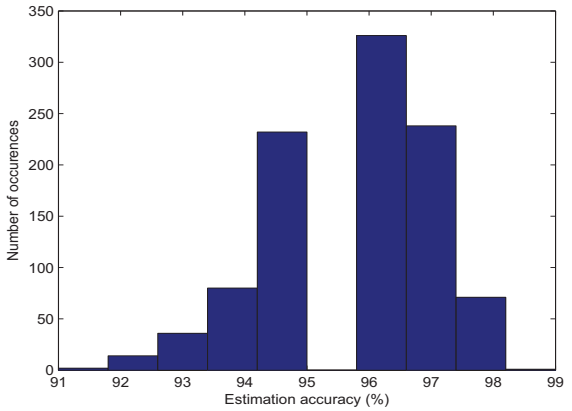

(b) Depiction of estimation accuracy of states in paging band (929.56 MHz).

Figure 4.3: Estimation accuracy of our Markov chain model over paging bands for 99 observation periods performed over 1000 iterations.

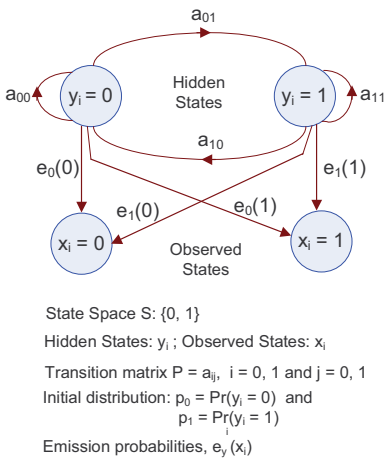

Figure 4.4: Hidden Markov model representation in spectrum sensing

An HMM is composed of two stochastic processes $Y_1, Y_2, \cdots$ and $X_1, X_2, \cdots$ with the following properties.

1. The process $Y_1, Y_2, \cdots$ is a Markov chain with finite state space S, π defined in the previous section.

2. The process $X_1, X_2, \cdots$ takes values in the alphabet space A = $\{1, 2, \cdots, m\}$. The conditional distribution of $X_1, X_2, \cdots, X_n | Y_1, Y_2, \cdots, Y_n$ is governed by an *emission matrix* $E = (e_j(i))_{m \times k}$, which has the following properties:

In the context of spectrum sensing, the true states Y of sub-band occupancy are never observable and are needed to be sensed using different sensing techniques. Hence, the Markov chain, constituting the true sequence Y, is hidden and the name for this type of model is *hidden Markov model* [40], [49]. A HMM is a stochastic process created by two interrelated probabilistic functions. One of these functions is the above mentioned Markov chain with a finite number of states. The other is a set of random functions, referred to as the *alphabet*, wherein each function generates a *symbol* related to a state in the Markov chain.

The general concept of HMM is illustrated in Figure 4.4. A system over discrete time $1, 2, 3, \cdots$ is moving stochastically from one state to another with states from a defined

state space S. Let Y_n be the state in which the system is in at time n. The process is assumed to be Markovian. The evolution of the sequence $Y_1, Y_2, \cdots$ is hidden. However, the hidden sequence can be represented by a sequence of symbols from the alphabet $\Omega = \{0, 1, 2, \cdots, N\}$. A state k can produce a symbol b from a distribution over all possible symbols $b = 0, 1, \cdots, N$ and its probability can be represented as:

$$e_k(b) = Pr(X_n = b|Y_n = k). \tag{4.3}$$

These probabilities are known as *emission probabilities* as shown in Figure 4.4. The system in state i can emit any one of the symbols from the alphabet with the following distribution:

$$\begin{aligned} State\ of\ the\ system &: i,\ \ i = 0, 1, 2, \cdots, M \\ Alphabet &: 0 \quad 1 \quad 2 \quad \cdots \quad N \\ Emission\ probability &: e_i(0)\ e_i(1)\ e_i(2)\ \cdots \quad e_i(N). \end{aligned}$$

Let X_n be the emitted symbol by the system at time n. The process $X_1, X_2, \cdots$ is independent with each X_n taking values $0, 1, 2, \cdots, N$ with the following distribution:

$$\begin{aligned} Pr(X_n = b|Y_n = i) &= e_i(b), \\ b &= 0, 1, 2, \cdots, N, and \\ i &= 0, 1, 2, \cdots, M. \end{aligned}$$

The process $X_1, X_2, \cdots$ is observable. Based on the observed process, the hidden sequence can be estimated, either by finding the most likely one, or alternatively by using a-posteriori distributions over states [40].

The output of spectrum sensing is now formulated on the basis of the generic HMM defined above. The hidden sequence is the sub-band occupancy sequence $Y = Y_1, \cdots, Y_{\mathcal{T}}$, the observed sequence $X_1, \cdots, X_{\mathcal{T}}$ is the sequence of decisions generated by the sensing technique used by a SU. In the spectrum sensing HMM, the challenge lies in framing emission probabilities which has precise correlation with output of any spectrum sensing technique. Once the emission probabilities are computed, *maximum likelihood* approach [40] can be adopted to estimate the hidden sequence Y.

Our research work emphasize on the following steps:

- Develop emission probabilities;
- Correlate these probabilities with a spectrum sensing technique; and
- Estimate the hidden sequence Y using maximum likelihood approach.

Once the sensed sequence is obtained from a sensing technique, the maximum likelihood approach calculates probabilities of all possible sub-band occupancy sequences, i.e., the joint occurrence of the sensed sequence and the occupancy sequence. This joint occurrence of both the sequences is interpreted as the joint distribution of the two sequences. The maximum likelihood approach consists of the following procedure:

- *Step 1*: Compute the joint distribution of the sensed sequence $x = X_1 = x_1, X_2 = x_2, \cdots, X_{\mathcal{T}} = x_{\mathcal{T}}$ and a possible sub-band occupancy sequence $y = Y_1 = y_1, Y_2 = y_2, \cdots, Y_{\mathcal{T}} = y_{\mathcal{T}}$;
- *Step 2*: Compute joint distributions for all possible sub-band occupancy sequences; and
- *Step 3*: Find the distribution which gives the maximum probability and the corresponding sub-band occupancy sequence is the estimate of the true sub-band occupancy.

We define $P(x; y)$ as the the joint distribution of the sequence x generated by the spectrum sensing technique and the occupancy sequence y. The joint distribution can be written as:

$$
\begin{aligned}
&Pr(x; y) \\
&\quad = Pr(x_1, x_2, \cdots, x_{\mathcal{T}}; y_1, y_2, \cdots, y_{\mathcal{T}}) \\
&\quad = Pr(\textit{getting the data } x \textit{ under the path } y) \\
&\quad = [Pr(Y_1 = y_1) Pr(X_1 = x_1 | Y_1 = y_1)] \times \\
&\qquad [Pr(Y_2 = y_2 | Y_1 = y_1) Pr(X_2 = x_2 | Y_2 = y_2)] \times \\
&\qquad [Pr(Y_3 = y_3 | Y_2 = y_2) Pr(X_3 = x_3 | Y_3 = y_3)] \times \cdots \\
&\qquad [Pr(Y_{\mathcal{T}} = y_{\mathcal{T}} | Y_{\mathcal{T}-1} = y_{\mathcal{T}-1}) Pr(X_{\mathcal{T}} = x_{\mathcal{T}} | Y_{\mathcal{T}} = y_{\mathcal{T}})].
\end{aligned}
\tag{4.4}
$$

Using notations for transition probability and emission probability defined in Eqs. (4.1) and (4.2), Eq. (4.4) can be further written as:

$Pr(x; y)$

$$\begin{aligned} &= [p_{y_1} e_{y_1}(x_1)] \times [a_{y_1 y_2} e_{y_2}(x_2)] \times \cdots \times [a_{y_{\mathcal{T}-1} y_{\mathcal{T}}} e_{y_{\mathcal{T}}}(x_{\mathcal{T}})]. \\ &= p_{y_1} \times \Pi_{i=1}^{\mathcal{T}} a_{y_i y_{i+1}} e_{y_i}(x_i). \end{aligned} \tag{4.5}$$

Eq. (4.5) shows that the probability $P(x; y)$ can be computed if the initial distribution, transition matrix, and emission probabilities are known. The occupancy sequence $Y_1 = y_1^*, Y_2 = y_2^*, \cdots, Y_{\mathcal{T}} = y_{\mathcal{T}}^*$, which maximizes $P(x; y)$ over all paths y, is the path y^* we seek. The predicted path $y^* = (y_1^*, y_2^*, \cdots, y_{\mathcal{T}}^*)$ is called the *maximum likelihood sequence*.

For a given data x, the likelihood prediction of the underlying path of the Hidden Markov chain requires computation of the joint probability $P(x; y)$ for every possible path y of length $\mathcal{T}$. Even for moderate values of $\mathcal{T}$, the set of all possible paths is astronomically large. For example, if $\mathcal{T} = 100$ and $M = 1$, the number of paths is 2^{100}, which is incomprehensible to handle. The computational complexity of the likelihood approach involves $2^{\mathcal{T}} \times (2\mathcal{T})$ multiplications. Computation time required to find the maximum likelihood sequence on a Intel 3.2 GHz processor with $1GB$ RAM is 21.303348 seconds for $\mathcal{T} = 10$, 86.221069 seconds for $\mathcal{T} = 12$, and 373.666768 seconds for $\mathcal{T} = 14$ for $10,000$ iterations.

4.6 Viterbi Algorithm and the Expectation Maximization Algorithm

4.6.1 Viterbi-based Sensing Algorithm

Viterbi-based sending algorithm is developed that uses a dynamic programming to find the optimal path, exploiting the structure of the relationship between various $P(x; y)$s. The basic idea is to successively compute $P(x; y)$ for $L = 1, 2, 3, \cdots$.

Step 1: Initialization:

$$\begin{aligned} L &= 1, \\ Data &: x_1, \end{aligned}$$

$$\begin{aligned} Compute\ v_i(1) &= p_i \times e_i(x_1), \\ ptr_1(i) &= i,\ \ i = 0, 1, 2, \cdots, M. \end{aligned}$$

• Step 2: Recursion:

$$\begin{aligned} L &= 2, \\ Data &: x_1, x_2. \end{aligned}$$

Determine the optimal path $y = (y_1, y_2)$ with $y_2 = 0$. For this, compute the following:

$$\begin{aligned} P(x_1, x_2; 0, 0) &= [p_0 \times e_0(x_1)][a_{00} \times e_0(x_2)] \\ P(x_1, x_2; 1, 0) &= [p_1 \times e_1(x_1)][a_{10} \times e_0(x_2)] \\ \cdots &\quad \cdots\cdots \\ P(x_1, x_2; M, 0) &= [p_M \times e_M(x_1)][a_{M0} \times e_0(x_2)]. \end{aligned}$$

For the optimal $y = (y_1, 0)$, we compute:

$$\begin{aligned} v_0(2) &= max\ \{P(x_1, x_2; i, 0) :\ 0 \le i \le M\} \\ &= e_0(x_2)\ max\ \{p_i e_i(x_1) a_{i0} :\ 0 \le i \le M\} \\ &= e_0(x_2)\ max\ \{v_i(1) a_{i0} :\ 0 \le i \le M\}. \\ ptr_2(0) &= argmax\ \{v_i(1) a_{i0} :\ 0 \le i \le M\}. \end{aligned}$$

For the optimal path $y = (y_1, y_2)$ with $y_2 = j$, compute the following:

$$\begin{aligned} v_j(2) &= e_j(x_2)\ max\{v_i(1) a_{ij} :\ 0 \le i \le M\}\ and \\ ptr_2(j) &= argmax\ \{v_i(1) a_{ij} :\ 0 \le i \le M\},\ \ j = 0, 1, 2, \cdots, M. \end{aligned}$$

• Step 3:

$$\begin{aligned} L &= 3 \\ Data &: x_1, x_2, x_3. \\ Compute & \\ v_j(3) &= e_j(x_3)\ max\{v_j(2) a_{ij} :\ 0 \le i \le M\}\ \ and \\ ptr_3(j) &= argmax\{v_j(2) a_{ij} :\ 0 \le i \le M\},\ \ j = 0, 1, 2, \cdots, M. \end{aligned}$$

Continue the same computations for $(L-1)$-th step. Finally the L-th step is executed as follows:

• Step L

$$\begin{aligned} Data \quad &: \quad x_1, x_2, \cdots, x_L \\ Compute & \\ v_j(L) \quad &= \quad e_j(x_L)\, max\{v_i(L-1)a_{ij} : \ 0 \le i \le M\} \ \ and \\ ptr_L(j) \quad &= \quad argmax\{v_i(L-1)a_{ij} : \ 0 \le i \le M\}, \quad j = 0, 1, 2, \cdots, M. \end{aligned}$$

• Termination step:

For the optimal path $y^* = (y_1^*, y_2^*, \cdots, y_L^*)$, calculate:

$$\begin{aligned} P(x; y) \quad &= \quad max\{v_j(L) : \ 0 \le j \le M\}, \\ y_L^* \quad &= \quad argmax\{v_j(L) : \ 0 \le j \le M\}, \\ y_{L-1}^* \quad &= \quad ptr_L(y_L^*), \\ y_{L-2}^* \quad &= \quad ptr_{L-1}(y_{L-1}^*), \\ \cdots \quad &\quad \cdots \\ y_1^* \quad &= \quad ptr_2(y_2^*). \end{aligned}$$

4.6.2 Expectation Maximization Algorithm

When the initial distribution, transition matrix, and emission probabilities are known, Viterbi algorithm can be employed to determine the optimal (likelihood) hidden path. Now, we consider the case when the underlying parameter values are unknown. The only information we have is the data $x = (x_1, x_2, \cdots, x_L)$. Following the paradigm of EM algorithm, we outline a method for estimating the unknown parameters. For a general exposition on EM algorithm, see [50].

• Step 1:

$$\begin{aligned} & Initial\ guesses \\ Initial\ distribution \quad &: \quad p^{(1)} = (p_0^{(1)}, p_1^{(1)}, \cdots, p_M^{(1)}) \\ Transition\ matrix \quad &: \quad P^{(1)} = (a_{ij}^{(1)}) \end{aligned}$$

Simulate the Markov chain to get a path $y_1^{(1)}, y_2^{(1)}, \cdots, y_L^{(1)}$ of length L.

• Step 2: Estimate the emission probabilities using the data and the simulated path as follows:

$$\begin{aligned} e_i^{(1)}(k) &= \frac{\#\{1 \le s \le L, 1 \le r \le L : x_s = k, y_r^{(1)} = i\}}{\#\{1 \le r \le L : y_r^{(1)} = i\}}, \\ k &= 0, 1, 2, \cdots, N, \\ i &= 0, 1, 2, \cdots, M. \end{aligned}$$

Since $e_i(k)$ is the conditional probability of emitting Letter k, given that the system is in State i, we count how many times the State i has occured along the path $(y_1^{(1)}, y_2^{(1)}, \cdots, y_L^{(1)})$. Among these tagged i's, we count how many times the Letter k occurs in the data $x_1, x_2, \cdots, x_L$. The ratio of these two counts is an estimate of $e_i(k)$.

• Step 3: Use the Viterbi algorithm to determine the optimal path $y^{(2)} = (y_1^{(2)}, y_2^{(2)}, \cdots, y_L^{(2)})$ using $p^{(1)}$, $P^{(1)}$ and $e_i^{(1)}(k)$s.

• Step 4: Using the path $y^{(2)}$, estimate the initial distribution $p^{(2)} = (p_0^{(2)}, p_1^{(2)}, \cdots, p_M^{(2)})$ and the transition matrix $P^{(2)} = (a_{ij}^{(2)})$.

Addendum:

The estimation proceeds in the standard way. More specifically,

$$\begin{aligned} p_i^{(2)} &= \frac{\#\{1 \le r \le L : y_r^{(2)} = i\}}{L}, \ \ i = 0, 1, 2, \cdots, M, \ \ \textit{and} \\ a_{ij}^{(2)} &= \frac{\textit{Number of one} - \textit{step transitions } y_r^{(2)} = i \textit{ and } y_{r+1}^{(2)} = j}{\textit{Number of one} - \textit{step transitions } y_r^{(2)} = i \textit{ and } y_{r+1}^{(2)} = s, \ \ 0 \le s \le M}, \\ & \textit{for } i = 0, 1, 2, \cdots, M \quad \textit{and} \quad j = 0, 1, 2, \cdots, M. \end{aligned} \tag{4.6}$$

• Step 5: Using the path $y^{(2)}$ and data x, estimate the emission probabilities $e_i^{(2)}(k)$s as in Step 2.

• Step 6: Use the Viterbi algorithm to determine the optimal path $y^{(3)} = (y_1^{(3)}, y_2^{(3)}, \cdots, y_L^{(3)})$ using $p^{(2)}$, $P^{(2)}$ and $e_i^{(2)}(k)$s.

Steps 4, 5, and 6 are repeated until each absolute difference of corresponding estimate ≤ 0.0001. The final set of parameter values are the desired estimates.

4.7 Hidden Markov Model in Spectrum Sensing

Spectrum sensing is a vital part of the dynamic spectrum access needed by the CR users. The SUs need to sense whether a particular sub-band is free for its communication or is currently being used by a PU. The possible states can be either a used sub-band (considered as 0 in our model) or a free sub-band (considered as 1 in our model). The general notation used in Section 4.3, M is 1. These states are monitored for a finite duration of time (24 hours), at intervals of 15 minutes. The transition of states between two adjacent intervals are assumed to be stochastically dependent. To be specific, we assume one-step memory model, also known as the Markov model, i.e., the current state of the sub-band is dependent only on the previous state and not on the other earlier states.

Now, to utilize the Markov model in spectrum sensing, we need two sets of parameters: *(i)* initial distribution, and *(ii)* transition matrix for all possible states. These two sets are not usually available in the context of CRN, but can be determined by adopting a learning process over an extensive time period. In this work, we study variations in the prediction accuracy of sensing when these two sets of parameters are changed.

Design of the emission probability matrix required for the hidden Markov model is more intriguing and demands the knowledge of the 802.22 standard [51]. The Dynamic Frequency Selection model imposed by the Federal Communications Commission (FCC) in the 5 GHz band [51], the *probability of detection* $(1 - \delta)$ is 90% when the PUs are either wireless phones or TV broadcasting. From the sensing perspective, this implies that the State 0 is detected correctly (State 0) for 90% of the time. Hence, the *probability of mis-detection* δ is only 10%. Similarly, the *probability of false alarm* ϵ is 10% for both wireless microphone and TV user incumbents (PUs in our context). Again, from the sensing perspective, the SUs can make an erroneous decision of a free sub-band (State 1) being declared as used by a PU (State 0). Now, we need to analyze their significance in terms of emission probability discussed in the previous section.

In the terminology of a Hidden Markov model, the letter space is $\Omega = \{0, 1\} = S$. The emission probabilities now acquire special significance.

$$e_0(0) \quad = \quad Pr(Cognitive\ radio\ identifies\ the\ state\ to\ be\ 0 \mid True\ state\ is\ 0)$$

Table 4.2: Emission Probability for Spectrum Sensing

Observed States	True States	
	0	1
0	$(1-\delta) = 0.9$	$\epsilon = 0.1$
1	$\delta = 0.1$	$(1-\epsilon) = 0.9$

$$
\begin{aligned}
&= 1-\delta; \\
e_0(1) &= Pr(Cognitive\ radio\ identifies\ the\ state\ to\ be\ 1 \mid True\ state\ is\ 0) \\
&= \delta; \\
e_1(0) &= Pr(Cognitive\ radio\ identifies\ the\ state\ to\ be\ 0 \mid True\ state\ is\ 1) \\
&= \epsilon; \\
e_0(0) &= Pr(Cognitive\ radio\ identifies\ the\ state\ to\ be\ 0 \mid True\ state\ is\ 0) \\
&= 1-\epsilon. \qquad (4.7)
\end{aligned}
$$

Here, the true state represents the actual scenario which is never known to a SU and an observed state depicts the sensed or detected scenario by a SU. As per the 802.22 standard, SU is supposed to sense the presence of a PU in the sub-band with 90% efficiency. This can be interpreted as the emission probability $e_0(0)$ of State 0 (the observed state = 0) when the PU is using the sub-band (true state = 0) is 0.9. Therefore, the emission probability $e_0(1)$ of State 1 (observed state = 1) when the true state is 0 is 0.1. Again, based on the 802.22 standard, the emission probability $e_1(1)$ of State 1 when the true state is 1 is 0.9. It is better explained in Table 4.1 below, with the true states run across the top row and the observed states are indicated in the left-most column.

With the initial distribution, transition matrix and the emission probability matrix, we can apply the Viterbi algorithm to predict the actual scenario of the availability of a particular sub-band over time and study the percentage accuracy in spectrum sensing. The additional information needed for the Viterbi algorithm by the SU is the observed sequence which is detected or sensed sequence of the availability of the sub-band over time. The percentage accuracy of the Viterbi algorithm is examined in the next section.

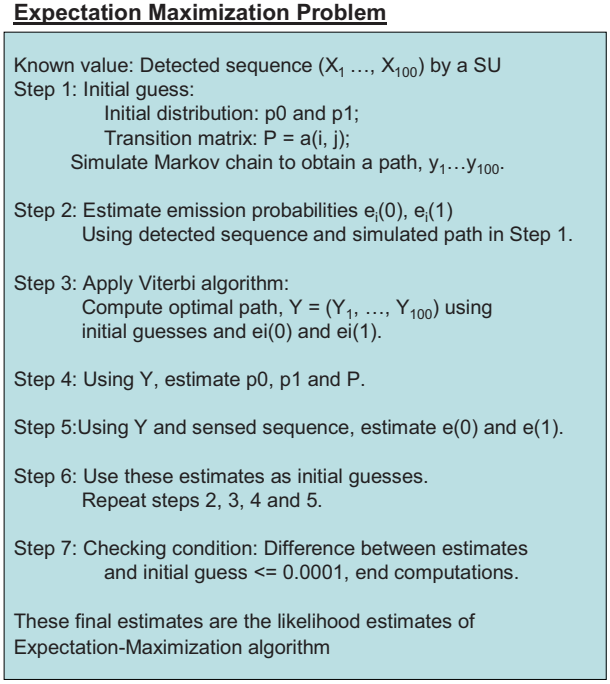

Figure 4.5: Expectation-maximization algorithm for estimating parameter values

However, the initial distribution, transition matrix and the emission probability matrix are not known in practice. The sensed sub-band availability sequence by the SU is the only information available. In such a case, we can apply the EM algorithm within the sensed sub-band sequence by estimating the initial distribution, transition matrix and emission probability matrix. A detailed general description of the EM algorithm was given in Section 4.4. The EM algorithm for estimation tailored to our needs is explained in Figure 4.5.

4.8 Validation and Simulation Results

In this section, we conduct some empirical studies of percentage accuracy of the Viterbi algorithm. The specifications are:
We have considered three cases to substantiate our validation and percentage accuracy of the Viterbi algorithm.

Case I:

$$Transition\ matrix\ P = \begin{pmatrix} 0.3 & 0.7 \\ 0.2 & 0.8 \end{pmatrix}.$$

Case II:

$$Transition\ matrix\ P = \begin{pmatrix} 0.4 & 0.6 \\ 0.6 & 0.4 \end{pmatrix}.$$

Case III:

$$Transition\ matrix\ P = \begin{pmatrix} 0.5 & 0.5 \\ 0.5 & 0.5 \end{pmatrix}.$$

The initial distribution for each case is determined by the following steady-state equation:

$$\begin{aligned} (p_0, p_1) \times P &= (p_0, p_1), \\ p_0 + p_1 &= 1. \end{aligned} \tag{4.8}$$

Emission probability matrix is specified in Table 4.2.

We have simulated the Viterbi algorithm under two different scenarios:
Scenario 1 : $\delta = 0.05$ and $(1 - \epsilon) = 0.95, 0.9, 0.85$ and 0.8, and
Scenario 2 : $\epsilon = 0.05$ and $(1 - \delta) = 0.95, 0.9, 0.85$ and 0.8.

In the simulation work under each case, the initial distribution and transition matrix are fixed.

• Step 1 : Using the initial distribution and transition matrix, simulate the Markov chain of length $L = 100$, leading to a path $y_1, y_2, \cdots, y_{100}$.

• Step 2 : Under each scenario for each choice of ϵ and δ, generate data $x_1, x_2, \cdots, x_{100}$ using the simulated path $y_1, y_2, \cdots, y_{100}$.

• Step 3 : Apply the Viterbi algorithm detailed in Section 4.4 to the data $x_1, x_2, \cdots, x_{100}$ to predict the underlying path as $y_1^*, y_2^*, \cdots, y_{100}^*$.

• Step 4 : Calculate prediction accuracy (PA) by:

$$PA = \frac{\#\{1 \le i \le 100 : y_i^* = y_i\}}{100} \times 100. \tag{4.9}$$

Repeat Step 1 to 4 for 10,000 times. The histogram of these PA percentages are as shown in Figure 4.6 (Scenario 1) and Figure 4.7 (Scenario 2) and also for different cases

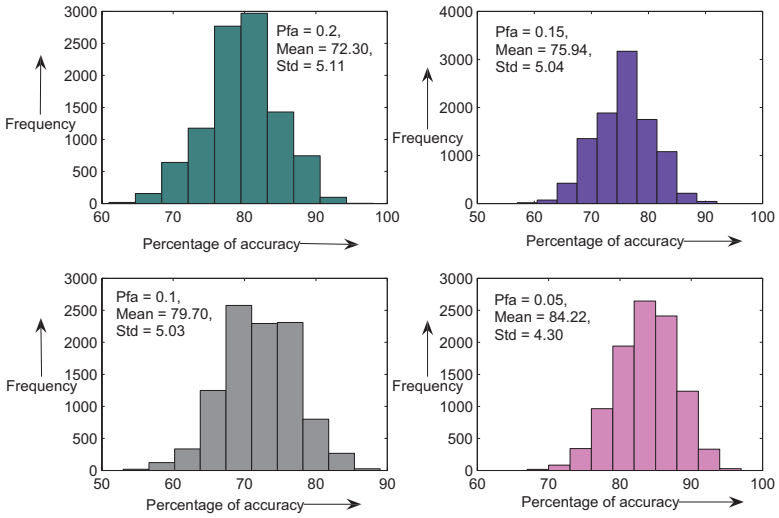

Figure 4.6: Frequency distribution of prediction accuracy percentage of the Viterbi algorithm with mis-detection probability (Pmd) $\delta = 0.05$ and false alarm probability (Pfa) ϵ specified in the inset of each histogram (Case I, Scenario 1)

shown in Figure 4.8 and Figure 4.9. The corresponding normal approximation curves are given in Figure 4.10 and Figure 4.11.

Under scenario 1 shown in Figure 4.6 ($\delta = 0.05$ and $\epsilon = 0.05, 0.1, 0.15, 0.20$), the prediction accuracy decreases as ϵ is increased. The standard deviation (Std) of accuracy is more or less stable around 5.0. For the chosen initial distribution and transition matrix, there will be high propensity of true state being 1 in the path generated by the Markov chain and transitions 0 to 1 and 1 to 1 are much more common. If the false alarm (reading 1 as 0) probability increases, the accuracy also decreases.

Under scenario 2 shown in Figure 4.7 ($\epsilon = 0.05$ and $\delta = 0.05, 0.1, 0.15, 0.2$), the prediction accuracy is more or less stable around 76% and the standard deviation of accuracy is also stable around 4.98. It is less frequent to have the State 0 in the path generated by the Markov chain and the percentage mis-readings (reading 0 as 1) do remain stable. The histograms are well-approximated by the normal curves shown in Figures 4.10 and 4.11. The Central Limit Theorem seems to be playing a major role in this situation.

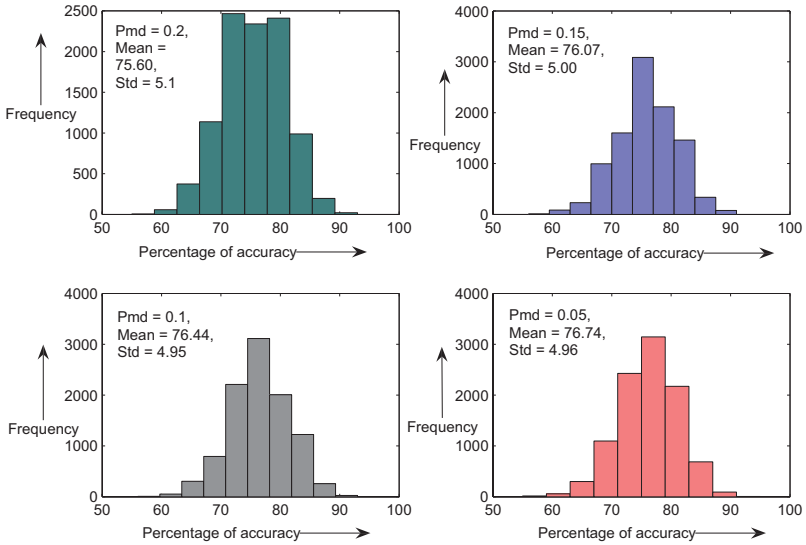

Figure 4.7: Frequency distribution of prediction accuracy percentage of the Viterbi algorithm with $\epsilon = 0.05$ and δ specified in the inset of each histogram (Case I, Scenario 2)

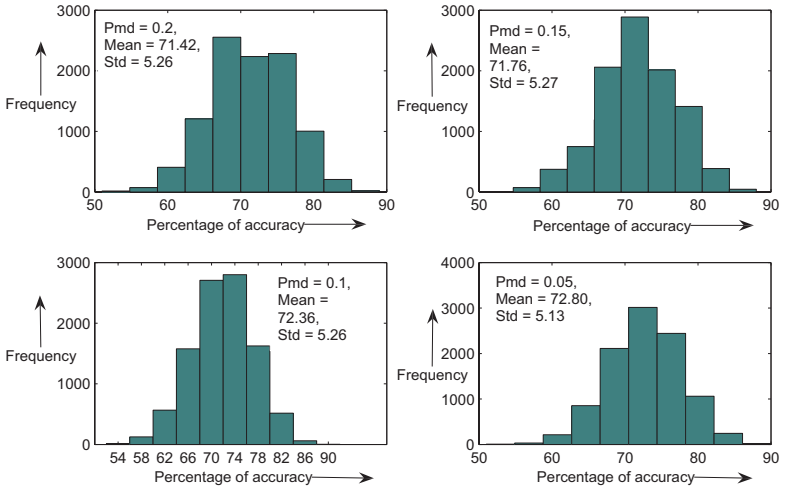

Figure 4.8: Frequency distribution of prediction accuracy percentage of the Viterbi algorithm with $\epsilon = 0.05$ and δ specified in the inset of each histogram (Case II, Scenario 2)

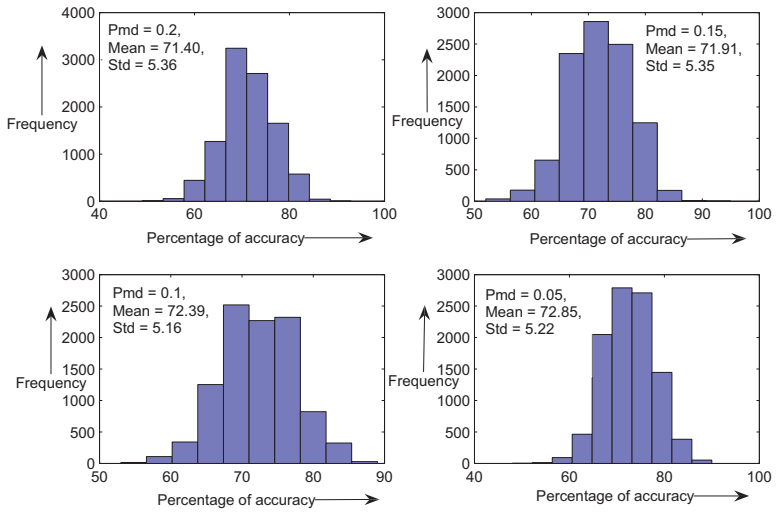

Figure 4.9: Frequency distribution of prediction accuracy percentage of the Viterbi algorithm with $\epsilon = 0.05$ and δ specified in the inset of each histogram (Case III, Scenario 2)

The prediction accuracy depends on the underlying initial distribution and transition matrix. In practice, these are unknown. One can estimate these entities if one observes the availability of the sub-band over a long stretch of time. One can use the EM algorithm developed in this work for estimation.

In order to assess how well the EM algorithm recaptures the underlying initial distribution, the transition matrix and the emission probabilities, we have performed extensive simulations. Initial distribution (p_0, p_1) and transition matrix P are taken to be the same as those described in the simulation work on the Viterbi algorithm for Case I. For emission probability matrix (EP), take $\delta = 0.05$ and $\epsilon = 0.1$. Using these specifications, generate data $x_1, x_2, \cdots, x_{100}$ of length 100 as explained for the simulations. We use these data to estimate the underlying parameter values. For utilizing the EM algorithm, we need a preliminary guess of the initial distribution and transition matrix. We enlisted below the preliminary guesses (p_0, p_1, and P) and final estimates ($\tilde{p_0}$, $\tilde{p_1}$, $\tilde{P}$, and $\tilde{EP}$).

We can compare the final estimates with true values of the set of parameters given in

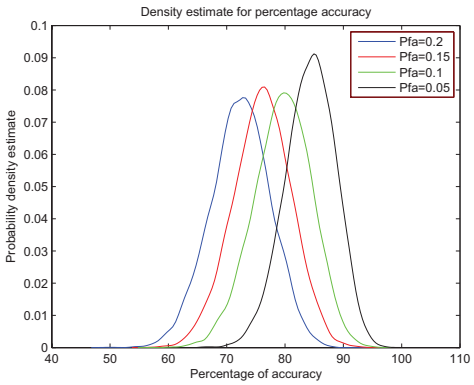

Figure 4.10: Normal approximation of the Viterbi algorithm for Case I with $\delta = 0.05$ and ϵ specified in the inset

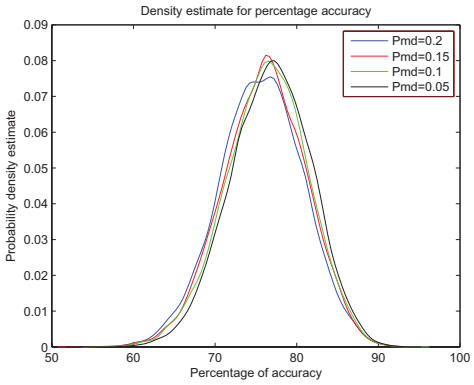

Figure 4.11: Normal approximation of the Viterbi algorithm for Case I with $\epsilon = 0.05$ and δ specified in the inset

Case I. As one can see from the list, the accuracy of estimates depends on the initial guess. If the initial guess do not differ markedly from the true values, the initial distribution can be well estimated to the actual values ($p_0 = 0.223$ and $p_1 = 0.777$). One of the important inference from the estimates of emission probability is that δ is well estimated by the Set I guesses of parameters and this estimation degrades as we move down to guesses in Set V. Additionally, ϵ is well estimated by the set of parameter in Set V and this estimation degrades as we move up to the guesses made in Set I.

Par. Set: (p_0, p_1), P, $(\tilde{p_0}, \tilde{p_1})$, $\tilde{P}$, $\tilde{EP}$

$$SetI : (0.4, 0.6), \begin{pmatrix} 0.4 & 0.6 \\ 0.6 & 0.4 \end{pmatrix}, (0.28, 0.72), \begin{pmatrix} 0.3704 & 0.6296 \\ 0.2361 & 0.7639 \end{pmatrix}, \begin{pmatrix} 0.9524 & 0.1519 \\ 0.0476 & 0.8481 \end{pmatrix}.$$

$$SetII : (0.5, 0.5), \begin{pmatrix} 0.5 & 0.5 \\ 0.5 & 0.5 \end{pmatrix}, (0.26, 0.74), \begin{pmatrix} 0.2308 & 0.7692 \\ 0.2740 & 0.7260 \end{pmatrix}, \begin{pmatrix} 0.9467 & 0.1350 \\ 0.0533 & 0.8650 \end{pmatrix}.$$

$$SetIII : (0.6, 0.4), \begin{pmatrix} 0.6 & 0.4 \\ 0.4 & 0.6 \end{pmatrix}, (0.26, 0.74), \begin{pmatrix} 0.2727 & 0.7273 \\ 0.2208 & 0.7792 \end{pmatrix}, \begin{pmatrix} 0.9331 & 0.1294 \\ 0.0669 & 0.8706 \end{pmatrix}.$$

$$SetIV : (0.7, 0.3), \begin{pmatrix} 0.7 & 0.3 \\ 0.3 & 0.7 \end{pmatrix}, (0.25, 0.75), \begin{pmatrix} 0.32 & 0.68 \\ 0.2297 & 0.7703 \end{pmatrix}, \begin{pmatrix} 0.9286 & 0.1244 \\ 0.0714 & 0.8756 \end{pmatrix}.$$

$$SetV : (0.8, 0.2), \begin{pmatrix} 0.8 & 0.2 \\ 0.2 & 0.8 \end{pmatrix}, (0.26, 0.74), \begin{pmatrix} 0.3077 & 0.6923 \\ 0.2466 & 0.7534 \end{pmatrix}, \begin{pmatrix} 0.9175 & 0.1125 \\ 0.0825 & 0.8875 \end{pmatrix}.$$

$$SetVI : (0.6, 0.4), \begin{pmatrix} 0.5 & 0.5 \\ 0.5 & 0.5 \end{pmatrix}, (0.24, 0.76), \begin{pmatrix} 0.3043 & 0.6957 \\ 0.2237 & 0.7763 \end{pmatrix}, \begin{pmatrix} 0.9389 & 0.1241 \\ 0.0611 & 0.8759 \end{pmatrix}.$$

Using each of the set of estimates in the list, we applied the Viterbi algorithm to predict the hidden states and compared them with the states generated by the true Markov chain

Table 4.3: Estimation accuracy for the EM algorithm

Par. Set	Estimated values	
	Mean	Std
Set 1	75.3904	5.3619
Set 2	75.4020	5.3882
Set 3	75.4738	5.3390
Set 4	75.3695	5.3411

and emission probabilities for prediction accuracy. The results are shown in Table 4.3. These estimated mean percentage accuracy and Std approaches quite close to the actual mean value (79.70) and actual Std (5.03) as also indicated in Figure 4.8. This validates the efficiency of the EM algorithm and we can conclude that the cognitive radio is capable of generating the set of unknown parameters and detect the availability of PUs in a sub-band with 75.5% prediction accuracy. We must remember that these values were computed in presence of the probability of false alarm and mis-detection.

4.9 Conclusion

One of the primary tasks of the cognitive radio is to sense whether or not a particular sub-band is free for a SU and true state determination of the sub-band (1 = Free; 0 = Not free) is the main objective. An incorrect reading of the true state could occur. The goal is to predict the true state of the sub-band given its reading. We treat this problem by the probability theory. We assume that the true states of the sub-band follows a Markov model. The true path of the states is hidden to the SU. The only data available to the SU are the readings of the states by the cognitive radio. In this chapter, we use the likelihood method for prediction of true states. The computational complexity that arises is solved by using the Viterbi algorithm. If the underlying parameter values are unknown, we have developed an Expectation-Maximization algorithm for estimation.

Chapter 5

Game Theoretic Approach in Spectrum Sharing

5.1 Introduction

Dynamic spectrum sharing [53], [54] depends upon detection and location of the PUs that implies information about the radio environment and the transmission power measurement for each channel in an operating spectrum. Coexistence of PUs and SUs leads to the following conflict problems: (i) Limitation on the transmission power in each channel for minimum interference to coexisting PUs, and (ii) Certain signal-to-noise ratio (SNR) required for data transmission of SUs without substantial performance degradation. Cooperation [54] among SUs has proved to be beneficial in solving such contradictory interests. Such cooperation can be achieved with the application of well-known concepts of Game Theory [55], [56].

Existing research work on Game theory [57], [58] have focused on transmission power allocation on available channels. Since the SUs coexist with the PUs in an operating spectrum, mere consideration of transmission power limits on a channel may not be sufficient. The presence of PUs in adjacent channels demand reduced signal power transmission on an available channel for minimum adjacent channel interference. Hence, the occupancy of the neighboring channels is a critical parameter for improved spectrum sharing. Some other research work [59] - [69] have developed pricing and utility functions in a multiple

buyers (SUs in the context of CR) and multiple sellers (PUs) environment. The basic assumption is that the PUs communicate with the SUs before spectrum allocation. Here, we do not make such assumption and develop a Game theoretic strategy among the SUs only. Therefore, there is no communication between the PUs and SUs.

In this chapter, we have addressed major shortcomings found in existing research by developing enhanced Game theoretic strategies for improved spectrum allocation. In our research work, the basic framework considered is that an operating spectrum is divided into sub-bands or channels. These channels, when not in use by the PUs, are allocated to SUs for enhanced spectrum efficiency. We contribute the following unique features in the spectrum sharing: *(i)* Classify the quality of a channel into five different types, depending upon the occupancy of its neighboring channels; *(ii)* Develop a multi-objective function optimization problem leading to a Game theoretic perspective [55], [56] among cooperative N cognitive users in order to allocate channels to these users, *(iii)* Define reward functions to determine Nash equilibrium strategy, *(iv)* Define idle durations and transmission rate for each channel during which the SUs are permitted to transmit, and *(v)* Develop a Game theoretic strategy to allocate single channel to each user, while taking the transmission rate and idle durations into account in defining the reward functions. In addition, we have considered parameters such as idle duration and transmission time in the context of spectrum sharing. The simple idea behind this approach is that each channel supports its own data transmission rates based on perceived channel conditions and multipath characteristics. During a specific time instant if the idle duration of a particular channel is less than the total transmission time required by the SU, then the channel is not allocated to this particular SU. We show that the spectrum allocation method that does not consider such aspects may lead to inefficient spectrum utilization.

The rest of the chapter is organized as follows. Section 5.2 presents a brief overview of existing research works in the area of spectrum sharing and application of Game Theory in CRN. Section 5.3 deals with the system model and the basic components used in our proposed spectrum sharing strategy. Next, Section 5.4 presents the proposal on channel capacity optimization and then develop the Game theoretic approach of allocating multiple channels to each SU in a CRN. Section 5.5 focuses on another Game theoretic spectrum sharing strategy of allocating a single channel to each SU while using spectrum sensing

information. The experimental results are discussed in Section 5.6. A 2-person game theoretic approach is dealt with in Section 5.7 for possible coexistence of PUs and SUs in the same spectrum. Finally, Section 5.8 includes the conclusion.

5.2 Related Work

Spectrum sensing is key for effective spectrum management as it enables SUs to detect PUs in the operating channels. The authors in [51] discuss spectrum sensing techniques which involves an integrated sharing of information between the PHY and MAC layers in the CRN. Detection of primary receivers [62] is achieved by sensing the leakage power emitted by their local oscillators. Spectrum sensing and detection of PU occupancy eventually provides us with the information of idle durations, i.e. intervals of time when the PUs do not (or are not likely to) use their corresponding channels. To the author's knowledge, existing cooperative communication techniques have not considered this aspect in spectrum sharing.

Cooperative algorithms for smart antenna communications [63] have also been used in reducing the time for detecting the presence of PUs. Once the spectrum is sensed and detected as white space, spectrum sharing among the SUs is triggered. The rate optimization approach [64] opts for maximizing the global channel capacity within specific power constraints in each band. But, the main obstacle for SUs in sharing the spectral bands with PUs is the transmission power limits on each channel, which rely on the probabilistic distribution of PUs in the entire spectrum. For example, SU on an available channel with two PUs operating on the adjacent channels should transmit at lower signal power than on a channel wherein both adjacent channels are vacant.

In [65], the authors use a well-known relay techniques among the cognitive radios operating in the same frequency band. The central concept used here is that one SU transmits information to the second SU in a time slot and in the next time slot, the second SU forwards the data packets to the desired destination. Therefore, two time slots are required to transmit the same information. In addition, in any two time slots only one SU listens to the other SU and transmits this user's information instead of its own information, resulting

in lower spectral inefficiency. The authors in [66] assign conflict free spectrum based on required user throughput, while maximizing the total system capacity. However, there is no discussion on the specific condition imposed on each SU and about the variations of the spectrum assignment based on the location of the PUs.

The two switch channel model [53] for capacity analysis introduces communication opportunities for two switches, modeling the transmitter and the receiver. The white spaces detected by the transmitter and the receiver may not be identical since they have different sensing ranges. The channel capacity is analyzed in a distributed nature based on correlated detection between the transmitter and the receiver and the dynamic use by the PUs. The two switch channel model investigates the capacity issue while opportunistically sharing multiple frequency slots, also called "frequency coding", and by sharing different time slots within a single frequency interval, also called "temporal coding".

The throughput analysis discussed in [67] and applied in [53] considers two different scenarios: (1) overlay models where the PUs and the SUs transmit within the same frequency band and (2) interweave models where the SUs operate in an unused channel. A significant improvement is shown in the throughput of SU transmissions in the overlay model as compared to the interweave model. However, an important disadvantage of the overlay model is that the information on PU transmission activity may not be always available at the SU. Another interesting work on capacity analysis [68] discusses the possibility of PU and SU coexistence and derives a mathematical model for the channel capacity enhancement. Though the authors stress on the experimental analysis, they do not quantify the degree of capacity improvements. Also, even though the interference detection and the tolerance level in used bands as well as coexistence using Carrier Interferometry multicarrier approach are described, no scheme is proposed for the implementation of such multicarrier approach in PU bands.

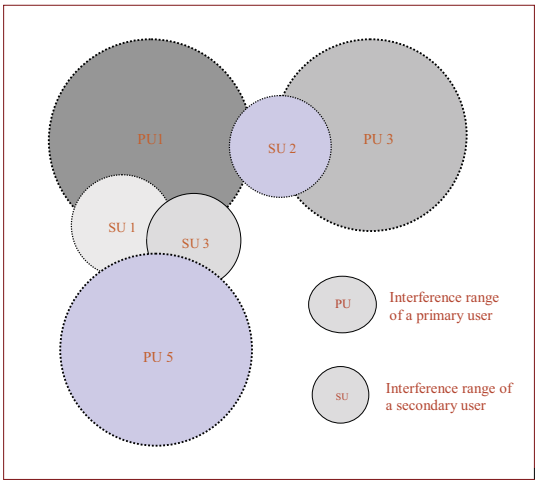

Figure 5.1: Distribution of PUs and SUs in one particular cell

5.3 Spectrum Model and Basic Components of Spectrum Sharing

Our proposed spectrum sharing model consists of M PUs denoted by $PU_1, PU_2, \cdots, PU_M$ located in specific channels represented as $Ch_1, Ch_2, \cdots, Ch_M$. Each channel is licensed to a single PU, as is the case of television band where the television transmitters are further away from each other to avoid interference. This framework is also valid for multiple PUs licensed to a particular channel as is done in the case of cellular communications. There are N SUs denoted as $SU_1, SU_2, \cdots, SU_N$. In the example of Figure 5.1, $M = 5$ and $N = 3$. In our model, the location of an SU_i determines its associated available channels. For example, as shown in Figure 5.1, since the SU_1 is within the interference range of PU_1, Ch_1 is not available for SU_1. On the contrary, Ch_1 is available to SU_2 as it is outside the interference range of PU_1.

The objective of our spectrum sharing approach is to allocate multiple available channels to an SU_i based on two factors: (i) The number of packets SU_i need to transmit and (ii) The transmission rate of each Ch_i. Below we define the components forming the core of our proposed spectrum sharing strategy.

Availability matrix: For any SU, the channels that are free to use, can be indicated by a

column vector. More specifically, for SU_j, let $(\delta_{1j}, \delta_{2j}, \ldots, \delta_{Mj})^T$ be the availability vector, where

$$\begin{aligned} \delta_{ij} &= 1 \; if \; Ch_i \; is \; free \; for \; SU_j, \\ &= 0, \; otherwise. \end{aligned} \tag{5.1}$$

We stack all these column vectors into a matrix $\Delta = (\delta_{ij})$ of order $M \times N$ and call this an "Availability matrix." The column vectors of Δ are indexed by the SUs and the channels that are available could vary from SU to SU.

The components of this matrix can be interpreted in both the settings of a single PU or multiple PUs licensed to a single channel. In case of a single PU in one channel, if the i^{th} channel is not utilized by the PU_i, then Ch_i is available to SUs and $\delta_{ij} = 1$ for all $j = 1, 2, \ldots, N$. In case of multiple PUs in Ch_i, $\delta_{ij} = 1$ if none of the PUs is using Ch_i at that time instant. If any one of the PUs is using Ch_i, $\delta_{ij} = 0$.

Interference matrix: It is a matrix $\Omega = (\omega_{ij})$ of order $N \times N$, where

$$\begin{aligned} \omega_{ij} &= 1 \; if \; SU_i \; and \; SU_j \; are \; in \; interference \; range, \\ &= 0, \; otherwise. \end{aligned} \tag{5.2}$$

By convention, $\omega_{ii} = 0$ for all i; i.e., we do not consider self-interference in our work.

In practical terms, every SU is aware of the spectrum with M channels and availability of the same. In other words, SU_i computes its availability vector, which is the i^{th} column of Δ. Again, SU_i calculates the interference vector, which is the i^{th} row of Ω. At this point, we assume that each SU communicates its availability and interference vectors to all other SUs competing for available licensed channels, using multi-hop communication. Upon receipt of the vectors, each SU puts together both availability and interference matrices.

Idle duration: Spectrum measurements indicate that channels in the entire radio frequency spectrum remain unused for substantial amount of time as depicted in Figure 2.1. Before a channel Ch_i, $i \in 1, 2, \cdots, M$, is allocated to an SU, it is critical to have the knowledge of those instances during which Ch_i is unused by PU_i licensed to it. These durations for any channel are known as idle durations. In our research work [39], we have developed and validated our spectrum occupancy model, which detects idle durations in the paging

band (928-948 MHz). For each channel in the spectrum, we assume that the idle periods for each Ch_i are communicated to each SU. Let I_i denote the idle period of channel Ch_i (in seconds), $i = 1, 2, \cdots, M$. As per our knowledge, this parameter is generally ignored in the spectrum sharing schemes though is vital in this context.

Transmission rate: Let r_i denote the transmission rate (in bits per seconds) supported by Ch_i, $i = 1, 2, \cdots, M$. This parameter has a vital connotation to the spectrum sharing. During any given time period, if the transmission time (ratio of the number of packets of SU_i to be transmitted (in bits) to the transmission rate r_i) is greater than I_i, then Ch_i is not allocated to SU_i.

Allocation matrix: Essentially, an allocation matrix is a summary of allocated channels to all SUs subjected to the availability and interference constraints. A channel may be allocated to a SU only if the channel is available to the SU. A channel may be allocated to two or more SUs if there is no interference among the SUs. Formally, an allocation matrix is a matrix $\Lambda = (\lambda_{ij})$ of order $M \times N$ with the following properties:
(i)

$$\begin{aligned} \lambda_{ij} &= 1 \; if \; Ch_i \; is \; allocated \; to \; SU_j, \\ &= 0, \; otherwise, \\ i &= 1, 2, \ldots, M \; and \; j = 1, 2, \ldots, N. \end{aligned} \tag{5.3}$$

(ii) $\lambda_{ij} = 0$ if $\delta_{ij} = 0$, i.e., Ch_i is not allocated to SU_j if the channel is not available to the SU.
(iii) $\lambda_{ij} + \lambda_{ik} \leq 1$ if $\omega_{jk} = 1$, i.e., if SU_j and SU_k are with in their interference range.

A comment is in order on (iii). If the Ch_i is available to both SU_j and SU_k and $\omega_{jk} = 1$, then the following allocations are feasible:
(a) $\lambda_{ij} = 0$ and $\lambda_{ik} = 0$, i.e., the Ch_i is not allocated;
(b) $\lambda_{ij} = 1$ and $\lambda_{ik} = 0$, i.e., Ch_i is allocated to only SU_j; or
(c) $\lambda_{ij} = 0$ and $\lambda_{ik} = 1$, i.e., the Ch_i channel is allocated to only SU_k.

To illustrate these properties, we include an example. Let us take the same availability matrix and interference matrix for the distribution shown in Figure 5.1 and then some of

the possible allocation matrices are:

$$\Lambda_1 = \begin{pmatrix} 0 & 0 & 0 \\ 1 & 1 & 0 \\ 1 & 0 & 0 \\ 0 & 1 & 1 \\ 0 & 1 & 0 \end{pmatrix}, \Lambda_2 = \begin{pmatrix} 0 & 0 & 0 \\ 0 & 1 & 1 \\ 0 & 0 & 1 \\ 1 & 1 & 0 \\ 0 & 1 & 0 \end{pmatrix},$$

$$\Lambda_3 = \begin{pmatrix} 0 & 0 & 0 \\ 0 & 1 & 0 \\ 0 & 0 & 1 \\ 1 & 1 & 0 \\ 0 & 1 & 0 \end{pmatrix}, \Lambda_4 = \begin{pmatrix} 0 & 0 & 0 \\ 0 & 1 & 0 \\ 1 & 0 & 0 \\ 0 & 1 & 1 \\ 0 & 1 & 0 \end{pmatrix}.$$

Maximal Allocation matrices: Let $\mathcal{A}$ be the collection of all allocation matrices. The set $\mathcal{A}$ is finite. We introduce a partial order on $\mathcal{A}$. Let $\Lambda = (\lambda_{ij})$ and $\Pi = (\pi_{ij}) \in \mathcal{A}$. We say that $\Lambda \leq \Pi$ if $\lambda_{ij} \leq \pi_{ij}$ for all i and j. This implies that if Ch_i is allocated to SU_j as per the allocation matrix Λ, then the channel remains allocated to the SU as per Π too. The relation $\leq$ here is a partial order but not a linear order since it is possible that two allocation matrices Λ and Π may not be comparable as per the order $\leq$. This is true in our example above where Λ_1 and Λ_2 are not comparable according to the order $\leq$. The following concept is useful to weed out potential allocation matrices which are inefficient.

Definition: A matrix $\Lambda \in \mathcal{A}$ is said to be maximal if $\Pi \in \mathcal{A}$ and $\Lambda \leq \Pi$ implies that $\Lambda = \Pi$.

It is now trivial to prove that given any Λ in $\mathcal{A}$, there exists a maximal Λ^* in $\mathcal{A}$ such that $\Lambda \leq \Lambda^*$. We will refer to our example for this assertion. The allocation matrices Λ_3 and $\Lambda_4 \in \mathcal{A}$. Note that Λ_3 is not maximal but Λ_2 is. Also, $\Lambda_3 \leq \Lambda_2$. Similarly, Λ_4 is not maximal but Λ_1 is. Also, $\Lambda_4 \leq \Lambda_1$.

Any maximal matrix Λ has an appealing property: *Each channel is allocated to a maximum number of SUs subject to the interference constraints. If a channel is available to only one SU, it is allocated to the SU.* From now on, $\mathcal{A}$ is used for the set of all maximal allocation matrices.

We now provide an upper bound for the total number of maximal allocation matrices. Let K_i be the sum of all entries in the $i-th$ row of Δ, $i = 1, 2, \ldots, M$. The entity K_i is the

total number of SUs to whom the $i-th$ channel is available. If $K_i = 0$, then the i^{th} channel is being used by a PU and is not available to any SU. Any allocation matrix has to have $(0, 0, \ldots, 0)$ in the i^{th} row perforce. Assume, $K_i > 0$. When filling up the i-th row of a maximal matrix, we have only at most K_i choices. In one extreme case of interferences, $\omega_{jk} = 0$ for all j and k and every channel is allocated to every SU to whom it is available. In this case, the i-th row can be filled only one way. Another extreme case of interference is $\omega_{jk} = 1$ for all $j \neq k$. In this case, each channel can be given to only one SU. It means that the i-th row of any maximal allocation matrix can have only one entry equal to 1 and the rest zero. Consequently, the i-th row can be filled in K_i different ways.

We now illustrate the cases where the i^{th} row of any maximal allocation matrix is filled out for any Ω other than the cases considered above. Assume, without loss of generality, that the i^{th} row of Δ is of the form $(1, 1, \ldots, 1, 0, 0, \ldots, 0)$, where the first K_i entries are each equal to one. In other words, the i^{th} channel is not available to SU_{K_i+1}, $SU_{K_i+2}, \ldots, SU_N$. Now, we consider the first row $(0, \omega_{12}, \omega_{13}, \ldots, \omega_{1N})$ of Ω. The maximal allocation of channels stemming out is $(1, 1-\omega_{12}, 1-\omega_{13}, \ldots, 1-\omega_{1K_i}, 0, 0, \ldots, 0)$. In this allocation, SU_1 is allocated the i^{th} channel and other SUs from SU_2 to SU_{K_i} depending upon their corresponding interferences with SU_1. Considering the second row $(\omega_{21}, 0, \omega_{23}, \ldots, \omega_{2N})$ of Ω, the maximal allocation is given by $(1-\omega_{21}, 1, 1-\omega_{23}, \ldots, 1-\omega_{2K_i}, 0, 0, \ldots, 0)$. Proceeding in the same way till SU_{K_i}, the i^{th} row of the allocation matrix is filled by any one of the following K_i rows:

$$
\begin{gathered}
(1, 1-\omega_{12}, 1-\omega_{13}, \ldots, 1-\omega_{1K_i}, 0, 0, \ldots, 0) \\
(1-\omega_{21}, 1, 1-\omega_{23}, \ldots, 1-\omega_{2K_i}, 0, 0, \ldots, 0) \\
\ldots \\
\ldots \\
(1-\omega_{K_i1}, 1-\omega_{K_i2}, \ldots, 1, 0, 0, \ldots, 0). \qquad (5.4)
\end{gathered}
$$

However, there may be some duplications among the rows. Again, some rows may not be feasible as illustrated in the following case study. Let L_i be the total number of distinct rows among the above after excluding infeasible ones. Note that $L_i \leq K_i$. We have the following results:

Theorem 5.1: The total number of maximal allocation matrices $\leq \prod_{i=1,K_i\neq 0}^{M} K_i$.
Theorem 5.2: The exact number of maximal allocation matrices is $\prod_{i=1,K_i\neq 0}^{M} L_i$.
We will walk through our example with Ω defined as:

$$\Omega = \begin{pmatrix} 0 & 0 & 1 \\ 0 & 0 & 0 \\ 1 & 0 & 0 \end{pmatrix},$$

and the availability matrix Δ to illustrate the results.

$$\Delta = \begin{pmatrix} 0 & 0 & 0 \\ 1 & 1 & 1 \\ 1 & 0 & 1 \\ 1 & 1 & 1 \\ 0 & 1 & 0 \end{pmatrix} \begin{matrix} K_1 = 0 \\ K_2 = 3 \\ K_3 = 2 \\ K_4 = 3 \\ K_5 = 1. \end{matrix}$$

The number of maximal allocation matrices is $\leq 3 \times 2 \times 3 \times 1$, i.e. ≤ 18. Forming all possible allocation matrices as per (5.4):

Row number of Δ	*Row vector and L − value*
1	(000) −,
2	(110) 1,
	(111) *Infeasible*,
	(011) 1 => 1 + 1 = 2,
3	(100) 1,
	(001) 1 => 1 + 1 = 2,
4	(110) 1,
	(111) *Infeasible*,
	(011) 1 => 1 + 1 = 2,
5	(010) 1.

(5.5)

The number of maximal allocation matrices is $(2 \times 2 \times 2 \times 1) = 8$. This validates *Theorem*

5.2. The matrices are enumerated below for the completeness of the text.

$$\Lambda_1 = \begin{pmatrix} 0 & 0 & 0 \\ 1 & 1 & 0 \\ 1 & 0 & 0 \\ 1 & 1 & 0 \\ 0 & 1 & 0 \end{pmatrix}, \Lambda_2 = \begin{pmatrix} 0 & 0 & 0 \\ 1 & 1 & 0 \\ 1 & 0 & 0 \\ 0 & 1 & 1 \\ 0 & 1 & 0 \end{pmatrix},$$

$$\Lambda_3 = \begin{pmatrix} 0 & 0 & 0 \\ 1 & 1 & 0 \\ 0 & 0 & 1 \\ 1 & 1 & 0 \\ 0 & 1 & 0 \end{pmatrix}, \Lambda_4 = \begin{pmatrix} 0 & 0 & 0 \\ 1 & 1 & 0 \\ 0 & 0 & 1 \\ 0 & 1 & 1 \\ 0 & 1 & 0 \end{pmatrix},$$

$$\Lambda_5 = \begin{pmatrix} 0 & 0 & 0 \\ 0 & 1 & 1 \\ 1 & 0 & 0 \\ 1 & 1 & 0 \\ 0 & 1 & 0 \end{pmatrix}, \Lambda_6 = \begin{pmatrix} 0 & 0 & 0 \\ 0 & 1 & 1 \\ 1 & 0 & 0 \\ 0 & 1 & 1 \\ 0 & 1 & 0 \end{pmatrix},$$

$$\Lambda_7 = \begin{pmatrix} 0 & 0 & 0 \\ 0 & 1 & 1 \\ 0 & 0 & 1 \\ 1 & 1 & 0 \\ 0 & 1 & 0 \end{pmatrix}, \Lambda_8 = \begin{pmatrix} 0 & 0 & 0 \\ 0 & 1 & 1 \\ 0 & 0 & 1 \\ 0 & 1 & 1 \\ 0 & 1 & 0 \end{pmatrix}. \tag{5.6}$$

Quality of a channel: In practice, some free channels are preferred over others for an SU. For example, a free band in between two bands with PUs is less preferred than a free band with adjacent unused bands. Each SU has a spectral mask on the maximum transmission power admissible in each channel. Therefore, this results in a low signal-to-noise-ratio (SNR). This compels us to delve into the different configurations of the free bands with adjacent PUs while focussing on a specific free channel, Ch_i. The channels are assumed to be orthogonal to each other. This assumption enables us to consider that

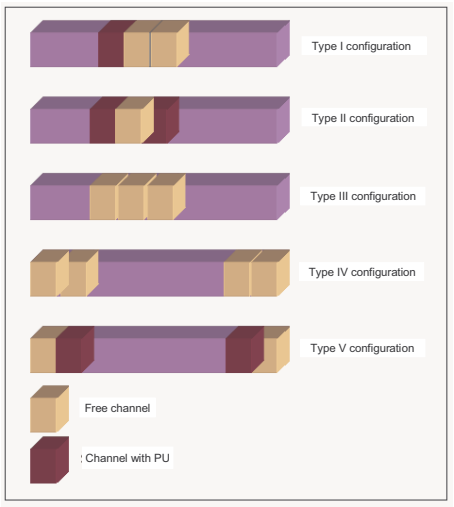

Figure 5.2: Type classifications of various configurations of free channels

adjacent channels do not interfere.

The five different configurations discussed in our research work are shown in Figure 5.2.

(i) Type I configuration: A free band Ch_i with one PU as $(i-1)$-th neighbor and one free band as the $(i+1)$-th neighbor and vice versa as shown in Figure 5.2.

(ii) Type II configuration: A free band Ch_i with two PUs as $(i-1)$-th and $(i+1)$-th neighbors as shown in Figure 5.2.

(iii) Type III configuration: A free band Ch_i with two free bands as $(i-1)$-th and $(i+1)$-th neighbors as shown in Figure 5.2.

(iv) Type IV configuration: A free band at the left or right edge of the entire operating spectrum with a free channel as its neighbor as shown in Figure 5.2.

(v) Type V configuration: A free band at the left or right edge of the entire spectrum with PU as its neighbor as shown in Figure 5.2.

SNR: Allowable transmission signal energy E_b on an available channel depends on its adjacent neighbors, categorized as five Types in our research work. For example, an available channel with two PUs as neighbors, i.e., Type II, will have smaller E_b than any other Types of configurations (Type I, III, IV and V). Since the SUs have been allowed to un-

licensed use of any channel imposing minimum interference to PUs, a SU on a Type II channel will have restricted transmission power as compared to channels of other types with one PU or a free band as neighbors. Formally,
$E_{b_{TypeII}} < E_{b_{TypeI}} < E_{b_{TypeV}} < E_{b_{TypeIV}} < E_{b_{TypeIII}}$.

Consequently,

$$\begin{aligned} SNR_{TypeIII} > SNR_{TypeIV} > SNR_{TypeV} \\ > SNR_{TypeI} > SNR_{TypeII}. \end{aligned} \tag{5.7}$$

Suppose Ch_i is allocated to SU_j. Here, it needs to be pointed out that the type of channel allocated to an SU depends on the availability matrix Δ. We now introduce the SNR matrix $\Sigma(\Lambda) = \sigma_{ij}$ of order $M \times N$, where,

$$\begin{aligned} \sigma_{ij} &= 0, \; if \; \delta_{ij} = 0, \\ &= SNR_{TypeK}, \; if \; Ch_i \; allocated \; as \; per \; \Lambda \; to \\ &\quad SU_j \; is \; of \; Type \; K. \end{aligned} \tag{5.8}$$

Using the SNR matrix, the admissible transmission power for each SU can be obtained under a prescribed allocation matrix Λ.

5.4 Channel Capacity Optimization and Game Theoretic Formulation

In this section, we initially formulate the channel capacity maximization problem in spectrum sharing among the SUs as multi-objective optimization. Lacking any unique solution which could satisfy all SUs, we have pursued two options: the first one is translating the problem into a single-objective optimization problem and the other is the game theory.

5.4.1 Channel Capacity Optimization

The basic problem is to choose an allocation matrix which is maximum. We need an objective function. One natural objective function is based on the SNR. For a given allocation matrix $\Lambda = \lambda_{ij}$, we define total SNR (TSNR) by:

$$TSNR(\Lambda) = \sum_{i=1}^{M} \sum_{j=1}^{N} \lambda_{ij}\sigma_{ij}. \tag{5.9}$$

Higher TSNR is an indication of high quality transmission. The goal is to find Λ for which $TSNR(\Lambda)$ is maximum. It is evident that it suffices to maximize $TSNR(\Lambda)$ over all maximal allocation matrices. This is a discrete optimization problem since the set of all maximal allocation matrices is finite. We have developed an algorithm to compute the Λ with its corresponding maximum $TSNR(\Lambda)$. The inputs to the algorithm are Δ, Ω, and the SNR matrix Σ.

Using the SNR matrix, one can obtain admissible transmission power for each SU under a prescribed allocation matrix Λ. Let us express the total admissible SNR of SU_j in the operating spectrum under the allocation matrix by $R_j(\Lambda)$. Hence, $R_j(\Lambda)$ can be expressed as:

$$R_j(\Lambda) = \sum_{i=1}^{M} \lambda_{ij}\sigma_{ij}(\Lambda), \;\; j = 1, 2, \ldots, N. \tag{5.10}$$

The number $R_j(\Lambda)$ is the sum of all admissible SNRs from the channels allocated to SU_j. Mathematically, it is the inner product of the j^{th} column of the allocation matrix Λ and j^{th} column of the SNR matrix $\Sigma(\Lambda)$.

The goal now is to maximize the channel capacity over the set $\mathcal{A}$ of all allocation matrices. Since the entries of the SNR matrix are non-negative, it follows from:

$$\Lambda, \Pi \in \mathcal{A}, \Lambda \leq \Pi \Rightarrow R_j(\Lambda) \leq R_j(\Pi) \; for \; all \; j. \tag{5.11}$$

5.4.2 Optimization, Game Theory, and Nash Equilibrium

In this section, we formulate a general optimization problem in which every SU_j is attempting to maximize his total admissible SNR, R_j. As an illustration, for the example

in (5.6), SU_1 can opt for Λ_1 since he is allocated three channels maximizing his SNR. On the other hand, SU_3 can opt for Λ_8 to maximize his own SNR. There is no universal allocation matrix Λ at which $R_j(\Lambda)$ is maximum for every SU_j. To resolve such competing choices, we introduce game theoretic ideas into the problem and explore existence of Nash equilibrium. We formulate the problem in general game theoretic terminology.

The basic components of a *perfect information* Game Theory [56] are: a set of N players; the strategy set of each player; and reward function of each player for the joint strategy adopted by all the players in the game. Let $\mathcal{A}_i$ be the strategy set of Player i, $i = 1, 2, \ldots, N$. Let g_i be the reward function of Player i, $i = 1, 2, \ldots, N$, i.e., if Player 1 chooses $A_1 \in \mathcal{A}_1$, Player 2 chooses $A_2 \in \mathcal{A}_2$ and so on till Player N chooses $A_N \in \mathcal{A}_N$, $g_i(A_1, A_2, \ldots, A_i, \ldots, A_N)$ is the reward obtained by Player i. In fact, g_i is a real-valued function from the Cartesian product space $\mathcal{A}_1 \times \mathcal{A}_2 \times \ldots \times \mathcal{A}_N$. The *perfect information* qualification refers to the paradigm that each player knows all the strategy sets and reward functions.

At the basic level, the goal for each player is to maximize his reward function. The problem is then considered to be under the realm of multi-objective function optimization. The objective is to find strategies $A_i^* \in \mathcal{A}_i$, $i = 1, 2, \ldots, N$, such that

$$g_i(A_1^*, A_2^*, \ldots, A_N^*) \quad = \quad \max\, g_i(A_1, A_2, \ldots, A_N), \tag{5.12}$$

where the maximum is taken over all $A_1 \in \mathcal{A}_1, A_2 \in \mathcal{A}_2, \ldots, A_N \in \mathcal{A}_N$, and the solution $(A_1^*, A_2^*, \ldots, A_N^*)$ is the same for each $i = 1, 2, \ldots, N$. If the strategies $A_i^* \in \mathcal{A}_i$ exist, adopting these strategies is optimal for every player. However, realistically, such universal set $A_1^*, A_2^*, \ldots, A_N^*$ may not exist. Two options are now possible. One option is to maximize $g_1 + g_2 + \ldots + g_N$, or some function of $g_1, g_2, \ldots, g_N$, over the set $\mathcal{A}_1 \times \ldots \times \mathcal{A}_N$. In such a case, this problem falls under the realm of traditional optimization. Typically, it is feasible to find $A_1^* \in \mathcal{A}_1$, ..., $A_N^* \in \mathcal{A}_N$ such that

$$\begin{aligned} g_1(A_1^*, A_2^*, \ldots, A_N^*) + g_2(A_1^*, A_2^*, \ldots, A_N^*) & \\ + \ldots + g_N(A_1^*, A_2^*, \ldots, A_N^*) \quad &= \\ \max\, (g_1 + g_2 + \ldots + g_N)(A_1, A_2, \ldots, A_N), & \end{aligned} \tag{5.13}$$

where the maximum is taken over all $A_1 \in \mathcal{A}_1, A_2 \in \mathcal{A}_2, \ldots, A_N \in \mathcal{A}_N$.

Another option is to search for a Nash equilibrium. A choice $(A_1^*, A_2^*, \ldots, A_N^*) \in \mathcal{A}_1 \times \ldots \times \mathcal{A}_N$ is said to be a Nash equilibrium if $g_i(A_1^*, A_2^*, \ldots, A_{(i-1)}^*, A_i^*, A_{(i+1)}^*, \ldots, A_N^*) \geq g_i(A_1^*, A_2^*, \ldots, A_{(i-1)}^*, A_i, A_{(i+1)}^*, \ldots, A_N^*)$, for all $A_i \in \mathcal{A}_i$ and $i = 1, 2, \ldots, N$. In other words, a Nash equilibrium strategy means that if Player i ($i = 1, 2, \ldots, N$) does not use A_i^* and all other players use their A_j^*s then the reward for Player i is at most $g_i(A_1^*, A_2^*, \ldots, A_i^*, \ldots, A_N^*)$. Note that if we maximize g_i over $\mathcal{A}_1 \times \mathcal{A}_2 \times \mathcal{A}_N$ using a greedy algorithm, for each i, there may not be a common solution $(A_1^*, A_2^*, \ldots, A_N^*)$ for all the players.

In our context, the players are the SUs. The strategy set for player i is $\mathcal{A}$, the collection of all maximal allocation matrices as described in Section III. The development of reward functions g_i's requires some tact. If each SU chooses the same allocation matrix Λ, there is no conflict and the reward for SU_j is given by:

$$g_j(\Lambda, \Lambda, \ldots, \Lambda) = R_j(\Lambda) = \sum_{i=1}^{M} \lambda_{ij}\sigma_{ij}(\Lambda). \tag{5.14}$$

If SUs choose different allocation matrices, there is certainly a conflict of interests. Suppose $\Lambda_j = (a_{rs}^{(j)}) \in \mathcal{A}$ is the allocation matrix chosen by SU_j, $j = 1, 2, \ldots, N$, a compromise allocation matrix is given by:

$$\Lambda = (a_{rs}) = \Lambda_1 \wedge \Lambda_2 \wedge \ldots \wedge \Lambda_N, \tag{5.15}$$

where $\wedge$ is the minimum operator, i.e., the $(r, s)^{th}$ entry of Λ is given by:

$$a_{rs} = min\,\{(a_{rs}^{(j)}) : 1 \leq j \leq N\}. \tag{5.16}$$

It is clear that Λ is an allocation matrix, i.e., $\Lambda \in \mathcal{A}$. All SUs agree upon the allocations indicated by Λ. We now define the reward function of SU_j by:

$$g_j(\Lambda_1, \Lambda_2, \ldots, \Lambda_N) = R_j(\Lambda) = \sum_{i=1}^{M} a_{ij}\sigma_{ij}(\Lambda), \tag{5.17}$$

where $j = 1, 2, \ldots, N$. It must be emphasized that $\Lambda_1 \vee \Lambda_2 \vee \ldots \vee \Lambda_N$ is not an allocation matrix if at least two of the Λ_i's are distinct, where $\vee$ represents the maximum operator. As a matter of fact, $\Lambda_1 \vee \Lambda_2 \vee \ldots \vee \Lambda_N$ is an allocation matrix if and only if all Λ_i's are equal.

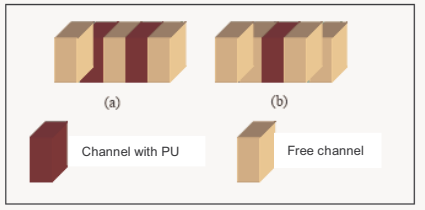

Figure 5.3: Free channel configurations for (a) SU_1 and (b) SU_2

For this game, we have several Nash equilibria. This is stated in the following theorem.

Theorem 5.3: Fix any $\Lambda \in \mathcal{A}$. Then $(\Lambda, \Lambda, \ldots, \Lambda)$ is a Nash equilibrium.

Proof: Let $\Lambda^{'}$ be any member of $\mathcal{A}$. Observe that $(\Lambda \wedge \Lambda^{'}) \leq \Lambda$. Consequently,

$$\begin{aligned} g_j(\Lambda, \Lambda, \ldots, \Lambda) &= R_j(\Lambda) \\ &\geq R_j(\Lambda \wedge \Lambda^{'}) \\ &\geq g_j(\Lambda, \Lambda, \ldots, \Lambda, \Lambda^{'}, \Lambda, \ldots, \Lambda), \end{aligned} \tag{5.18}$$

where $\Lambda^{'}$ is in the j^{th} position and $j = 1, 2, \ldots, N$. Hence, $(\Lambda, \Lambda, \ldots, \Lambda)$ is a Nash equilibrium.

Note that the number of Nash equilibria is equal to the cardinality of $\mathcal{A}$.

In practical terms, once Δ and Ω are available to each SU, he can work out all maximal allocation matrices and reward functions.

Since this is a "perfect information" game, every SU is capable of determining the options and the attendant solutions with respect to all other SUs. Using a single objective function optimization approach, there may not be a universal agreement (sum, product, or any other way) in combining the reward functions. In the game theoretic approach, if there is a unique Nash equilibrium, the players pursue the solution offered by the equilibrium. If there are several equilibria, the players need to cooperate in resolving the choices. These issues are further illustrated in the context of the following case study.

5.4.3 Case Study

We illustrate the details of our N-person game using the example as shown in Figure 5.3 with two SUs. As we see from Figure 5.3, only five channels are considered for both

SU_1 and SU_2. Ch-bands 1, 3, and 5 are available to SU_1 which are of Types V, II, and V, respectively. Ch-bands 1, 2, 4, and 5 are available to SU_2 which are of Types IV, I, I, and IV, respectively. Hence with reference to (5.1), (5.2) and (5.8), the "Availability matrix, Δ", the "Interference matrix, Ω" and the "SNR matrix, Σ" for SU_1 and SU_2 can be expressed as follows:

$$\Delta = \begin{pmatrix} 1 & 1 \\ 0 & 1 \\ 1 & 0 \\ 0 & 1 \\ 1 & 1 \end{pmatrix}, \ \Omega = \begin{pmatrix} 0 & 1 \\ 1 & 0 \end{pmatrix}.$$

As a prelude to the development of σ_{ij}'s in (5.7) and (5.8), we have considered the following values of SNR for various types of free channels. For illustration:

$$\begin{aligned} SNR \ = \ & 0, \ \textit{for a channel not free}, \\ & 1, \ \textit{for Type II channel}, \\ & 2, \ \textit{for Type I channel}, \\ & 3, \ \textit{for Type V channel}, \\ & 4, \ \textit{for Type IV channel, and} \\ & 5, \ \textit{for Type III channel}. \end{aligned} \tag{5.19}$$

Now, we list the maximal allocation matrices of these two players, SU_1 and SU_2, as follows:

$$\Lambda_1 = \begin{pmatrix} 1 & 0 \\ 0 & 1 \\ 1 & 0 \\ 0 & 1 \\ 0 & 1 \end{pmatrix}, \ \Lambda_2 = \begin{pmatrix} 1 & 0 \\ 0 & 1 \\ 1 & 0 \\ 0 & 1 \\ 1 & 0 \end{pmatrix},$$

$$\Lambda_3 = \begin{pmatrix} 0 & 1 \\ 0 & 1 \\ 1 & 0 \\ 0 & 1 \\ 1 & 0 \end{pmatrix}, \ \Lambda_4 = \begin{pmatrix} 0 & 1 \\ 0 & 1 \\ 1 & 0 \\ 0 & 1 \\ 0 & 1 \end{pmatrix}.$$

Using our optimization approach, we compute the maximum channel capacity. Using (5.10), we write the following admissible SNR for SU_1 as: $R_1(\Lambda_1) = 4$, $R_1(\Lambda_2) = 7$, $R_1(\Lambda_3) = 4$, and $R_1(\Lambda_4) = 1$. Similarly, for SU_2, the admissible SNRs are: $R_2(\Lambda_1) = 8$, $R_1(\Lambda_2) = 4$, $R_1(\Lambda_3) = 8$, and $R_1(\Lambda_4) = 12$. Hence, $TSNR(\Lambda)$ can be written as:

$$\begin{aligned} TSNR(\Lambda_1) &= 12, \\ TSNR(\Lambda_2) &= 11, \\ TSNR(\Lambda_3) &= 12, \\ TSNR(\Lambda_4) &= 13. \end{aligned} \tag{5.20}$$

Now, the two SUs could have conflicting interests, with different allocation strategies selected by each one of them so as to maximize their individual benefits. This can be resolved using (5.16) and computed as follows:

$$\Lambda_1 \wedge \Lambda_2 = \begin{pmatrix} 1 & 0 \\ 0 & 1 \\ 1 & 0 \\ 0 & 1 \\ 0 & 0 \end{pmatrix}, \ \Lambda_1 \wedge \Lambda_3 = \begin{pmatrix} 0 & 0 \\ 0 & 1 \\ 1 & 0 \\ 0 & 1 \\ 0 & 0 \end{pmatrix},$$

$$\Lambda_1 \wedge \Lambda_4 = \begin{pmatrix} 0 & 0 \\ 0 & 1 \\ 1 & 0 \\ 0 & 1 \\ 0 & 1 \end{pmatrix}, \ \Lambda_2 \wedge \Lambda_3 = \begin{pmatrix} 0 & 0 \\ 0 & 1 \\ 1 & 0 \\ 0 & 1 \\ 1 & 0 \end{pmatrix},$$

Table 5.1: Reward table to achieve Nash Equilibria

$\mathcal{A}$ for SU 1	$\mathcal{A}$ for SU 2			
	Λ_1	Λ_2	Λ_3	Λ_4
Λ_1	4, 8	4, 4	1, 4	1, 8
Λ_2	4, 4	7, 4	4, 4	1, 4
Λ_3	1, 4	4, 4	4, 8	1, 8
Λ_4	1, 8	1, 4	1, 8	1, 12

$$\Lambda_2 \wedge \Lambda_4 = \begin{pmatrix} 0 & 0 \\ 0 & 1 \\ 1 & 0 \\ 0 & 1 \\ 0 & 0 \end{pmatrix}, \ \Lambda_3 \wedge \Lambda_4 = \begin{pmatrix} 0 & 1 \\ 0 & 1 \\ 1 & 0 \\ 0 & 1 \\ 0 & 0 \end{pmatrix}.$$

Finally, we calculate the reward functions for all the allocation strategies shown in Table 5.1.

Table 5.1 provides all the ingredients of the proposed game. The strategy set is $\mathcal{A} = \{\Lambda_1, \Lambda_2, \Lambda_3, \Lambda_4\}$. Note that

$$max_{B,C\in\mathcal{A}}\, g_1(B, C) = g_1(A_2, A_2) = 7,$$

and

$$max_{B,C\in\mathcal{A}}\, g_2(B, C) = g_2(A_4, A_4) = 12.$$

There is no universal $(\Lambda_1^*, \Lambda_2^*)$ at which both g_1 and g_2 are maximum. If we combine g_1 and g_2 additively, the total channel capacity $TSNR(\Lambda)$ is maximized at (Λ_4, Λ_4) following (5.20). If g_1 and g_2 are combined in a different way, an optimal solution can be similarly worked out. For example, if the reward functions are combined using multiplication, (Λ_1, Λ_1) and (Λ_3, Λ_3) are the solutions to the optimization problem. However, combining the reward functions may not be acceptable to some of the SUs. In such a case, exploring the existence of a Nash equilibrium is a natural pursuit. We observe that there are four Nash equilibria: (Λ_1, Λ_1), (Λ_2, Λ_2), (Λ_3, Λ_3), and (Λ_4, Λ_4). If SUs plan to pursue a Nash

equilibrium, they need to work out a choice collaboratively. As in Table 5.1, the choice (Λ_4, Λ_4) not only is a Nash equilibrium, but also maximizes the SNR. The main goal of this section is to present a chain of ideas that can be pursued in problems of the type characterized above. In some problems with a different formulation of reward functions, pursuing the chain of ideas presented above can be illuminating and rewarding as we will see later.

In the next section, we revisit the optimization problem by considering additional critical parameters like idle period and transmission time. To the best of our knowledge, this is the first work to take these spectrum sensing parameters into account for improved spectrum sharing.

5.5 Game Theoretic Perspective using Spectrum Sensing Parameters

A natural strategy set for a SU is to allocate all channels available to itself. Let A_i denote the collection of channels free for SU_i, $i = 1, 2, \cdots, N$. Therefore, in this section, instead of multiple channels as discussed in the previous section, we focus on allocating a single channel. In this spectrum allocation game, we consider the presence of a central controller, a base station, who is in control of taking all the decisions and imposing restrictions on the players.

To accomplish this, we initially assume idle durations $I_1, I_2, \cdots, I_M$ of the M channels and their respective transmission rates r_i, $i = 1, 2, \cdots, M$, are known. These parameters can be estimated using accurate spectrum occupancy model design discussed in [39]. In addition, a threshold time τ is set to prevent an SU, with a smaller number of packets, to opt for a channel with a larger idle duration. If an SU with small transmission time selects a channel with large I_i, then the SU is penalized with half the signal energy allowed on the channel.

For simplicity of notation, let the channels be numbered serially from 1 to M. Suppose SU_1 chooses i_1, SU_2 $i_2, \cdots, SU_N$ i_N. The choices of channels now is a vector $(i_1, i_2, \cdots, i_N)$. We propose the following reward function g_j for SU_j.

Case I: If SU_j's choice, namely i_j is the same as that of SU_k and $\omega_{jk} = 1$ (i.e., they are

within their interference range), then SU_j cannot use i_j. Consequently,

$$g_j(i_1, i_2, \cdots, i_N) = 0. \tag{5.21}$$

Case II: Suppose SU_j can use i_j. The transmission time t_j required is the ratio of SU_j's number of data packets to r_{i_j}. Two cases may arise:
Case II.1: If $I_{i_j} - t_j \geq 0$, SU_j can transmit the data on channel i_j. Now if $I_{i_j} - t_j \leq \tau$, SU_j is allowed to transmit on i_j with its allowable signal power limits. In such a case, reward for SU_j is given by:

$$g_j(i_1, i_2, \cdots, i_N) = t_j(e_b)_{i_j}, \tag{5.22}$$

where $(e_b)_{i_j}$ is the signal energy on the i^{th} channel for the j^{th} SU.
Case II.2: If the idle time is substantially larger than the required transmission time, i.e., $I_{i_j} - t_j > \tau$, then SU_j is punished to transmit with half the allowable signal energy limited to i_j. The reward for SU_j is written as:

$$g_j(i_1, i_2, \cdots, i_N) = 0.5 t_j(e_b)_{i_j}. \tag{5.23}$$

Case III: If $I_{i_j} - t_j < 0$, SU_j does not prefer to use the channel since it wastes time and incurs latency in shifting its data transmission to another channel due to an incoming PU. The reward for this case is $g_j(i_1, i_2, \cdots, i_N) = 0$.

Now, we incorporate all these scenarios in the following expression:

$$\begin{aligned} g_j(i_1, i_2, \cdots, i_N) &= [t_j(e_b)_{i_j} I(0 \leq I_{i_j} - t_j \leq \tau) + \\ &\quad 0.5 t_j(e_b)_{i_j} I(I_{i_j} - t_j > \tau)],\ i_j \neq i_k, \\ &= [t_j(e_b)_{i_j} I(0 \leq I_{i_j} - t_j \leq \tau) + \\ &\quad 0.5 t_j(e_b)_{i_j} I(I_{i_j} - t_j > \tau)] \times \\ &\quad \prod_{k=1}^{N} (1 - \omega_{jk}),\ i_j = i_k. \end{aligned} \tag{5.24}$$

5.5.1 Case Study

With the reward functions in place, we now explore the existence of Nash equilibrium for this Game. In order to do that, we utilize real-time spectrum measurement data obtained

from the experiment conducted on the paging channels (928-948 MHz) over 500 sweeps [39]. The details of the experiment and instruments used are described in Section 2.2. Each sweep duration is of 1.68 seconds. The 10 channels under considerations are in the range of 929-929.18 MHz with resolution bandwidth of 20 KHz. We have randomly selected the 84^{th} sweep and determined Δ, idle durations I_{dur}, and the transmission rates r_i (in Kbps) of these channels as:

$$\Delta = \begin{pmatrix} 0 & 0 \\ 1 & 1 \\ 0 & 0 \\ 0 & 0 \\ 0 & 0 \\ 0 & 0 \\ 0 & 0 \\ 0 & 0 \\ 0 & 0 \\ 0 & 0 \end{pmatrix}, \; I_{dur} = \begin{pmatrix} 5.04 \\ 3.36 \\ 10.08 \\ 3.36 \\ 1.68 \\ 1.68 \\ 1.68 \\ 16.80 \\ 3.36 \\ 10.08 \end{pmatrix}, \; r_i = \begin{pmatrix} 512 \\ 256 \\ 768 \\ 256 \\ 512 \\ 768 \\ 256 \\ 768 \\ 256 \\ 512 \end{pmatrix}.$$

As in the Game described in the previous section, we consider two SUs, namely, SU 1 and SU 2 with $24,000$ and $2,000$ transmission packets, respectively. The type of each of the 10 channels are determined based on the occupancy of their adjacent users. As described in Section III, these channels are of Types 1, 2, 3, 4, or 5. Additionally, an used channel is regarded as Type 0. Based on the r_i's and the number of transmission packets of SU 1 and SU 2, the transmission times T_{trans} are given by:

$$Type_{Ch} = \begin{pmatrix} 5 \\ 0 \\ 1 \\ 3 \\ 3 \\ 3 \\ 3 \\ 3 \\ 3 \\ 3 \end{pmatrix}, \; T_{trans} = \begin{pmatrix} 0.0469 & 0.0039 \\ 0.0938 & 0.0078 \\ 0.0313 & 0.0026 \\ 0.0938 & 0.0078 \\ 0.0469 & 0.0039 \\ 0.0313 & 0.0026 \\ 0.0938 & 0.0078 \\ 0.0313 & 0.0026 \\ 0.0938 & 0.0078 \\ 0.0469 & 0.0039 \end{pmatrix}.$$

The threshold τ in Eq. 5.24 is set to 1.6722, which is the minimum value for SU 2 to be allocated one channel without being penalized. Thus, based on Eq. 5.24, the rewards are calculated using the above matrices. The signal energy e_b is computed based on 5.7 and the values assigned for our Game theoretic strategy are as follows:

$$\begin{aligned} e_b \;=\; & 0, \;\; for\ unavailable\ channel, \\ & 1, \;\; for\ Type\ II, \\ & 1.5, \;\; for\ Type\ V, \\ & 2, \;\; for\ Type\ I, \\ & 2.5, \;\; for\ Type\ IV, and \\ & 3, \;\; for\ Type\ III. \end{aligned} \tag{5.25}$$

Referring to the reward table, we have neglected the rewards for the g_{21} and g_{22}. The reason for this is that the second channel, i.e., 929.12 MHz, is used by a PU and the reward for using this channel is always 0. From Tables 5.2, 5.3, and according to Eq. (5.13), the single objective function optimization also achieves a maximum at g_{71}, g_{72} with total reward of 0.3040. As observed from Tables 5.2 and 5.3, a unique Nash equilibrium is also achieved at g_{71}, g_{72} with rewards $(0.2814, 0.0234)$. This implies that the seventh channel, i.e., 929.14 MHz, is allocated to both SU 1 and 2 for maximum signal power on this channel during the 84^{th} sweep. Additionally, the difference $I_{dur} - T_{trans}$ for the seventh channel is the

Table 5.2: Reward table to achieve Nash Equilibria with 10 strategies for $SU1$ and 6 for $SU2$

$SU1$	$SU2$					
	g_{12}	g_{32}	g_{42}	g_{52}	g_{62}	g_{72}
g_{11}	0.035,0.003	0.035,0.001	0.035,0.012	0.035,0.006	0.035,0.004	0.035,0.023
g_{31}	0.016,0.003	0.016,0.001	0.016,0.012	0.016,0.006	0.016,0.004	0.016,0.023
g_{41}	0.140,0.003	0.140,0.001	0.140,0.012	0.140,0.006	0.140,0.004	0.140,0.023
g_{51}	0.140,0.003	0.140,0.001	0.140,0.012	0.140,0.006	0.140,0.004	0.140,0.023
g_{61}	0.095,0.003	0.095,0.001	0.095,0.012	0.095,0.006	0.095,0.004	0.095,0.023
g_{71}	0.281,0.003	0.281,0.001	0.281,0.012	0.281,0.006	0.281,0.004	0.281,0.023
g_{81}	0.016,0.003	0.016,0.001	0.016,0.012	0.016,0.006	0.016,0.004	0.016,0.023
g_{91}	0.141,0.003	0.141,0.001	0.141,0.012	0.141,0.006	0.141,0.004	0.141,0.023
g_{101}	0.070,0.003	0.070,0.001	0.070,0.012	0.070,0.006	0.070,0.004	0.070,0.023

Table 5.3: Reward table to achieve Nash Equilibria with 10 strategies for $SU1$ and remaining 3 for $SU2$

$SU1$	$SU2$		
	g_{82}	g_{92}	g_{102}
g_{11}	0.035,0.004	0.035,0.012	0.035,0.006
g_{31}	0.016,0.004	0.016,0.012	0.016,0.006
g_{41}	0.140,0.004	0.140,0.012	0.140,0.006
g_{51}	0.140,0.004	0.140,0.012	0.140,0.006
g_{61}	0.095,0.004	0.095,0.012	0.095,0.006
g_{71}	0.281,0.004	0.281,0.012	0.281,0.006
g_{81}	0.016,0.004	0.016,0.012	0.016,0.006
g_{91}	0.141,0.004	0.141,0.012	0.141,0.006
g_{101}	0.070,0.004	0.070,0.012	0.070,0.006

least (1.5862, 1.6722 seconds) among all the other channels. For better appreciation, higher differences ($I_{dur} - T_{trans}$) are noticed for 3^{rd}, 8^{th}, and 10^{th} channels with (10.0487, 10.0774 seconds), (16.7687, 16.7974 seconds), and (10.0331, 10.0761 seconds), respectively.

5.6 Experimental Results

In this section, we provide some important observations deduced from the proposed Game theoretic strategies. For our first game theoretic model, the reward function to achieve maximum channel capacity depends on the quality of available channels and the SNR admissible on them. For our second strategy, the reward function depends on a number of parameters: (i) Idle duration of each channel at any specific time instant, (ii) Transmission time for the allocated SU in each available channel, and (iii) Signal energy admissible on each channel depending upon its quality. The reward functions, based on the parameters laid above, are computed using the real-time spectrum measurement data taken on the paging channels (928-948 MHz) over 500 sweeps each of duration 1.68 seconds [39]. These extensive measurements have been performed by the Wireless Innovation Laboratory of Worcester Polytechnic Institute.

Figure 5.4 refers to the transmission power (dBm) received by the antenna used in the experimental set-up on 10 channels ranging from 928.8 MHz to 929 MHz. The average received power is -115 dBm over the range of frequencies between 928 MHz and 928.9 MHz over all 500 sweeps. Increased received power of around -100 dBm are noticed on the channel 928.95 MHz to 929 MHz over almost all 500 sweeps. This figure indicates that the paging band was partially used by the PUs during the time the experiment was conducted.

Figure 5.5 refers to the transmission power (dBm) received by the antenna used in the experimental set-up on 10 channels ranging from 929 MHz to 929.2 MHz. A substantial amount of received power around -65 dBm is observed on the channel 929.1 MHz to 929.16 MHz for all 500 sweeps. It is clear from this figure that the PUs use this channel 929.1 MHz to 929.16 MHz during the measurement campaign.

The idle durations are shown in Figure 5.6 over 10 idle intervals in both channels (928.8

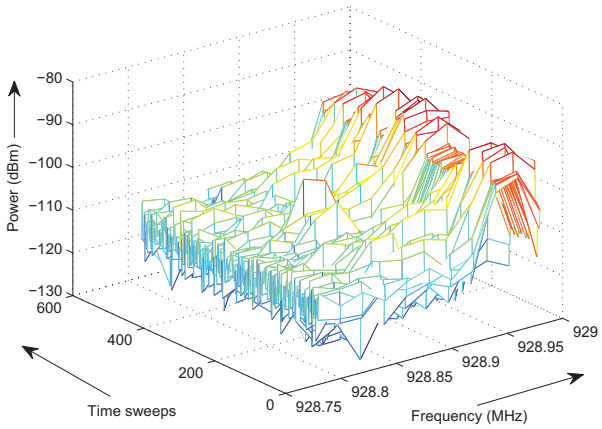

Figure 5.4: Transmission power variation over 10 frequency slots, i.e., 928.8 MHz to 929 MHz.

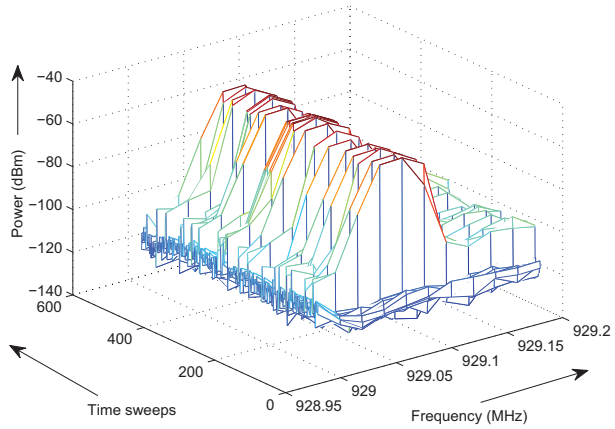

Figure 5.5: Transmission power variation over 10 frequency slots, i.e., 929 MHz to 929.20 MHz.

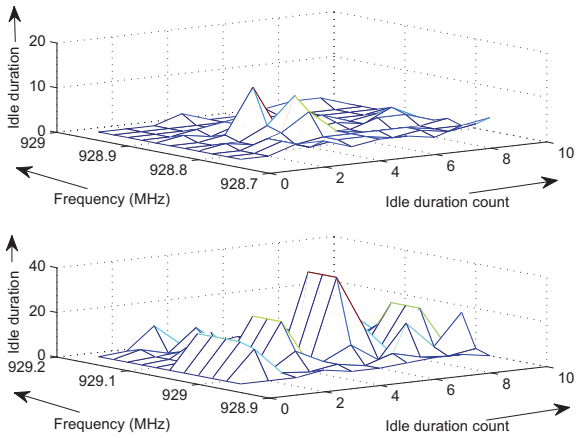

Figure 5.6: Idle durations over 10 consecutive idle intervals in both paging bands, i.e., 928.8 MHz to 929 MHz and 929 MHz to 929.20 MHz.

MHz to 929 MHz and 929 MHz to 929.20 MHz). Since there is no definitive method to comprehend PU's occupancy, we have used traditional energy detection method to predict PU occupancy. The threshold is set to -108.5 dBm. If the received power on a channel during any time sweep is above this threshold, a binary variable PU_{occ}, designated for PU occupancy, is set to 0, *i.e.*, used channel. Otherwise, it is 1, i.e., unused channel. Hence, K consecutive time sweeps with $PU_{occ} = 0$ is defined as one idle duration of duration K. In Figure 5.6, we consider 10 such idle durations. As shown in Figure 5.6, the magnitude of each idle duration in channel 929 MHz-929.20 MHz is higher than in other channel 928.8 MHz-929 MHz.

Using the categorization presented in Figure 5.2, we have also computed the Types of the paging channels, i.e., 928.8 MHz to 929 MHz and 929 MHz to 929.20 MHz and this is shown in Figure 5.7. As noticed from the figure, there is a larger number of Type III channels in 929 MHz to 929.20 MHz paging spectrum as compared to 928.8 MHz to 929 MHz. As discussed earlier, Type III channel are the most suitable for SUs and higher signal energy is allowed in these channels compared to other types.

The intention of Figure 5.8 is to prove the significance of quality of channels in spectrum allocation. The results shown in Figure 5.7 are utilized for obtaining results in Figure 5.8 where in we have considered five sets of PU occupancy configurations during time

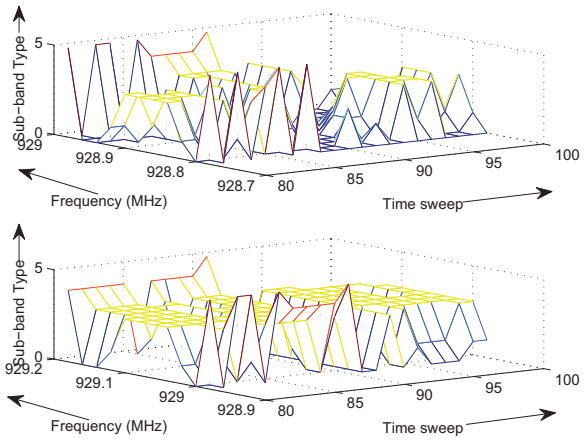

Figure 5.7: Quality of channels over sweeps 80 to 100 based on their neighboring channels considered for both paging bands, i.e., 928.8 MHz to 929 MHz and 929 MHz to 929.20 MHz.

sweeps 80-100. The x-axis refers to the 20 sweeps. As explained in Section III, PU occupancy during each configuration results in varying types of channels (Types I, II, III, IV, and V). Based on the values of SNR matrix in Eq. 5.19, the rewards are computed for a single SU using Eq. 5.17 for all its possible maximal allocation matrices. The top figure in Figure 5.8 refers to 10 channels, i.e., 928.8-929 MHz and the one below refers to 929-929.2 MHz. As observed, higher SNR is obtained in paging channels 929-929.2 MHz with a maximum of 44 units of SNR. The maximum SNR obtained in channels 928.8-929 MHz is 33 units. The reason for higher SNR values are due to the larger number of Type III channels in the paging band 929-929.2 MHz during the 20 sweeps.

Figure 5.9 demonstrates the significance of additional parameters like idle durations and transmission times in spectrum sharing. The results of Figure 5.6 are utilized for obtaining results in Figure 5.9. We have considered five sets of PU occupancy configurations as described above. The signal energy allowed on each channel are obtained from Eq. 5.25. The x-axis refers to the 20 sweeps namely, 80-100 sweeps. The reward functions are now calculated on the basis of Eq. 5.24 for two different SUs with $24,000$ and $2,000$ data packets. The threshold is set to 1.6722, as explained earlier. As mentioned in Section 5.5, the Game theoretic strategy allocates a single channel to an SU, as opposed to our

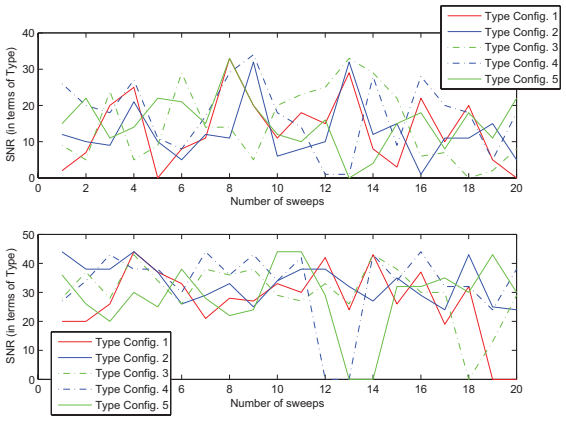

Figure 5.8: SNR computations based on our reward function defined in Eq. 5.17 for both paging bands, i.e., 928.8 MHz to 929 MHz and 929 MHz to 929.20 MHz.

first spectrum sharing strategy. Hence, the SNR values obtained are much less than that obtained in Figure 5.8. Additionally, since we have introduced a penalty for selection of a channel with a larger idle duration as compared to an SU's transmission time, that explains the substantial reduction in SNR as compared to that in Figure 5.8. The top of Figure 5.9 is for SU with $24,000$ packets and the one below for SU with $2,000$ packets. The SNR's for the second SU is an order less than the SU with higher number of data packets because of small transmission times (an integral part of our defined reward function).

5.7 2-Person Game Formulation for Coexistence of PUs and SUs

In this section, we focus on a single SU. Suppose the SU is using a particular free sub-band. Technically, it can entertain any amount of transmission power. However, the prospect of a PU entering the sub-band at any time is real. If the SU uses power greater than the FCC's spectral mask for the TV spectrum, it has to leave the sub-band the moment the PU enters, thus incurring a loss of power. For simplicity, assume the SU entertains the following three options whenever the sub-band is free to use:

a_1 : Use the sub-band at transmission power < FCC spectral mask.

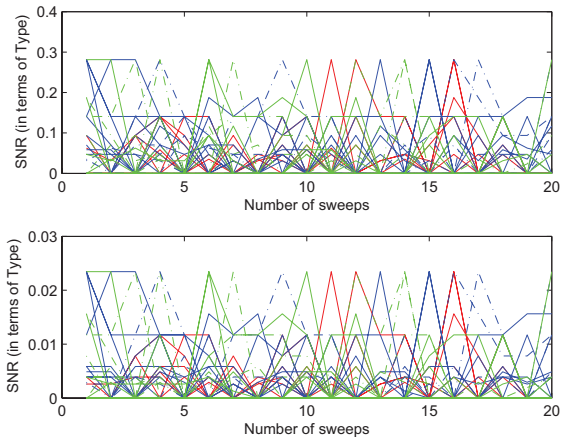

Figure 5.9: SNR computations for SU 1 and SU 2 based on their utility functions defined in Eq. 5.24 for paging bands 929 MHz to 929.20 MHz.

a_2 : Use the sub-band at transmission power comparable to FCC's spectral mask.

a_3 : Use the sub-band at the transmission power higher than the FCC's specified spectral mask for the TV spectrum.

Now, assume that the PU which owns the sub-band, arrives in the sub-band presently used by the SU, creating a conflict. Technically, the SU has to stop using the sub-band. On the other hand, the PU can entertain one of the following two options:

b_1 : Allow the SU share the sub-band.

b_2 : Do not allow the SU share the sub-band.

With this information in place, we now formulate the pay-off functions for the PU and the SU.

$Pay-off\ function\ of\ SU$:

$g_1(a_1, b_1)$ = Gain in SU transmission power in the allocated sub-band, a positive value.

$g_1(a_2, b_1)$ = Gain in SU transmission power in the allocated sub-band, a positive value.

$g_1(a_3, b_1)$ = Loss in SU transmission power for leaving the allocated sub-band, a negative value.

$g_1(a_1, b_2)$ = Loss in SU transmission power for not allowing SU in the allocated sub-band, a negative value.

$g_1(a_2, b_2)$ = Loss in SU transmission power for not allowing SU in the allocated sub-band,

Table 5.4: Pay-off table to achieve Nash Equilibria

SU	PU	
	b_1	b_2
a_1	$0.17 \times 10^{-5}, 0.371 \times 10^{-3}$	$-0.17 \times 10^{-5}, 0.37 \times 10^{-3}$
a_2	$0.37 \times 10^{-5}, 0.373 \times 10^{-3}$	$-0.37 \times 10^{-5}, 0.37 \times 10^{-3}$
a_3	$-0.67 \times 10^{-5}, 0.37 \times 10^{-3}$	$-0.67 \times 10^{-5}, 0.37 \times 10^{-3}$

a negative value.

$g_1(a_3, b_2)$ = Loss in SU transmission power for not allowing SU in the allocated sub-band, a negative value.

$Pay-off\ function\ of\ PU$:

$g_2(a_1, b_1)$ = Gain in total signal power ($SU + PU$) in the allocated sub-band, a positive value.

$g_2(a_2, b_1)$ = Gain in total signal power ($SU + PU$) in the allocated sub-band, a positive value.

$g_2(a_3, b_1)$ = Loss in total signal power (*only PU*) in allocated sub-band, a positive value.

$g_2(a_1, b_2)$ = Loss in total signal power (*only PU*) in allocated sub-band, a positive value.

$g_2(a_2, b_2)$ = Loss in total signal power (*only PU*) in allocated sub-band, a positive value.

$g_2(a_3, b_2)$ = Loss in total signal power (*only PU*) in allocated sub-band, a positive value.

We illustrate identification of the Nash equilibrium using a simple example with admissible transmission power limits of 0.37×10^{-5} mW/5MHz (i.e., 100 MHz of TV spectrum is divided into 20 sub-bands, each of 5 MHz with spectral mask of $-61.3 dBm/MHz$ in each sub-band [4]). The transmission power for the PU is taken to be $-41.3 dBm/MHz$ which is equivalent to 0.370×10^{-3} mW/5MHz.

From the pay-off functions defines in Table 5.4, we can identify (a_2, b_1) strategy as a unique Nash equilibrium. This implies that the SU wants to optimize its transmission power closer to the admissible power constraint of 0.37×10^{-5} while the PU accommodates the SU to achieve higher signal power which in turn, increases the channel capacity.

In some situations, a free sub-band is used by two or more SUs when the PU, which owns the channel, enters the sub-band. In such scenarios, the other SU(s) can initiate the

2-person Game with the PU as discussed above. But, the PU informs the initiating SU(s) about the ongoing communication of an existing SU in the same sub-band. This resolves the serious problem we posed before: *While a SU coexists with a PU restricting itself within the admissible power limit, how can the other SU(s) be informed about the existing SU's communication in the same sub-band?* The lack of this information can encourage a new SU to initiate communication within admissible power limits in the same sub-band of a PU. This additional power from the new SU can prove to be detrimental as it can create inadmissible interference to the PU, thereby violating the FCC's spectral mask for coexistence in the same sub-band.

A game theoretic paradigm can be developed to resolve conflicts between the PU and the SU(s) which could form a coalition analogous to the above 2-person Game. Details are planned as a future work.

5.8 Conclusion

Two game theoretic strategies have been proposed to achieve maximum channel capacity. Initially, a free channel has been classified uniquely as one of the five types depending on its neighboring channels. We have shown that the type of available channel has definite impact on the SNR. In our first spectrum allocation strategy, multiple available channels are allocated to SUs, subjected to availability and interference constraints. Maximal allocation matrices are then characterized. Optimization of channel capacity over all maximal allocation matrices are discussed. To resolve conflicts due to allocation matrices by SUs, a Game theoretic ideas is introduced and Nash equilibria are identified. Further, we have identified a unique Nash equilibrium allocation for the SUs that can maximize the channel capacity. Next, we have developed a second Game to allocate a single channel to each SU, as opposed to our first strategy. In such a scenario, we have developed reward functions based on idle duration of each available channel, transmission time for an allocable SU, and the signal energy limited to each channel. Finally, we have provided extensive simulation results on the game theoretic approached proposed. It would be interesting to study the dependence of variable transmission power requirements of SUs and the corresponding

interference imposed on the PUs in adjacent channels.

To resolve conflict between SU and PU, a two-person game is introduced and Nash equilibrium is identified. It would be interesting to develop a computational algorithm to enumerate all possible maximal allocation matrices for a given availability matrix and the interference matrix. This will be pursued as our future research work. Additionally, the probability of detecting a free sub-band in the entire TV spectrum changes over time. So, our future work will focus on the probabilistic characterization of the distribution of free sub-bands with temporal and spatial variations of the locations of the PUs in the entire TV spectrum.

Acknowledgments

The authors would also like to thank Prof. Alexander M. Wyglinski for sharing the real-time measurements taken on the paging band (928-948 MHz) under the project supported by the National Science Foundation (NSF) sponsored project “NeTS-WN: Quantification of Spectrum Availability for Wireless Network Access” with project number CNS-0754315.

Chapter 6

Priority-based Spectrum Allocation for Cognitive Radio Networks Employing NC-OFDM Transmission

6.1 Introduction

For higher spectral efficiency, multiple access techniques can be employed such that multiple SUs can transmit data on the same section of the spectrum. Le and Hossain [69] employed code division multiple access (CDMA) technique while allocating resources in spectrum sharing among the SUs satisfying their quality of service (QoS) constraints for the BER. The interference imposed on the PUs is also taken into account in their proposed spectrum allocation technique. *Orthogonal frequency division multiplexing* (OFDM) [70] is known for its spectral efficiency. Additionally, OFDM converts a high data rate serial signal stream into several parallel low rate symbol streams transmitted in parallel over multiple number of sub-carriers. These sub-carriers possess narrow bandwidth in comparison to the original transmission data, which means that a frequency selective fading channel is effectively transformed into a collection of approximately flat fading sub-channels. Attar *et al*. [71] proposed resource allocation among several SUs in an OFDM-based network with the intention of increasing the system throughput while limiting interference to the PUs. The optimization problem in [71] can be challenging when considering the spec-

trum occupancy characteristics of the PUs. *Spectrum pooling* [72], a concept where data is transmitted only on active or unoccupied sections of an operating spectrum, can be implemented using OFDM. To support co-existence, the SUs need to use modulation techniques to transmit data on only smaller idle sections of the spectrum. Qu *et al*. [73] studied the performance of multi-carrier CDMA-based cognitive networks with the joint allocation of frequency and power among the SUs while ensuring limited interference on the PUs. Prior to the joint allocation strategy, the subcarrier availability has been computed using multitaper spectrum estimation, and channel states using linear minimum mean square estimation. These *a-priori* knowledge about spectrum utilization made their study much more interesting and realistic in the context of cognitive radio networks. Zhang and Liang [74] utilized multiple antennas at the SU terminals to exploit spatial multiplexing in order to maximize the system throughput.

Although efficient resource allocation strategies have been proposed in the open literature, there are a series of issues that need to be considered in the context of CRNs performing dynamic spectrum access: (*i*) Prioritize SUs based on their varying performance requirement metrics such as BER and delay constrains, (*ii*) Prioritize sub-bands based on their BER support and fraction of unoccupied bandwidth, and (*iii*) Utilize information of spectrum occupancy statistics in designing dynamic and truly opportunistic spectrum sharing approach. Consequently, spectrum measurements [5,8] are critically important in order to characterize the degree of utilization of the available sub-bands.

In this chapter, we propose three priority-based spectrum allocation techniques for enabling dynamic spectrum access by the SUs in licensed spectrum. The proposed techniques use critical *a-priori* information, *i.e.*, spectrum occupancy statistics [75] in deciding the priorities of the spectrum allocations. Furthermore, the proposed techniques are specifically designed for a variant of OFDM transmission, namely non-contiguous OFDM (NC-OFDM) [75], in order to enable efficient spectrum sharing among prioritized SUs. Specifically, it allows usage of idle non-contiguous sections of sub-bands by de-activating sub-carriers in sections of sub-bands that are occupied by the PUs. Our proposed strategies depend on two priority metrics:

- NC-OFDM sub-carriers and BER support in each sub-band to define preferred sub-

bands; and

- Priorities among applications generated from the SUs based on BER and delay requirements. [1]

The proposed spectrum allocation schemes can be divided into two categories: *(i)* allocation of a single SU in each sub-band, and *(ii)* allocation of multiple SUs in each sub-band. Under the first category, two allocation strategies are proposed namely, (*i*) *First Available First Allocate* (FAFA), which employs the traditional OFDM approach without the knowledge of active and inactive sub-carriers, and (*ii*) *Best Available Selective Allocate* (BASA), which utilizes the information of the NC-OFDM active sub-carriers and BER information for each sub-band to allocate a sub-band to a single SU satisfying its request. Unlike the first category, the second category introduces *Best Available Multiple Allocate* (BAMA), a multiple access scheme using *non-contiguous orthogonal frequency division multiple access* (NC-OFDMA), a technique that works on the same principle of NC-OFDM while supporting multiple access on its non-contiguous sub-carriers.

The rest of the chapter is organized as follows. Section 6.2 briefs the spectrum occupancy model which facilitates our priority scheduling algorithms. Section 6.3 gives detailed description of the three proposed algorithms. Section 6.4 describes the implementation of the algorithms and compares their performance using bandwidth utilization and achieved throughput. Finally, Section 6.5 draws several conclusions.

6.2 System Model

Cognitive radios are capable of spectrum sensing, which is essential in order for the SUs to avoid interference with the PUs. Real-time spectrum measurements coupled with the spectrum occupancy statistics are critical for spectrum sharing. Our research exploits the spectrum utilization information of the PUs in allocating spectrum among the SUs. The central idea is to allocate preferred sub-bands in a prioritized order of SUs' requests.

[1] For example, a real-time application can sustain delay less than or equal to 40 ms with BER requirement of 10^{-7}, while a typical high quality audio application can sustain a maximum of 200 ms delay over a channel with BER of 10^{-5} [76].

Preference of a sub-band depends on the experienced channel conditions as well as the number of unoccupied frequencies. Idle durations also play a vital role in deciding the priority of a sub-band. For example, spectrum blocks with longer mean idle times are assigned to requests with longer transmission durations. Moreover, attenuation profiles can be utilized to assign frequency bands with less attenuation to communication links requiring high error robustness.

In this chapter, we consider a wireless network with a cognitive radio base station and several queued applications. In Figure 6.1, the SUs generate M applications represented by the order $i_{\text{app}} = 1, 2, \cdots, M$. The users are within one-hop transmission range of the base station. Each request is received at the base station, which assigns a priority value based on the BER and delay requirements of user i_{app}. The cognitive base station also detects the unoccupied blocks in N sub-bands of an operating spectrum. Each sub-band is represented by $j_{\text{sb}} = 1, 2, \cdots, N$. Based on the size of the detected block in a sub-band, the base station computes the number of active sub-carriers $(P - m)$ in sub-band j_{sb}, where m represents the number of occupied or inactive sub-carriers in an NC-OFDM symbol of total P sub-carriers. This process is iterated over all sub-bands $1, 2, \cdots, N$ in the target spectrum of operation.

The base station also computes the BER supported by sub-band j_{sb} while taking fading channel coefficients into consideration. As shown in Figure 6.1, the base station maintains a priority table of BER and the number of active sub-carrier values of all sub-bands. This

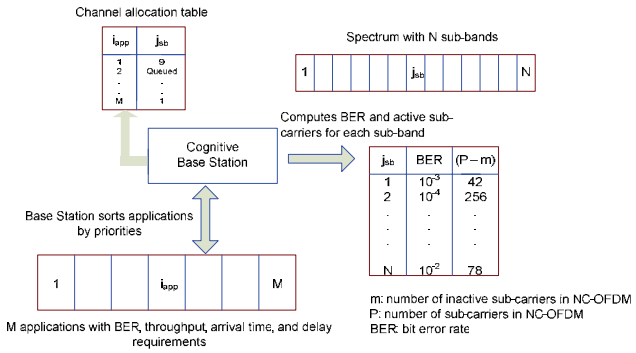

Figure 6.1: Schematic diagram of the system model used for proposed priority scheduling techniques among SUs.

database needs to be updated over time, using the PU occupancy statistics obtained from the spectrum occupancy model. As a result, the base station maps a suitable sub-band j_{sb} to a request i_{app}, based on its priority derived from its BER and the delay requirements. The channel allocation table maintains recent allocation status performed by the base station to satisfy requests generated from M SUs. Note that an application is queued if no sub-band can be scheduled to satisfy its requirements.

6.2.1 Wireless Multicarrier Transmission Format

Let the bandwidth assigned for an NC-OFDM symbol with P sub-carriers be denoted by BW [Hz]. Hence, the bandwidth for a single sub-carrier of NC-OFDM is (BW/P) [Hz]. The effective bandwidth BW_{eff} for data transmission in an NC-OFDM system, with m inactive sub-carriers, is expressed as:

$$BW_{\text{eff}} = BW - \left(\frac{BW}{P}\right)m = BW\left[1 - \frac{m}{P}\right]. \tag{6.1}$$

Therefore, the effective capacity C_{eff} of an NC-OFDM symbol is:

$$\begin{aligned} C_{\text{eff}} &= BW_{\text{eff}} \log(1+\gamma) \\ &= BW\left[1 - \frac{m}{P}\right]\log(1+\gamma) \\ &= \left(1 - \frac{m}{P}\right)BW \log(1+\gamma) \\ &= \left(1 - \frac{m}{P}\right)C, \end{aligned} \tag{6.2}$$

where C is the Shannon capacity of the NC-OFDM system, and γ is the signal-to-noise ratio of the NC-OFDM symbol. Observe that $0 \leq \frac{m}{P} \leq 1$, for $m = 0, \cdots, P$. Eq. (6.2) implies that the fraction m/P plays a decisive role in defining the effective capacity. In other words, for a fixed value of P, smaller value of m, *i.e.*, few inactive sub-carriers in a block of sub-bands, yields a higher C_{eff} as compared to higher values of m. This idea leads to the core concept of our unique spectrum allocation strategy using NC-OFDM. The following section describes our proposed approaches in details taking the model illustrated in Figure 6.1 into consideration.

6.3 Proposed Priority-based Spectrum Allocation Techniques

Our proposed priority allocation techniques are specifically designed for NC-OFDM-based wireless links that can support dynamic spectrum access. Suppose that each NC-OFDM symbol consists of P narrow-band sub-carriers divided over a fixed bandwidth BW. This bandwidth can span across a definite number of sub-bands in the spectrum considered. Hence, it is essential to have the knowledge of the following:

- PU occupancy in the sub-bands to compute idle durations; and
- Bandwidth occupied by each PU in these sub-bands to compute number of inactive NC-OFDM sub-carriers.

Once this information is available, the cognitive base station can then decide on the number of sub-carriers to be made inactive. Suppose that the i^{th} PU occupies a bandwidth BW_i in sub-band $i_{sb} = 0, 1, \cdots, N$. The number of NC-OFDM sub-carriers in sub-band i_{sb} is $\frac{BW_i}{BW/P}$. Hence, the number of inactive sub-carriers m can be expressed as:

$$m = \sum_{i=1}^{N} BW_i \left(\frac{P}{BW}\right). \tag{6.3}$$

If we assume that all the PUs occupy the same bandwidth BW_{equal} in their respective sub-bands, then Eq. (6.3) can be re-written as:

$$m = (NP)\left(\frac{BW_{equal}}{BW}\right). \tag{6.4}$$

Consequently, the cognitive node can compute the effective capacity C_{eff} by substituting value of m in Eq. (6.2) as:

$$C_{\text{eff}} = \left(1 - N\frac{BW_{equal}}{BW}\right)C. \tag{6.5}$$

Given this framework for performing prioritized spectrum allocation in NC-OFDM-based wireless networks, we now proceed with three allocation techniques.

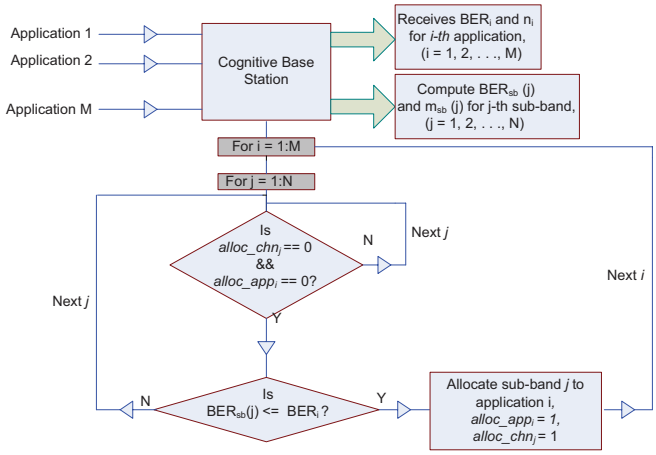

Figure 6.2: Flow diagram of the proposed FAFA approach.

6.3.1 First Available First Allocate (FAFA) Spectrum Allocation Approach

In this scheme, the cognitive base station constructs a priority queue based on the arrival time of each application into the queue. This strategy follows the spectrum pooling technique illustrated in [72]. FAFA selects the first application from the queue and allocates the first available sub-band that satisfies the BER requirement of the application. The scheme follows the same strategy for the subsequent sub-bands. This type of spectrum allocation does not compare BER requirements of other applications in the queue before allocating a sub-band to its requesting application. A situation can arrive when an application with BER requirement of 10^{-2} is allocated a sub-band which supports BER of 10^{-4} or above. In such a case, an error sensitive application may suffer at the cost of the error-prone application due to lack of sub-bands with better BER support. As is evident, this scheme gives a lower bound of performance and serves as the base case for comparison with other two proposed schemes.

The flow diagram of FAFA is depicted in Figure 6.2. On receiving M requests from the SUs, the base station prioritizes an i^{th} request, for $i = 1, 2, \cdots, M$, into a queue on the basis of its arrival time. It also computes the BER support of the j^{th} sub-band, $BER_{\text{sb}}(j)$, and its number of inactive sub-carriers m of NC-OFDM symbol, $m_{\text{sb}}(j)$, computed using

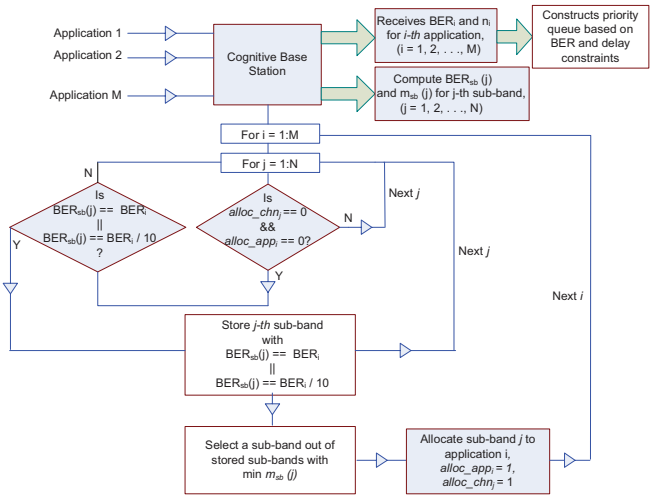

Figure 6.3: Flow diagram of the proposed BASA approach.

Eq. (6.3), for $j = 1, 2, \ldots, N$. For convenience, we define two vectors, $alloc_chn_j$ and $alloc_app_i$ to keep track of the channel numbers assigned and the indices of SUs which have been allocated sub-bands for their requests, respectively. Now for every user i, the base station performs a search for a suitable sub-band out of the N sub-bands. The decision block ensures that an allocated j^{th} sub-band is never allocated again to a requesting SU (*i.e.*, $alloc_chn_j == 0$) as well as that a i^{th} SU is never allocated two or more sub-bands at the same time instant (*i.e.*, $alloc_app_i == 0$). After this decision, a sub-band is allocated only after checking that the $BER_{\text{sb}}(j)$ is better or equal to the i^{th} SU's requested BER, BER_i. In the final stage of Figure 6.2, once a channel is allocated, the status of j^{th} sub-band and i^{th} SU request are set appropriately to prevent duplicate allocation of sub-bands and user requests (i.e., $alloc_chn_j == 1$ and $alloc_app_i == 1$). This process is iterated over all the M requests.

6.3.2 Best Available Selective Allocate (BASA) Spectrum Allocation Approach

In this approach, the cognitive base station constructs a priority queue based on the joint requirement of BER and delay requirements. It is important to notice that all applications

share a common relation between BER and delay requirements. All real time applications (implying better BER performance), such as streaming media, video conference, and online video games, are delay sensitive. Hence, they can sustain only a minimum transmission delay (< 40 ms). Similarly, all non-real time applications, such as data applications, are robust against fading channel and hence can be served on sub-bands with lower BER performance. Additionally, these non-real time applications can sustain delays in the order of 200 to 400 ms. This priority allocation scheme does not consider throughput in assigning priorities along with BER and delay constraints. The reason for this consideration is that there are many typical applications. For example, applications from public safety require less bandwidth and better BER performance. Similarly, there are applications, such as high quality audio requiring 940 kb/s throughput and BER of 10^{-5}, that demand higher bandwidth while simultaneously robust against fading channels. Therefore, to maintain fairness among the requesting applications, priorities are defined based on only the delay and the BER constraints.

In BASA, the cognitive base station allocates the best available sub-band that satisfies the selective requirement of a SU. This selective allocation is based on the prioritized BER and delay requirements and as well as the throughput, *i.e.*, bandwidth demand. Intuitively speaking, the BASA definitely performs better than FAFA with respect to throughput maximization and bandwidth utilization. The performance results in Section 6.4 illustrate our assertion.

The potential of NC-OFDM is emphasized in the BASA scheme. It has already been proved [75] that higher number of active sub-carriers in NC-OFDM results in better BER performance. In BASA, we exactly utilize this valuable information wherein the base station computes the number of non-contiguous active sub-carriers in each sub-band. This information is also critical to calculate the throughput supported by each sub-band. With this information available, the base station allocates the best sub-band that satisfies not only the user prioritized BER and delay requirements but also has the maximum number of active sub-carriers to support throughput requirement desired by the SU applications.

The flow diagram of BASA is depicted in Figure 6.3. On receiving M requests from the SUs, the base station prioritizes i^{th} request, $i = 1, 2, \ldots, M$, into a queue on the basis of its BER and sustainable delay requirements. It also computes the BER support $BER_{\text{sb}}(j)$

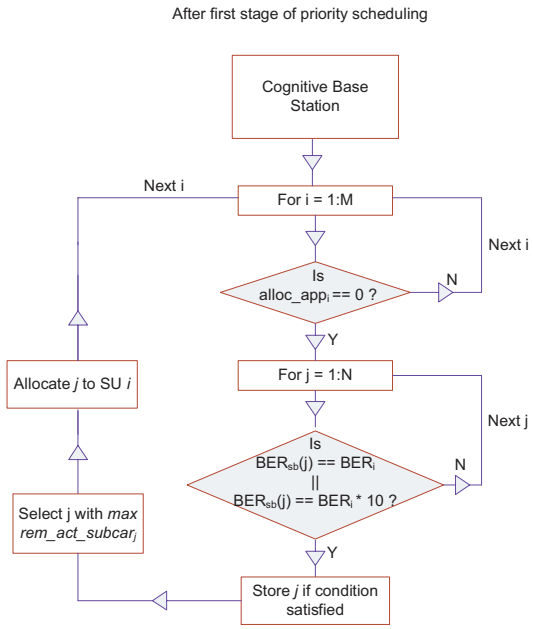

Figure 6.4: Flow diagram of the proposed BAMA approach.

and the number of inactive sub-carriers of NC-OFDM symbol $m_{\text{sb}}(j)$ for each j^{th} sub-band using Eq. (6.3), $j = 1, 2, \ldots, N$. The two vectors, $alloc_chn_j$ and $alloc_app_i$ are as defined for FAFA, respectively. Similar decision, as described in FAFA, is performed in the first decision block. The improvement in BASA over FAFA evolves from the following decision blocks. Those sub-bands with BER support $BER_{\text{sb}}(j)$ equal to or one order better than the requested BER BER_i of the i^{th} SU are stored. Out of these stored sub-bands, a sub-band with the highest number of active sub-carriers (i.e., minimum $m_{\text{sb}}(j)$) is allocated as illustrated in Figure 6.3. Finally, the status of the j^{th} sub-band and i^{th} SU request are set appropriately to prevent duplicate allocation of sub-bands and user requests (i.e., $alloc_chn_j$ == 1 and $alloc_app_i$ == 1). This process is iterated over all the M requests.

6.3.3 Best Available Multiple Allocate (BAMA) Spectrum Allocation Approach

This multiple access technique using NC-OFDMA has an initial operation similar to that of BASA described above. BAMA performs its priority allocation in two stages as follows:

- *First stage*: Scheduling of prioritized requests to selective sub-bands similar to BASA; and
- *Second stage*: Detects un-allocated user requests and schedules them to previously allocated sub-bands, which satisfies the BER and throughput requirements. This feature is unique of NC-OFDMA. This differentiates BAMA from the other two proposed schemes.

Hence, the flow diagram in Figure 6.3 also applies for the execution of the first stage in BAMA. The operations involved in the second stage is illustrated in Figure 6.4. For each i^{th} SU request in the priority queue, the cognitive base station checks the i^{th} index of the vector $alloc_app_i$. If it detects a zero value, it interprets an un-allocated request. For each un-allocated request in the priority queue, it searches and stores sub-bands with equal or one order lower in magnitude of BER support (*i.e.*, $BER_{\mathrm{sb}}(j) == BER_i$ or $BER_{\mathrm{sb}}(j) == BER_i \times 10$ in Figure 6.4). The reasons for including a checking condition for a sub-band with lower order BER are as follows:

- Possibility of absence of a sub-band, even during the first stage of operation, with equal order of BER support $BER_{\mathrm{sb}}(j)$ as that of BER_i; or
- Possibility of consuming all the sub-bands of equal order of BER support as that of BER_i during the first stage of execution of BAMA, to requests higher in priority than this un-allocated user request.

Thus, instead of queuing the packet for the next time instant, the base station makes an attempt to allocate the waiting request to a sub-band, only if, its BER support is of equal or with one order lower in magnitude as that of the BER requirement of the requesting user.

In the final stage, the base station allocates previously allocated sub-band with maximum number of remaining un-allocated active sub-carriers (*i.e.*, maximum $rem_act_subcar_j$). This supports the name of our priority allocation scheme since the base station allocates the best (*i.e.*, the sub-band with maximum number of un-allocated active sub-carriers) to an un-allocated user request. The reason for selecting the best sub-band is to make sure that this allocation poses limited interference to the PU occupying this sub-band. Consequently, the larger the number of active sub-carriers, either contiguous or non-contiguous, the better the BER performance [75] and better interference mitigation the system and network will possess.

The unique characteristic of BAMA is that it allows flexibility to the user requests with variations in throughput requirements. The priorities are defined based on the BER and the delay requirements of the users' requests. Now, for user with lower throughput but a higher BER constraint will be treated with the same priority as that of an user request with a higher throughput and a similar BER requirement. This allows fairness among the users from the perspective of throughput constraints.

6.4 Simulation Results

In this section, the performance is evaluated for each of the three proposed schemes namely, FAFA, BASA, and BAMA. The schemes are evaluated in terms of bandwidth utilization and throughput achieved for equal number of SUs requests arriving at the base station. The allocation efficiency is evaluated in terms of the number of un-allocated requests per allocation time slot.

We have collected real-time data in the paging band (928-948 MHz) located at latitude $42°16'24.94''$ N and longitude $71°48'35.29''$ W. During the measurement campaign, 500 scans or sweeps have been conducted between 3:31 - 4:30 PM over the entire paging band. The frequency resolution was set to 20 KHz. Using a pre-defined threshold of -68.7 dBm ($\mu + 6\sigma$, where μ and σ are the mean and standard deviation of the power distribution over the entire paging band during any time sweep), it has been observed that a maximum of 17 PU signal were detected. This enables us to compute the active and inactive blocks in

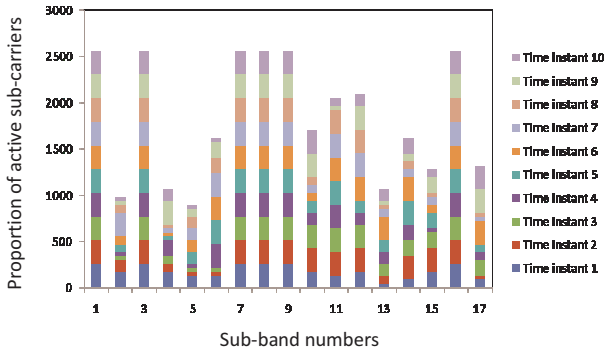

Figure 6.5: Proportion of active sub-carriers for NC-OFDM for all sub-bands for ten time instants.

each sub-band over the entire paging band. Using Eq. (6.4), the number of inactive or unoccupied NC-OFDM sub-carriers for each sub-band are then obtained.

6.4.1 Computation of Priority Metrics from Real-time Measurements

The study is conducted on a spectrum bandwidth of 20 MHz with the sub-bands of 20 KHz bandwidth. As mentioned above, PU signal are detected in only 17 sub-bands out of the total of 1000 sub-bands in the entire paging band. The simulation is performed over a stretch of 10 time sweeps, spanning over 1000 ms. Each allocation slot is of 100 ms duration. Hence, there are 10 allocation slots over the time sweeps considered. Within a allocation period, we assume that the PU occupancy status remains unchanged once they have started using their respective sub-bands. This assumption is valid since allowing changes in PU occupancy within a allocation period would change the parameters (*i.e.*, number of inactive sub-carriers m as well as the active sub-carriers $(P - m)$) utilized in our allocation policy. For our simulation, the term "active sub-carriers" gives a total of all contiguous and non-contiguous sub-carriers in a sub-band. Each NC-OFDM symbol is implemented with 256 sub-carriers. The reason we chose a lower value of the number of sub-carriers is to have reduced impact of peak-to-average-power ratio, an impairment for OFDM systems, on the licensed spectrum users.

One of the critical parameters for our spectrum priority allocation is the number of active sub-carriers $(P - m)$ in each sub-band of the simulated spectrum. Figure 6.5 refers

to $(P - m)$ for each of the 17 sub-bands during a simulation period of 1000 ms. Therefore, as shown in Figure 6.5, during the first time instant sub-bands 1, 3, 7 - 9, and 16 have idle bandwidth equivalent to 256 active sub-carriers, indicating that these sub-bands are idle for that time duration. From the context of the SUs, these sub-bands are preferred to other sub-bands, which are occupied by PUs. Sub-band 13 is the least preferred during the first time instant since it has 34 active sub-carriers. Over the entire simulation duration, it is noted that sub-bands 1, 3, 7 - 9, and 16 have the maximum number of active sub-carriers, *i.e.*, 256 sub-carriers over all 10 time instants. Sub-band 5 has least number of active sub-carriers, *i.e.*, a total of 912 over all the 10 instants. This suggests that sub-band 5 is heavily used by a PU during the entire simulation duration.

Other important parameter for our spectrum priority allocation is the BER supported by each sub-band. Figure 6.6 refers to this parameter for each of the 17 sub-bands during a simulation period of 1000 ms, consisting of 10 instants each of 100 ms allocation duration. Figure 6.6(a) presents the results obtained on first 12 sub-bands during each of the 10 instants of time while Figure 6.6(b) for the rest of 5 sub-bands. During the first time instant, the maximum BER support achieved is of the order of 0.0092 on sub-bands 6, 10, 12, 14, and 15 while in the second instant, sub-bands 9, 10, 11, and 15 can support BER of the order of 0.00028, *i.e.*, 2.8×10^{-4}.

6.4.2 Comparative Analysis of Proposed Algorithms

Combining information retrieved from Figure 6.5 and Figure 6.6, it is concluded that higher priority application requests with BER of the order of 0.001 are queued during the first time instant because of unavailability of suitable sub-bands. On the contrary, during the second time instant, sub-band 9 is best preferred with 256 active sub-carriers and BER support of 0.00028. Since FAFA and BASA allocation schemes allocate one SU per sub-band, only one higher priority request will be served on sub-band 9 while other higher priority requests have to be queued. The BAMA scheme, being a multiple access scheme, will allocate sub-band 9 to its capacity of 256 active sub-carriers to a number of high priority SU requests. This explicitly explains higher bandwidth and better throughput performance of BAMA over FAFA and BASA.

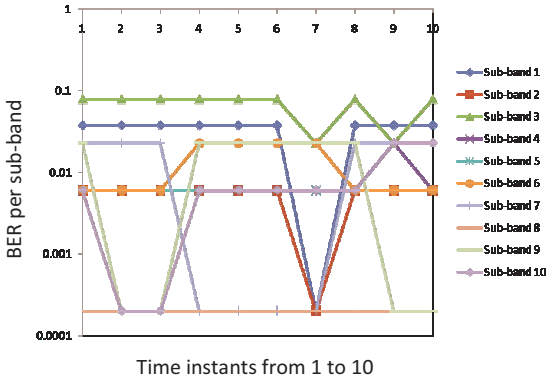

(a) BER support of 10 sub-bands during each of the 10 instants of time.

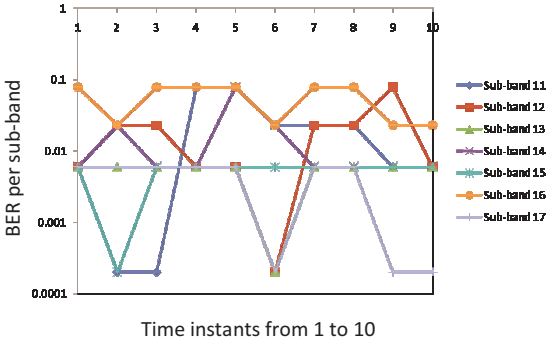

(b) BER support of 7 sub-bands, 11 to 17, during each of the 10 instants of time.

Figure 6.6: BER of all the sub-bands in the spectrum for all ten time instants of our simulation.

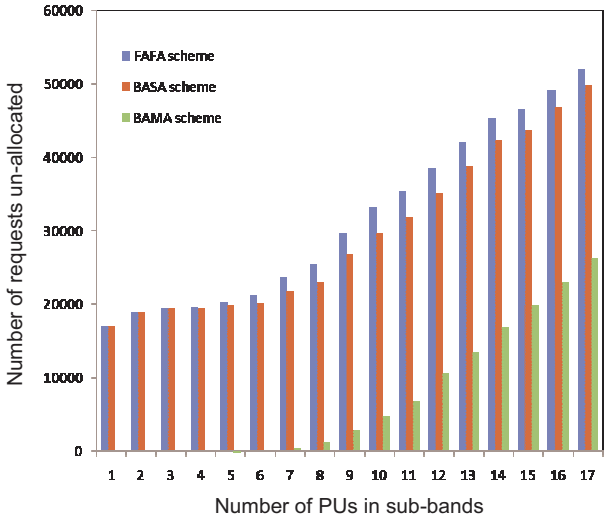

Figure 6.7: Comparison between FAFA, BASA and BAMA schemes for the number of un-allocated requests per time instant for increasing PU occupancy.

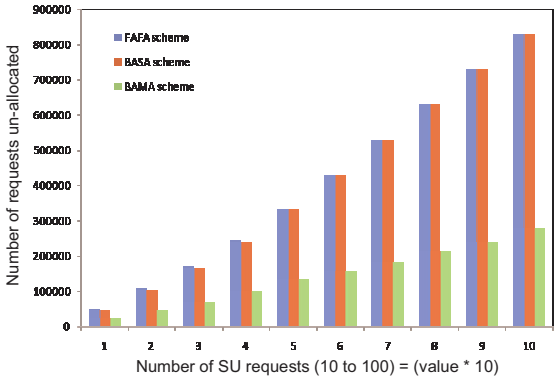

Figure 6.8: Comparison between FAFA, BASA and BAMA schemes for the number of un-allocated requests per time instant for increasing SU requests.

The above conclusion is further emphasized by Figures 6.7 and 6.8 where the simulation is conducted over 1000 iterations, with each iteration involving a complete scenario of PU occupancy over a period of 1000 ms. Again, 10 allocation slots are divided into 100 ms each within the PU occupancy interval of 1000 ms. In Figure 6.7, the *x*-axis represents the increasing number of PU occupancy from 1 to 17 while the *y*-axis refers to the number of requests un-allocated during each allocation slot. In Figure 6.8, the *x*-axis plots the increasing number of application requests from 10 to 100 at the base station while the *y*-axis refers to the number of requests un-allocated during each allocation slot. Figures 6.7 and 6.8 indicate that the allocation performance degrades for FAFA and BASA for increasing PU occupancy or SU requests while BAMA performs the best with its NC-OFDMA approach, supporting multiple users on each of the sub-bands. Figure 6.8 considers a total of 10^6 requests generated at the base station when 13 out of 17 sub-bands were occupied by PUs. As seen, almost 830000, i.e., 83% of the requests were un-allocated by FAFA and BASA while only 280219, *i.e.*, 28.02% requests were unallocated by BAMA. We have similar plots for increasing number of PUs when the applications requests are fixed to a specific number.

One of the critical parameters of performance evaluation is the bandwidth utilization. Figure 6.9 refers to the bandwidth utilization of BASA and BAMA for increasing number of SU requests, considering 10, 20, 50, and 100 applications generated at the base station. The aggregate bandwidth utilization is the sum of bandwidth scheduled to all the allocated requests during one simulation duration of 1000 ms. For 1000 iterations, the time instant on the *x*-axis refers to each one of 1000 ms time durations. The *y*-axis plots the aggregate bandwidth for each instant of 1000 ms. For clarity of information and better appreciation, the figure is plotted only for the duration of 300 to 600 ms, instead of from 1 to 1000 ms. As seen from Figure 6.9(a) there is no improvement in bandwidth utilization in BASA, even when the SU requests increase from 50 to 100. The aggregate bandwidth achieved for 100 user requests is around 50 MHz over a period of 1000 ms and on average 5 MHz over a allocation slot of 100 ms. On the contrary, BAMA achieves a bandwidth utilization of 180 MHz over a period of 1000 ms for 100 users and therefore, clearly outperforms BASA with respect to bandwidth utilization. The other measure of performance evaluation is throughput achieved by a priority allocation scheme. Figure 6.10 presents the aggregate

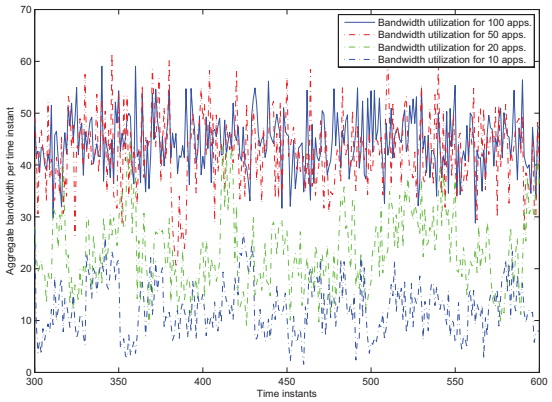

(a) Bandwidth utilization of the FAFA scheme with increasing number of SU requests.

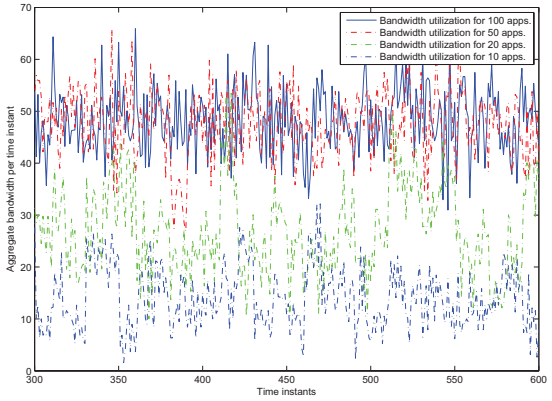

(b) Bandwidth utilization of the BASA scheme with increasing number of SU requests.

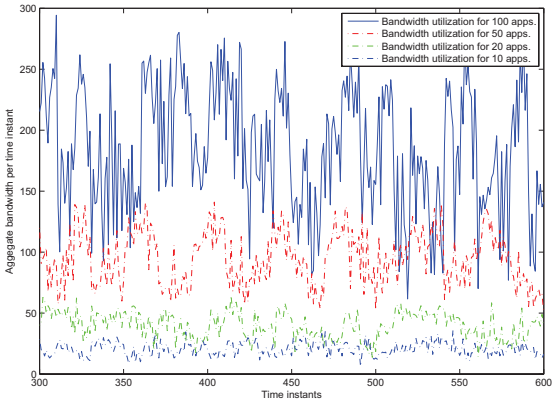

(c) Bandwidth utilization of the BAMA scheme with increasing number of SU requests.

Figure 6.9: Aggregate bandwidth utilization in BASA, and BAMA schemes for varying number of SU requests.

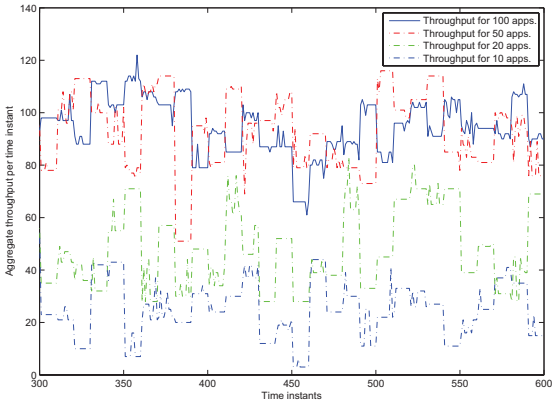

(a) Throughput of the FAFA scheme with increasing number of SU requests.

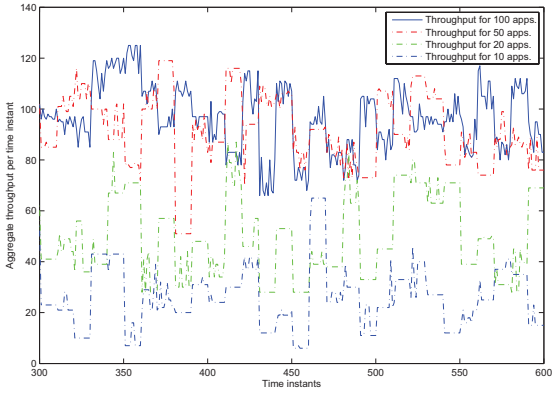

(b) Throughput of the BASA scheme with increasing number of SU requests.

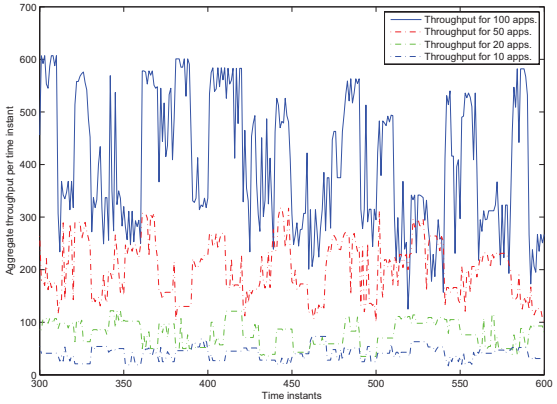

(c) Throughput of the BAMA scheme with increasing number of SU requests.

Figure 6.10: Aggregate throughput achieved in BAMA scheme for varying number of SU requests.

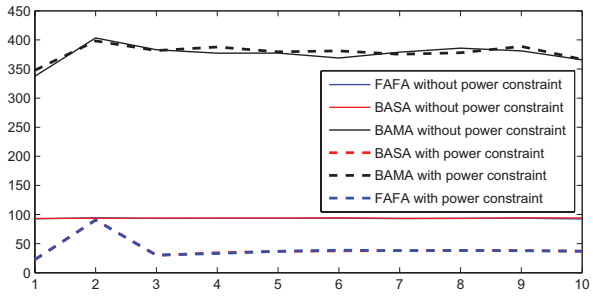

Figure 6.11: Average throughput comparison of FAFA, BASA, and BAMA

throughput for BAMA for increasing number of SU requests, considering 10, 20, 50, and 100 applications generated at the base station. The aggregate throughput is the sum of throughput requirements of all the allocated requests during one simulation duration of 1000 ms. For 1000 iterations, the time instant on the x-axis refers to each one of 1000 ms time durations. The y-axis plots the aggregate throughput for each instant of 1000 ms. For clarity of information, the figure is plotted only for the duration of 300 to 600 ms, instead of from 1 to 1000 ms. With increasing number of SU requests, there is an increasing value of aggregate throughput. We also have similar results for FAFA and BASA spectrum priority allocation schemes, but BAMA outperforms both the schemes substantially.

To test the three schemes, we added power constraint. The power constraint is set such that bands occupied by PUs are allowed transmission power for SU to only -60 dB. The SUs are assigned transmission power level randomly such that there is a chance of 20% that the secondary user does not have enough transmission power to establish successful connection. This setting is to simulate the case with selective channel fading. Figure 6.11 shows the average performance of the three schemes over 50 simulations. With transmission power constraint, FAFA and BASA suffer great performance degradation, while BAMA still has the same performance.

In the result, the performance of FAFA and BASA are almost the same and their performance curves overlap in Figure 6.11, which means the first available band is almost always the best available band. This is because in TV broadcasting channels, primary users either

occupy the channel almost entirely or not at all. Thus, first available allocation scheme is the same as best available allocation scheme in single allocation cases.

6.5 Conclusion

In this chapter, we have developed three unique spectrum allocation techniques to satisfy requests generated from prioritized secondary users (SUs). First, we have extracted PU occupancy statistics from real time measurements collected in the paging band (928-948 MHz). Second, priorities have been assigned to SU requests based on their bit error rate (BER) and delay requirements. Since several portions of the wireless spectrum may be heavily attenuated due to frequency-selective fading resulting from multipath propagation, BER support on each sub-band are separately computed. Additionally, to assign aggregate bandwidth to requesting users, we have exploited the concept of non-contiguous orthogonal frequency division multiplexing (NC-OFDM) to compute the number of active sub-carriers (contiguous as well as non-contiguous) in each sub-band of the entire paging band. Finally, we have presented and compared three novel priority allocation schemes based on bandwidth utilization and achieved throughput.

Acknowledgment

The authors would like to thank the University Research Council (URC) Graduate Student Research Fellowship Program at the University of Cincinnati for generously supporting this research project.

Chapter 7

Cross-layer Architecture for Joint Power and Link Allocation

7.1 Introduction

Ultra Wideband (UWB) [77] techniques are used extensively for higher data rates over short transmission ranges, especially for multimedia traffic. UWB spans over a 7.5 GHz (3.1-10.6 GHz) bandwidth at a power level near the noise floor. However, the UWB transmissions can increase the noise floor and introduce interference to adjacent channels. This may result in substantial performance degradation to existing users. To avoid such undesirable situations, Federal Communications Commission (FCC) defined the spectral mask of -41.3 dBm/MHz for the UWB transmissions in certain overlapping bands. For example, the radar and satellite systems span over a bandwidth of 1.6 GHz (3.1 - 4.7 GHz). Therefore, power control mechanisms and reduction of channel interference are important design issues in an UWB receiver.

UWB communications are rich in multipath effects. In this chapter, we make an effort in utilizing Rake filtering and Power aware Scheduling (ROPAS) architecture to exploit effects of the multipath channels. In our ROPAS design, the unique multi-objective Rake optimization ensures minimal bit error rate (BER) for the receiving applications while strategically selecting an optimal number of multipaths among many possible propagation paths. The joint optimization helps in reducing the computation complexity at the Rake

receiver while minimizing interference for enhanced estimation of transmitted bits.

Design of the MAC layer for the UWB network is significantly different from the traditional multihop ad hoc networks. The reason for this difference in the design is due to the transmission power restrictions imposed by the FCC on such UWB signals in the licensed bands. The MAC layer protocol design should possess the salient features: (i) Minimize power consumption due to communications to reduce interference on the licensed users, and (ii) Fair and efficient sharing of resources between the communicating devices.

Power aware MAC layer, with minimum interference can now be efficiently developed when information can be exchanged with the PHY layer before allocating links to the data traffic. This exactly is the central idea of our ROPAS architecture. In this chapter, we take advantage of cross-layer design between the PHY and MAC layers for CR aided dynamic channel assignment with the use of UWB technology. However, the CR-based dynamic channel assignment can not be achieved in a straightforward manner and involves inter-related issues such as "free" (i.e., idle) channel detection, interference measurement, multipath selection, and power control. For example, the interference and channel fading characteristics have to be considered from the PHY layer so that the data frames can be transmitted with less interference. Furthermore, transmission power control over the links is performed by the MAC layer, with an objective of limiting power while satisfying the packet transmission requirement (e.g., delay, distance). Thus, the cross-layer sharing of information between these two layers is indispensable, especially for CR-based mobile nodes in a dynamic network, since the channel conditions vary randomly with different mobility patterns. At the same time, the cross layer based power control and link scheduling strategy in ROPAS helps the CR in imposing a limit on the transmit power for each frame interval. The CR uses increased transmission power for delay sensitive traffic to reach the destination in the minimum number of hops and hence, minimum delays, while employing reduced transmission power for delay tolerant services.

In our cross layer design and simulation, we have chosen the UWB (3.1-10.6 GHz) for link allocation and for traffic communication purposes due to its high data rate on each sub-channel of 528 MHz bandwidth [77]. The main contributions of this chapter [78] are as follows:

- We present a multi-objective optimization problem for the Rake receiver to reduce computational complexity,
- We present a cross-layer multi-objective optimization design for dynamic frequency selection with optimal transmission powers allocated to each subframe, an optimal partition of a licensed sub-band, and
- We discuss the cross-layer design of the CR-based priority based scheduling while supporting the maximum number of parallel transmissions within a frame interval.

The rest of this chapter is organized as follows. Section 7.2 deals with the previous work on dynamic channel allocation strategies. Our proposed algorithm, ROPAS is described in Section 7.3. Section 7.4 illustrates the optimal power allocation strategy based on distance and priority differentiations. Simulation results are discussed in Section 7.5 followed by the conclusion in Section 7.6.

7.2 Related Work

Dynamic channel allocation in mobile networks has been addressed by previous works in myriad ways. The distributed, fault-tolerant allocation [79] depends much on the channel usage information by the interfering neighbors of a requesting user, which can be used to compute the best channel allocation. This strategy involves a high message complexity due to exchange of channel usage information of all its one-hop neighbors. The other research on dynamic channel allocation [80] is based on a mutual exclusion between the "request" and "reject" messages for allocating a group of channels. But, this strategy suffers from the problem of fairness among requesting users, with additional limitation of exchange of "request" and "reject" messages. An improved version of the channel allocation is discussed in [81] where the channel allocation is based on the ratio of the serviced data rate to the required data rate. Additionally, the power distribution algorithm in this research work "adjusts" the average transmit power of the channel based on the received signal-to-noise ratio per user. But, this allocation strategy may give rise to a serious problem: *Assume a channel is allocated to a loss-sensitive application and the channel suffers from deep*

fading while their power distribution strategy decides to decrease ("adjust") the average transmit power on this channel. This will result in loss of the entire transmission due to poor channel conditions and cause a dramatic performance degradation. Our proposed ROPAS cross-layer architecture has a novel solution to this problem. Scheduled links are allocated power by the CR based on the retrieved information about the channel conditions from the physical layer.

The design of efficient MAC layer protocol with lower power consumption and strict computational complexity is a persisting research challenge. The authors in [82] have dealt with this issue of interference using the margin based power allocation scheme that maintains power constraint along with an exclusive region based scheduling. But, this work suffers from an inherent problem of centralized decisions taken by a centralized controller for power allocation and slot allocation. Therefore, the system becomes much more complex with an increase in the number of UWB devices, resulting in heavy overhead due to sharing of varying number of users with a centralized controller. The location based MAC layer protocol and routing [83] depends on the distance information to achieve low power levels and increased lifetime and improved network performance. Saving of power in each UWB device is achieved by using a sleep interval when the devices are not participating in active transmissions. Again, this provides a trade-off between the power constraints and the network latency when our main focus is for power constrained protocol design. The application of CR [84] deals with the network layer perspective in UWB-based networks. The routing decisions are made on the basis of a cognitive cost function that takes care of important issues like synchronization, end-to-end delays and coexistence with licensed PUs. Our proposed architecture deals with a cross-layer MAC optimization protocol where the CR in each UWB device upon allocation of channels to its applications decides about the imposed power constraints. Additionally, proportional fairness is achieved by a unique priority scheduling performed by the CR.

7.3 The ROPAS Architecture

In our proposed ROPAS architecture, the two essential ingredients are the cross-layer design and the multi-objective optimization principles.

Cross-layer design: The motivation behind a cross-layer design is three-fold [85]. First, sharing of information across layers aims to solve problems created by wireless links. For example, the misinterpretation of a wireless error by a TCP sender to be an indication of network congestion. Second, the cross-layer design attempts to exploit the fundamental characteristics of wireless medium like channel variations due to fading, at higher layers. This particular attribute is a potential candidate, especially for CRNs, in developing adaptive protocol stack to adapt dynamically to changes in network conditions. Finally, the cross-layer design can take advantage of the new modalities like node cooperation, multi-packet reception, and cognitive radio [85] offered by wireless medium. This is not viable in traditional layered architecture. Recent research on cross-layer design [86]- [87] showed a substantial improvement in the routing efficiency, throughput, fairness and delay variance among different applications. Physical layer information exchange [88] with the MAC and network layer has also exhibited a superior network performance.

Especially, cross-layer design seems to be an essential component in cognitive networks since it not only provides network functionalities to various applications, but also adapts to their needs, prevailing network traffic conditions as well as the wireless medium.

Multi-objective Optimization: Optimization problems [89] are generally formulated using a single-objective function complying with a series of constraints. A single-objective optimization problem is expressed as:

$$\text{Optimize [minimize/maximize] } f(x) \tag{7.1}$$

$$\begin{aligned} \text{subject to} \quad & Y(x) = 0 \\ & Z(x) \leq 0. \end{aligned}$$

In the above problem, $f(x)$ is the optimization function and x is an independent variable. It may be noted that x can also represent a vector of independent variables. The functions $Y(x)$ and $Z(x)$ are the constraints of the model. But, in real life, problems can be complex

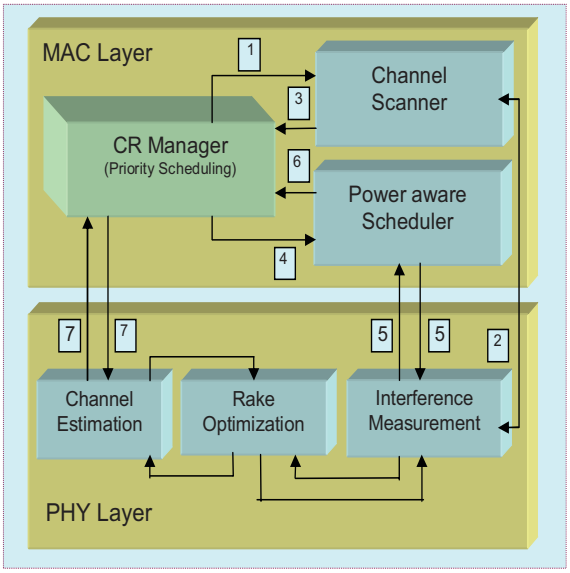

Figure 7.1: Cross-layer design of the ROPAS architecture

enough to optimize more than one objective function. This gives rise to the evolution of multi-objective optimization [90]. A multi-objective optimization problem is expressed as:

$$\text{Optimize [minimize/maximize] } f(x) = f_1(x), f_1(x), \ldots, f_n(x) \tag{7.2}$$

$$\begin{aligned} \text{subject to} \quad & Y(x) = 0 \\ & Z(x) \leq 0. \end{aligned}$$

Here, $f(x)$ is a set of n functions jointly optimized with constraints functions $Y(x)$ and $Z(x)$.

In our research, we made an effort in utilizing multi-objective optimization techniques in the CR-based cross layer design which involves the MAC and PHY layers.

The ROPAS architecture is shown in Figure 7.1 and the entire protocol is described in several steps (i.e. marked by the numbers). In the proposed ROPAS, in addition to traditional CR modules in the PHY and MAC layers, several functional modules are included in order to improve the collaboration between the PHY and MAC functionalities as shown in Figure 7.1. All the central decisions are taken by the **CR Manager (CRM)** which also has the capability of interaction between different modules. The other two modules

in the MAC layer are responsible for an efficient dynamic channel allocation among mobile nodes with limiting power constraints. The **Channel Scanner (CS)** divides the entire UWB into smaller sub-bands and scans these sub-bands in periodic intervals for possible "free" (not used by licensed users) channels. The next module is called the **Power-aware Scheduler (PAS)** which aims at a multi-objective joint power control and link scheduling of data frames. Additionally, it also performs the hybrid queuing strategy to achieve fairness among requesting applications. The three modules at the bottom of Figure 7.1 are associated with the PHY layer of each node in the network. One of the modules is the **Interference Measurement (IM)** which measures the interfering power sensed in each sub-band due to users in adjacent sub-bands. The PAS works with the IM to limit the transmission power in any particular sub-band within the permissible limits (- 41.3 dBm/MHz [77] or 0.039 mW/528 MHz for UWB communications). The **Rake Optimization Module (ROM)** deals with the PHY layer Rake receiver. This multi-objective optimization computes a minimal number of Rakes or fingers needed by the Rake receiver for maximum signal power and hence maximum signal-to-noise ratio (SNR) at minimal BER. The **Channel Estimation Block (CEB)** estimates the fading condition of the channel as well as the channel error rates. The CEB shares the cross-layer information with the CRM to select the best link (in terms of fading and error rate) for data transmission among the adjacent one hop neighbors.

Our proposed architecture addresses these two issues: the dynamic channel allocation for the transmitting applications and the Rake optimization for receiving processes. The Rake optimization is a pure PHY layer issue and utilizes the interference power information from the IM to optimize the number of propagation paths selected for minimal BER. For dynamic channel allocation, let us consider an example to get a better understanding of our cross-layer design of ROPAS. Seven steps are involved in the entire channel allocation process:

- **Step 1**: An application arrives at the CRM with its link request and the delay constraint. The CRM refers to the CS for possible "free" channels.

- **Step 2**: The CS with ready reference to the IM module for probable interference power, detects the "free" channels. It is noted that the IM module is located in the

PHY layer.

- **Step 3**: Upon the response from the IM, the CS sends the detected free channels with their respective identifications to the CRM. Therefore, the CRM has the complete information about the free channels for the requesting applications.

- **Step 4**: The CRM requests the PAS module for transmit power limits on each of these "free" channels. The CRM also sends information about the delay constraints for the requesting application.

- **Step 5**: The PAS refers to the IM for signal-to-interference and noise ratio needed for joint power control and link scheduling; the PAS module divides the MAC layer frames into subframes (based on delay constraints of the requesting applications) and assigns a group of links to each subframe. The module also allocates a group of transmit powers based on the delay constraints.

- **Step 6**: The PAS sends the information to the CRM about the frame interval, fraction of each subframe and probable group of transmit power allocation to each subframe.

- **Step 7**: Finally, the CRM checks with the CEB for probable error rates and fading conditions based on the information received from the PAS module. Then, the CRM allocates the power constrained links to the frames determined by the PAS.

It can be seen from these steps that for a power constrained link, an appropriate collaboration between different modules enables the data transmission in an optimal manner in terms of current channel and link status (i.e., delay constraint of the requesting user, utilization of the channel with power constraints, and the interference of link). The collaboration considers two critical issues in the subframe transmission: Channel characteristics for dynamic channel allocation and the transmission power for reducing the interference. In the following subsections, we describe each module in detail and illustrate the interactions between these modules.

7.3.1 Rake Optimization Module

In this subsection, we discuss the Rake optimization, which is an enhanced module in the PHY layer shown in Figure 7.1. We employ a multi-objective optimization strategy for an optimal selection of multipaths out of the several possible propagation paths.

Since UWB communications are rich in multipath effects, Rake receivers are used to accumulate significant energy from multipath components in UWB networks. It consists of a bank of correlators or fingers where each finger is synchronized to a multipath component. The output of each finger is coherently combined using different techniques like Maximal Ratio Combining (MRC) [91], Minimum Mean Square Error, etc.

The complexity in computing the Rake receiver output involves two parts: (i) Multiplications of $\{N \times M\}$ matrix with $\{M \times N\}$ matrix gives $O(MN^2)$ [91] and (ii) Additions of the two matrices of similar dimensions, resulting in a complexity of $O((M-1)N^2)$, where M and N denote the number of correlators and the weights assigned to each correlator respectively. Our idea of developing an optimized Rake receiver stems from the intention of reducing the computation complexity in terms of the number of multiplications and additions needed for the weight derivation attached to each finger of the Rake receiver. We have chosen MRC Rake receiver for its lower computation complexity as compared to other Rake receivers.

To illustrate our assertion, we assume that the i-th received signal at time instant t is $r_i(t)$. The output of the Rake receiver $y_i(t)$ for the i-th received signal with R fingers or correlators can be given by:

$$y_i(t) = \gamma^T \times \sum_{j=0}^{R-1} r_i(t - \delta_j), \tag{7.3}$$

where $\gamma = [\gamma_0, \cdots, \gamma_{R-1}]^T$ are the weights associated with each finger, T is the transpose operation and δ_j is the delay associated with j-th correlator of the Rake receiver to capture the multipath signal from its predefined delayed path. Now, the computation complexity depends on the number of fingers used and their corresponding finger weights. In order to reduce the computation complexity, we can strategically select an optimal number of fingers out of many multipaths in UWB communications. If the value of M and N can be reduced, then the computation complexity can be reduced to a great extent. Hence, the

basic idea of our optimal selection of a few fingers is to reduce M and the corresponding reduction in N.

Let $\mathbf{K} = \{1, 2, \cdots, k, \cdots, K\}$ be the set of all multipaths. The energy-to-noise ratio (ENR_k) in k-th multipath can be written as [77]:

$$ENR_k = \frac{P_k \times \tau_c}{N_0 \times W \times \sigma_T}, \tag{7.4}$$

where P_k is the average power received in the k-th multipath, τ_c is the coherence bandwidth of the UWB channel, N_0 is the one-sided power spectral density of the background Additive White Gaussian Noise (AWGN), W is the signal bandwidth and σ_T is the standard deviation of the AWGN noise within the symbol duration T.

The Rake optimization is to strategically select only a few of the multipaths out of all the possible ones. The reason behind this is two fold: *(i)* Received signal energy from each and every multipath may not improve the total desired signal energy at the Rake receiver, and *(ii)* Delayed multipaths may suffer from severe fading or may have been corrupted due to channel interference, thereby resulting in increased BER. The idea is to optimize the number of multipaths chosen so as to maximize the ENR_k for the k-th path. On the other hand, the optimization needs to minimize the overall system BER, which implies minimization of the overall bit energy E_b. Therefore, it becomes a multi-objective optimization.

The multi-objective function in multipath k with power P_i^k for the i-th UWB receiver in the presence of interfering U nodes can be represented as:

$$max\left(\frac{P_i^k}{\sum_{j=0, j\neq i}^{U-1} P_j^k}\right),\ k \in \mathbf{K}. \tag{7.5}$$

Then, maximizing Eq. (7.5) for all $k \in K$.

$$\begin{aligned} min\left(\frac{E_b}{N_0}\right) &= min\left(\sum_{k=0}^{K-1} P_i^k + \sum_{j=0, j\neq i}^{U-1} \sum_{k=0}^{K-1} P_j^k\right) \\ &= min\left(\sum_{k=0}^{K-1} P^k\right) over\, all\, the\, users. \end{aligned} \tag{7.6}$$

Next, let $\phi = \{1, 2, \cdots, k^{'}, \cdots, K^{'}\}$ be a selection from $\mathbf{K}$ i.e., $\phi \subset \mathbf{K}$. Hence, our goal is to choose a subset ϕ that maximizes the power given in the first objective while maintaining a low BER. Therefore, $K^{'}$ is the optimized number of paths in the set of paths ϕ and $\mathbf{K}$ is the number of multipaths in the set of possible propagation paths. Therefore, the optimization problem with two maximizing functions $f_0(k)$ and $f_1(k^{'})$ can be rewritten as:

$$\begin{aligned} max\, f_0(k) &= \frac{P_i^k}{\sum_{j=0, j\neq i}^{U-1} P_j^k},\ k = 0, \cdots, K-1, \\ max\, f_1(k^{'}) &= \sum_{l=0}^{K^{'}-1} P^l. \end{aligned} \tag{7.7}$$

To solve this multi-objective functions, we can either create Pareto-optimal charts [92] and select the best solution from the same or combine them as done here. In fact, another approach is to select a set of real values λ_i which refers to the multiplier for the i-th maximizing objective function, $f_0(i)$. Hence, our new objective function $L(\phi)$ becomes:

$$L(\phi) = f_1(k^{'}) - \sum_{i=0}^{K^{'}-1} \lambda_i \times f_0(i). \tag{7.8}$$

This is still a combinatorial optimization problem. To reduce it to a linear Integer Programming (IP) [92], we introduce a set of variables X_i defined as:

$$\begin{aligned} X_i &= 1, if\ multipath\ is\ selected\ and, \\ &= 0, if\ multipath\ is\ not\ selected. \end{aligned}$$

Therefore, the problem in Eq. (7.8) can be reformulated over the set X (constitutes individual $X_i^{'}s$) as:

$$\begin{aligned} L(X) &= X \times f_1(k^{'}) - \sum_{i=0}^{K^{'}-1} \lambda_i \times f_0(i) \\ &= \sum_{i=0}^{K^{'}-1} \left[X_i \times P^l - \lambda_i \frac{X_i \times P_j^i}{\sum_{l\neq j} P_l^i} \right], \\ &\quad subject\ to\ X_i \in [0, 1]. \end{aligned} \tag{7.9}$$

It is easy to see that this is a linear IP problem and can be easily addressed using a standard solver like the Branch-and-Bound method. We have used GLPK [93] (version 4.10)

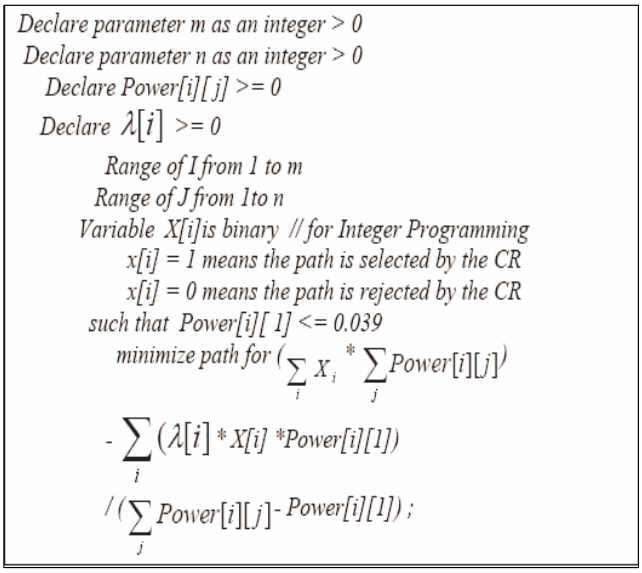

Figure 7.2: Pseudo code for the Rake multi-objective optimization

for solving this multi-objective optimization problem.

Our implementation of the IP and the pseudo-code is shown in Figure 7.2. First, we declare a variable, $Power[i][j]$ which represents the power received by the Rake receiver from the i-th multipath carrying information of the j-th user. The entity $Power[i][1]$ is the power received by the desired UWB Rake receiver ($j = 1$) from the i-th multipath. This implies that $Power[i][j]$ with $j \neq 1$ is the received interference power from i-th multipath. We have also declared the multiplier, λ_i (i.e., $\lambda[i]$ in Figure 7.2) and the binary variable, X_i (i.e., X_i or $x[i]$ in Figure 7.2) for our joint optimization. The transmission power constraint on each multipath for UWB communication is limited to 0.039 mW. Therefore, for any correlator, we impose a power constraint of 0.039 mW as any multipath with higher power values may be corrupted due to interference. With this underlying logic for our optimization problem, we solve Eq. (7.9) for the optimal selection of paths as shown in Figure 7.2.

7.3.2 Interference Measurement (IM)

The IM is another module in the PHY layer involved in Steps 2 and 5 as shown in Figure 7.1. This module is needed to calculate the signal-to-interference noise ratio (SINR) which estimates the ratio of power due to the allocated link to power due to other adjacent interfering links at a soft-decision variable. Let us assume that M information bearing symbols, $S_k(1), \cdots, S_k(M)$ independently and identically distributed (i.i.d) are chosen from a finite set with zero mean. The mean $E[S_k(m)]$ and variance, $E[\mid S_k(m) \mid^2]$ for the k-th link are defined as:

$$\begin{aligned} E[S_k(m)] &= 0, \textit{ and} \\ E[\mid S_k(m) \mid^2] &= P_k, \\ 1 \leq m \leq M, \;\; 1 \leq k \leq L, & \end{aligned} \tag{7.10}$$

where, P_k represents the signal power on the k-th link.

Then, the expected value of SINR at the k-th link among L links is given by:

$$\begin{aligned} SINR_k(P) &= \frac{G_k \times P_k}{\sum_{l=1}^{L} P_l \times G_{k,l} + \sigma_k^2}, \\ &= \frac{P_k}{\sum_{l=1}^{L} P_l \times \left(\frac{G_{k,l}}{G_k}\right) + \frac{\sigma_k^2}{G_k}}, \\ & 1 \leq k \leq L, \end{aligned} \tag{7.11}$$

where $P_k \geq 0$ is the transmitted power on link k. We further define the transmit power vector, P as:

$$P = (P_1, \cdots, P_L) \in \Re_+^L, \tag{7.12}$$

where P is also referred to as the power allocation vector. The first term in the denominator of Eq.(7.11) gives us the interference power in the k-th sub-band prior to link's data transmission. This interference is called the *interference temperature* caused by concurrent communications in adjacent channels. This value is exchanged with the PAS module for link allocation. $G_k \geq 0$ is the path gain on the allocated link k and depends on the channel allocation and the state of the wireless channel. $G_{k,l} \geq 0, l \neq k$ is the path gain between the link l and link k. Therefore, if the transmit power on link l is P_l , then the expected

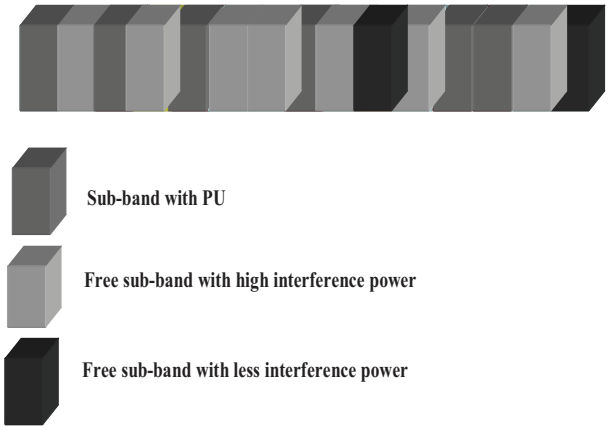

Figure 7.3: Channel assignment based on the "free" channels detected by the IM in the UWB (3.1-10.6 GHz)

interference on link $k \neq l$ is $P_l G_{k,l}$. Additionally, if $G_{k,l} = 0$, then the link k is said to be orthogonal to link l. Again, $G_{k,k} \geq 0$ represents the self and inter-symbol interference which occurs due to the time dispersive nature of the wireless channel. $\sigma_k^2 > 0$ is the Gaussian noise variance at the output of link, k.

7.3.3 Channel Estimation Block (CEB)

The CEB module is involved in Step 7 of our cross-layer dynamic channel allocation strategy. The minimum mean square estimation (MMSE) [94] algorithm runs at the CEB to determine existing channel conditions between the network nodes within their communicating ranges. The CEB also gets an estimate of the error rate due to existing channel conditions. These estimates are calculated in short durations to take care of changing topology/routes caused by mobility of the nodes. The CRM refers to these estimates for the requesting service and assigns the link out of a possible multiple set of selected links chosen by the PAS module. For example, the CRM would decide to assign links with channel error rate 10^{-3} (rapid fading characteristics) to frames of a speech telephony application and will assign a link with channel error rate 10^{-5} (slow fading characteristics) to frames of a video telephony application.

7.3.4 Channel Scanner

The Channel Scanner is involved in Steps 1, 2, and 3 of our channel allocation strategy shown in Figure 7.1. The CR divides the UWB into narrow sub-bands or channels of bandwidth 528 MHz [77]. CR scans each of these sub-bands and detects them as "free channels" based on the "interference temperature" obtained from Eq. (7.11). These "free channels" can be assigned for its own data transmission or for forwarding traffic of its one hop neighbors. The CR detects the "free" channels with the help of the IM and stores them in a "free channel pool" as shown in Figure 7.3.

7.3.5 Power Aware Scheduling

The CR divides a MAC layer frame into smaller synchronized subframe intervals, assigns a set of links to each subframe, and allocates transmitting power to each of the set of links. This process is done by the PAS module, which is involved is Steps 4, 5, and 6 as shown in Figure 7.1. Let us assume a finite frame interval F and each subframe interval to be SF, a perfect multiple n of F. Thus, we have a set of subframe intervals $\chi = \{1, 2, \cdots, n\}$. Again, the PAS module divides the entire sub-band of N links of 528 MHz into smaller subsets M of bands or links of bandwidth $(528/n)$ such that $M \times n = N$ as illustrated in Figure 7.4.

We consider that any one of these subsets M can be allocated to each subframe based on the power constraint. We also assume that $A = \{SF_i : i \in \chi\}$ be a system of subsets of F with:

$$\bigcup_{i \in \chi} SF_i = F \ \ and \ \ \forall_{i \in \chi} SF_i \bigcap SF_j = 0, \ i \neq j. \tag{7.13}$$

Eq. (7.13) indicates that a frame is divided into disjoint subframes within the frame interval. One additional point to note is that F can also represent a frame and correspondingly, SF is a subframe of F. Let ξ represents the real function that denotes the fraction of frame occupied by the subframe, $\xi : A \rightarrow [0, 1]$ such that

$$\begin{gathered} \forall_{i \in \chi} \xi(SF_i) \geq 0, \ \ \xi(0) = 0, \ \ and \\ \xi(\bigcup_{i \in \chi} SF_i) = \sum_{i \in \chi} \xi(SF_i) = \xi(F) = 1. \end{gathered} \tag{7.14}$$

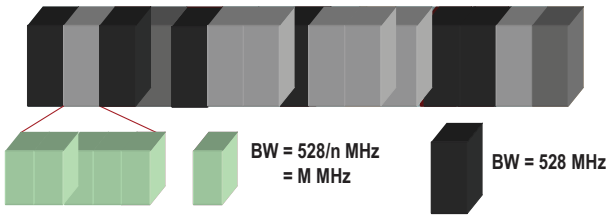

Figure 7.4: Sub-band division into multiple frmaes in Power Aware Scheduling illustrated in UWB

Here $\xi(SF_i)$ denotes the i-th fraction of the frame with interval SF. We have also related $\xi(SF_i)$ with the frequency of allocation of the power vector $P(SF_i)$ to the links allocated to i-th subframe. $\xi(SF_i) = 0$ implies that the power vector $P(SF_i)$ is not utilized by the links for that subframe.

Now, for each link within a set M, $l \in M$, we associate a set function $P_l : A \rightarrow \Re_+$ (a positive real space). Let us define a power vector P as the set of possible transmit powers which satisfy $P = (P_1, \cdots, P_l) : A \rightarrow \Re_+^L$. If we define $\phi(SINR_k(P(SF_i)))$ as the average data rate for link k in the subframe with $SINR_k(P(SF_i))$ defined as in Eq. (7.11), then the expected data rate $\tau_k(P, \xi)$ can be written as:

$$\tau_k(p, \xi) = \sum_{i \in \xi} \xi(SF_i)\phi(SINR_k(P(SF_i))). \tag{7.15}$$

Now, with the above expected data rate and SINR, we define the joint power control and link scheduling strategy as: *With given values of A and F, ξ decides the length of each subframe and based upon the subframe interval, assigns a group of links to each subframe*. This is similar to frequency division multiplexing, where the entire bandwidth is divided into frequency slots. Therefore, link scheduling can be modeled as a function of ξ. Now power scheduling relates to allocating transmit power to the links in each subframe. Therefore, the joint power control and link scheduling can be mathematically defined as:

- Choosing $\xi : A \rightarrow [0, 1]$ while satisfying Eq. (7.14) and
- Determining $P : A \rightarrow \Re_+^L$.

The CR computes the joint power control and link scheduling in two different ways for two different traffic patterns:

Delay Sensitive Traffic: For delay sensitive packets (e.g., delay less than 100 ms), higher power vector needs to be assigned to each subframe which results in higher transmit power within each frame interval. Therefore, the joint strategy tries to minimize the value of ξ fraction of each subframe and maximize the power vector in each subframe. In other words, it maximizes the transmit power in each link. The joint optimization can be expressed as:

$$\begin{aligned} &min \quad \xi \\ &max \quad \sum_{k=1}^{M} P_k, \;\; k = 1, 2, \cdots, M, \end{aligned}$$

such that

$$\sum_{i \in \chi} P(SF_i)\xi(SF_i) + \sum_{i=1}^{n}\sum_{k=1}^{M}\sum_{l=1}^{L} \xi(SF_i)P_l G_{k,l} \leq 0.039. \tag{7.16}$$

Delay Tolerant Traffic: Similarly, the strategy for delay tolerant packets (e.g., delay greater than 100 ms) is to maximize the value of ξ while re-using the links with higher frequency). As we mentioned earlier, the value ξ has a direct correlation with the frequency of using a certain power vector. Since we use larger subframes, the transmit power has to be limited in each subframe in this case. This joint optimization can be written as:

$$\begin{aligned} &max \quad \xi \\ &min \quad \sum_{k=1}^{M} P_k, \;\; k = 1, 2, \cdots, M, \end{aligned} \tag{7.17}$$

with constraint defined as in Eq. (7.16).

Here, L is the total number of links in the entire UWB. This optimization is solved in a similar way as computed by a Rake Optimization. Choice of ξ also plays a vital role in the power control. Higher value of ξ implies higher subframe duration (rather less number of subframes), and higher frequency of usage of power vector, $P(SF_i)$ for links used in i-th subframe (since $\xi(SF_i)$ relates to the frequency of allocation of power vector $P(SF_i)$ in i-th subframe). Thus, Eq. (7.16) limits the transmit power dissipated over the frame duration. On the other hand, lower values of ξ implies lower frequencies of utilization of a certain power vector and encourages the use of higher transmit powers with the allocated links in each subframe. In addition, we can further define priority according to the requirement of given applications. To illustrate this point, the CR can use smaller values of ξ for real

time traffic (i.e., delay sensitive) which encourage higher values of transmit power in each subframe. Thus, it increases the transmission range of each UWB node while reducing the number of hops to its destination, thus results in minimum transmission delay. Again, the non-real time applications (i.e., delay tolerant) can be assigned higher values of ξ to use lower transmit power in each subframe, resulting in decreased transmission range.

7.4 Priority Based Scheduling

In this sub-section, we formulate the optimization problem for joint power control and link scheduling for different application originating from one UWB node or from other competing nodes. We know that higher spectral efficiency can be achieved with increasing parallel transmissions in minimum number of time slots per frame. Thus, we concentrate our attention in scheduling the maximum number of parallel transmissions in minimum number of time slots which is defined by a variable NP where $NP_{i,j}$ represents the i^{th} bit of the j^{th} user application. The other aspect of our constrained optimization would be to restrict the multi-access interference (MAI) within the FCC's permissible limits.

$$\begin{aligned} max \quad & NP_{i,j} \\ s.t. \quad & \frac{P_{i,k}}{\sum_{p=0,p\neq k}^{M-1} P_{i,p} \sum_{l=0}^{N-1} c_p^l c_p^k + \sigma_k^2} \geq SNR_{th}, \end{aligned} \tag{7.18}$$

where σ_k^2 is the additive White Gaussian noise power SNR_{th} is the minimum SNR for transmission power in a particular slot. If the SNR of a user is higher than the SNR_{th}, the signal can be received successfully. Otherwise, the transmission fails. The signal power for the i^{th} bit for the k^{th} user is represented by $P_{i,k}$ and that for the p^{th} interfering users is represented by $P_{i,p}$. The l^{th} chip of the spreading sequences for the p^{th} and k^{th} users are denoted by c_p^l and c_p^k respectively. The cross-correlation of two different spreading sequences is not negligible. Hence, this term is added in the interference term of Eq. (7.18). The first term in the denominator of the expression for the constraint represent the MAI from $(M-1)$ users.

Now, the signal power for an application is defined in our work as a function of chan-

nel conditions, priority level in the queue, and the distance between the transmitting UWB node and the receiving node.

According to the FCC's restriction on transmission power, the maximum transmitting range can be 10m [77]. Again, near-far interference is a persisting issue in case of Code Division Multiple Access (CDMA) systems. To reduce the near-far interference, the transmitter requires less power if the receiver is close by and more power for a receiving node far away from it. We represent the distance variable between the i^{th} transmitter and j^{th} receiver by $d_{i,j}$. So, if the distance between a transmitting node and receiving node is less than $d_{i,j}$, the transmission power level is reduced by half its current value. If greater than $d_{i,j}$, the existing power level is increased twice its current transmission power level.

Next, we consider the channel conditions. This gives rise to the cross-layer sharing of information between the MAC and PHY layers. In our research, we have considered the BER as the measure of the channel conditions. The BER value is evaluated by the CEB and shared with the BER. For BER values in the order of 10^{-3} or higher, the channel is considered to be poor and data from the low priority queue will be preferred. For BER smaller than this value, data from a higher priority queue is preferred or data is transmitted at higher power levels and can also support higher data rates.

Finally, we consider the priority queue operated by the CR. This module is depicted in the CRM module of Figure 7.1. Priority is decided based on the data rate requested by an application or higher transmit power requests, which in turn requires lower BER ($< 10^{-3}$). Now, based on these demands, the CR maintains 2 queues, one with higher priority ($P = 2$) and the other with low priority ($P = 1$). The unique feature added to our priority queuing strategy is the frequency of requests by the same application. If irrespective of its priority level, the same application requests for channel assignment more than once, the signal power is reduced by the value of its corresponding frequency of request. This is done to achieve fairness among the requesting applications.

Now, the signal power $P_{i,j}$ for the j^{th} user application in the i^{th} slot is proportional to the priority of an application, BER and the distance between the transmitter-receiver pair. Additionally, $P_{i,j}$ is inversely related to the frequency of request of an application.

Therefore, the expression for the $P_{i,j}$ can be expressed as:

$$P_{i,j} = K \frac{P \times 10_j^{\gamma} \times d_{j,k}}{f}, \tag{7.19}$$

where, γ is the positive exponent of the BER, K is the proportionality constant, $d_{j,k}$ is the distance between the j^{th} transmitter and the k^{th} receiver. Here, f represents the frequency of the requesting application.

The constraint in Eq. (7.18) can now be expressed as:

$$\frac{K \times P \times 10_j^{\gamma} \times d_{j,k}}{f \times IP_j} \geq SNR_{th}, \tag{7.20}$$

which can be re-written for interference power IP_j as:

$$\frac{K \times P \times 10_j^{\gamma} \times d_{j,k}}{f \times SNR_{th}} \geq IP_j. \tag{7.21}$$

7.5 Simulation Results

In this part, we study the performance of our proposed optimal power allocation with the scheduling performed by the CR. The simulation is done using software models written in C++. This optimal priority based scheduling is simulated using the GLPK [93] tool. The UWB is divided into 15 sub-channels, each of 528 MHz bandwidth. The IM computes the SINR in each sub-channel and based on the joint power control and link scheduling policy, links are assigned to different slots within frame duration of 0.5 ms. The proportional constant is considered to be 10^{-18} [82] and the SNR threshold is taken to be 10dB. The maximum transmission power is set to 10^{-13} W. The channel is assumed to have Gaussian noise power of 10^{-20} W. The performance of our proposed optimization architecture is evaluated from three aspects:

- Optimal number of correlators needed by a Rake receiver to improve the overall system BER.
- Power limits in different subframe intervals within a frame interval when joint power control and link scheduling is used in our ROPAS design.
- Optimal value of slot assignment and its variations with improvements in BER values.

Path 1	Path 2	Path 3	Path 4	Path 5	Path 6	Path 7	Path 8	Path 9	Path 10
0.0896	0.0509	0.0972	0.143	0.31	0.18	0.08	0.136	0.124	0.38

(a)

Path 2	Path 3	Path 4	Path 5	Path 6	Path 7	Path 8	Path 9
2.19×10^{-3}	1.79×10^{-3}	2.1×10^{-3}	1.26×10^{-3}	4.82×10^{-3}	4.4×10^{-3}	1.86×10^{-3}	6.41×10^{-3}

(b)

Figure 7.5: (a) Values of Lagrange multiplier's, $\lambda_i^{'}s$ for all 10 paths and (b) Strategic selection of propagation paths based on BER values by our optimization algorithm when path P1 is already selected

7.5.1 Multi-objective Rake Optimization

The simulation results in the PHY layer for multi-objective optimization for Rake receivers are discussed in three phases:

- Selection of values, $\lambda_i^{'}s$,
- Strategic selection of multipaths by CR-equipped optimal Rake receiver, and
- Joint optimization achieved using the GLPK tool with the selected multipaths and as well as achieving desirable BER values.

Selection of $\lambda_i^{'}s$: The UWB signal experiences multipath fading. Depending upon the channel delay profile, the signal energy reaching the receiver via certain multipaths with considerable delay but are still resolvable, can still be selected by the S-Rake. But, a smaller value of λ may select path 1 but may exclude path 9 or 10 since it does not maximize the second term in Eq. (7.9). The values of $\lambda_i^{'}s$ for different multipaths for its selection by the S-Rake are detailed in Figure 7.5(a).

Strategic selection of multipaths: The optimization algorithm selects path $P1$ with assigned value of λ_i. The BER achieved through our simulation is 2.34×10^{-3}. This result validates our optimization algorithm as we know that the first multipath component

Selection of paths (P)	Bit-error rate
P1, P2, P3, P8	2.29×10^{-3}
P1, P3, P8	1.9×10^{-3}
P1, P3, P4, P8	1.75×10^{-3}

Figure 7.6: Strategic selection of paths for optimal BER

will always be the strongest path with most of the received signal power. Again, with the selection of the Lagrange multipliers for all 10 multipaths, all the 10 propagation paths are selected by our algorithm, but the BER achieved is 3.82×10^{-2}. The degradation in BER is due to the addition of all the remaining 9 paths with the strongest first multipath. This result validates the fact that all the multipaths do not carry adequate signal power, but also MAI power introduced in multiple access based UWB networks. The predominance of the MAI power in certain paths leads to such increased BER. These results help us to check the correctness of our optimization algorithm by varying the values of the Lagrange multipliers $\lambda_i^{'}s$ of Figure 7.5(a). When path 10 is chosen along with path 1, BER is 1.6×10^{-2}.

Now, if we carefully look at Figure 7.5(b), we see that paths 2, 3, 4 and 8 can be chosen along with path 1 for a better BER performance.

Let us see how it can be achieved by varying the values of the Lagrange multipliers $\lambda_i^{'}s$. The strategic selection of the selective multipaths by the S-Rake is demonstrated in Figure 7.6. Therefore, the optimization algorithm computes a combination of paths 1, 3, 4, and 8 as the final optimal path selection which maximizes the desired signal power over the MAI power and as well as minimizes the BER. This observation is supported by our simulation results obtained with the GLPK tool in Figure 7.7 by increasing iterations for the path selection.

Joint optimization for acceptable BER: Initial value of Path 1 is stored in a database that results in a BER of 2.34×10^{-3}. We have chosen the reference BER of 2.54×10^{-3}, a stringent value closer to the BER of the strongest path, Path 1 to obtain better results. Therefore, the optimization algorithm now runs with the dual constraints of $BER < 2.54 \times$

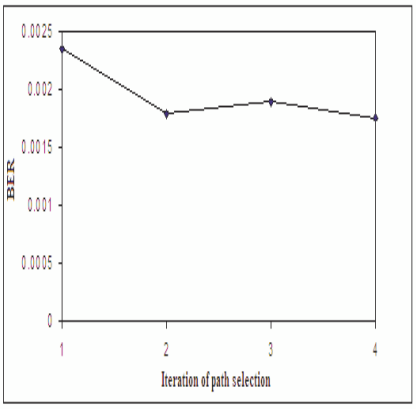

Figure 7.7: Reduction of BER with increase in iteration of path selection

10^{-3} as well as $X_i \in [0, 1]$. Figure 7.6 explains the lists of path selections and the optimized path selection. Figure 7.7 shows the next strategic selection is Path P3 with BER of 1.79×10^{-3} (refer to Figure 7.5(b)). Now, it can choose either Path 2 or 4 to satisfy the constraint of BER. Finally, it selects Path 4 in the third iteration with BER of 1.9×10^{-3}. The final selection with BER constraint is Path 8 with BER of 1.75×10^{-3}, supporting the assertion that addition of selective paths results in minimal BER. Additional iterations lead to the paths that do not satisfy the constraint, thereby terminating the optimization algorithm after the fifth iteration.

7.5.2 Power Aware Scheduling in ROPAS

The simulation for the joint power control and link scheduling provides informative results concerned with the varying applications and different delay constraints. Figure 7.8 describes the scenario for four subframe intervals in one frame interval with $\xi = 0.5$. The unit value of ξ also implies that the lower frequency of using a particular power vector, $P(SF_i)$ for a group of links, $l \in L$ assigned to the i-th subframe. As shown in Figure 7.8, magnitudes of the sum of power vectors assigned (with frequency, $\xi = 1$) by our optimization strategy to 4 subframes are 0.02mW, 0.01mW, 0.005mW, and 0.002mW. This also satisfies the constraint imposed by Eq. (7.16) where P = 0.037 mW (the admissible spectral mask in UWB communications = 0.039 mW). This suggests that a smaller value

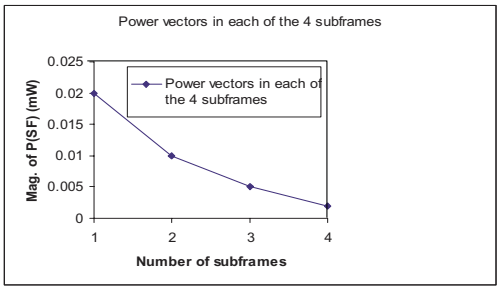

Figure 7.8: Magnitude of power vectors allocated in each subframe with unit frame interval

of ξ is suitable for a real-time traffic. Higher power allocation (e.g., 0.02 mW, 0.01 mW) during the frame interval results in increased transmission range such that the nodes can reach the destination nodes in a smaller number of hops.

Figure 7.9 shows the scenario with 2 subframes with $\xi = 1$. Higher value of ξ indicates higher frequency of allocation of certain power vector, $P(SF_i)$ for the i-th subframe. As shown in Figure 7.9, the magnitudes of power vectors allocated to 2 subframes are 0.01 mW (frequency =3) and 0.001 mW (frequency =7), much smaller in magnitude as compared to the scenario with $\xi = 0.5$. This indicates that higher values of ξ are suitable for delay tolerant non-real-time applications.

7.5.3 Priority based Joint link and Power Scheduling

Figure 7.10 depicts an important aspect of our optimization algorithm. Two applications, App. 1 and App. 3, have been enqueued twice for the service requests. Thus, according to Eq. (7.19), power assigned to these applications have been reduced for their second requests. This shows a unique design of our priority protocol. Additionally, since the power level for each of the slots assigned by the CR is quite high, it could accommodate only 6 slots in a frame. This is in tune with Eq. (7.21).

Figure 7.11 gives us an estimate of the scheduling algorithm performed by the CR based on the power constraints and the MAI observed at each node. As in Eq. (7.20), we observe that the signal power increases with improvement in BER values. So, increased power is assigned to each application with improvement in BER from 0.1 to 0.0001. This has a negative impact on the number of slots per frame. Higher signal power increases MAI

among the transmitting nodes, which in turn, restricts the number of parallel transmissions. Higher number of parallel transmissions (15 for BER of 0.1 as shown in Figure 7.11) is possible at higher values of BER which gradually decreases with improvement in the BER values. The power allocations for the six slots assigned for BER of 0.0001 are also shown in Figure 7.10.

7.6 Conclusion

In this chapter, we have proposed a novel cross-layer based ROPAS architecture applicable for mobile UWB networks. The Rake optimization in our ROPAS receiver achieves minimal BER with an optimal selection of correlators in the MRC-based Rake receiver. The optimization also reduces the computation complexity by reducing the number of fingers selected for signal estimation and their corresponding weight coefficients. The CR-based cross-layer optimization of joint power control and link scheduling has been simulated in each mobile UWB node. Our proposed optimization algorithm is capable of allocating "free" channel bandwidth dynamically to requesting application within power constraints in finite frame intervals. Additionally, non-real time and real-time applications are differentiated by designing a novel queuing strategy in ROPAS, which provides fairness and higher throughput among services with varying delay constraints in a mobile UWB network. The optimal division of a frame into slots is computed to support maximum number of parallel transmissions with dependence on parameters like the distance between transmitter-receiver pair and BER values. Finally, fairness among applications is taken care of while allocating power to each slot based on the frequency of request of a requesting application.

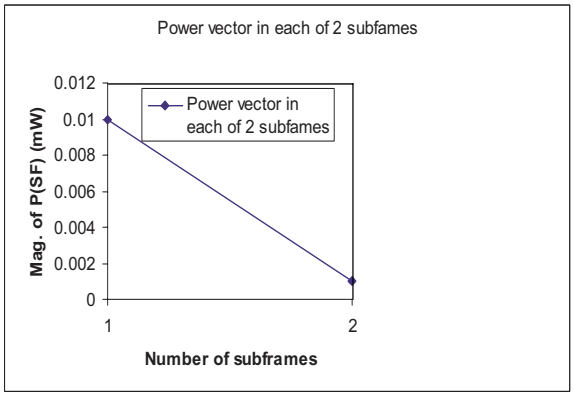

Figure 7.9: Magnitude of power vectors allocated in each subframe with frame interval=2units

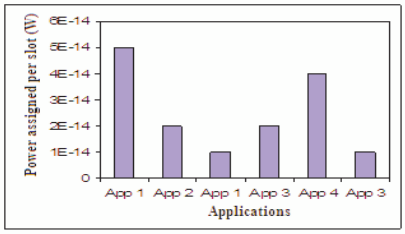

Figure 7.10: Power allocations for each application request in 6 time slots

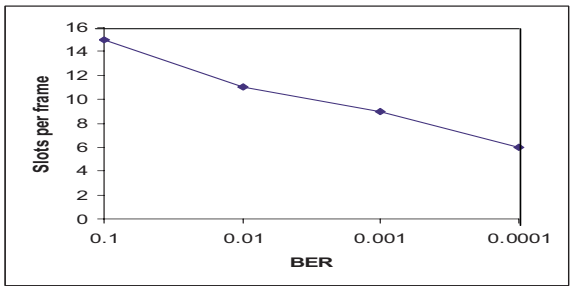

Figure 7.11: Number of slots assigned per frame for varying values of BER

Chapter 8

Conclusions and Future Work

Cognitive Radios are expected to play an important role in enhancing the spectrum efficiency without adding any new frequency spectrum to the wireless communications. In this dissertation, we have outlined numerous results obtained in different chapters. We summarize our results as follows.

In Chapter 2, we have proposed a novel spectrum occupancy model to accurately generate both the temporal and frequency behavior of various wireless transmissions. Using statistical characteristics from actual radio frequency measurements, first and second-order parameters are obtained and employed in a statistical spectrum occupancy model based on a combination of several different probability density functions (PDFs). The output characteristics of the proposed spectrum occupancy model are compared with spectrum measurements obtained from the USRP measurement system.

In Chapter 3, we have conducted a probabilistic analysis of free and contiguous sub-bands in the cognitive radio network. The critical entity in our analysis is the distribution of total number of free sub-bands. As we have shown, the computation of the exact distribution of the total number of free sub-bands (i.e., N_{free}) is prohibitively time-consuming and thus an efficient approximation approach is presented and analyzed. We labeled this novel approach as a Poisson-normal approximation and the time taken to execute this method is reasonable as indicated by the simulation. In addition, we focused on the analysis of contiguous sub-bands of a free sub-band, characterizing five different types of free sub-

bands. An algorithm is developed to compute the distribution of total number of sub-bands of each type. Exploiting probability distributions computed, we have outlined ways of selecting preferable sections of a spectrum for further sensing.

In Chapter 4, we have employed hidden Markov model to improve the decisions obtained from existing spectrum sensing techniques. The decisions obtained from the spectrum sensing approach are referred to as the observed sequence while the actual sub-band occupancy (true states) by a PU is unknown or in other words, hidden to a SU. The goal is to predict the true states of a sub-band given its observed sequence. We treat this problem by the probability theory. We assume that the sequence of true states of a sub-band follows a Markov model. In this chapter, we use the likelihood method for prediction of the true sequence for each sub-band. The computational complexity that arises is solved by using the Viterbi algorithm. If the underlying parameter values of the Markov chain are unknown, an Expectation-Maximization algorithm has been developed for the estimation of true sequences.

In any spectrum with M sub-bands, a sub-band can become free at an instant of time with probability p and is assumed to be constant with respect to the sub-bands. A free sub-band can be classified as one of the five types depending on who the neighbors of the free sub-band are. In Chapter 5, we have calculated the expected number of free sub-bands of each type. The type of free sub-band has impact on SINR. The free sub-bands can be allocated to the SUs subject to availability and interference constraints in many different ways. Maximal allocation matrices are characterized. Optimization of channel capacity over all maximal allocation matrices is discussed. To resolve conflicts that arise on preference of allocation matrices by SUs, game theoretic ideas are introduced in this chapter and Nash equilibria identified. Further, we have identified a unique Nash equilibrium allocation for the SUs that can optimize the channel capacity.

In Chapter 6, we have proposed a novel cross-layer based ROPAS architecture applicable for mobile UWB networks. The Rake optimization in our ROPAS receiver achieves minimal BER with an optimal selection of correlators in the MRC-based Rake receiver. The

optimization also reduces the computation complexity by reducing the number of fingers selected for signal estimation and their corresponding weight coefficients. The CR-based cross-layer optimization of joint power control and link scheduling has been simulated in each mobile UWB node. Our proposed optimization algorithm is capable of allocating "free" channel bandwidth dynamically to requesting application within power constraints in finite frame intervals. Additionally, non-real time and real-time applications are differentiated by designing a novel queuing strategy in ROPAS which provides fairness and higher throughput among services with varying delay constraints in a mobile UWB network. The optimal division of a frame into slots is computed to support maximum number of parallel transmissions with dependence on parameters like the distance between transmitter-receiver pair and BER values. Finally, fairness among applications is taken care of while allocating power to each slot based on the frequency of request of a requesting application.

8.0.1 Future Work

The following are the proposed work that will be pursued for completion of this Ph.D. dissertation.

Adaptive Spectrum Sensing

Adaptive spectrum sensing deals with spectrum sensing while exploiting the information available from the spectrum occupancy statistics. In Chapter 3, we have made an extensive probabilistic analysis of spectrum occupancy as well as the quality of a free subband with respect to its adjoining neighbors. In Chapter 4, we have utilized the hidden Markov model to estimate the real-time spectrum occupancy by the PUs. We can combine results from our probabilistic analysis into the hidden Markov model for enhancing the spectrum sensing efficiency. The central idea of our proposed work will be reduction in sensing time by utilizing the analysis carried out in Chapter 3. This type of spectrum sensing is known as ***adaptive spectrum sensing***.

Queuing model definition in Spectrum Occupancy Analysis

We have designed and validated a spectrum occupancy model in Chapter 2 based on different probabilistic distributions. The time slots t_{ON} and t_{OFF} represents the duration of time occupied by the PU and a set of SUs, respectively in each sub-band. We can represent such a sequence of t_{ON} and t_{OFF} in a sub-band as two M/M/1 queues for the PU and SUs, respectively, where M stands for the exponential distribution of inter-arrival rate of the users, where the arrival rate is governed by Poisson distribution. The main focus of our future work could be to study the average waiting time for the SUs in each sub-band. This information can serve as a historical data to the CR. Based on the average waiting time for each sub-band, the CR may allocate the real-time applications to those sub-bands with minimum waiting time.

There are many other open problems in the CRN area and it would be interesting to work on some of these challenging issues.

Appendix

Publications

Book Chapters:

- **C. Ghosh** and D. P. Agrawal. *NC-OFDM in Cognitive Radio Networks*. Cognitive Radio Networks: Architectures, Protocols and Standards, Auerbach Publications, Taylor & Francis Group, July, 2008.
- **C. Ghosh**, V. Ramesh Babu, and D. P. Agrawal. *OFDMA for Cognitive Wireless Networks*. OFDMA, Auerbach Publications, Taylor & Francis Group, February, 2009.

Accepted Journals:

- **C. Ghosh**, S. Pagadarai, D. P. Agrawal, and A. M. Wyglinski, "Statistical Spectrum Occupancy Modeling and Validation against real-time Measurements," accepted with revisions for publication in *IEEE Transactions on Wireless Communications*, Fall 2009.
- **C. Ghosh**, D. P. Agrawal, M. B. Rao, and C. Cordeiro, "Channel Capacity Optimization in Cooperative Cognitive Radio Networks using Game Theory," submitted to *ACM MC2R Special Issue on Dynamic Spectrum Access and Cognitive Radio*, September 2009.
- **C. Ghosh**, B. Xie and D. P. Agrawal, "ROPAS: Cross-Layer Cognitive Architecture for Mobile UWB Networks," *Springer Journal of Computer Science and Technology (JCST)*, Invited submission as one of the best paper from 4th IEEE International

Conference on Mobile Ad hoc and Sensor Systems, MASS '07, Vol. 23, No. 3, May 2008, pp. 413-423.

Submitted Journal:

- **C. Ghosh**, D. P. Agrawal, and M. B. Rao, "Probabilistic Analysis of Spectrum Occupancy in Cognitive Radio Networks," revised and re-submitted to *IEEE Transactions on Mobile Computing*, December 2008.

- **C. Ghosh**, S. Chen, D. P. Agrawal, and A. M. Wyglinski, "Priority Scheduling for NC-OFDM-based Cognitive Radio Networks," submitted to *Elsevier Computer Communications Special Issue on Dynamic Spectrum Access*, December 2008.

Journals in preparation:

- **C. Ghosh**, D. P. Agrawal, and M. B. Rao, "Enhanced Spectrum Sensing and Detection using Hidden Markov Models in Cognitive Radio Networks," to be submitted to *IEEE Transactions on Wireless Communications*, January 2009.

- **C. Ghosh**, D. P. Agrawal, and A. M. Wyglinski, "Priority-based Scheduling and Network Selection using Cognitive Radio in SDR-based Heterogeneous Networks," to be submitted to *IEEE Communications and Surveys*, February 2009.

- V. R. Babu, **C. Ghosh**, and D. P. Agrawal, "Enhancing Wireless Mesh Network Performance using Cognitive Radio with Smart Antenna," to be submitted to *IEEE Transactions on Wireless Communications*, February 2009.

- R. Dhekne, **C. Ghosh**, S. Swami, D. P. Agrawal, and K. Berman, "Graph Theoretic Approach to QoS-Guaranteed Spectrum Allocation in Cognitive Radio Networks," to be submitted to *IEEE Transactions on Parallel and Distributed Computing*, February 2009.

Conferences and Workshops:

- **C. Ghosh**, D. P. Agrawal, C. Cordeiro, and M. B. Rao, "Markov Chain Existence and Hidden Markov Models in Spectrum Sensing," invited paper to appear in *Fifth*

IEEE PerCom Workshop on Pervasive Wireless Networking, PWN'09, 9-13 March, 2009, Galveston, Texas.

- S. Swami, **C. Ghosh**, R. Dhekne, and D. P. Agrawal, "Graph Theoretic Approach to QoS Guaranteed Spectrum Allocation in Cognitive Radio Networks," *1st IEEE International Workshop on Dynamic Spectrum Access and Cognitive Radio Networks in conjunction with IPCCC'08*, 7-9 December, 2008, Austin, Texas.

- **C. Ghosh**, D. P. Agrawal, S. Chen, and A. M. Wyglinski, "Priority Scheduling for Cognitive Radio Networks Employing NC-OFDM Transmission," submitted to *IEEE Vehicular Technology Conference - Fall 2009, VTC*, 20-23 September, 2009, Anchorage, Arkansas.

- **C. Ghosh**, D. P. Agrawal, S. Pagadarai, and A. M. Wyglinski, "Statistical Spectrum Occupancy Modeling Employing Radio Frequency Measurements," submitted to *IEEE Vehicular Technology Conference - Fall 2009, VTC*, 20-23 September, 2009, Anchorage, Arkansas.

- V. K. Babu, **C. Ghosh**, and D. P. Agrawal, "Enhancing Wireless Mesh Network Performance using Cognitive Radio with Smart Antenna," submitted to *2009 IEEE Global Telecommunications Conference, GLOBECOM'09*, 29 November - 3 December, 2009, Honolulu, Hawaii.

- **C. Ghosh** and D. P. Agrawal, "Cross-layer architecture for Cognitive UWB Networks," *4th IEEE International Conference on Mobile Ad-hoc and Sensor Systems, MASS'07*, October 8-11, 2007, Pisa, Italy.

- **C. Ghosh** and D. P. Agrawal, "Cross layer optimization with Cognitive power aware scheduling and queuing in UWB Networks," accepted in *ACM International Wireless Communications and Mobile Computing Conference, ACM IWCMC*, August 12-16, 2007, Turtle Bay Resort Hotel, Honolulu, Hawaii.

- **C. Ghosh**, D. P. Agrawal and A. Chakraborty, "Performance of UWB receiver with Cognitive channel allocation and Rake optimization," *IEEE Cognitive Radio Ori-*

ented Wireless Networks and Communications, IEEE CROWNCOM, August 1-3, 2007, Orlando, Florida.

- **C. Ghosh** and D. P. Agrawal, "Cross layer performance evaluation of a Software Defined Radio receiver using Turbo decoding," *IEEE Software Defined Radio Workshop in conjunction with IEEE SECON*, June 18, 2007, San Diego, CA.

- **C. Ghosh** and D. P. Agrawal, "Channel assignment with route discovery (CARD) using cognitive radio in multi-radio wireless mesh networks," *IEEE Software Defined Radio Workshop in conjunction with IEEE SECON*, Sept 2006, Alexandria, Virginia.

- T. Banerjee, **C. Ghosh** and D. P. Agrawal, "Wireless Sensor Network based dynamic channel selection in cellular communication," *IEEE Cognitive Radio Oriented Wireless Networks and Communications, IEEE CROWNCOM*, June 8-11, 2006, Mykonos Island, Greece.

- R. Biswas, V. Jain, **C. Ghosh** and D. P. Agrawal, "On-demand reliable medium access in Sensor Networks," *IEEE International Symposium on a World of Wireless Mobile and Multimedia Networks, WoWMoM '06*, June 26-29, 2006, Niagara Falls, NY.

Bibliography

[1] W. Tuttlebee, *Software Defined Radio: Enabling Technologies*, John Wiley Pub., 2002.

[2] W. Tuttlebee, *Software Defined Radio: Origins, Drivers and International Perspectives*, John Wiley Pub., 2002.

[3] J. Mitola III, *Cognitive radio: an integrated agent architecture for software defined radio*. Ph.D. Thesis, Swedish Royal Institute of Technology, 2000.

[4] B. Fette, *Cognitive Radio Technology*, Communication Engineering Series, Elsevier, First Ed., 2006.

[5] M. A. McHenry, P. A. Tenhula, D. McCloskey, D. A. Roberson, and C. S. Hood, "Chicago spectrum occupancy measurements & analysis and a long-term studies proposal," *Proceedings of the First International Workshop on Technology and Policy for Accessing Spectrum, TAPAS'06*, ACM International Conference Proceeding Series; Vol. 222.

[6] M. A. McHenry and K. Steadman, "Spectrum occupancy measurements, location 2 of 6: Tyson's Square center, Vienna, Virginia, April 9, 2004," *Shared Spectrum Company Report*, August, 2005.

[7] F. H. Sanders, B. J. Ramsey, and V. S. Lawrence, "Broadband spectrum survey at Los Angeles, California," *NTIA Report 97-. 336*, May 1997.

[8] D. A. Roberson, C. S. Hood, J. L. LoCicero, and J. T. MacDonald, "Spectral occupancy and interference studies in support of Cognitive Radio Technology Deployment," *1st IEEE Workshop on Networking Technologies for Software Defined Radio Networks (SDR)*, Virginia, 25 Sept. 2006, pp. 26-35.

[9] M. Wellens, A. d. Baynast, and P. Mahonen, "Exploiting historical spectrum occupancy information for adaptive spectrum sensing," *IEEE Wireless Communication and Networking Conference (WCNC)*, March 31st - April 3, 2008, pp. 717-722.

[10] C. Ghosh, B. Xie, D. P. Agrawal, and M. B. Rao, "Probabilistic analysis of spectrum occupancy in cognitive radio," submitted in *IEEE Trans. on Mobile Computing*, May, 2008.

[11] A. J. Gibson, L. Arnett, "Statistical modelling of spectrum occupancy," *Electronics Letters*, Vol. 29, Issue 25, Dec. 1993, pp. 2175 - 2176.

[12] S. Geirhofer, L. Tong, and B. M. Sadler, "A Measurement-Based Model for Dynamic Spectrum Access in WLAN Channels," *Proceedings of the Military Communications Conference, MILCOM*, 23-25 Oct. 2006, pp. 1 - 7.

[13] B. Wang, Z. Ji, K. J. R. Liu, "Primary-Prioritized Markov Approach for Dynamic Spectrum Access," *Proceedings of the Second IEEE International Symposium on New Frontiers in Dynamic Spectrum Access Networks, DySPAN*, 17-20 April 2007, pp. 507 - 515.

[14] H. Kushwaha, Y. Xing, R. Chandramouli, and H. Heffes, "Reliable Multimedia Transmission Over Cognitive Radio Networks Using Fountain Codes," *Proceedings of the IEEE*, Vol. 96, Issue 1, Jan. 2008, pp. 155 - 165.

[15] F. H. Campos, M. Karaliopoulos, M. Papadopouli, and H. Shen, "Spatio Temporal Modeling of Traffic Workload in a Campus WLAN," *Proceedings of the ACM WICON*, 2006.

[16] A. Papoulis and S. U. Pillai, *Probability, Random Variables and Stochastic Processes*, Mc Graw Hill, Fourth Edition, 2002.

[17] M. Tanner, *Practical Queuing Analysis*, The IBM McGraw-Hill Series, 1995.

[18] S. Haykin, "Cognitive radio: brain-empowered wireless communications," *IEEE Journal on Selected Areas in Communications*, Vol. 23, Issue 2, Feb. 2005, pp. 201 - 220.

[19] J. Mitola, III and G. Q. Maguire, Jr., "Cognitive radio: making software radios more personal," *IEEE Personal Communications,*, Vol. 6, Issue 4, Aug. 1999, pp. 13 - 18.

[20] Z. Quan, S. Cui, and A. H. Sayed, "Optimal linear cooperation for spectrum sensing in cognitive radio networks," *IEEE Journal of Selected Topics in Signal Processing*, Vol. 2, Issue 1, Feb. 2008, pp. 28 - 40.

[21] G. Ganesan and Y. Li, "Cooperative spectrum sensing in cognitive radio, part I: two user networks," *IEEE Transactions on Wireless Communications*, Vol. 6, Issue 6, June 2007, pp. 2204 - 2213.

[22] G. Ganesan and Y. Li, "Cooperative spectrum sensing in cognitive radio, part II: multiuser networks," *IEEE Transactions on Wireless Communications*, Vol. 6, Issue 6, June 2007, pp. 2214 - 2222.

[23] L. Lou and S. Roy, "Analysis of search schemes in cognitive radio," *4th Annual IEEE Sensor, Mesh and Ad Hoc Communications and Networks '07, SECON '07*, 18-21 June 2007, San Diego, CA, pp. 647-654.

[24] S. Deng, J. Chen, H. He, and W. Tang, "Collaborative strategy for route and spectrum selection in cognitive radio networks," *Future Generation Communication and Networking*, Vol. 2, 6-8 Dec. 2007, pp. 168 - 172.

[25] P. Demestichas, G. Dimitrakopoulos, K. Tsagkaris, K. Demestichas, and J. Adamopoulou, "Reconfigurations selection in cognitive, beyond 3G, radio infrastructures," *1st International Conference on Cognitive Radio Oriented Wireless Networks and Communications, CROWNCOM '06*, 8-10 June 2006, pp. 1 - 5.

[26] Q. Wang and H. Zheng, "Route and spectrum selection in Dynamic Spectrum Networks," *3rd IEEE Consumer Communications and Networking Conference, CCNC '06.*, Vol. 1, 8-10 Jan. 2006, pp. 625 - 629.

[27] S-Y. Tu, K-C. Chen, and R. Prasad, "Spectrum sensing of OFDMA systems for cognitive radios," *18th Annual IEEE International Symposium on Personal, Indoor and Mobile Radio Communications, PIMRC'07*, Athens, Greece, 3-7 Sept. 2007, pp. 1 - 5.

[28] F-S. Chu and K-C. Chen, "Radio resource allocation in OFDMA cognitive radio networks," *18th Annual IEEE International Symposium on Personal, Indoor and Mobile Radio Communications, PIMRC'07*, Athens, Greece, 3-7 Sept. 2007, pp. 1 - 5.

[29] G. Ganesan, Y. Li, B. Bing, and S. Li, "Spatiotemporal sensing in cognitive radio networks," *IEEE Journal on Selected Areas in Communications*, Vol. 26, Issue 1, Jan. 2008, pp. 5 - 12.

[30] FCC Spectrum Policy Task Force. *Report of spectrum efficiency working group.* [Available online], First note and Order, Federal Communications Commission, ET-Docket 98-153, adopted February 14, 2002, released April 22, 2002.

[31] R. B. Ash, *Real Analysis and Probability*, Academic Press, Orlando, Florida, 1972, pp. 337.

[32] K. Lange, *Applied Probability*, Springer, New York, 2003.

[33] P. M. Lee, *Bayesian Statistics: An Introduction*. Oxford University Press, Third Ed., 2004.

[34] T. W. Rondeau, C. J. Rieser, T. M. Gallagher, and C. W. Bostian, "Online modeling of wireless channels with hidden markov models and channel impulse responses for cognitive radios," *2004 IEEE MTT-S Digest*, pp. 739-742.

[35] K. Kim, I. A. Akbar, K. K. Bae, J-S. Um, C. M. Spooner, and J. H. Reed, "Cyclostationary approaches to signal detection and classification in cognitive radio," *IEEE 2007*, pp. 212-215.

[36] C-H. Park, S-W. Kim, S-M. Lim, and M-S. Song, "HMM based channel status predictor for cognitive radio," *IEEE Proc. of Asia-Pacific Microwave Conference*, 2007.

[37] I. A. Akbar and W. H. Tranter, "Dynamic spectrum allocation in cognitive radio using hidden markov models: Poisson distributed case," *IEEE Southeast Conference*, 2007, pp. 196-201.

[38] Q. Zhao and A. Swami, "A decision-theoretic framework for opportunistic spectrum access," *IEEE Wireless Comm. Mag.*, vol. 14, no. 4, pp. 14-20, August 2007.

[39] C. Ghosh, D. P. Agrawal, S. Pagadarai, and A. M. Wyglinski, "Statistical Spectrum Occupancy Modeling Employing Radio Frequency Measurements," submitted to *IEEE Trans. on Wireless Communications*, Nov. 2008.

[40] R. Durbin, S. Eddy, A. Krogh, and G. Mitchison, *Biological Sequence Analysis*, Cambridge University Press, UK, 2004.

[41] C. Ghosh and D. P. Agrawal, "Enhanced Spectrum Sensing and Detection using Hidden Markov Models in Cognitive Radio Networks," to be submitted to *IEEE Trans. on Wireless Comm.*, August 2008.

[42] Y. Zeng and Y. C. Liang, "Maximum-minimum eigenvalue detection for cognitive radio," *Proc. IEEE PIMRC '07*, 2007.

[43] M. Ghosh, "DTV Signal Sensing using the PN511 Sequence," *Available online:IEEE 802.22-07/0186r01*, May 2007.

[44] G. Turkenich, V. Gaddam, and M. Ghosh, "Dual FPLL pilot sensing," *Available online: IEEE 802.22-07/0296r2*, May 2007.

[45] S. Y. Chang, L. Lv, Z. Wu, M. Jie, J. Zhang, L. Qian, and J. Wen, "Spectral correlation sensing with real DTV signals," *Available online: IEEE 802.22-07/0284r1*, May 2007.

[46] H. S. Chen and W. Gao, "Cyclostationary feature detector for spectrum sensing," *Available online: IEEE 802.22-07/0283r0*, May 2007.

[47] Y. Zeng and Y. C. Liang, "Covariance based signal detections for cognitive radio," *Available online: IEEE 802.22-07/0294r2*, May 2007.

[48] Y. Zeng and Y. C. Liang, "Covariance based sensing for wireless microphone," *Available online: IEEE 802.22-07/0295r3*, May 2007.

[49] T. Koski, *Hidden Markov Models for Bioinformatics*, Kluwer Academic Publisher, 2001.

[50] G. McLachlan and T. Krishnan, *The EM algorithm and extensions*, John Wiley, New York, 1997.

[51] C. Cordeiro, M. Ghosh, D. Cavalcanti and K. Challapali, "Spectrum sensing for Dynamic Spectrum Access of TV bands," *IEEE CROWNCOM '07*, Aug. 1-3 2007, Orlando, Florida, pp. 1-6.

[52] S. Ragusa, J. Palicot, C. Roland, and C. Lereau, "Adjacent channel power ratio analysis for an OFDM signal," *IEEE International Symposium on Signal Processing and Information Technology*, 2005, pp. 495-500.

[53] S. A. Jafar and S. Srinivasa, "Capacity limits of Cognitive Radio with distributed and dynamic spectral activity," *IEEE J. on Selected Areas in Communications*, vol. 25, no. 3, April 2007, pp. 529-537.

[54] Z. Ji and K. J. Ray, "Dynamic Spectrum Sharing: A Game Theoretic Overview," *IEEE Communication Magazine*, vol. 45, no. 5, May 2007, pp. 88-94.

[55] G. Owen, *Game Theory*, Academic Press, 1995.

[56] M. J. Osborne, *An Introduction to Game Theory*, Oxford University Press, 2004.

[57] J. E. Hicks, A. B. MacKenzie, J. Neel, and J. H. Reed, "A Game theory perspective on interference avoidance," *IEEE Global Telecommunications Conference, GLOBECOM*, vol. 1, 29 Nov. - 3 Dec. 2004, pp. 257 - 261.

[58] N. Nie and C. Comaniciu, "Adaptive channel allocation spectrum etiquette for cognitive radio networks," *First IEEE International Symposium on New Frontiers in Dynamic Spectrum Access Networks, DySPAN'05*, 8-11 Nov. 2005, pp. 269 - 278.

[59] Y. Xing, R. Chandramouli, and C. Cordeiro, "Price dynamics in competitive agile spectrum access markets," *IEEE J. on Selected Areas in Communications*, vol. 25, no. 3, April 2007, pp. 613-621.

[60] D. Niyato and E. Hossain, "Competitive pricing for spectrum sharing in cognitive radio networks: dynamic game, inefficiency of Nash equilibrium, and collusion," *IEEE J. on Selected Areas in Communications*, vol. 26, no. 1, Jan. 2008, pp. 192-202.

[61] D. Niyato and E. Hossain, "Competitive spectrum sharing in cognitive radio networks: a dynamic game approach," *IEEE Trans. on Wireless Comm.*, vol. 7, no. 7, July 2008, pp. 2651-2660.

[62] B. Wild and K. Ramchandran, "Detecting primary receivers for Cognitive Radio applications," *First IEEE International Symposium on New Frontiers in Dynamic Spectrum Access Networks, DySPAN'05*, 8-11 Nov. 2005, pp. 124-130.

[63] H. Sun, J. Jiang, and M. Lin, "Adaptive cooperation algorithm for Cognitive Radio Networks," *International Conference Wireless Communications, Networking and Mobile Computing, WiCOM'06.*, 22-24 Sept. 2006, pp. 1-4.

[64] R. Etkin, A. Parekh, and D. Tse, "Spectrum sharing for unlicensed bands," *IEEE J. on Selected Areas in Communications*, vol. 25, issue 3, April 2007, pp. 517 - 528.

[65] G. Ganesan and Y. G. Li, "Agility improvement through cooperative diversity in Cognitive Radio," *IEEE Global Telecommunications Conference, GLOBECOM'05*, vol 5, 28 Nov. - 2nd Dec., 2005, pp. 1-5.

[66] L. Cao and H. Zheng, "Distributed spectrum allocation via local bargaining," *Second Annual IEEE Communications Society Conference on Sensor and Ad Hoc Communications and Networks, SECON'05*, 26-29 Sept. 2005, pp. 475 - 486.

[67] S. Srinivasa and S. A. Jafar, "The throughput potential of Cognitive Radio: a theoretical perspective," *Fortieth Asilomar Conference on Signals, Systems and Computers, ACSSC'06*, Oct.-Nov. 2006, pp. 221-225.

[68] Z. Wu and B. Natarajan, "Interference tolerant agile Cognitive Radio: maximize channel capacity of Cognitive Radio," *4th IEEE Consumer Communications and Networking Conference, CCNC'07*, Jan. 2007, pp. 1027-1031.

[69] L. B. Le, and E. Hossain, "Resource allocation for spectrum underlay in cognitive radio networks," *Proceedings of the IEEE Transactions on Wireless Communications*, Vol. 7, Issue 12, Part 2, December 2008, pp. 5306 - 5315.

[70] U. S. Jha and R. Prasad, *OFDM towards Fixed and Mobile Broadband Wireless Access*. Artech House, London, 2007.

[71] A. Attar, O. Holland, M. R. Nakhai, and A. H. Aghvami, "Interference-limited resource allocation for cognitive radio in orthogonal frequency-division multiplexing networks," *Proceedings of the IET Communications*, Vol. 2, Issue 6, July 2008, pp. 806 - 814.

[72] T. A. Weiss and F. K. Jondral, "Spectrum pooling: an innovative strategy for the enhancement of spectrum efficiency," *IEEE Communications Magazine*, Vol. 42, Issue 3, March 2004, pp. 8 - 14.

[73] Q. Qu, L. B. Milstein, and D. R. Vaman, "Cognitive Radio Based Multi-User Resource Allocation in Mobile Ad Hoc Networks Using Multi-Carrier CDMA Modulation," *Proceedings of the IEEE Journal on Selected Areas in Communications*, Vol. 26, Issue 1, January 2008, pp. 70 - 82.

[74] R. Zhang and Y-. Liang, "Exploiting Multi-Antennas for Opportunistic Spectrum Sharing in Cognitive Radio Networks," *Proceedings of the IEEE Journal of Selected Topics in Signal Processing*, Vol. 2, Issue 1, February 2008, pp. 88 - 102.

[75] R. Rajbanshi, A. M. Wyglinski, and G. J. Minden, "An efficient implementation of NC-OFDM transceivers for cognitive radios," *Proceedings of the 1st International Conference on Cognitive Radio Oriented Wireless Networks and Communications, Crowncom'06*, Mykonos Island, Greece, June 2006.

[76] G. Aggelou, *Mobile Ad Hoc Networks*. McGraw-Hill Pub., 2005.

[77] J. H. Reed, *An introduction to Ultra Wideband communication system*, Prentice Hall, Upper Saddle River, NJ, 2005.

[78] C. Ghosh, B. Xie, and D. P. Agrawal, "ROPAS: Cross-Layer Cognitive Architecture for Mobile UWB Networks," *Springer Journal of Computer Science and Technology (JCST)*, Invited submission as best paper from 4th IEEE International Conference on Mobile Ad hoc and Sensor Systems (MASS), 2007, pp. 413-423.

[79] J. Yang, Q. Jiang, D. Manivannan, and M. Singhal, "A fault-tolerant distributed channel allocation scheme for cellular networks," *IEEE Trans. on Computers*, vol. 54, no.5, May 2005, pp. 616-629.

[80] A. Boukerche, T. Huang, and K. Abrougui, "Design and performance evaluation of a QoS-based dynamic channel allocation protocol for wireless and mobile networks," *IEEE MASCOTS'05*.

[81] J. Heo, I. Cha, and K. H. Chang, "A novel transmit power allocation algorithm combined with dynamic channel allocation in reuse partitioning-based OFDMA/FDD system," *IEEE ICC'06*, pp. 5654-5659.

[82] J. Cai, K. H. Liu, X. Shen, J. W. Mark, and T. D. Todd, "Power allocation and scheduling for MAC layer design in UWB networks," *IEEE QShine '05*, 22-24 Aug. 2005, 8 pp.

[83] L. D. Nardis, G. Giancola, and M. G. D. Benedetto, "Power-aware design of MAC and routing for UWB networks," *IEEE Globecom 2004*, 29 Nov.-3 Dec. 2004, pp.:235 - 239.

[84] M. G. D. Benedetto and L. D. Nardis, "Cognitive routing in UWB networks," *IEEE ICUWB '06*, Sept. 2006, pp.:381 - 386.

[85] Q. H. Mahmoud, *Cognitive Networks: Towards Self-Aware Networks*, Wiley, 2007.

[86] V. Srivastava and M. Motani, "Cross-layer design: a survey and the road ahead," *IEEE Comm. Mag*, vol. 43, no. 12, Dec. 2005, pp.: 112-119.

[87] L. Qingwen, Z. Shengli, and G. B. Giannakis, "Cross-layer scheduling with prescribed QoS guarantees for adaptive wireless networks," *IEEE Jour. in Sel. Areas in Comm.*, vol. 23, no.5, May 2005, pp.:1056-1066.

[88] G. Dimic, N. D. Sidiropoulos, and R. Zhang, "Medium access control-physical cross layer design," *IEEE Signal Processing Mag.*, vol. 21, Issue 5, Sept. 2004, pp.: 40 - 50.

[89] Y. Donoso and R. Fabregat, *Multi-Objective Optimization in Computer Networks Using Metaheuristics*, Auerbach Publications, 2007.

[90] C-L. Hwang and A. S. Md. Masud, *Multiple Objective Decision Making - Methods and Applications*, Springer-Verlag, 1979.

[91] H. Sato and T. Ohtsuki, "Computational complexity and performance of Rake receivers with channel estimation for DS_UWB," *IEEE Trans. Fundamentals*, vol. E88-A, no. 9, Sept. 2005, pp. 2318-2326.

[92] S. Boyd and L. Vandeberghe, *Convex Optimization*, Cambridge University Press, 2004.

[93] www.gnu.org/software/glpk

[94] H. Harada and R. Prasad, *Simulation and Software Radio for Mobile Communications*, Artech House, London, 2002.